MAGNETIC INTERACTIONS AND ORDERING IN SOME

TRANSITION METAL ALLOYS.

Thesis submitted for the degree of Doctor of Philosophy

University of London

by

PON-WEI HOU.

Physics Department,

Imperial College of Science and Technology,

London, S.W.7.

July, 1975.

ABSTRACT

Recently the interest in alloy research has been shifting from the extremely dilute region to the more concentrated region in which the interactions between impurities can be no longer neglected. Studies of some transition metal alloy systems by means of magnetic and resistivity measurements in the presence of such interactions are presented in this thesis.

Measurements taken at temperatures above Kondo temperature, T_K, of the magnetization M and the susceptibility X of three "dilute" AgMn alloys of nominal concentration 630, 1000 and 1370 ppm Mn are presented. Both M and X follow scaling laws well and, thus, verify the geometrical decreasing with distance cubed characteristics of the RKKY interaction. The strength V_0 of the RKKY interaction between two Mn impurities has been determined from the high field behaviour to be $(3.9 \pm 1) \times 10^{-25}$ eV cm^3. The effective $|J|$ value estimated from V_0 is (0.9 ± 0.1)eV.

Other measurements taken at temperatures below T_K are presented of the magnetization of several "dilute" Al-3d alloys. It is experimentally shown that the impurity interaction persists below T_K in these alloys.

A series of PtMn alloys (0.09, 2, 3, 5.4, 8, 11, and 12 at.% Mn) has been studied magnetically from 1.4 to 70K. The behaviour of the most dilute alloy (0.09 at.% Mn) approximates to a free spin system. For other alloys, the paramagnetic–superparamagnetic–magnetic spin glass states transitions have been observed. The temperature T_{max} of the susceptibility maximum follows a linear relation of the impurity

concentration n. For alloys of n from 2 to 8 at.% Mn, the Weiss temperature follows a linear relation of n and susceptibility follows the same power law of the reduced temperature (T/n) at high temperatures. The magnetic phase diagram of the $\underline{Pt}Mn$ alloy system has been established.

Three $\underline{Pt}Cr$ alloys (n = 10, 14.1 and 17 at.% Cr) have been studied magnetically from 1.4 to 70K. A magnetic spin glass state is observed for alloys of n = 14.1 and 17 at.% Cr, and the superparamagnetic state has been seen. These three alloys and another more dilute $\underline{Pt}Cr$ alloy (7 at.% Cr) have been studied by resistivity measurements and the results are consistent with that of the magnetic measurements. The magnetic phase diagram of the $\underline{Pt}Cr$ alloy system has been established.

The $Pd_{1-x}Pt_xMn$ alloy system has been studied mainly by magnetic measurements from 1.4 to 20K and also by some resistivity measurements. The magnetic phase diagram of paramagnetic-ferromagnetic-magnetic spin glass states has been established. For $Pd_{1-x}Pt_xMn$ alloys containing 3 at.% Mn, the ferromagnetism dominates for $x < 0.1 \pm 0.02$, and the magnetic spin glass state is observed for higher x alloys.

An extension of ultraviolet transmission spectrum to 21 eV into the far vacuum ultraviolet was achieved in previous work carried out on uracil thin film at Queen Elizabeth College after registration for a higher degree of the University of London, and this work is included as supplementary matter.

ACKNOWLEDGEMENTS

TABLE OF CONTENTS

MAGNETIC INTERACTIONS AND ORDERING IN SOME TRANSITION METAL ALLOYS

SUPPORTING MATERIAL

SUBMITTED TO PHYSICAL REVIEW LETTERS

APPENDIX A   MAGNETIC INTERACTIONS IN "DILUTE"

AgMn ALLOYS

Pon-Wei Hou and B.R. Coles, Department of

Physics, Imperial College, London SW7

APPENDIX B   EXTENDED FAR VACUUM ULTRAVIOLET

TRANSMISSION SPECTRUM OF URACIL

THIN FILM

Pon-Wei Hou, Department of Physics,

Imperial College, London SW7

R.P. Rampling, Department of Physics,

Queen Elizabeth College, London W8

PREFACE

Magnetism was first discovered over five thousand years ago and, along with the inventions of printing technology and dynamite, is one of the three major scientific contributions made by the Chinese in an early age. The frontiers of knowledge are always on the move. Magnetism in solids is a subject which continues to attract the attention of research workers. The study of dilute alloys was a major break-through which occurred in the early sixties. This single-impurity effect has been studied reasonably well. The next stage of the research will be to find out the physical properties of non-dilute alloys in which the impurity-impurity interaction can no longer be neglected. These non-dilute AgMn, Al-3d, PtMn, PtCr, and PdPtMn alloy systems are the subjects studied and presented in this work.

In Chapter 1, an introductory description of theoretical and experimental work of dilute and non-dilute alloys is presented in Sections I and II respectively. In Chapter 2, a description of experi-mental apparatus and procedures is presented. The ideas and experi-mental results of the AgMn and Al-3d alloy systems, the PtMn and PtCr alloy systems, and the PdPtMn alloy system are presented in Chapters 3, 4, and 5, in sequence.

An extension of the ultraviolet transmission spectrum of uracil thin film into the far vacuum ultraviolet was achieved and is included as supplementary matter.

The attitude of writing in this work is intended for physicists who have a general knowledge of physics, but not necessarily specialization in the alloy field; therefore, a self-consistent manner of presentation in each chapter as well as in the overall frame of the work is used.

CHAPTER 1 INTRODUCTION TO TRANSITION METAL ALLOYS

General Introduction

A certain amount of a transition element(s) with magnetic proper-
ties originally, when put as the impurity into an otherwise non-magnetic
metallic host, can form a transition metal alloy. The magnetic prop-
erties of the impurity will be influenced and can be completely quenched
by this alloying. The alloy, under appropriate conditions, will be
magnetic, defined by its initial susceptibility X(t) as described by the
Curie-Weiss law, $X(t) = \frac{C}{T-\theta}$, where C is the Curie constant, T is
the absolute temperature, and θ is the Weiss temperature.

The problem of alloys has attracted a considerable amount of
attention in solid state physics research. Starting from dilute alloys
with a simple metal host, the research later shifted to more concen-
trated solid solutions and even used transition metals as the host. In
beginning to examine this problem, there are several possible inter-
actions to be considered:

(A) interactions between the magnetic electrons of the same
impurity atom with the influence of the host,

(B) interactions between the magnetic electrons of the impurity
atom and the conduction electrons of the host, and

(C) interactions between different impurity atoms with the
influence of the host.

Obviously, the properties of the alloys will depend upon the types
and combinations of impurities and hosts, the impurity concentrations,

and the temperature range under consideration; however, for purposes

here, it is preferable to divide the alloys into two rough categories:

(I) the isolated solute atoms alloy in which the interactions (A)/(B)

dominate, and (II) the interacted solute atoms alloy in which the

interaction (C) dominates. These two categories will be discussed in

sequence in Sections I and II.

Section I. The Isolated Solute Atoms Alloy

I-1. Introduction

An extremely small amount of a transitional element(s) with magnetic properties originally, when put as the impurity into an otherwise non-magnetic metallic host, can form a dilute transition metal alloy. Several general phenomenological characteristics of dilute alloys formed by a combination of host and impurity have been found experimentally (the so-called single-impurity, Kondo-like, dilute alloys can also be characterized by these general attributes). These characteristics are stated as follows:

(1) the magnitudes of the measured bulk properties are directly proportional to the impurity concentrations (3), i.e. additive,

(2) the Weiss temperature θ is nearly a constant and is insensitive to the impurity concentrations (4,5),

(3). there exists a resistivity minimum (6). The temperature of this resistivity minimum is quite insensitive to the impurity concentration $n(\propto n^{1/5})$ (7) and the low temperature resistivity scales with n (3,8). In addition, a one-to-one correspondence between the resistivity minimum and the magnetic property has been found (9).

Moreover, the neutron diffraction results of some alloys, such as NiFe and NiMn, suggest that the magnetic moment on a near neighbor solvent atom is unaffected by the impurity (10,11). Therefore, from the above evidence, it is suggested that the formation of magnetic property of dilute alloys can be isolated to a question of the formation of a local magnetic moment of a single isolated transition metal atom

interacting with a sea of host conduction electrons and having nearly the characteristics of free, non-interacting, ensemble of spins behaviour.

1-2. Virtual Bound State

The concept of virtual bound state (VBS) was introduced to the research of dilute alloys by Friedel (12). VBS is a state lying between the impurity magnetic d electrons and the host conduction s electrons. The energy band of the host s electrons is so broad that sometimes the energy level of the impurity d electrons, E_d, which is a much narrower band, lies within it (13).

VBS is a particular case of the degeneracy resonance phenomena which is well-known in atomic and nuclear physics. It arises when one puts together two systems with similar eigenenergies (14). The degeneracy resonance process is shown in Fig. 1.
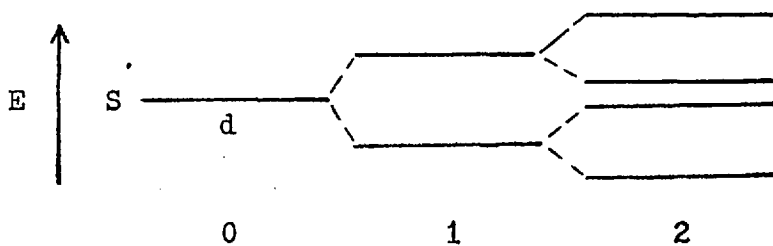
Fig. 1   Degeneracy resonance process (after Friedel (12)).

The region in space and in the energies where each of the extended states presents in the alloy has an amplitude larger on the impurity atom than in the matrix, with strong d characteristics and build-up VBS.

VBS can also be approached as a scattering resonance phenomena which arises when the host s electrons are scattered by the impurity d

electrons and cause a phase shift. If the s electrons and d electrons

have similar energy, then resonance causes an anomalous phase shift

(15) and builds up a VBS. This scattering resonance phenomena is

shown in Fig. 2.
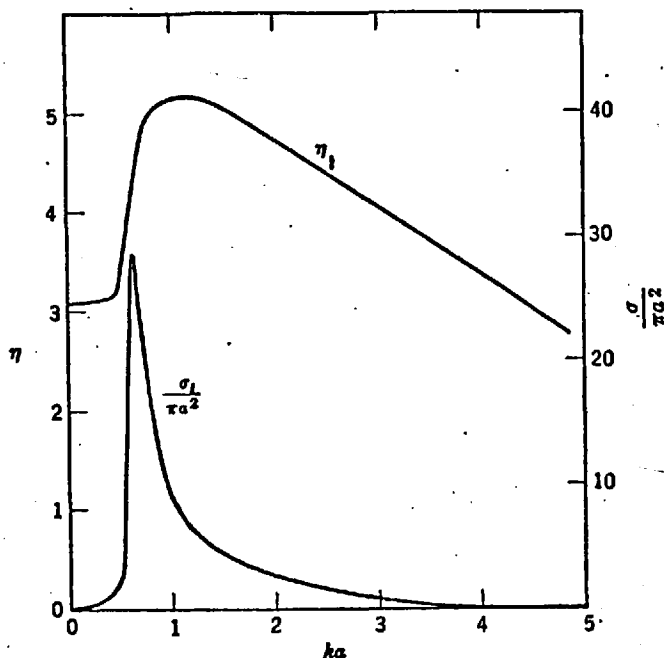
Fig. 2 Phase shift η_1 and partial cross section δ_1 for p-wave of

electron with mass m scattering from square well of radius

a and depth b such that $(2mb)^{1/2}a = 6.2$ (after Merzbacher (15)).

A spherical potential will give rise to a change in the electron

density $\Delta\rho(r)$ at location $\underset{\sim}{r}$ from the scattering center at origin as:

$$\int_0^\infty \Delta\rho\,(r)d\underset{\sim}{r} = \frac{2}{\pi}\sum_l (2l + 1)\,\eta_l(E_F)$$

with $\eta_l(E_F)$ being the phase shifts of the incident wave of angular

momentum l at the Fermi level. If the impurity has an excess charge

Z compared to the host, it follows the necessary condition of neutrali-

zation, or Friedel's sum rule, such that Z should equal the total

screening charges:

$$Z = \frac{2}{\pi} \sum_l (2l + 1) \, \eta_l(E_F)$$

The VBS resonates with the l spherical components of the incident waves and broadens in a region of energy Δ with the average energy being E_d. The relations among the phase shift $\eta_l(E)$ at energy E, the energy width Δ, and the excess charge density $\Delta\rho(r)$, and the corresponding density of localized states $\rho_l(E)$ are shown in the following equations and in Fig. 3 and 4.

$$\Delta \sim |V_{sd}|^2 \, n_s(E_F)$$

$$\Delta\rho(r) \propto \frac{\cos(2K_F r)}{r^3} \quad \text{(for large r)}$$

$$\rho_l(E) = \frac{2l + 1}{\pi} \frac{d\,\eta_l(E)}{dE}$$

where V_{sd} is the interaction between s and d electrons, $n_s(E_F)$ is the electron density at Fermi level, and K_F is the wave number at Fermi level.
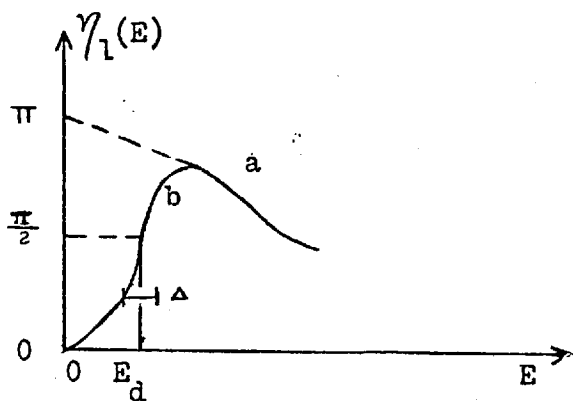
Fig. 3 Phase shift $\eta_l(E)$ for a free-electron gas (a) bound state, (b) VBS versus energy E (after Friedel (12)).
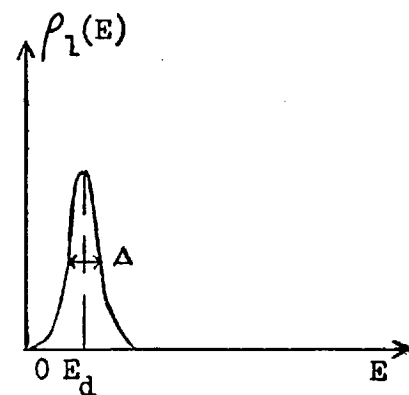
Fig. 4 Corresponding density of localized states $\rho_l(E)$ versus energy E (after Friedel (12)).

1-3. The Anderson Model

The rapid variation of phase shift with electron energy near the

virtual level makes the properties of an alloy having its Fermi level

in this region highly sensitive to the electron concentration (a phase

shift diagram has been shown in Fig. 2). The magnetic moment in

Bohr magnetons of an Fe atom dissolved in various second row

transition metals and alloys as a function of the electron concentration

is exhibited in Fig. 5.
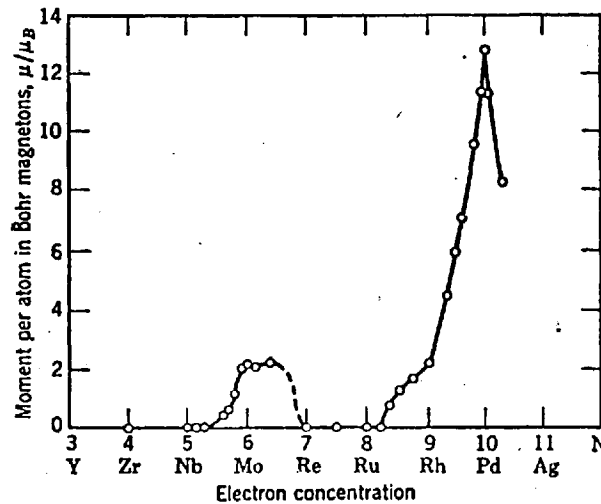
Fig. 5   Magnetic moment of an Fe atom in different solvents (after

Clogston et al (16)).

It is clear that a sharply defined region where localized moments

are absent or present exists.   Since varying the electron concentration

varies the width of the virtual level and the position of the Fermi level,

a local moment is developed when the Fermi level is close to a vir-

tual level, and the virtual level is sufficiently narrow.

Anderson (17) started from these experimental results and intro-duced the Anderson Hamiltonian: $H = H_s + H_d + H_{corr} + H_{sd}$ where H_s is the unperturbed energy of the free-electron system, and H_d is the unperturbed energy of the "d" states on the impurity atom. The third term, $H_{corr} = U n_{d\uparrow} n_{d\downarrow}$, is the repulsive energy among the d functions, where U is the Coulomb potential between d electrons of opposite (up and down) spins, and $n_{d\delta}$ is the occupation number operator with spin δ : $n_{d\delta} = C^*_{d\delta} C_{d\delta}$, where the $C_{d\delta}$ is the second quantization operator. The last term, $H_{sd} = \sum_{k,\delta} V_{kd} (C^*_{k\delta} C_{d\delta} + C^*_{d\delta} C_{k\delta})$, with momentum k, represents the covalent admixture interaction of conduction and localized d state.

The Anderson picture is a simplified single orbital model: the impurity as a localized extra orbital with an energy somewhere in the conduction band of the host representing the d state of the transitional atom in an otherwise free electron gas. The repulsive energy U between the up and down state electrons causes the level to split into two halves. This emphasis of U is, as we have pointed out in the General Introduction section, the interaction (A). The relative mag-nitude of this splitting and width 2Δ of the level (which is caused by V_{kd} that allows electrons to hop on and off the impurity with the result that the energies of the localized levels are no longer well-defined, but are broadened with electron lifetime $\mathcal{T}_\Delta$, $\mathcal{T}_\Delta = \hbar/\Delta$) determines whether the state is magnetic or not, with a sharp transition. The Anderson picture of the density of state distributions in a magnetic case is shown in Fig. 6.
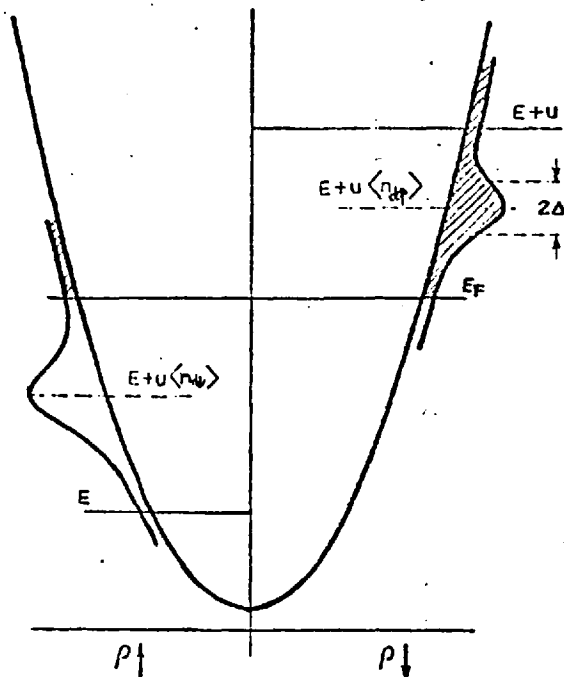
Fig. 6   Density of state distribution in a magnetic case (after

Anderson (17)).

The numbers of electrons $\langle n_{d\uparrow} \rangle$ and $\langle n_{d\downarrow} \rangle$ occupying

the virtual d "levels" of width 2Δ are to be computed from the

area of the unshaded portion below the Fermi surface. If a local

magnetic moment exists on the impurity site, then the spin, $|S|$, of

the virtual state must not equal zero, i.e. $\langle n_{d\uparrow} \rangle \neq \langle n_{d\downarrow} \rangle$.

Anderson made calculations through a self-consistent Hartree-Fock

approximation taken at the $\frac{U}{\Delta} < 1$ limit and found that for a localized

magnetic moment to exist, the condition $\frac{U}{\Delta\pi} > 1$ must be satisfied.

As the transition metal impurity might have more than one d

orbital, Yosida, Kiji, and Chikazumi (18), and Klein and Heeger (19)

later considered the Anderson model with (2l + 1) degenerate localized

impurity orbitals. They also took account of Hund's rule (intra-atomic-

like exchange $J_{dd} > 0$), providing there is no crystal field splitting.

Hence, the condition favorable for magnetic moments to exist becomes:

$$\frac{U + 4J}{\pi \Delta} \geq 1$$

where U is the Coulomb repulsion, J is the intra-atomic exchange

integral, and Δ is the width of the VBS. This expression is of the

same form as the Stoner condition for band ferromagnetism (20).

I-4. The s-d Model

The formation of a localized magnetic moment on impurity site

can also be treated as a scattering problem in which the free conduc-

tion electrons scatter from the perturbing impurity potential (21,22).

Actually, the problem of a magnetic impurity in metal (Mn in Cu, for

example) was first treated with the s-d exchange interaction model by

Zener (23), Ruderman and Kittel (24), Kasuya (25), and Yosida (26).

The s-d exchange Hamiltonian V_{sd} can be expressed as:

$$V_{sd} = -J \underset{\sim}{S} \cdot \underset{\sim}{s}$$

between the spin operator $\underset{\sim}{S}$ and $\underset{\sim}{s}$ for the spin momenta of impurity

and host conduction electron, and J is the exchange integral.

Since the resistivity minimum occurs in a dilute alloy which

exhibits the localized magnetic moment (9), with the basic assumptions

that the impurity moments exist and have an infinite lifetime, Kondo

(7) derived the anomalous rise of the low temperature resistivity of

dilute magnetic alloys by using the s-d model and calculating in the

second Born approximation, taking the Pauling exclusion principle into account in the intermediate states. The interference between single and two electron scattering processes leads to the correlations which account for the internal degree of freedom of the magnetic impurity scattering center. This emphasis of s-d interaction, as we have pointed out in the General Introduction section, is the interaction (B). The magnetic contribution to the resistivity has the form of:

$$\rho = n \, \rho_m [1 + N(o) \, J \ln(k_B T/D)]$$

where n is the impurity concentration, ρ_m is the first Born scattering term, $N(o)$ is the density of states in a flat band of width 2D, and k_B is the Boltzmann constant.

With an effective negative J (antiferromagnetic) (27,28), the magnetic contribution to the resistivity increases logarithmically with decreasing temperature and, combined with the phonon contribution, gives a minimum in the total resistivity at some temperature T_{min}.

But, in this calculation, the logarithmic singularity in the scattering amplitude will occur below a characteristic temperature (Kondo temperature T_K), and the perturbation approach will break down. This characteristic temperature has been considered by different authors and through different approaches (29): Yosida (30,31) (variational method), Abrikosov (32) (modified diagrammatic method), Suhl and Wong (33) (dispersion theoretical method), Nagaoka (34) (who solves a truncated set of double-time thermodynamic Green's function equations) and Bloomfield and Hamann (35) (who solve a

double-time thermodynamic Green's function equation of motion).

The unity among these apparently diverse methods was soon realized

(36,37), and all yield the Kondo temperature of:

$$T_K = T_F \; \exp(\; -1/N(o) \; |J| \;)$$

The order of magnitude "Kondo temperatures" for 3d elements in

several simple metal hosts are shown in Table 1, and it is clear that

T_K decreases as the impurity moves closer to the center of the

transition series in a given host.

TABLE 1

Order of Magnitude "Kondo Temperatures" for 3d Elements

in Simple Metal Hosts *

Solvent \ Solute	V	Cr	Mn	Fe	Co	Ni
Cu .	----	1.0	0.01	25	2000	>5000
Ag	----	~0.02	0.040	3(?)	----	----
Au	300	~0.01	<0.01	0.3	200	----
Zn	----	3	1.0	90	----	----
Cd	----	----	~0.02	----	----	----
Al	----	1200	530	>5000	----	----

*Values in degrees Kelvin (after Rizzuto (38)).

Nagaoka (34) suggested that below T_K the onset of spin compensation of the impurity spin is due to conduction-electron spin polarization condensing around it, such that the localized moment would be quenched. On the other hand, Bloomfield et al (39) suggested that the disappearance of the local moment with decreasing temperature was due to an increase in the spin correlation between conduction-impurity electrons. Experimentally, there is an apparent decrease of the local moment as the temperature decreases (40); therefore, only at temperatures higher compared to the Kondo temperature does the impurity moment presumably break free from the conduction-electron polarization cloud and a localized moment appear.

I-5. Local Spin Fluctuations

The fundamental validity of the s-d model relies on the assumption of a well-defined impurity spin with an infinite lifetime. The basic interaction for magnetic moment is the local particle-particle Coulomb interaction between electrons of opposite spins when on the impurity site. The Anderson Hartree-Fock approximation is incomplete since it excludes the dynamics, and it overestimates the tendency to magnetism (41). Since the temperature departs from 0K, the fluctuation in the spin density needs to be considered; therefore, we need to consider the attraction between an electron and a hole of opposite spin on the impurity site and repeated scattering between them. This mechanism is the so-called local spin fluctuation (42).

The localized spin fluctuation approach starts off with a non-magnetic (as opposed to the s-d interaction approach) virtual bound state descrip-

tion of the solute atom, and then builds in magnetism as a dynamic interaction. A conduction electron can hop on and off the impurity site where it stops for a time $\tau_\Delta \simeq h/\Delta$, i.e. one electron decay time from virtual state to continuum, where Δ is the width of single resonance. Memory of its spin, however, is kept for a longer time because of the Coulomb repulsion U between electrons of opposite spin at the impurity. This memory time is the lifetime of the spin fluctuation τ_{sf} (43)

$$\tau_{sf} = \frac{\pi \rho_d}{1 - U\rho_d}$$

where ρ_d is the density of d-state at the Fermi level. The lifetime τ_{sf} equals T_K^{-1} and is essentially temperature-independent (44). In order for a moment to exist, the condition $\tau_\Delta < \tau_{sf}$ must be satisfied.

The thermal fluctuations in the conduction electron gas should also be considered. A conduction electron will have an intrinsic spin memory time $\tau_K \simeq \hbar/k_BT$ at temperature T. The condition for a moment to exist should be such that the spin fluctuation is slower than the thermal fluctuation: $\tau_K < \tau_{sf}$, i.e. $T_K < T$. Thus, if τ_{sf} is sufficiently long, the above two conditions can be met and a static localized moment will appear.

I-6. The Relationship Between the Anderson Model and the s-d Model

The essential aspect of the Anderson model (17) is that the electrons hop between the localized "d" states and spatially extended conduction states more or less freely, depending on V_{kd}, but there is no mixing of s and d electron states.

The s-d model (7) states essentially that the s electrons are exchange scattered by a well-defined localized impurity spin whose only structure is the (2l + 1) fold spin degeneracy.

Wolff (21) has shown that the most important matrix elements of the exchange potential in the s-d model correspond to the Anderson form $Un_{d\uparrow} n_{d\downarrow}$. The Kondo effect has also been obtained following from a functional integral form of Anderson's dilute alloy model by Hamann (44a). Schrieffer and Wolff (45) have also shown that in the extremely magnetic limit, where s-d interaction is small, the Hamiltonian of Anderson model can be transformed into a form similar to that of the s-d model; and the basic interaction involved in the two approaches has been proved to be essentially the same (43).

Therefore, it is concluded that these two models are essentially equivalent in the extremely magnetic limit, i.e. $\frac{U}{\pi \Delta} \gg 1$; and it is obvious that, in the opposite limit, $U \rightarrow 0$, the system will be non-magnetic; however, when the nearly-magnetic boundary region, $\frac{U}{\pi \Delta} \approx 1$, is under consideration, the situation will be more involved. This will be discussed in the next section.

I-7. Magnetic and Non-magnetic Dilute Alloys

According to the Anderson model (17), there is a sharp transition between the magnetic and the non-magnetic state of dilute alloys, and it occurs at $\frac{U}{\pi\Delta} \simeq 1$. But, as pointed out by many authors such as Schrieffer (46), Kume (47), Narath et al (48), and Launois (49), if such a "phase transition" exists, it cannot be a sharp one, because the condensation will be localized in real space about the impurity and, therefore, a finite, probably small, number of degrees of freedom will be involved, and thermal fluctuation will broaden the transition. This Kondo magnetic problem can be linked to the one-dimensional phase transition problem (50) which apparently has no sharp phase transitions (51,52).

Doubts about the adequacy of the Hartree-Fock treatment of Anderson Hamiltonian have been raised (53), such as when the impurity is nearly magnetic the many body effects (d-d electron correlations) must be taken into account. A dynamic extension of the non-magnetic limit of the Anderson model is suggested by the local spin fluctuation theory which allows for the probability of a temporary moment occurring even when $\frac{U}{\pi\Delta} < 1$ (41).

Meanwhile, the effect of the temperature should also be taken into consideration. As pointed out by Anderson (54) and Schrieffer and Mattis (53), at sufficiently low temperature the Kondo effect may lead to the spin of the localized moment being totally compensated by the conduction electrons (34,39). Even with an infinite U, the Anderson model will lead to non-magnetic behaviour at $T < T_K$ (55). Since the magnitude of T_K may vary through several decades from alloy to alloy,

as from the mK region to well above room temperature (46) (see for

example Table 1), the dilute alloy will exhibit at low temperature

$(T < T_K)$ non-magnetic transport properties with possibly some weak

additional contribution of the spin fluctuation. As the temperature goes

up to T_K, the spin fluctuations behave classically as would a well-

defined magnetic spin, i.e. when the temperature becomes of the order

T_K, the spin fluctuations are slower than the thermal fluctuation of the

temporary moment.

Therefore, some "non-magnetic" dilute alloys, in the sense they

displayed temperature independent properties within the conventional

experimental range, may be regarded as the end product of a very

high temperature spin-correlated state arising from the Kondo effect.

Thus, the T_K, possibly varying from 10^{-3} to $10^3 K$, may be considered

to be the boundary between the magnetic and the non-magnetic behaviours

of dilute alloys.

In order to investigate this "sharp or smooth" transition between

the magnetic and the non-magnetic states of dilute alloys, it will be

most straight-forward to study some dilute alloy system, such as

AlMn alloy $(\frac{U + 4J}{\pi \Delta} \sim 0.7$ (56) to 1.5 (57)), which is somewhere in

the transition region. Since the basic assumption of the s-d model is

on one side (assuming the impurity is magnetic) and local spin fluctuation

on the other side, AlMn alloys represent a typical case of near magne-

tism where both approaches should join; therefore, a series of Al-3d

alloys has been studied experimentally through the magnetic measure-

ments. This is presented in Chapter 3.

Section II.   The Interacting Solute Atoms Alloy

II-1. Introduction

For the extremely dilute alloy, the single-impurity Kondo effect

will dominate. This has been discussed in Section I. As the impurity

concentration increases, the region in which $T_K < T_I$ (where T_K is the

Kondo temperature and T_I is the measure of average interactions

between solute atoms) will be reached where the interactions between

atoms (single atoms and/or clusters) of the impurity can no longer be

neglected. In addition, the impurity-impurity interactions may change

the properties of the alloys drastically from the Kondo-effect dominated

systems. This emphasis on the interactions between impurity atoms

with the influence of the host, just as we have pointed out in the General

Introduction section, is the interaction (C).

If the impurity concentration is extremely low, the alloy system can

be treated as a single-impurity system in which each impurity atom is

considered to be an isolated atom. The single-impurity Kondo effect,

as studied so far, is reasonably clear. If the impurity concentration is

sufficiently high, then the Kondo-like effects will be suppressed by the

impurity-impurity interactions.

When the impurity concentration is high enough, then the system

can be treated as a whole through the methods of statistical mechanics

at the thermodynamics limit by an effective-field approximation ; but,

for impurity concentrations lying in between these lower and higher

limits, the system becomes much more involved. In this case, we

have to face the traditionally complicated many body problem;

however, some efforts have been made to study the two-impurity Kondo effects and the cluster effects as a local treatment. Some concepts of the impurity interactions and treatments and some properties of the non-dilute alloys will be discussed in this section.

II-2. The Impurity Interactions

The idea that a contact, hyperfine interaction between s-state electrons and nuclear moments could lead to a polarization of the nuclear moments was proposed a long time ago (58). The actual form of this interaction was obtained by Ruderman and Kittel (24) when they investigated the nuclear moment-conduction electron interaction to the second order and interpreted the anomalous broadening of nuclear magnetic resonance (NMR) lines in metal due to the indirect coupling of nuclear spins.

The cooperative effects arising from the interaction of two d electrons on a single impurity atom under favorable circumstances may result in an isolated impurity in a metallic host forming a local moment. There will be a direct interaction between the magnetic moments on individual impurity atoms and, in an analogy with the nuclear coupling, also an indirect interaction between moments through the electron-electron interaction, in addition to the interaction between two possible local moments as nearest neighbors.

Physically, this indirect interaction between moments arises from a conduction electron scattering from one impurity, sensing the corresponding local spin, propagating with this spin information to the second impurity, and scattering from the second in a way dependent

upon its local spin. Zener (23) proposed that this was the origin of ferromagnetic coupling between atomic moments. Kasuya (25) investigated the interaction between localized d electron spins on a solute atom and conduction electrons to second order perturbation which produces a coupling between the atomic moments, particularly with respect to its effect on spin waves and electrical resistivity. Yosida (26) also employed this interaction to interpret the magnetic properties of $\underline{Cu}$Mn alloys. As a result of these developments, the indirect coupling of magnetic moments through the conduction electrons is referred to as the Ruderman-Kittel-Kasuya-Yosida (RKKY) inter-action.

Assuming the s-d exchange interaction, $V_{sd} = -J\underset{\sim}{S}\cdot\underset{\sim}{s}$ between the spin operators $\underset{\sim}{S}$ and $\underset{\sim}{s}$ for the spin moments of the impurity and the host conduction electron respectively, where $|J|$ is the effective exchange interaction constant, the RKKY interaction between the localized impurity spins is of the form:

$$V_{RKKY} = - \frac{3J^2 K_F^3}{8 E_F D} F[2K_F |\underset{\sim}{r_i} - \underset{\sim}{r_j}|] \underset{\sim}{S_i}\cdot\underset{\sim}{S_j}$$

where K_F is the Fermi momentum, E_F is the Fermi energy, D is the electron density, $F(x) = \frac{1}{x^4}(x\cos x - \sin x)$ is the Wolff function (59), and $r = |\underset{\sim}{r_i} - \underset{\sim}{r_j}|$ is the distance between impurity spin operators $\underset{\sim}{S_i}$ and $\underset{\sim}{S_j}$. From the free electron density, $D = \frac{K_F^3}{3\pi^2}$, we obtain the following equation of the RKKY interaction (60):

$$V_{RKKY} = - \frac{9\pi^2 J^2}{64 E_F K_F^3} \frac{\cos(2K_F r)}{r^3} \underset{\sim}{S_i}\cdot\underset{\sim}{S_j} \quad (K_F r \gg \pi)$$

Magnetization of a free electron gas in the neighborhood of a point

magnetic moment at the origin $r = 0$, according to the RKKY theory,

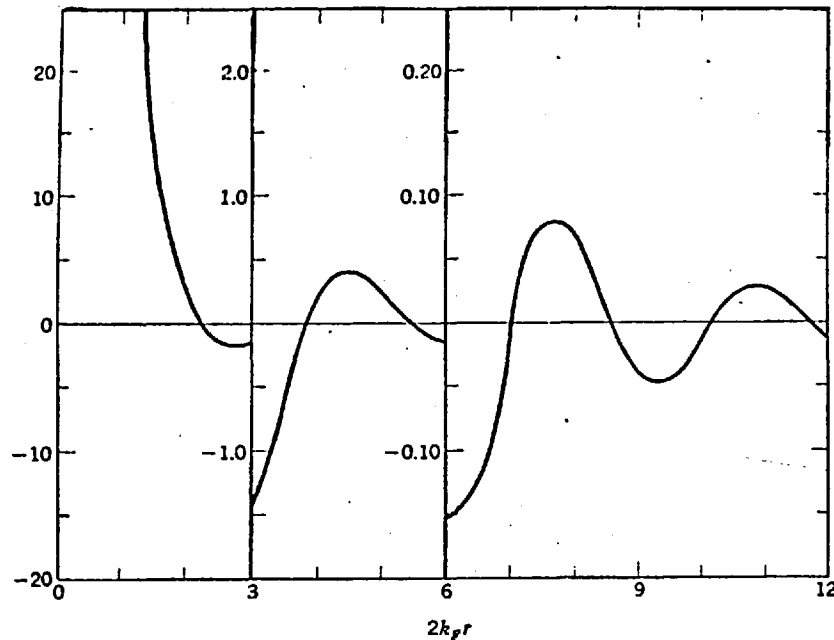will oscillate and is shown in Fig. 7.

Fig. 7 Magnetization of a free electron gas in the neighborhood of a

point magnetic moment at the origin $r = 0$ (after de Gennes (61)).

Thus, we can see that when a localized moment is introduced into a

metal, the conduction electron spins develop an oscillating polarization

in the vicinity of this moment. These spin-density oscillations have the

same form as the Friedel charge-density oscillation (12,62), as have

been shown in Section I-2, that results when an electron gas screens

out a charge impurity, and the phase shifts for the spin up and spin down

scattered conduction electrons will be different (this is the so-called

interaction between virtual bound states approach). This spin perturba-

tion with an RKKY oscillatory form has been experimentally verified by

comparing the NMR, the Mössbauer, and bulk susceptibility results, for example, on $\underline{Cu}Fe$ alloys, where no long-range negative definite part near the impurity site is found (63,64). Moreover, the distance dependence is the same as the RKKY oscillation, as confirmed by G o libersuch's (64) measuring the effect of the electronic mean free path in, for example, $\underline{CuAl}Fe$ alloys.

Since the nature of the RKKY interaction also depends on the density of conduction electrons through the Fermi momentum, theoretically Mattis (65) calculated the stability condition for ferromagnetism and antiferromagnetism to appear alternately as the number of conduction electrons increases. It should be experimentally possible to change the magnetic order continuously by alloying. Such an effect has been observed by doping the ferromagnetic semiconductor EuSe with gadolinium and lanthanum. For every Eu^{2+} ion replaced by a Gd^{3+} or La^{3+} ion, the number of conduction electrons increases by one. In addition to a large increase in the conductivity, the paramagnetic Weiss temperature changes from positive to negative, as shown in Fig. 8.
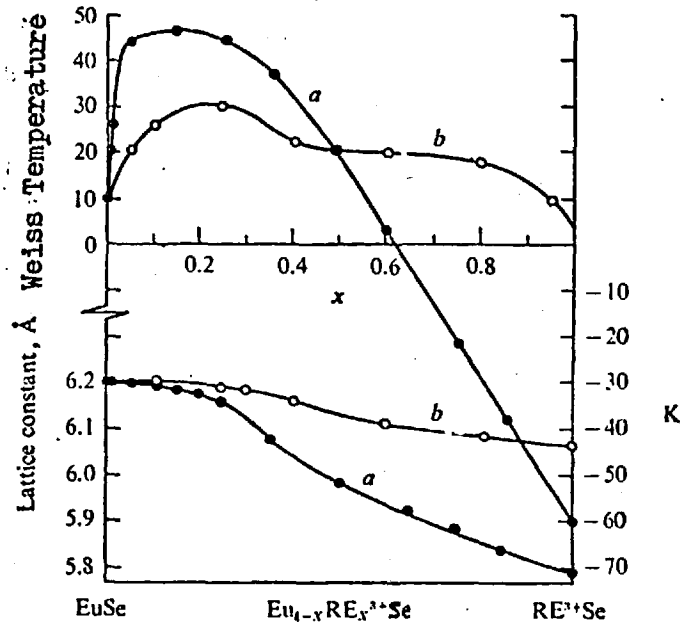
Fig. 8 Variation of the paramagnetic Weiss temperature of EuSe with

RE^{3+} substitution: (a) $Eu_{1-x}Gd_xSe$, (b) $Eu_{1-x}La_xSe$ (after

Holtzberg et al (66)).

The wavelength of the RKKY oscillation is small, even at the scale

of the interatomic distances ($2K_Fd \approx 7$ for Ag, Au, or Cu, where d

is the distance between first neighbors). The effective strength of the

RKKY interaction slowly decreases with the distance between the

impurities and, therefore, may exert a substantial influence on the

thermodynamic functions, even for small impurity concentrations; and

the RKKY interaction is expected to persist in the presence of the Kondo

effect and modify the experimental behaviours of the various Kondo

anomalies down to very dilute concentrations ($T_I < T_K$) (67).

This slowly decreasing character ($\sim 1/r^3$) of the RKKY interaction

has been experimentally verified by us on the AgMn alloys and is

presented as part of this work. The details of the experimental idea, procedures, and results will be discussed in Chapter 3.

The direct interaction between two neighboring localized moments in the transition metal and alloys was first studied by Moriya (68). By using the Anderson model (17) generalized to the case of five-fold degenerate d-orbitals, the effective exchange energy and the change of the localized moments due to the d-d covalent admixture have been calculated. The results of the effective exchange energy between two atoms with N_1 and N_2 localized electrons which are evaluated for $\dfrac{U + 4J}{\triangle} = 10$, are not very sensitive to the exact value of this latter parameter, and are presented in Fig. 9. It is explained qualitatively why Cr and Mn are antiferromagnetic while Fe, Co, and Ni are ferromagnetic. The estimated exchange energies for these 3-d metals compare fairly well with the observed values of the Curie temperatures.
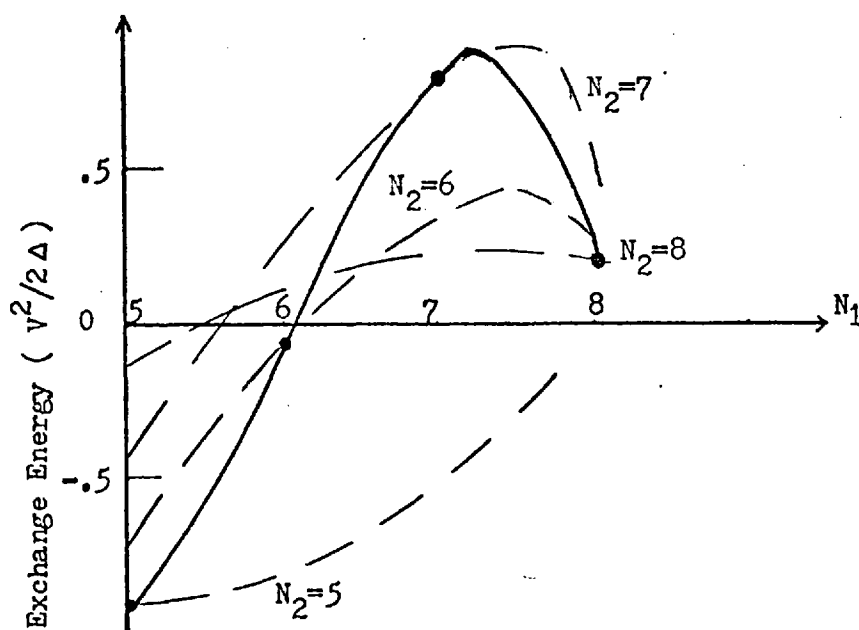

Fig. 9 Effective exchange energy between two atoms with N_1 and N_2 localized electrons for $(U + 4J)/\triangle = 10$ (after Moriya (68)).

These ferromagnetic and anti-ferromagnetic effective exchange energies between two neighboring localized moments can have decisive influence over the alloy behaviours when the impurity concentration varies. The most significant experimental results can be seen from the magnetic phase diagram of PdMn alloys (69), and this will be shown and discussed in Section II-6.

II-3. The Internal Field Treatments

The effective field theory has been of value in the study of magnetic ordering problems. The theory is based on the method of statistical mechanics. The Weiss molecular-field theory postulates the existence of an effective field acting on each of the spins. This field originates from the mutual interaction of all the spins, and its value is assumed to be proportional to the spontaneous magnetization. If the fluctuation of the effective field on a spin due to the various possible alignments of the neighboring spins is also taken into consideration (70), as a result, there exists a number of values for the effective field, each weighted by a temperature T dependent probability. As the temperature increases, the most probable value of the effective field shifts to lower values.

In an alloy where the distribution of spins on the matrix is random, the effective field has another source of fluctuation that is due to all possible distances between pairs of interacting spins. Moreover, the indirect RKKY interaction has a long-range, oscillatory nature. Thus, each impurity is surrounded by a different environment and, therefore,

experiences a different effective field.

Marshall (71) proposed the existence of a continuous probability distribution of internal field $P(H_I, T)$ acting on the solute atoms having varying magnitude and sign. In this case, the thermodynamic variables of the system can be obtained by integrating the expression for the thermodynamic variables of a single spin in a fixed internal field H_I over the distribution of all fields. Klein and Brout (72) and Klein (73) adopted Marshall's proposal, using the Ising model for the solute atom moment, and considered two particles correlation functions. They calculated the $P(H_I)$ statistically by expanding the partition function diagrammatically in a power series in solute concentration. The obtained low-temperature specific heat of dilute CuMn, CuFe, and CuCo alloys were in close agreement with the measured values.

The weakness of the above theory lies in the cutting off of the cluster expansion of the partition function at the two-spin correlation term; therefore, this procedure seems to be valid only for very dilute concentrations. In order to treat larger concentrations and carry out the analysis at finite temperatures and external magnetic field, Liu (74) suggested that the effective-field distribution satisfied a self-consistent condition which made it suitable to describe the collective effects of the spins. A symmetric distribution of effective field $P(H_I)$ about the origin is of the form shown in Fig. 10.
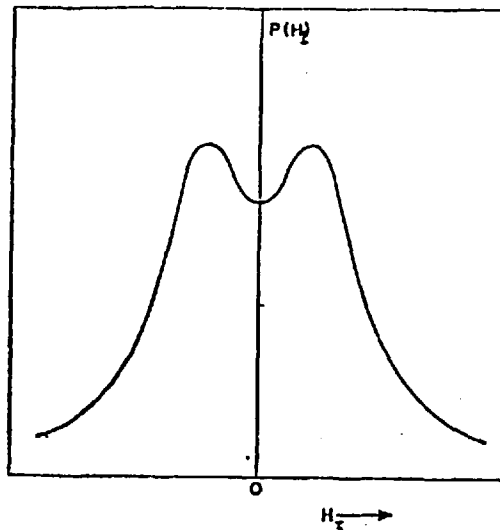
Fig. 10   The effective-field distribution   (after Liu (74)).

For simplicity, the curve is parameterized by:

$$P(H_I) = \frac{a}{(H_I - b)^2 + c^2} + \frac{a}{(H_I + b)^2 + c^2} \quad \text{for } H_I < H_c$$

$$= 0 \qquad\qquad\qquad\qquad \text{for } H_I > H_c$$

The parameters b and c determine the shape of the curve, and the value of a is the normalization constant. H_c is the cut-off field to keep the moments distribution finite.

Roughly, the curve $P(H_I)$ peaks at H = b and has a width c under the peak. Hence, b represents the most probable value and c the fluctuation of the effective field. In comparison with the Weiss theory, b depends on the temperatures according to:

$$b = b_o \, \xi$$

where b_o is proportional to the concentration and:

$$\mathcal{J} = \int_0^\infty P(H_I) B_s(\beta H_I)\, dH_I$$

where β is the inverse temperature and $B_s(X)$ is the Brillouin function. Through a series of calculations, and assuming in a very dilute alloy a random distribution and an antiferromagnetic interaction, the following predictions have been proposed: a peak in susceptibility X only appears for those alloys for which c is relatively small compared with b_0; the size of the peak is insensitive to the impurity concentration; and the position of the peak is proportional to the impurity concentration.

The validity of these predictions varies from alloy to alloy. As an illustration, the size of the peak for the AuMn (n = 1 to 2 at.% Mn) alloys (75) is much more insensitive to the impurity concentration n compared to that of the AuCr (n = 0.5 to 1 at.% Cr) alloys (75); also, the position of the peak of the PtMn (n = 2 to 12 at.% Mn) alloys (1) is linearly proportional to the impurity concentration, but that of the AuMn (n = 1 to 10 at.% Mn) alloys (76) is proportional to the 2/3 power of the impurity concentration. The actual interaction within some different alloy systems of higher impurity concentrations are, perhaps, more involved than Liu's original picture, and the behaviours can be categorized as magnetic spin glass and/or mictomagnets. These will be discussed in later sections.

Recently, Southern (77) predicted through a local stability condition for the orientation of each spin calculation that the initial susceptibility exhibits a cusp at an ordering temperature proportional to the power from 1/2 to 1 of the impurity concentration. These results agree with the wider range of experimental data.

A numerical study in a cluster approximation done by taking into account the cluster of as high as five atoms in disordered systems has been carried out by Takahashi and Shimiju (78). Calculations were performed on the density of states for vibrations in one-dimensional random lattice. It was found that the shapes of peaky structure of the density of state were changed by the short-range order, but the positions of the peaks were no so changed.

Tsay and Klein (79) investigated the system in which two-impurity Kondo effect dominates. In this case, the Hamiltonian will be the two-impurity s-d Hamiltonian with an added exchange term of the form V $(\underset{\sim}{S}_i \cdot \underset{\sim}{S}_j)$, where $\underset{\sim}{S}_i$ and $\underset{\sim}{S}_j$ are the spin operators of the two impurities. All the $\ln T$ terms arising in the single-impurity Kondo effect (7) are modified and replaced by $\ln(T^2 + V^2)^{1/2}$, where V is an energy approximately equal to the two impurity exchange interaction. This results in an effective Kondo temperature $T_K{}^E$, where $T_K{}^E = T_K [1 - (V/T_K)^2]^{1/2}$. Thus, the effective Kondo temperature decreases as the impurity-impurity interaction increases and, when V is greater than T_K, the Kondo divergence is removed by the impurity-impurity interaction.

This form of the incremental resistivity has also been obtained by using the localized spin fluctuation (lsf) model (80) modified to include both potential (81-83) and spin-flip (84) scattering. It yields the general equation $\rho(T)/n = A + B \ln[(T^2 + \theta_s^2)^{1/2}]$, where A and B are constants, and n is the impurity concentration, while θ_s measures the lsf lifetime $\tau_{sf} \approx h/k_B \theta_s$. Therefore, the temperature dependences of $\rho(T)$ as in T^2, T, $\ln T$, and $1 - (T/\theta)^2$, as have generally been observed, can be reproduced depending on the magnitude of the ratio (T/θ).

Furthermore, the sign of constant B can be obtained via (81-83):

$$B \propto \sin^2 [\pi S/(2l + 1)] \cos [\pi Z/(2l + 1)]$$

Here, S is the impurity spin, (2l + 1) accounts for the orbital degeneracy of the impurity state, and Z is the host-impurity charge difference. Hence, the sign of the temperature dependence of the incremental resistivity can be determined.

II-4. The Scaling Laws

The scaling laws (85) are applied to the magnetic alloys in which the indirect Ruderman-Kittel-Kasuya-Yosida (RKKY) interaction (24-26) dominates. The laws underline the simple correspondences which are expected between the bulk properties and the solute concentrations. These correspondences derive directly from the geometrical character-istics of the RKKY interaction (62).

The electrons' polarization around a magnetic impurity follows the form of the Ruderman-Kittel oscillation: $\cos (2K_F r)/r^3$ (24,62), where r is the distance from the impurity and K_F is the Fermi momentum. The rapid nature of this oscillation has been discussed in Section II-2. Therefore, for an alloy system whose impurity concentration is not too high (i.e. when the probability of two impurities being the nearest or next-nearest neighbors is small) this oscillation can be well-approximated by a null mean value; and, the impurity interaction will decrease merely with the cube of the distance.

Since the impurity interaction has this r^{-3} geometrical characteristic, Blandin (86) observed that any cloud of impurities that one imagines to

represent a dilute alloy of impurity concentration n may, in a liquid model, be used to represent an alloy of different impurity concentration n'. All that is necessary is to change the unit of measurement of distance, i.e. if $r \to r'$, then $n \to n'$, where $nr^3 = n'r'^3$, follows because there are the same numbers of particles in the new volume. This argument is based on the assumptions that the alloy is random, and the number of all the particles under consideration are conserved; therefore, the quantity nr^3 is "concentration-independent."

The normalized probability density distribution, $P(H_I) = \dfrac{dN}{dH_I}$, gives the probability for the value of the internal field H_I on a site being in the range dH_I around H_I, where N is the total number of impurity atoms (71,72,74). Since $P(H_I) = \dfrac{dN}{dH_I} = \dfrac{dN}{dH_I/n} \times \dfrac{1}{n}$, it implies that $n P(H_I) = F(H_I/n)$. Similarly, we can obtain:

$$n P (H_I, T, H) = F\left(\frac{H_I}{n}, \frac{T}{n}, \frac{H}{n}\right)$$

where F is a universal function independent of the impurity concentration, T is temperature, and H is the external field.

The magnetization M of the alloy can be written as:

$$M(H,T) = Nn \int P(H_I, T, H) \, \mu \, B_s \left[\frac{\mu(H_I + H)}{k_B T}\right] dH_I$$

$$= Nn \int n P(H_I, T, H) \mu B_s \left[\frac{\mu(H_I/n + H/n)}{k_B T/n}\right] d(H_I/n)$$

$$\frac{M(H_I T)}{n} = F_1\left(\frac{T}{n}, \frac{H}{n}\right)$$

where μ is the effective moment of the impurity atom, k_B is the

Boltzmann constant, and $B_S(x)$ is the Brillouin function. Similarly, the

initial susceptibility X can be written as:

$$X(T) = \lim_{H \to 0} \frac{\partial M}{\partial H}$$

$$= \lim_{H \to 0} F_2 \left(\frac{T}{n}, \frac{H}{n}\right)$$

$$= F_2 \left(\frac{T}{n}\right)$$

Both functions F_1 and F_2 are universal functions independent of the

impurity concentration.

The "reduced temperature," (T/n), and the "reduced field," (H/n),

will act as the new arguments in this "reduced diagram," and the

impurity concentration n acts as the significant scaling parameter. The

scaling laws propose that the alloy ordering temperatures are propor-

tional to the impurity concentration (62,86) which coincides with the

proposal in the internal field treatment made by Liu (74).

An experiment has been carried out on the Ag Mn alloys and is

presented in Chapter 3. The experimental results follow the scaling

laws well and, therefore, verify the geometrical characteristic, the

r^{-3} dependence, of the RKKY interaction (1).

II-5. Virial Expansion for Magnetic Impurities in Metals

The concept of the indirect Ruderman-Kittel-Kasuya-Yosida (RKKY) interaction (24-26) in alloys has been well-known for a long time. The significant characteristics of this interaction, such as the dependence on the density of conduction electrons through the Fermi momentum, the oscillation of polarization, and the slow geometrical falling off have all been discussed and verified in the previous sections.

The next stage of the research will be to find out quantitatively the effects of the RKKY interaction on the thermodynamic functions of magnetic alloys. In this area, Larkin and Khmel'nitskii (87) have used a virial expansion of the free energy in power series of the concentration of magnetic impurities to investigate these effects.

Since the RKKY interaction falls off slowly with distance and, thus, can turn out to be significant even at a low concentration of the impurities (67), after averaging over the conduction electrons, the effective Hamiltonian H of the impurities with spin operator $\underset{\sim}{S}$ and exchange integral V may be written in the form of (87):

$$H = \sum_{ij}^{N} V_{ij} \underset{\sim}{S_i} \cdot \underset{\sim}{S_j} - g \mu_B \underset{\sim}{H} \cdot \sum_{i}^{N} \underset{\sim}{S_i}$$

by taking the sum of all the impurities within the applied field $\underset{\sim}{H}$, where g is the Lande g factor, and μ_B is the Bohr magneton. The inter-action between spins at large distances is given by:

$$V(r) = V_0 \frac{\cos 2K_F r}{r^3} \qquad (K_F r \gg \pi)$$

where V_0 is the strength of the RKKY interaction, and r is the distance between spins.

This interaction will influence the thermodynamic functions, and for a limited concentration, the thermodynamic functions may be obtained by an expansion in powers of the density of impurities. This approach is based on the assumption that the distribution of the impurities in an alloy is independent of the temperature.

The free energy of N impurities is determined by:

$$F_{1,2...N} = -Nk_BT \ \ln\left\{ \exp\left[-1/T \left(\sum_{ij}^{N} V_{ij} \ \underset{\sim}{S}_i \cdot \underset{\sim}{S}_j - g\mu_B H \cdot \sum_{i}^{N} \underset{\sim}{S}_i\right)\right]\right\}$$

In order to obtain a virial expansion, the quantity f defined by the recurrence relation is introduced:

$$f_i = F_i$$

$$F_{ij...m} = \sum_k f_k + \sum_{kr} f_{kr} + ... \sum_{kr...m} f_{kr...m}$$

where the summation is carried out over different sets of the indices ij...m. The function f vanishes if the distance between any two impurities tends to be infinity. For example, $f_{ij} = F_{ij} - (F_i - F_j)$. Averaging this expression over the distribution of the impurities and going to the thermodynamic limit $N \rightarrow \infty$, an expansion of the free energy in powers of the impurity concentration n is obtained and has the following form:

$$F = -NT \left(\frac{nV_0}{T}, \frac{\mu_B H}{T}\right)$$

By differentiating up to the second order of the free energy, a temperature independent expression for the magnetization M at the $k_B T \ll \mu_B H$ limit can be obtained as:

$$M = g \mu_B \bar{S} n [1 - 2(2\bar{S} + 1) n V_o / 3g \mu_B H]$$

where $\bar{S} = (S(S + 1))^{1/2}$. However, under practical laboratory conditions (say H = 45KOe) the $k_B T \ll \mu_B H$ limit might be difficult to achieve, and the effect of temperature should be considered as well. This can be done, as Larkin and Khmel'nitskii (87) suggested, by introducing the free energy in second order:

$$F^{(2)} = -(2/3) n^2 V_o Re \; \psi \; [1/2 - (i/2\pi) \ln (1 + 2ch \frac{g \mu_B H}{k_B T}) \;]$$

where ψ is the logarithmic derivative of the Γ function. We obtained (1) the following temperature-dependent expression for the small $k_B T / \mu_B H$ case:

$$M = g \mu_B \bar{S} n \left\{ 1 - 2(2\bar{S} + 1) (n V_o / 3g \mu_B H)[1 + (1/3)(\pi k_B / g \mu_B H)^2 T^2] \right\}$$

In a weak field, the susceptibility χ may be written in the form of (87):

$$\chi^{-1} = \frac{3}{N \mu_B^2 S(S + 1)} (T + \theta)$$

and $\theta k_B C_s = V_o n$, where C_s is a spin-dependent constant of the order unity.

An experiment has been carried out on the AgMn alloys and is presented in Chapter 3. From the experimental results and the virial expansion theory, the strength V_o of the RKKY interaction and the effective $|J|$ value are therefore determined.

II-6. Magnetic Spin Glass and Mictomagnets

In the extremely dilute alloys, the impurities are mainly non-interacting, and the single-impurity Kondo effect (7) dominates. As the impurity concentration increases, the long-range, indirect interaction via the Ruderman-Kittel-Kasuya-Yosida (RKKY) mechanism (24-26) between impurities will begin to dominate. Even as the temperature is lowered in zero external field, the impurity spins "freeze out" or become "locked" in random directions with no long-range, magnetic ordering, so that the net macroscopic magnetization is zero. This freezing occurs in a certain kind of alloy at a well-defined, impurity concentration n dependent temperature T_o (n). Above this T_o, the alloy behaves as, or close to, the Curie-Weiss law. This phenomenon can be seen from the behaviours of the reciprocal of the low-field susceptibility of, say, "dilute" CuMn alloys at very low temperatures as in Fig. 11.
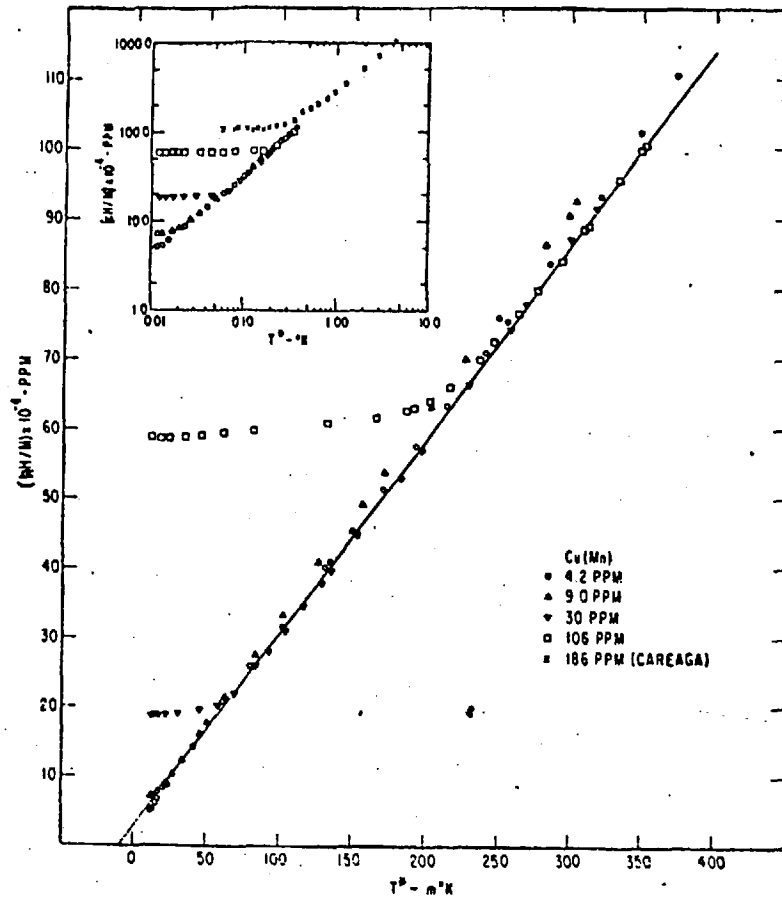
Fig. 11   The reciprocal of the low-field susceptibility of "dilute"

CuMn alloys   (after Hirschoff et al (88)).

The impurity concentration n at which the spin correlations become

dominant can be estimated either by setting the freezing temperature

equal to the Kondo temperature T_K (89), or by finding the condition

$nV_o = k_BT_K$, where V_o is the strength of the interaction, and k_B is the

Boltzmann constant (5). For this region, the thermodynamic parameters

will scale as universal functions of (T/n) and (H/n) where T is the

temperature and H is the field, and the freezing temperature is a

function of n. The scaling laws (85) have been discussed and experi-

mentally verified in the previous sections.

If the impurity concentration increases further, the scaling laws will be broken down. Because the short-range correlations are becoming more important, small groups of impurity clusters will begin to interact with each other. These non-dilute alloys, when there is a random freezing at a distinct temperature of impurity moments, give rise to a sharp peak in the low field susceptibility and a sudden splitting of the Mössbauer spectrum, along with remanence, irreversibility, and relaxation. There are currently two descriptive terms being used for the above non-dilute alloy systems: magnetic spin glass and mictomagnets.

The term magnetic spin glass was first suggested by Coles in 1970 (90). Magnetic spin glass refers mainly to the lower concentration-region where the long range, indirect RKKY interaction is mainly responsible for the cooperative freezing of the spins. The term mictomagnetism was suggested by Beck (91) and Kouvel at about the same time. Micto-magnetism is more appropriate in describing the magnetic clusters which form in the spin matrix at higher concentration due to nearest or next-nearest local exchange, or when there is a tendency towards short-range atomic ordering.

In order to study the magnetic spin glass/mictomagnetic systems, it is natural to start with the less complicated alloys of simple host materials with no partly filled d or f shells and with a broad energy band. The alloys are required to have both the properties of "good moment" and "random impurities"; therefore, the alloys should have a low Kondo temperature and favorable solubility. There are several systems which meet these requirements, such as AuCr, AuMn, AuFe, AgMn, and CuMn alloys.

The low field susceptibility (92) and the electrical resistivity (76)

exhibit very similar properties for these alloy systems. The deviation

from randomness is reflected in the low field susceptibility by the

sharp peaks at temperature T_{max} changing into broad maxima by

increasing either the impurity concentrations (75,93) or the applied

fields (94). These changes with concentrations or with fields are
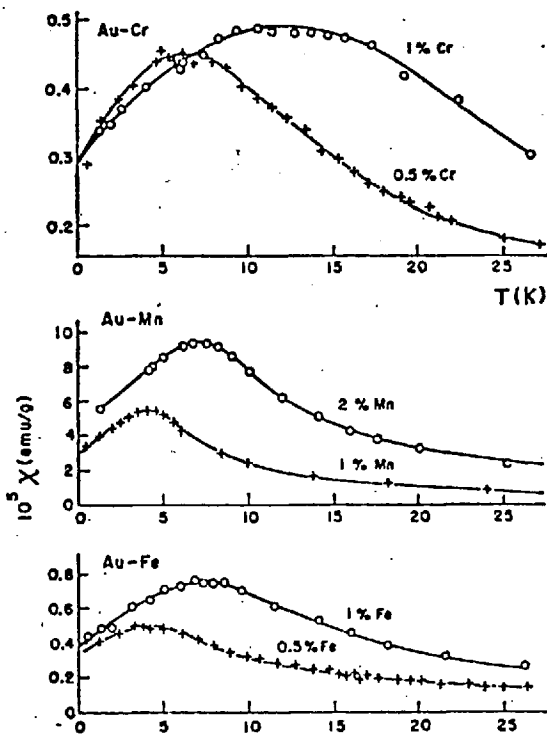
illustrated in Fig. 12 and in Fig. 13, respectively.

Fig. 12 Magnetic susceptibility

versus the temperature of

several alloys of different

impurity concentrations

(after Lutes and Schmit

(75)).
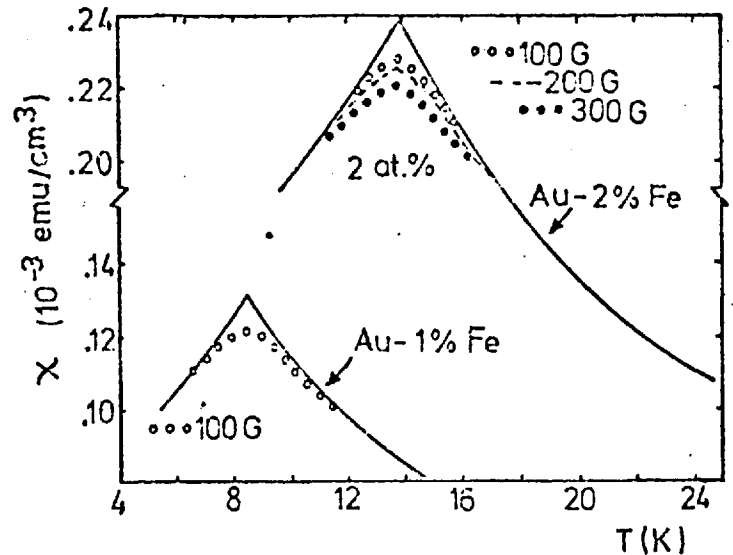
Fig. 13 Magnetic susceptibility

versus temperature with

increasing external field

(after Cannella and

Mydosh (94)).

When the impurity concentrations increase further, the phenomena

of the long range magnetic ordering of alloys can be seen, say for AuFe

alloys, to be ferromagnetic. The dramatic change of the low field

susceptibility behaviours with concentrations of AuFe alloys is shown

in Fig. 14, and the dependences of the spontaneous magnetizations with

concentrations and temperatures of AuFe alloys is shown in Fig. 15
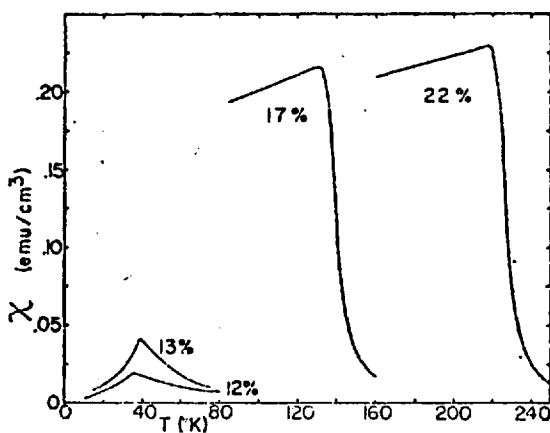
as a good comparison.

Fig. 14 Magnetic susceptibility

versus the temperature of

several non-dilute AuFe

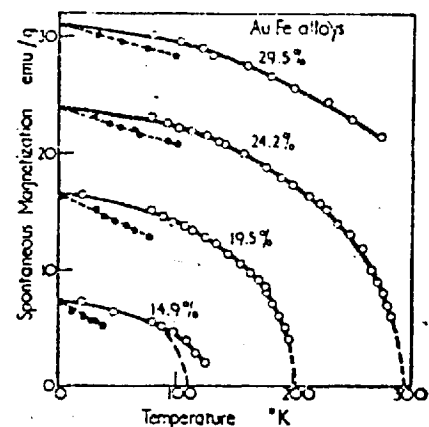alloys (after Cannella et al

(95)).

Fig. 15 Dependence of spontaneous

magnetization on the

temperature of several

non-dilute AuFe alloys

(after Crangle and Scott

(96)).

For alloys of binary combinations of transition metals, the band

structures are expected to have close widths between impurity and host,

and the specific exchange character of impurity site effects should

manifest itself more clearly. These alloys can be classified into simple

and enhanced transition hosts. In simple transition hosts where there

is no evidence for significant exchange enhancement, alloys of such

simple transition hosts such as RhFe (97,98) and RhCo (99), for

example, require a sufficiently large concentration of magnetic impurity

before magnetic spin glass behaviour manifests itself. Below this

impurity concentration, the paramagnetic spin fluctuations are present

without any evidence of a region where ferromagnetism is stabilized.

The Rh-3d alloy system has been studied extensively.

In the enhanced transition host Pd, for example, where the low

field susceptibility of alloys is significantly different from what has been

estimated from the electronic specific heat, NMR and Mössbauer

techniques, sometimes a strong tendency towards "giant moment"

exists even at low impurity concentrations (100). This effect can be

clearly seen from the giant moment of the Fe atom in PdFe alloys as

has already been shown in Fig. 5.

The magnitude of the moment localized on the Fe impurity atom has

been studied with the electronic specific heat (101), NMR (102), and

Mössbauer techniques (103) and resulted in a small moment of about

3 μ_B. The implication of this is clear---the giant moment arises

from a long-range polarization of the host metal. The range of this

polarization has been studied directly in the neutron diffraction experi-

ments on Fe in Pd (104). The results indicate a roughly exponential

fall-off with sizeable spin polarization on 200Pd atoms in the neighbor-

hood of the Fe impurity.

In the PdMn alloy system, for example, the behaviours are

different. Although PdMn for concentrations up to about 3 at.% Mn

resembles PdFe (but with Curie temperatures almost a factor of 10

smaller), there is a keen competition between this long range order

and the mixed antiferromagnetic correlations between nearest neighbors
(68) of the random alloys; therefore, the magnetic spin glass state may
overcome the ferromagnetism at certain concentrations. This character-
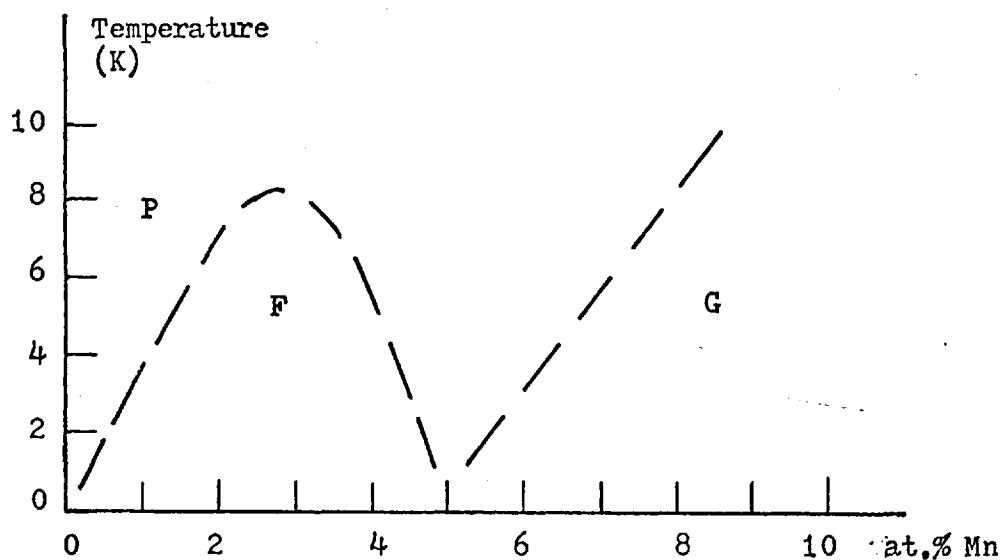istic property can be seen in the magnetic phase diagram of PdMn alloy
as in Fig. 16.

Fig. 16   Magnetic phase diagram of PdMn alloy system, F = ferromag-
netism,   P = paramagnetism, and G = magnetic spin glass
(after Coles (69)).

A brief summary of some alloy systems with simple metal, simple
transition metal, and enhanced transition metal hosts is presented in
Table 2.

TABLE 2

A brief summary of some alloy systems with simple metal, simple transition metal, and enhanced transition metal hosts.

$T_K(K)$	10^{-3}	10^0	10^3
Solute Type → / Host Type ↓	Good moments	Kondo moments	No moments
Simple metal	AuGd CuMn ZnMn AuMn AuFe	CuFe	AuCo AlMn AlFe CuNi
Simple transition metal	MoFe	MoCo RhFe	NbFe TiFe VFe RhCo RhNi
Enhanced transition metal	PdFe	PtFe PtCo PdCo	PtNi PdNi

The transition metal host Pt, in the respect of the magnitude of the exchange enhancement, can be classified as intermediate between, for example, Rh and Pd. A study on the PtMn and PtCr alloy systems has been carried out and is presented in Chapter 4.

II-7.   The Magnetic Environmental Effects

When 3d transition metal is dissolved as the impurity in a 4d and/or 5d transition metal host to form disordered alloys, the magnetic properties of such alloys provide a wide variety of characteristics.

For the dilute alloys, because of the relatively small number of parameters involved, a model could almost be deduced from the experimental results; however, for the more concentrated alloys, the number of parameters is much larger, and the behaviours are much more involved. In the present state of experiments, a model must be chosen a priori. The magnetic environmental effect in alloys provides a brief description of the causes of these wide behaviours.

The investigation of this magnetic environment effect in alloys has been approached through two models of opposing directions: the local environmental effect and the cooperative effect.

The model of the local environmental effect on magnetic moment formation was first considered by Jaccarino and Walker (106). The alloy is assumed to be random and perfectly disordered, and a well-defined magnetic moment is assigned to each solute atom with a certain number of atoms within a critical range, say the nearest neighbor (106) and the second neighbor (107,108), of one of the constituents of the matrix host. The magnetization process may be essentially a discontinuous one, the moment being either zero or some well-defined value on a solute atom (in analogy to the Chinese abacus model approach).

This local environmental model has successfully interpreted the occurrence of magnetism on Fe atoms in the Nb-MoFe alloys and Co

atoms in the Rh-PdCo alloys (106). In Nb-MoFe alloys the results can be interpreted by assuming the moment of Fe atoms is at its well-defined value when surrounded by 7 Mo atoms and is zero otherwise. In Rh-PdCo alloys, the situation is a little more involved. As the compositions of the host vary, the increased polarization of the matrix with increasing Pd concentration will increase the effective moment per Co atom compared to the simple model. This model has also been experimentally verified by Geballe et al (109), through the Fe behaving magnetically in a similar way, and the analysis yields the same values for the effective moment and the Weiss temperature in the alloys of $Ir_{0.9}Pt_{0.1}Fe$ (1 at.% Fe), $Os_{0.1}Ir_{0.8}Pt_{0.1}Fe$ (1 at.% Fe) and $Os_{0.05}Ir_{0.85}Pt_{0.1}Fe$ (1 at.% Fe). The constancy of the observed behaviour of the Fe atom in these alloys can be attributed to the fact that they have about one nearest Pt neighbor, regardless of whether Os is present.

On the other hand, Garland and Gonis (110) have suggested another model with a gradual variation in the magnitude of the moment with the size of a cluster above some critical value due to the possibility of the importance of the cooperative effect.

The results of neutron scattering experiments on alloys of Pd-Fe (104) and on Ni-Cu (111), for example, show an inhomogenous distribution of atomic moments. The idea of giant moments can also be verified by other approaches, such as by comparing the difference between the local and bulk properties. The measurements of the existence of such giant moments suggest that magnetic atoms are in clouds of host spins within which they are strongly coupled. These

clouds are more or less independent in the paramagnetic range and give rise to superparamagnetism.

By accepting this giant moments dominant idea, the magnetic ordering temperature T_0 should be proportional to the impurity concentration n. The prediction agrees with the PtMn alloys (1), for example, but alloys, say, where T_0 varies as n^2 or n^3, suggesting that the magnetic entities participating in the magnetic order are magnetic pairs or triplets of strongly coupled magnetic moments. Hence, it is clear that these two models both have their own validity and, perhaps, can be adopted simultaneously but with different weights.

In comparing the different behaviours of 3d transition metal impurities in Pd or Pt host, the main reason there is such a wide variety of characteristics possible is the wide difference of the exchange enhancement factor D. This Stoner factor D is defined as $X = D X_p$, where X is the enhanced magnetic susceptibility, and X_p is the paramagnetic spin susceptibility, $\mu_B^2 n(E_F)$ from d and s bands, where μ_B is the Bohr magneton and $n(E_F)$ is the electron density at the Fermi level.

The enhancement factors include the effects from the electron-phonon interaction and from spin fluctuations. The enhancement factor from the electron-phonon interaction can be obtained by the equation $D_{sp} = \dfrac{\gamma_{exp}}{\gamma_{band}}$, where the γ_{exp} is the coefficient of the linear term of the low temperature specific heat from the experimental results, and the γ_{band} is that from the one-electron theory with the rigid band approximation. The values of γ_{exp}, γ_{band}, and D_{sp} of some interested transitional metals are listed in Table 3.

TABLE 3

The electronic specific-heat coefficients of Ir, Rh, Pt, and Pd

	Ir	Rh	Pt	Pd
Experimental γ (mJ/mole K^2)	3.27	4.65 $\pm$ 0.02	6.56 $\pm$ 0.03	9.42 $\pm$ 0.02
Theoretical γ (mJ/mole K^2)	2.39	3.24	4.02	5.67
Enhancement factor D_{sp}	1.37	1.44	1.63	1.66

(after Anderson (112)).

The magnetic susceptibility and the electronic specific heat versus the valance electron density of Pd-Pt, Rh-Pd, Ir-Pt, Ir-Pd, and Ir-Rh alloys at 20K are plotted in Fig. 17.
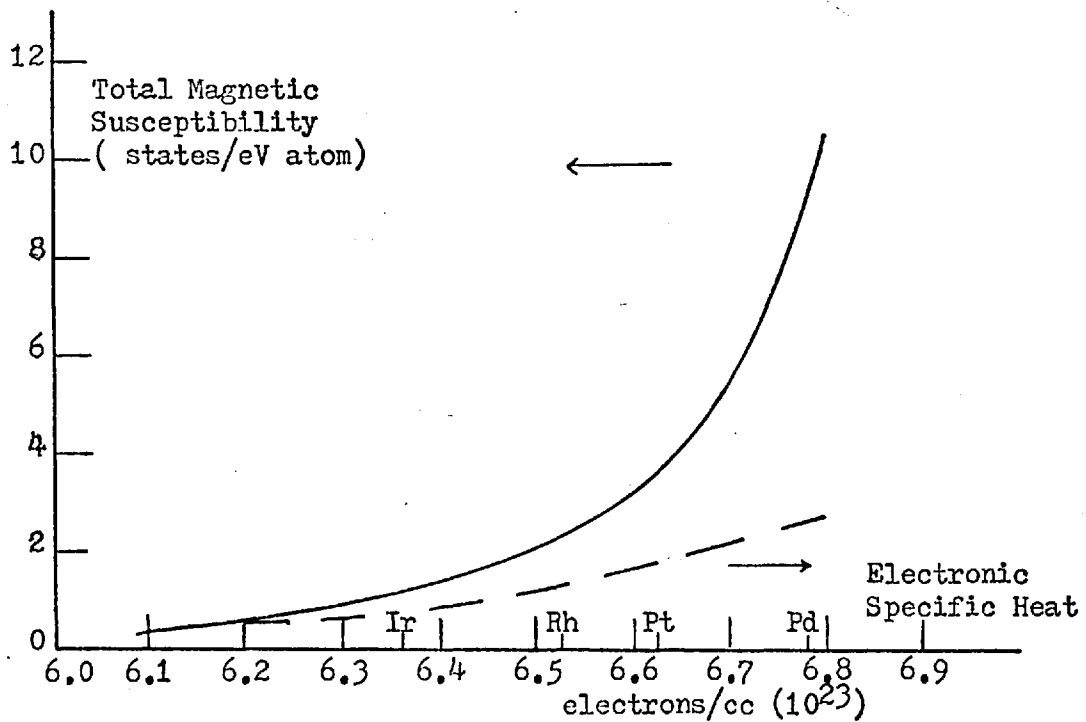
Fig. 17   Magnetic susceptibility and electronic specific heat versus

valance electron density of some binary transition alloys

(after Andres and Jensen (113)).

The enhancement factors D_{sp} increase in the same order as does

the density of states, and this increase is fairly close to Ir and Rh;

but, the increase is too small compared with the increase of the

magnetic susceptibility of Pt and Pd. The giant susceptibility values

of Pt and Pd are far beyond what the D_{sp} effect can reach; therefore,

the effect of the enhancement factor from the effect of spin fluctuation

is the main cause for Pt and Pd alloys.

In addition to the paramagnetic spin susceptibility X_p from d and s

bands, the susceptibility of a transition metal includes orbital para-

magnetism, Landau diamagnetism, and core diamagnetism. For Pt,

it has been estimated that the observed susceptibility is, in fact, equal

to the d-spin susceptibility because the other terms tend to cancel (114).

For Pd, the exchange enhancement of the d-spin susceptibility is so large that the latter terms overshadow all other contributions (115); therefore, we can use the Landau theory (116) which predicts that the Coulomb interactions between the electrons will enhance the spin susceptibility X_p through the exchange interaction:

$$X = DX_p = \frac{1}{1 - n(E_F)U} \, \mu_B^2 \, n(E_F)$$

where $n(E_F)$ is the electron density at the Fermi level, and U is a parameter associated with an electron-electron interaction potential. From the experimental values of the low temperature and low field susceptibility of 1.08×10^{-6} emu/gm and 6.9×10^{-6} emu/gm for Pt and Pd (117), respectively, the enhancement factors D over the d-spin susceptibility have been estimated to be 3.8 and 9.4 respectively (112,163).

For these large exchange enhancements of Pt and Pd, we can reach the interpretation that when a transition element , Fe for instance, is dissolved in a matrix of Pt or Pd, the long range magnetic coupling results from the overlapping of strong spin polarization of the matrix, which aligns itself in the direction of and centered on the magnetic moment of the solute atoms. The Curie temperature rises rapidly with solute content, and only at very low Fe concentration in Pt (82) and Pd (118) is there evidence for the usual magnetic spin glass phase of good moment system, like CuMn and AuFe.

In the PdMn alloy system, for example, the behaviours are different. PdMn for concentrations up to about 3 at.% Mn resembles PdFe (but with Curie temperatures almost a factor of 10 smaller); at concentrations above 5 at.% Mn, however, the ferromagnetism disappears and an

enfeebled version of the CuMn magnetic spin glass appears. This

behaviour has been shown clearly in the magnetic phase diagram of the

PdMn alloy system   as in Fig. 16. This difference between Fe and Mn

is due to a difference in sign of the nearest neighbor Fe-Fe (ferromag-

netic) and Mn-Mn (antiferromagnetic) interactions (68), which become

important as the impurity concentration increases (69).

The PtMn alloys, on the other hand, show a magnetic spin glass

phase behaviour with impurity concentrations n ~ 1 at.% Mn and no

observation of ferromagnetic phase at low concentrations (1). The

different behaviours between PtMn and PdMn must be due to the

difference of the exchange enhancements of the host Pd and Pt. In the

"dilute" PdMn alloys, although the Mn atoms are rather further apart

from each other, the long range magnetic coupling which results from

strong spin polarization clouds centered at Mn atoms overlap and cause

ferromagnetism. But for the "dilute" PtMn alloys, the less strong

spin polarization clouds centered at Mn atoms are not overlapping yet

and cause only superparamagnetism. As the Mn concentration

increases, the nearest neighbor Mn antiferromagnetic interaction

becomes important. There is a keen competition between this anti-

ferromagnetic interaction and long range ordering, and a magnetic

spin glass phase appears.

The striking difference between the low concentration of Mn

impurity in Pt and Pd hosts has been thus well interpreted (1). But,

what will happen if we had a small amount of Mn as an impurity into

the $Pd_{1-x}Pt_x$ binary matrix host? For a low concentration of Mn

impurity, say 3 at.% Mn, in the $\underline{Pd_{1-x}Pt_x}$ binary host at low temperatures, on the one hand, $\underline{Pt}Mn$ (x = 1) is of magnetic spin class state and, on the other hand, $\underline{Pd}Mn$ (x = 0) is of ferromagnetic state. Where and how will these two states meet each other? To determine this, a study on the $\underline{Pd_{1-x}Pt_x}Mn$ alloy system has been carried out and is presented in Chapter 5.

CHAPTER 2 EXPERIMENTAL APPARATUS AND PROCEDURES

Section I. Preparation of Samples

The alloys which have been studied in this work include:

(1) an $\underline{Ag}Mn$ alloy system with respective nominal impurity concen-
trations n of 630, 1000, and 1370 ppm Mn,

(2) an $\underline{Al}$-3d alloy system with n of 700 and 3100 ppm Mn, 4000 ppm
Cr, and 600 ppm V,

(3) a $\underline{Pt}Mn$ alloy system with n of 0.09, 2, 3, 5.4, 8, 11, and 12
at.% Mn,

(4) a $\underline{Pt}Cr$ alloy system with n of 7, 10, 14.1, and 17 at.% Cr and,

(5) a $\underline{Pd_{1-x}Pt_x}Mn$ binary matrix alloy system with a series of
nominal combinations of x = 0.02, 0.05, 0.15, 0.25, 0.35, 0.50, 0.75,
and 1.00 binary matrix with 3 at.% Mn, a $\underline{Pd_{.75}Pt_{.25}}Mn$ (4 at.% Mn)
alloy and a $\underline{Pd_{.98}Pt_{.02}}Mn$ (1.5 at.% Mn) alloy.

All the alloys which were studied belong to the FCC structure.
Except for the samples of $\underline{Al}$-3d alloy system which were obtained from
Gruner (119) (Hungarian Academy of Sciences), all other samples were
made in the Metal Physics Laboratory, Imperial College of Science and
Technology. The starting materials were 99.99% pure Pt, and 99.999%
"Specpure" Pd, all from Johnson Matthey Ltd., and 99.99% pure Mn
and 99.99% pure Cr from Koch-Light Labs. Ltd.

The samples of the $\underline{Ag}Mn$ alloy system were made by diluting an
$\underline{Ag}Mn$ (5.43 at.% Mn) master alloy in an arc furnace, within which
a circular cavity on a water cooled copper hearth was filled with two-
thirds atmosphere argon. The alloys were melted, turned over, and

remelted several times and then formed into short cylinders of about

3mm diameter. All samples were cleaned by a solution containing

equal amounts of 25% NH_4OH and 20 vols. H_2O_2.

The samples of A1-3d alloy system were obtained from outside (119)

and were in the form of cylinders of about 3mm diameter and 1.5cm

long. All samples were cleaned by a solution of 30% NHO_3 and homo-

genized at 600°C for one hour, then quenched in cold water before

measuring. Since the samples were made outside, the impurity con-

centrations of the AlMn alloys were checked for reference. The com-

position of the alloys was monitored by measuring the residual resistance

ratio. A typical apparatus for residual resistance ratio measurement

has been constructed according to the following Fig. 18:
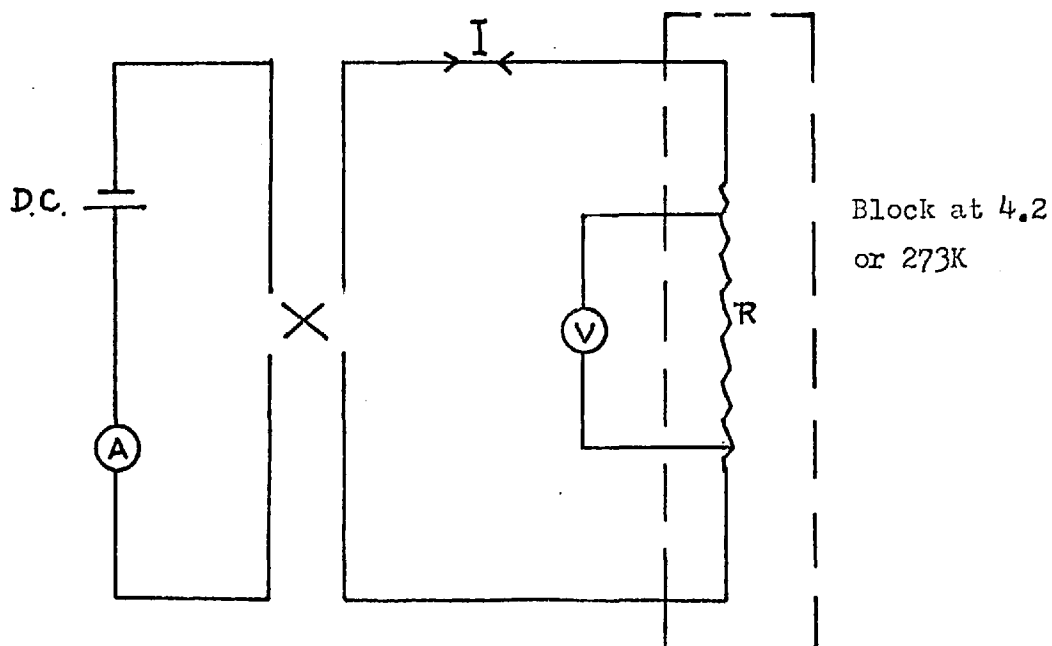
Fig. 18 The schematic diagram of the resistivity ratio measuring

apparatus (1,120).

The concentrations of the AlMn alloys have been determined to be 3110 and 705 ppm Mn, very close to the given values of 3100 and 700 ppm Mn. It is, thus, suggested that the given values of the impurity concentrations of the samples of the Al-3d alloys are reliable.

The solubilities when putting Mn and Cr in Pt to form disordered alloys are about 17 and 19 at.% respectively (121,122); therefore, no special technique is needed to make the samples of the PtMn, PtCr, and $Pd_{1-x}Pt_xMn$ alloy systems being studied. All samples were made similarly to the AgMn alloys, except without a previous master alloy making stage. The samples were short cylinders and were formed either by the casting method or by stretching through iron-free tools. All alloys were cleaned by an aqua regia solution and homogenized in a vacuum at $1000^{\circ}C$ for about five hours, then quenched in cold water before measuring.

Section II. Apparatus and Procedures of Magnetic Measurements

The magnetic measurements of all the samples presented in this work were taken by a force (Faraday) method and by using an apparatus built by Bell (123). The main features of this apparatus are: (1) a stainless steel cryostat with an insert dewar to keep the desired temperatures, (2) a superconducting main field solenoid with separate superconducting gradient field coils to supply the main field and the gradient field, (3) a suspension and a suspension tube in the insert dewar to position the sample, and (4) a balance to measure the magnetic force on the sample. These features, as shown in the schematic diagram Fig. 19, and the experimental procedures will be discussed in detail in the following sections.

II- 1. The Cryostat

The main dewar, with the insert dewar and the solenoid in position, is shown in Fig. 19. The liquid nitrogen jacket and liquid helium vessels (main bath) are of integral construction and share a common vacuum interspace with a pressure of about 2×10^{-6} torr and a 77K radiation shield fixed to the lower rim of the nitrogen jacket. This cryostat is supplied by B.O.C. At the bottom of the main bath, a dished circular 0.01" thick copper sheet is placed. On the copper sheet a main bath heater consisting of six 6-watt resistors, a liquid nitrogen detector consisting of an OA-95 point contact diode and a copper-constantan thermocouple with a reference junction in liquid nitrogen outside the dewar is attached.

BALANCE

BALANCE PLATFORM

SUPPORT FRAME

OVER PRESSURE SAFETY VALVE

TOP PLATE

RADIATION SHIELD

NITROGEN JACKET

HELIUM LEVER DETECTOR

CURRENT LEAD GUIDES

NEEDLE VALVE

HELIUM PICK-UP TUBE

INSERT DEWAR

COPPER HEAT EXCHANGER

MAIN BATH HEATER

PUMP-DOWN BOSS

NITROGEN LEVEL DETECTOR

INTERSPACE

RADIATION PLATE
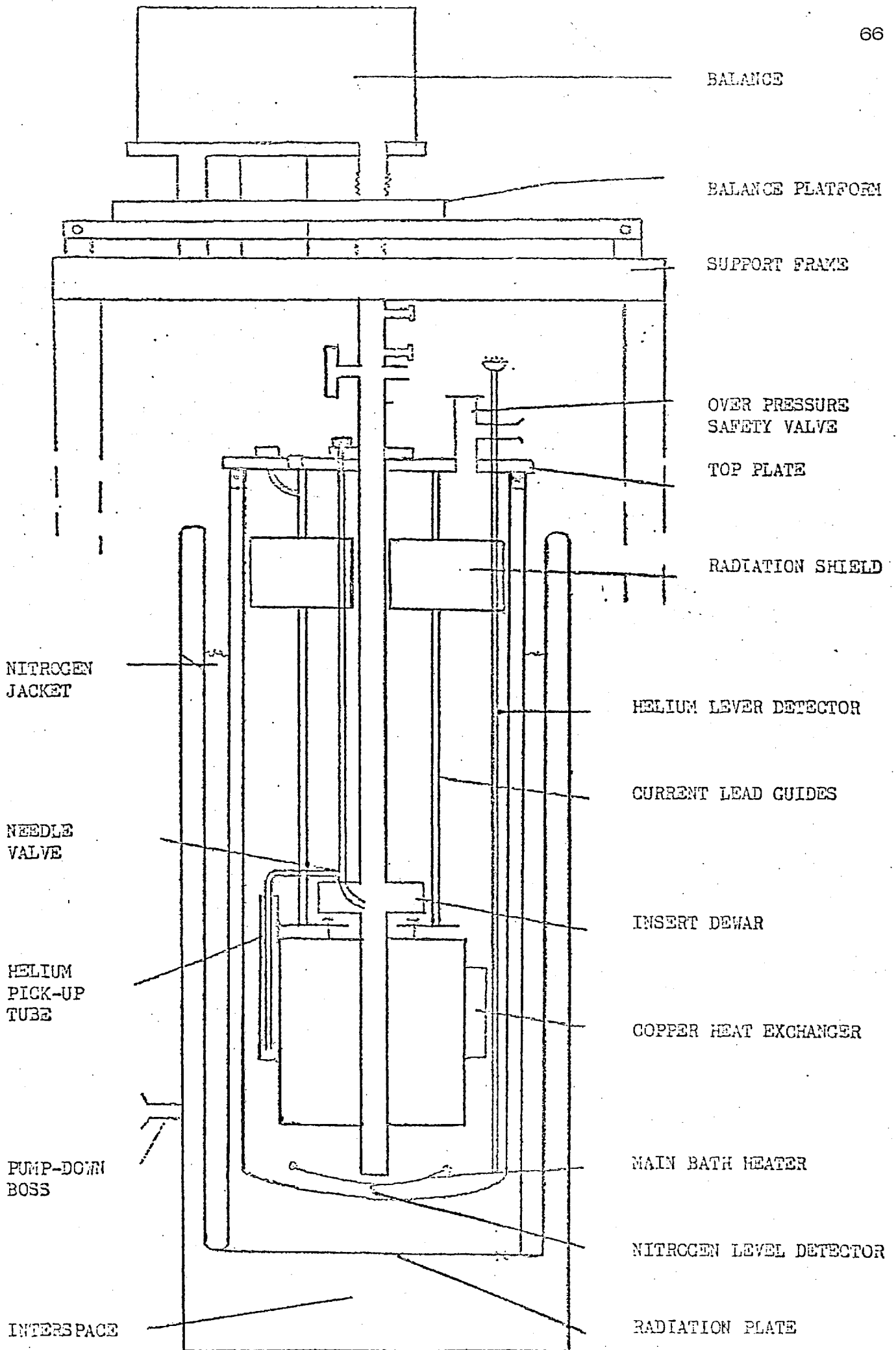
Fig. 19 The schematic diagram of the magnetic measuring apparatus (after Bell(123

The level of the liquid helium in the main bath can be detected by a liquid helium detector which is composed of a set of nine vertically-located Allen Bradley carbon resistors. The boil off rate of the liquid helium depends on the current (0 to 100 Amp) passing through the solenoid varying from 3 to 30 l/min of helium vapour.

II-2. The Superconducting Solenoid

The superconducting solenoid is supplied by B.O.C. and consists of two independent windings, main field and gradient field. Each are wound using a multifilamentary superconductor which contains 61 filaments of Nb-Ti (50 at.% Ti) superconducting alloy.

The main field winding has an inductance of 0.7 Henries and comprises a main section of 5984 turns in series with two correction coils, each of 414 turns. The field has a rating of 523 Oe/Amp, and the quench field is about 50KOe. At the center, the main field is fairly uniform. For instance, in the field of 45KOe the variation is only about 1 in 10^4 for 2 cm along the direction $\underline{k}$ of the suspension (123). The main field winding may be operated in the persistent current mode controlled by a heat switch to reduce the liquid helium boil off rate. A field decay of one part in 10^5 per sec was observed for fields of 30KOe, being worse at higher fields. The current is supplied by a B.O.C. PS100A supply. The DC current is stabilized to better than one in 10^3 over one hour, and the field is a linear function of the current to better than 0.1%. A pair of leads connects the shunt of the supply and a DANA D.V.M.. This will give a current supply reading to 5 significant positions. In

the event of a magnetic quench, a voltage trip circuit automatically

switches off the supply.

The gradient field winding consists of an anti-Helmholtz pair, each

composed of 743 turns and producing a field of the form $GZ\underset{\sim}{k}$, where

$Z = 0$ is the center of symmetry for the main field. The magnetic

field gradient G is linear to within 0.3% over the 20mm diameter sphere

centered at $Z = 0$ and is produced at the rate of 11.87 (± 0.2%) Oe/cm

per Amp. The critical current (84 Amps) corresponds to a maximum

attainable field gradient of about 1 KOe/cm. The discharge rate is

limited to a 1 volt constraint imposed by a thyristor connected in

parallel with the winding. The uniformity of the gradient field along $\underset{\sim}{k}$

has been checked by making a Hall probe vertically in a constant-

current gradient field only. The linearity is shown clearly in Fig. 20.

A current supply capable of 20 Amp outputis used; the drift in the

current is 2 parts in 10^3 over a period of 10 minus. An electronic

ramp generator has been constructed to drive the power supply (1),

and it will be discussed in Section IV.

Outside the superconducting solenoid, a copper matrix is attached

in order to provide better thermal contact between the superconducting

solenoid and the liquid helium.
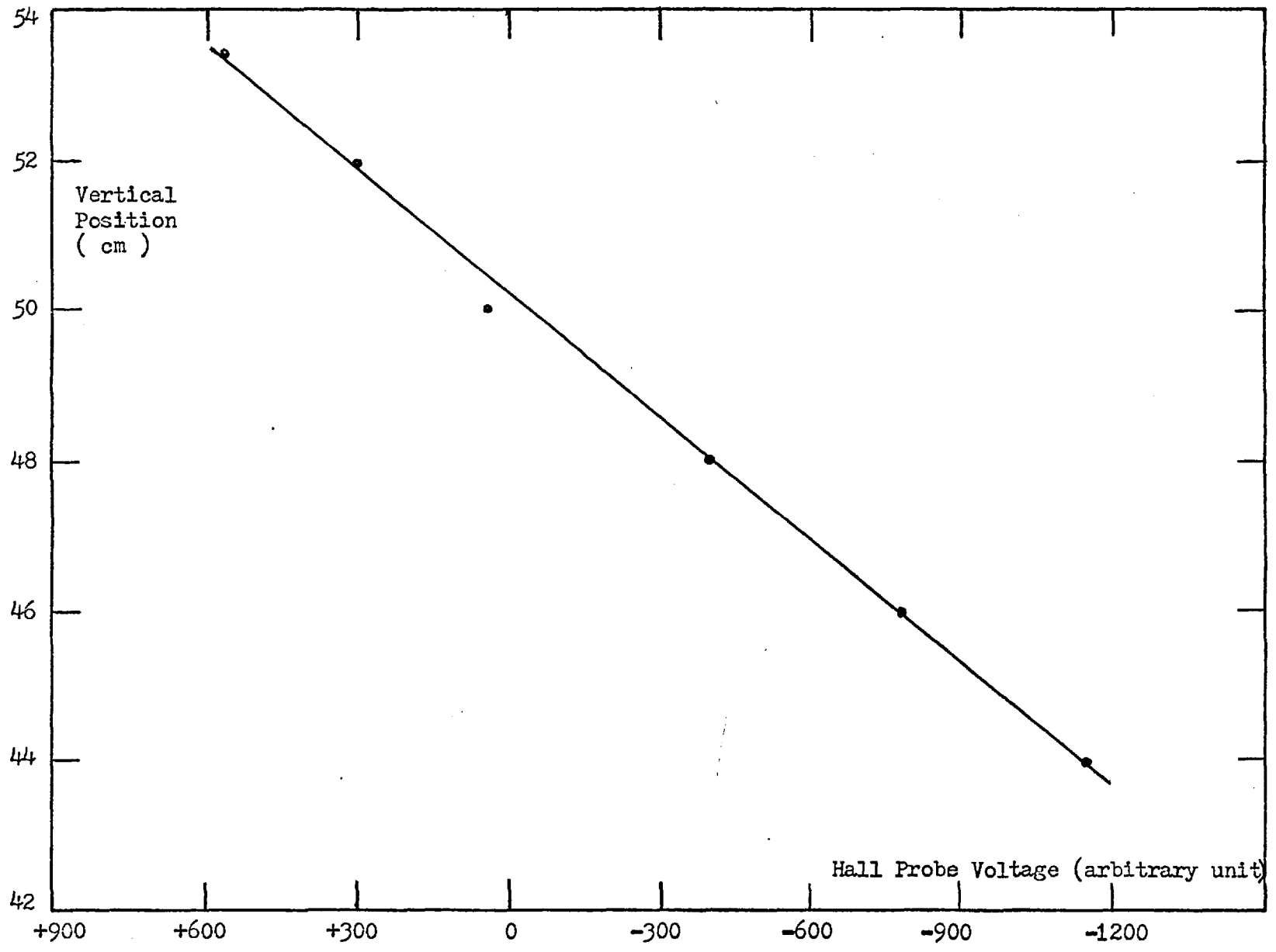
Fig. 20 Gradient Field versus Vertical Position

II-3. The Insert Dewar and Suspension

The insert dewar is a standard method for providing a thermally

isolated region in which the experiment may be performed within the

bore of an operational superconducting solenoid. In this apparatus,

sitting within the insert dewar, the sample chamber is made of brass

and covered with a thin copper foil, and the stainless steel suspension

tube is housed in it. A capillary of about 1mm diameter bridges the

interspace between the insert dewar and the main bath; therefore, the

liquid helium can be syphoned from the main bath to the insert dewar,

which can be controlled externally. The level of the liquid helium in the

insert dewar can be detected by a liquid helium detector which is similarly

constructed as the one in the main bath except it consists of only five

carbon resistors.

On the sample chamber there are several attachments: (1) an

AuFe (0.03 at.% Fe) versus chromel thermocouple with a reference

junction in the bottom liquid helium, (2) an Allen Bradley carbon resis-

tor with 110 Ω resistance at 300K, (3) a copper-constantan thermo-

couple with a reference junction in outside liquid nitrogen and, (4) a

sample chamber heater consisting of a length of 37 swg enamel-covered

copper wire.

Temperatures below 4.2K are achieved and stabilized fairly well

by using a rubber diaphragm manostat to pump the liquid helium in the

insert dewar, and the sample chamber now is emerged in the liquid

helium. Temperatures are derived from the helium vapour pressure of

reference to the standard table or from the resistance of the carbon

resistor. Temperatures above 4.2K are achieved and stabilized to within $\pm$ 0.1K for the time period of taking a data point by passing a controlled amount of current through the sample chamber heater. At this time, the sample chamber will be out of the liquid helium. Temperatures are derived from the reading of the AuFe versus chromel thermocouple or from the resistance of the carbon resistor from 4.2 to 25K and, at higher temperatures, from the reading of the copper-constantan thermocouple.

The effects of the magnetic field on the thermometry have been discussed by a number of authors (124-126). We did not make any further systematic investigation on the effects. A significant effect on thermometry might happen only when the magnetic field is sufficiently high. This high field is only used when a magnetic isotherm is being taken; meanwhile, the temperature is stable enough, and any minor changes (less than one percent) on thermometry will not affect the confidence in the isothermal stability. On the other hand, when a low field susceptibility is taken, although the temperature is not as stable as when taking the magnetic isotherms, the magnetic field is low, and any effect on the thermometry by this low magnetic field should be very small. This judgement has been verified by the good Curie-Weiss law fit of some Kondo alloys.

At the middle of the insert dewar, the suspension tube assembly, comprised of two concentric stainless steel tubes, hangs vertically. The inner tube has a 0.75" diameter at the upper portion and 0.5" diameter at the lower portion. The upper end forms the lower section of the demountable joint and is, thus, coupled to the balance platform.

The inner tube has been taken out and cleaned before the start of each run. The bottom of the inner tube is made of a piece of Lectrokit circuit board and a small transverse cryogenic Hall probe (Seimens THY17, B706) is glued on by GE 7031. During the run, the samples can be exchanged without warming up the insert dewar. During the operation of changing samples, pure helium gas flows down from the top of the cylindrical gap between the outer and inner suspension tubes, through the holes in the pegboard endpiece, and up the inside of the inner suspension tube. This counterflow severely restricts the influx of air from outside as the top of the tube is open during the change of the samples. By moving the inner suspension tube and, thus, the attached Hall probe vertically, the Hall probe can be located and used to measure the local strength of main field and/or gradient field. The Hall probe is used most of the time to locate the center of the magnetic field and, thus, the sample will be set at the same position.

The sample suspension is about 124 cm long; the top part is a hook fabricated from construction wire to connect to the balance. Below the hook, glued on the main section of the suspension, is a quartz fibre of about 0.1mm diameter. A low magnetic susceptibility aluminum wire-aluminum bar-aluminum wire combination is connected between the quartz fibre and the hanging sample to avoid the effect of possible ferromagnetic contamination of the quartz. The aluminum bar is to keep the suspension straight. Two aluminum radiation shields are glued onto the quartz fibre to reduce the radiation from the open top at the balance platform. In order to reduce the effect of the thermo-molecular force on the suspension, especially on the radiation shields,

by the exchange gas inside the tube, an improvement has been done by

attaching a twenty cm long copper ring with better thermal conductivity

onto the outside of the stainless steel inner suspension tube at the

location of the radiation shields. This application has improved the

effects of the thermomolecular force drift obviously (1). The sample is

hung on a loss hook at the bottom of the suspension and can be changed

very quickly.

The force on the suspension has been checked experimentally, and

the correction needed is negligible compared to the force of the sample

reading (123); therefore, in all of the later calculations, the only

correction made of the force on the sample is the aluminum wire

surrounding the sample which hangs from the suspension hook.

The pressure of the exchange helium gas within the sample chamber

is kept at about ~ 1 torr, and the mean free path of the helium molecules

will be of the order of 10^{-2} cm at 10K. The order of the size of the

sample chamber is certainly larger than that of the mean free path of

the exchange helium gas molecules; hence, the kinetic theory of thermal

conductivity can be applied. By comparing the thermal conductivity

between the sample and the sample chamber and the radiation energy

from the top of the suspension tube to the sample, a difference between

the temperature of the sample and that of the sample chamber (in which

the thermometers are attached) should be smaller than 0.1 K at 10K and

even less at higher temperatures; therefore, the temperature from the

reading of thermometers has been assumed to be that of the sample.

This judgement has been verified by the good Curie-Weiss law fit of

some Kondo alloys.

II-4. The Balance

A Beckman-Riic LM600 electronic microbalance is used to measure the magnetic force on the sample. The balance is sitting on a horizontal aluminum balance platform and is housed in a perspex cover.

The hooks from which the sample suspension and the counterweight are hung pass through a 1mm diameter hole drilled in the center of each scalepan. A calibrated weight of a known mass of platinum wire is controlled externally by an energized relay to calibrate the balance output reading before each run. The balance plate can be moved vertically and horizontally to locate the position of the sample and also allow exchange of the sample when it moves far back away from the suspension tube.

By changing the force applied on one end of the balance beam, an opposing torque is automatically provided by amplifying the photocell output by out of the balance position and feeding the resultant current back through a restoring coil until equilibrium. The potential drop across a pre-set resistor by passing the restoring current can be measured either by an internal potentiometer coupled to a duodial on the control unit, or externally by a D.V.M. The latter mode was used during the run, and the range was chosen as 10 mg/100mV. The balance is capable, on this range, of a linear output for differential pan leads up to 300mg. The noise component in the voltage output from the pre-set resistor is reduced, at the expense of increased response time, by a capacitor connected in parallel to the resistor. The output filter 3 on the control unit was chosen so as to reduce the noise to $\pm$ 1μgm in a response time of about 5 seconds.

When the temperature at the bottom of the suspension tube changes as for reset of a sample temperature, the top of the suspension tube still remains at room temperature; therefore, a redistribution of exchange gas molecules along the suspension tube will happen according to the Maxwell-Boltzmann statistics. This redistribution of exchange gas molecules will have a thermomolecular force exerted on the sample suspension system (127-129). This thermomolecular force can be reduced by keeping the pressure of the exchange gas low; however, the pressure of the exchange gas cannot be kept too low, otherwise the temperature of the sample will be rather different from that of the thermometers on the sample chamber. A calculation of this has been presented in the previous section.

This thermomolecular force will affect the force reading of the balance, and it will be impractical to wait until the redistribution of the exchange gas molecules to settle down; therefore, an alternative approach has been adopted. By assuming the force drift is smooth, then the initial condition can be achieved by taking the average value of the readings before and after the gradient field being applied, which only takes a very short period of time. In this way, the problem has been converted to a time-independent, linear response question; hence, it can be solved straight-forwardly.

II-5. Experimental Procedures

In a typical run, it takes about 36 hours after the filling of the liquid nitrogen jacket with liquid nitrogen to cool the main bath and the magnetic coils from room temperature down to around 150K. Then, the liquid nitrogen will be poured directly into the main bath and also by pumping the liquid nitrogen to cool the main bath and the magnetic coils further down to around 70K. After emptying the liquid nitrogen by pressured helium gas and by the main bath heater out of the main bath, any liquid nitrogen left can be checked by the liquid nitrogen detector. Then, it will begin to transfer the liquid helium slowly into the main bath. The first time, a dewar of liquid helium of about 15 litres will be transferred and, subsequently, a smaller amount of liquid helium will be added according to need. The level of the liquid helium in the main bath can be known through the main bath liquid helium detectors. The liquid helium can be transferred into the insert dewar by syphoning the liquid helium from the main bath through the externally controlled capillary, and the level of the liquid helium in the insert dewar can be known through the insert dewar liquid helium detector.

Temperatures below 4.2K are achieved and stabilized by pumping the liquid helium in the insert dewar. The temperatures are derived from the helium vapour pressures. Temperatures above 4.2K are achieved and stabilized by passing a controlled amount of current through the sample chamber heater. The temperatures are derived from the readings of an AuFe versus chromel thermocouple with a reference junction in liquid helium, or from the resistance of an Allen Bradley

carbon resistor from 4.2 to 25K and, at higher temperatures, from the

reading of a copper-constantan thermocouple with a reference junction

in liquid nitrogen.

At first, a low temperature magnetic isotherm is generally taken.

The value of the main field chosen for low field susceptibility measure-

ments is at the linear region of the magnetic isotherm in order to avoid

the effect of the magnetic spin saturation; however, for alloys of ferro-

magnetic and magnetic spin glass state, the magnetic remanence after

taking the magnetic isotherm through high fields may be significant

and will affect the later measurements; therefore, the procedure is to

go to high temperatures to break the possible magnetic ordering and

then cool down the sample in zero field to take the low fields suscepti-

bility. Even while taking the low field susceptibility, the main field

used is no more than 500 Oe, the persistent current mode is not used,

and the field has been turned on and off alternatively while taking data

and changing temperature periods.

Section III. Apparatus and Procedures of Electrical Resistivity Measurements

The apparatus of the electrical resistivity measurements of all the PtCr alloys was constructed by Barber (130); and that of the PdPtMn alloys was similar to it and constructed by Tari (131). Both of the apparatuses utilize the standard four-terminal D.C. technique and sit in the standard two-layer glass dewar. The samples are housed in an isothermal copper sample chamber and are connected in series for current passing with each other and also connected with an external 0.01 manganin standard resistor which is kept in an isothermal water bath.

The current leads, as well as the potential leads, use fine Cu wires and are attached to the long, cylindrically-shaped samples by a multi-positioned, spot-welded method in order to have better contact and more strength. The other ends of the leads are soldered onto the lead beads of the apparatus.

The current is supplied by a Tinsley regulated current supply 5753, with a stability of better than one part in 10^5 over a one-hour period. A Julie zener provides the necessary stable reference voltage to the current supply. The current passing through the samples-standard resistor system which is usually set as low as 130mA to minimize the Joule heating is obtained by the potential drop across the standard resistor. The potential drop across the standard resistor and each sample is measured by a potentiometer in conjunction with a galvanometer amplifier, which allows the out-of-balance voltage observed. The reading of the potential difference has a resolution of 1 nV; however, the order of 10 nV reading is the lowest value we have used.

Temperatures below 4.2K are achieved and stabilized fairly well by using a rubber diaphragm manostat to pump the liquid helium which is in the inner dewar as the sample chamber, and the sample chamber now is emerged in the liquid helium. Temperatures are derived from the helium vapour pressure of reference tc the standard table or from the resistivity of an Allen Bradley carbon resistor (Tari's apparatus) which is attached to the sample chamber. The vast amount of liquid helium will act as a heat resolvor in relation to the relatively small Joule heating and, therefore, the samples will be at the same temperature as the liquid helium and the thermometer. Temperatures above 4.2K are achieved and stabilized within $\pm$ 0.1K for the time period of taking a data point by passing a controlled amount of current through the sample chamber heater. At this time, the sample chamber will be out of the liquid helium and is of about one atmosphere pressure of helium vapour. Temperatures are derived from the reading of an $\underline{Au}Fe$ (0.03 at.% Fe) versus a chromel thermocouple (Barber's apparatus) with a reference junction in liquid helium or from the resistance of the carbon resistor (Tari's apparatus) from 4.2 to 25K. Higher temperatures are derived from the reading of a copper–constantan thermocouple (Barber's apparatus) with a reference junction in outside liquid nitrogen or from the resistance of a platinum resistor (Tari's apparatus). The space in between the samples and the thermometers is full of helium vapour of about one atmosphere with good heat conductivity; therefore, the temperature of the samples is assumed to be the same as that of the thermometers, and this assumption has been verified by the smooth change of the resistivity of some samples at below and above 4.2K.

Typically, it takes over two hours after filling up the outer liquid nitrogen jar with liquid nitrogen to cool the sample space down to below 150K. Then it will begin to transfer the liquid helium slowly into the inner dewar, usually taking about two litres of liquid helium for a low-temperature run.

Section IV. The Electronic Ramp Generator

In order to drive the current supply for the superconducting gradient field coils, an adequate electronic ramp generator having the following characteristics is required:

(1) a voltage output which can be set easily and which can be arrived at rapidly and accurately after each sweep and from there on maintained steadily,

(2) a smooth sweep with an adjustable sweep rate,

. (3) construction costs that are minimal.

To meet all of the above requirements, it was, therefore, decided to design and construct our own electronic ramp generator (1). The cost was less than £ 20. The circuit is shown in Fig. 21 and comprises power supply, integrator, and voltage follower three parts.

A set of commercial batteries with 15V output was used as the power supply. The voltage output sweeping up and down was decided merely by the position of the two-way switch, S_2, at U or D respectively. The sweep up time and down can be set by adjusting the potentiometer RVU and RVD respectively. A transistor, T, together with the resistors, R_5 and R_6, works as a current limiter, and combined with the Zener diode, D_3, limits the voltage output upper limit. Since the magnitude of the current is under control, the Zener diode and then the output will reach a stable state rapidly. The diodes, D_1 and D_2, were used to prevent voltage output going negative. The upper voltage output can be set by adjusting the potentiometer, RVO, which has been connected to a digitalmeter for the value-reading. The calibrated correspondence between voltage output and RVO's reading was set by adjusting the
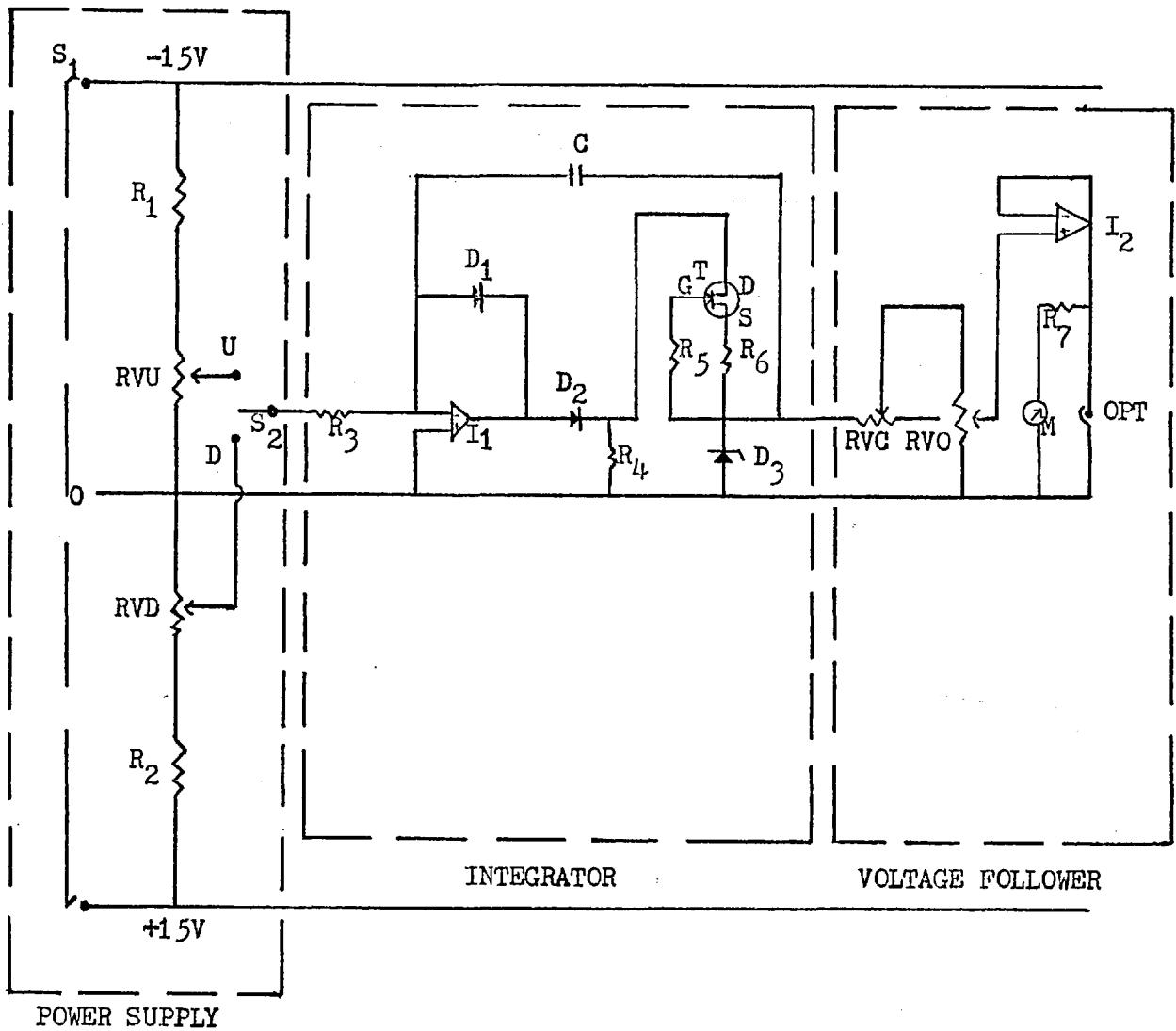
Fig. 21   Circuit Diagram of the Electronic Ramp Generator

R_1, R_2: 39KΩ, ¼W

R_3 :100KΩ, ¼W

R_4, R_5: 10KΩ, ¼W

R_6 :330 Ω, ¼W

R_7 : 1KΩ, ¼W

RVU,RVD:1KΩ

RVO : 10KΩ

RVC : 10kΩ

I_1, I_2: SN72741P

C   : 2@2.2uF

D_1, D_2: 1N914

D_3 : 5V

T   : 2N5245

S_1 : 2P

S_2 : 1P 2way

M   : 5V

potentiometer RVC and then fixed generally. For reference, a voltmeter was connected parallel to the output.

The current output of this ramp generator is approximately 14mAmp. The voltage output can be set up to 5V and has about 400 μV initial drift in the first 40 seconds after reaching the stable stage; it then remains constant within $\pm$ 100 μV. After each sweep, the voltage output will reach the same level repeatedly and accurately with 0.1 percent. The sweep time can be set between 5 and 40 seconds, and the sweep rate of voltage output can be decided by adjusting the combination of both upper voltage output and sweep time.

The performance of this electronic ramp generator was found to be adequate for our purposes.

CHAPTER 3 MAGNETIC INTERACTIONS IN "DILUTE" AgMn ALLOYS

AND MAGNETIC MEASUREMENTS ON SOME "DILUTE"

Al-3d ALLOYS

Abstract

Measurements taken at temperatures above Kondo temperature T_K of the magnetization M up to 50KOe between 1.8 and 4.2K and the suscep-tibility X from 1.8 to a maximum of 100K of three "dilute" AgMn alloys of nominal concentrations n of 630, 1000, and 1370 ppm Mn are presented. Both M and X follow scaling laws well, and thus verify the geometrical decreasing with the cube of the distance characteristics of the RKKY interaction. The strength V_0 of the RKKY interaction between two Mn impurities has been determined from expressions for the high field behaviour of M in the presence of such interaction, yielded by a virial expansion of the free energy. The value obtained for V_0 is $(3.9 \pm 1) \times 10^{-25}$ eV cm^3. The effective $|J|$ value estimated from V_0 is (0.9 ± 0.1)eV.

Other measurements taken at temperature below T_K are presented of the magnetization and the susceptibility of several "dilute" Al based alloys, including two AlMn (n = 700, 3100 ppm Mn) alloys, one AlCr (n = 4000 ppm Cr) alloy and one AlV (n = 600 ppm V) alloy. It is experimentally shown that the impurity interactions persist below T_K in these alloys.

Section I.　Magnetic Interactions in "Dilute" AgMn Alloys

I-1.　Introduction

Since the discovery of the electrical resistivity minimum phenomena, the Kondo effect (7), of dilute alloys in which localized magnetic moments exist on magnetic impurities' sites, an enormous amount of research has proceeded in this field. Most of the research has concentrated on the extremely dilute alloys ($T_I < T_K$, where T_I is the measure of average interactions between solute atoms and T_K is the Kondo temperature) in which the single-impurity Kondo effect dominates, and the impurity spins are considered to be independent to each other. The single-impurity Kondo effect has been studied reasonably well now; hence, in recent years, the interest in alloy research has been shifting from the extremely dilute region to the more concentrated region in which the interactions between impurities can no longer be neglected.

As the concentration of the magnetic impurities increases to just above the extremely dilute region, the impurity atoms are still too little and too apart to react to each other as near neighbors. In this impurity concentration region, the long-range indirect Ruderman-Kittel-Kasuya-Yosida (RKKY) interaction (24-26), $V(r) = V_0 \cos(2K_F r)/r^3$ (for $K_F r >> \pi$), will begin to dominate, where K_F is the Fermi momentum and r is the distance from the impurity.

The RKKY interaction has the following characteristics:

(A) the nature of this interaction depends on the density of conduction electrons through the Fermi momentum;

(B) the conduction electron spins develop a rapid oscillating polarization in the vicinity of the impurity;

(C) the interaction will decrease with the cube of the distance from the impurity.

The characteristics (A) and (B) have been discussed and experimentally verified in Chapter 1.

Obviously, it will be interesting if the characteristic (C), $(V \ (r) \sim r^{-3})$, can also be verified and, also, if the strength V_O of the RKKY interaction between two impurities can be quantitatively determined; therefore, an experiment has been designed and carried out, and three AgMn alloys with respective nominal concentrations n of 630, 1000, and 1370 ppm Mn were examined.

The RKKY interaction decreasing with the cube of the distance, r^3, has been verified through the fitting of the scaling laws (85). The strength of V_O of the RKKY interaction between two Mn impurities and the effective $|J|$ value in AgMn alloys have been determined by magnetization measurements at high fields and are presented here.

The AgMn alloy system was chosen because Kondo temperature, T_K, is very small, so that in the dilute limit the solute has a good magnetic moment down to very low temperature; and, because the electronic structure of Ag is simple, it can be safely approximated to by a free electron model. It is, thus, unlike AuFe, for example, where the effect of T_K on the interaction behaviour is clear, as shown in the results of Laborde and Radhakrishna (132), and those of Tholence and Tournier (133).

Although the RKKY interaction is expected to persist (67) in the presence of the Kondo effect and modify the experimental behaviour of the various

Kondo anomalies down to very dilute impurity concentrations, up to the present, no systematic experimental or theoretical studies have been made in this region where $T_I < T_K$. If the Mn concentration n is too low, the alloy will fall into the $T_I < T_K$ region, and if n is too high, the interactions in the alloy will be much more involved than the RKKY interaction alone. Hence, these three Mn concentrations of $\underline{Ag}Mn$ were chosen because when n lies between 630 and 1370 ppm Mn, the RKKY interaction dominates (experimental evidence in later section).

I-2. Experimental Procedures

Three AgMn alloys with respective nominal concentrations of 630, 1000,
and 1370 ppm Mn were made. The alloys belong to the FCC structure.
The starting materials were 99.999% "Specpure" Ag from Johnson Matthey
Ltd. and 99.99% pure Mn from Koch-Light Labs Ltd. The samples were
made by diluting an AgMn (5.43 at.% Mn) master alloy in an arc furnace
within which was a circular cavity on a water cooled copper hearth
filled with two-thirds atmosphere argon. The alloys were melted, turned
over, and remelted several times, and then formed into short cylinders
of about 3mm diameter. All samples were cleaned by a solution containing
equal amounts of 25% NH_4OH and 20 vols. H_2O_2.

Measurements were carried out by a force (Faraday) method using a
superconducting solenoid (0-50KOe) with separate superconducting gradient
field coils in a B.O.C. cryostat; the forces were measured with a
Beckman microbalance LM-600. Temperatures were derived from the
helium vapour pressure with reference to the standard table from 1.8 to
4.2K, from the resistance of an Allen Bradley carbon resistor from 4.2
to 25K and at higher temperatures from the readings of a copper-constantan
thermocouple with a reference junction in liquid nitrogen.

Three $\underline{Ag}Mn$ alloys with respective nominal concentrations n of 630, 1000, and 1370 ppm Mn and a pure Ag sample were examined. The magnetic isotherm M_{Ag} and the magnetic susceptibility X_{Ag} of Ag have been measured, and the M_{Ag} taken at 4.2K versus field H has been plotted in Fig. 22. A deviation from a straight line occurs at low field, indicating the contamination of a small amount of ferro-impurity. The X_{Ag} can be obtained, at this temperature, from the slope of the M_{Ag} at the high field, straight line portion. The X_{Ag} has a change of less than 3% in the 1.8 to 50K temperature range which agrees with the existing data.

The magnetization M and magnetic susceptibility X of the Mn solute are assumed to be $(M_{alloy} - M_{Ag})$ and $(X_{alloy} - X_{Ag})$ respectively, where M_{alloy} and X_{alloy} are, respectively, the magnetization and the suscepti-bility of the alloy. Since X_{Ag} changes only very slight with temperature compared with the change of X, the value -1.86×10^{-7} emu/gm for X_{Ag} was used as the correction for the whole of this temperature range. The initial susceptibility X and the reciprocal of the susceptibility (1/X) versus temperature T of these three $\underline{Ag}Mn$ alloys have been plotted in Fig. 23-25. These alloys all follow the Curie-Weiss law behaviour, and from the Curie constant $C = n \ \mu_{eff}^{2} / 3k_B = ng^2 \mu_B^2 S(S+1) / 3k_B$, where μ_{eff} is the effective moment, μ_B is the Bohr magneton, and k_B is the Boltzmann constant, spin $S = 2.23 \pm 0.01$ per Mn atom was determined, which is in good agreement with the values of Mizuno (134) and Flouquet (135), where in this and later calculations the assumption g = 2 was made.
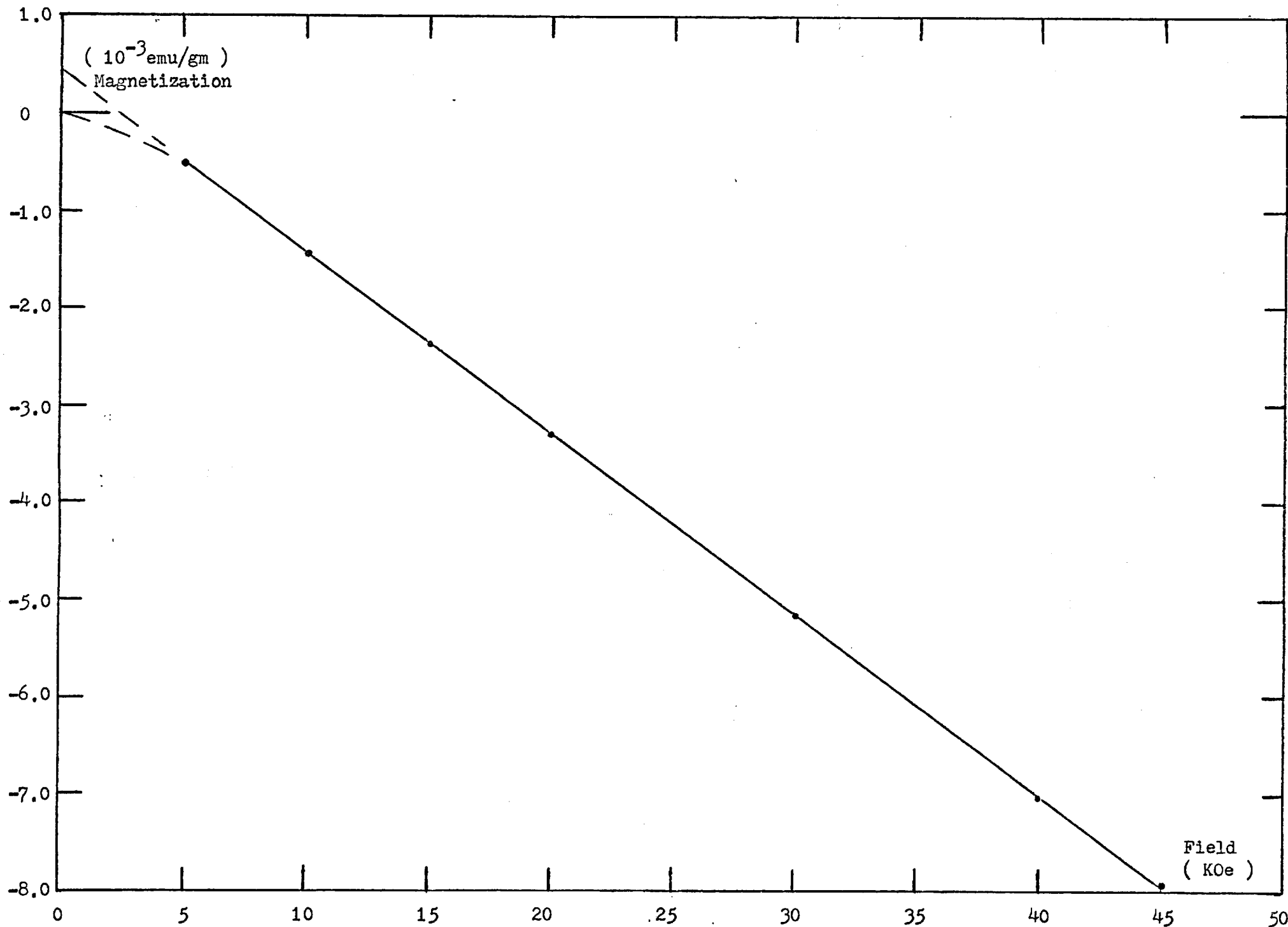
Fig. 2.2 Magnetization versus Field at 4.2K for Ag

90
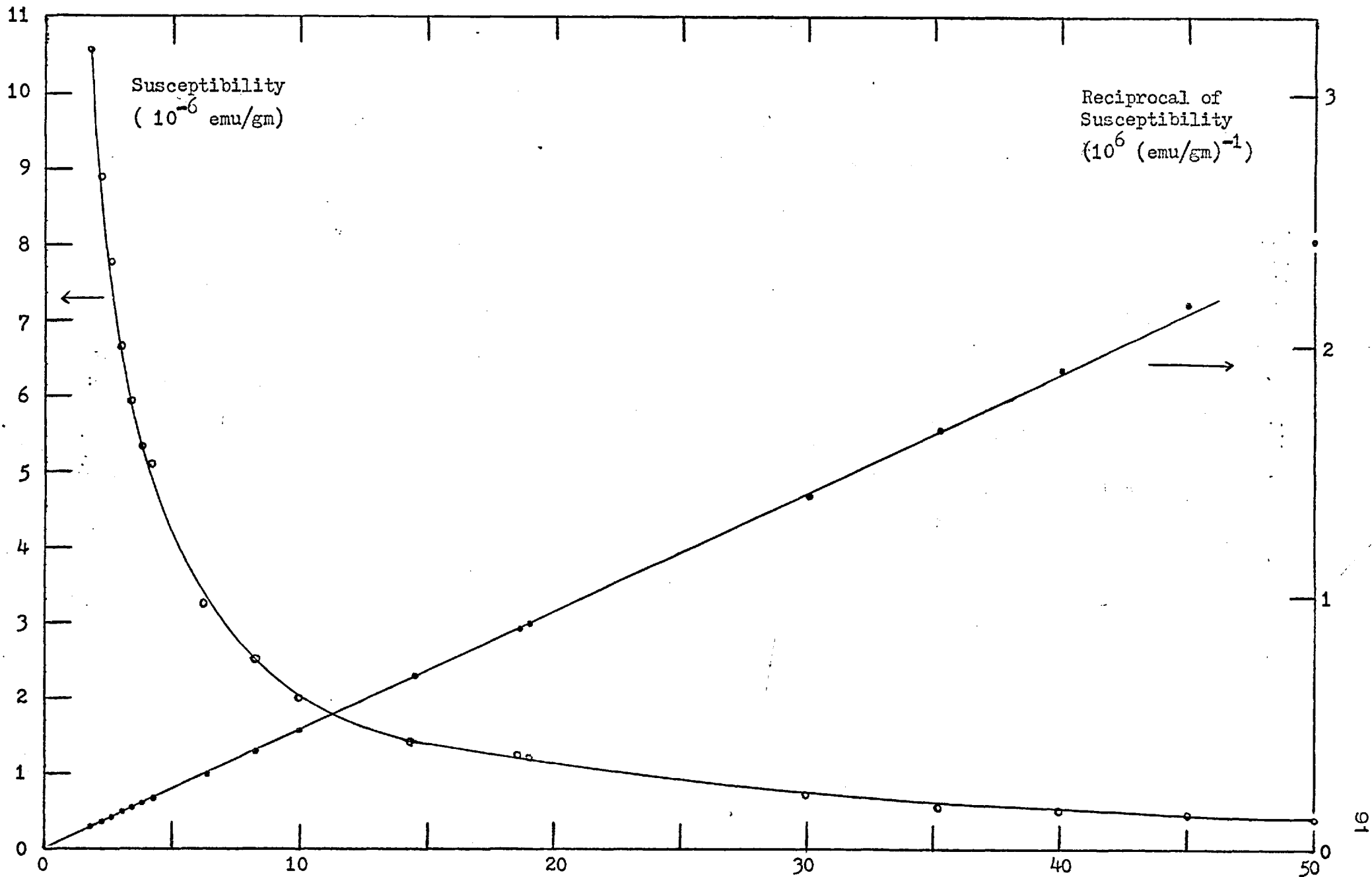
Fig. 23 Susceptibility and Reciprocal of Susceptibility versus Temperature for AgMn (630 ppm Mn) Impurity
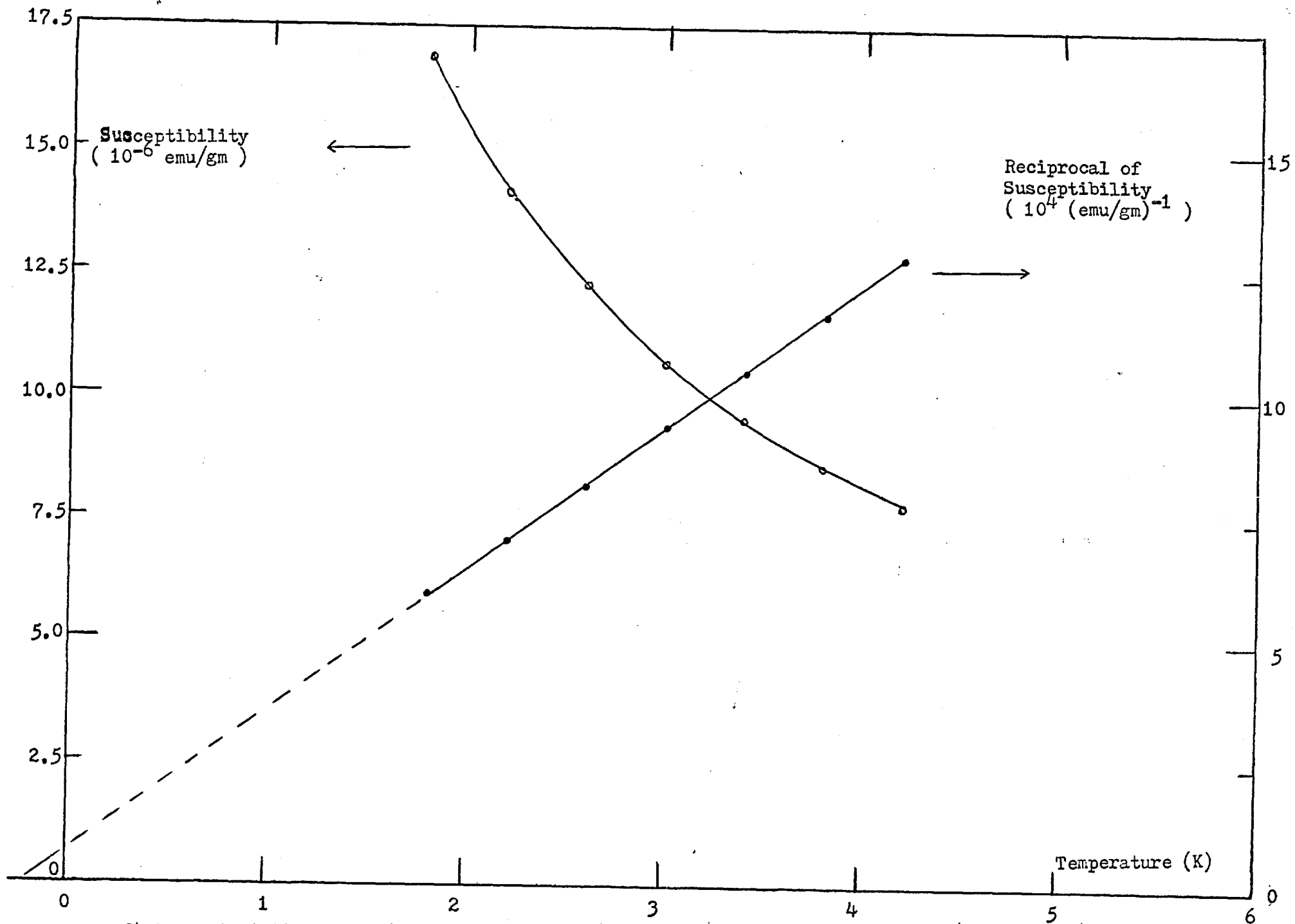
Fig. 24 Susceptibility and Reciprocal of Susceptibility versus Temperature for A̲gMn (1000 ppm Mn) Impurity

92
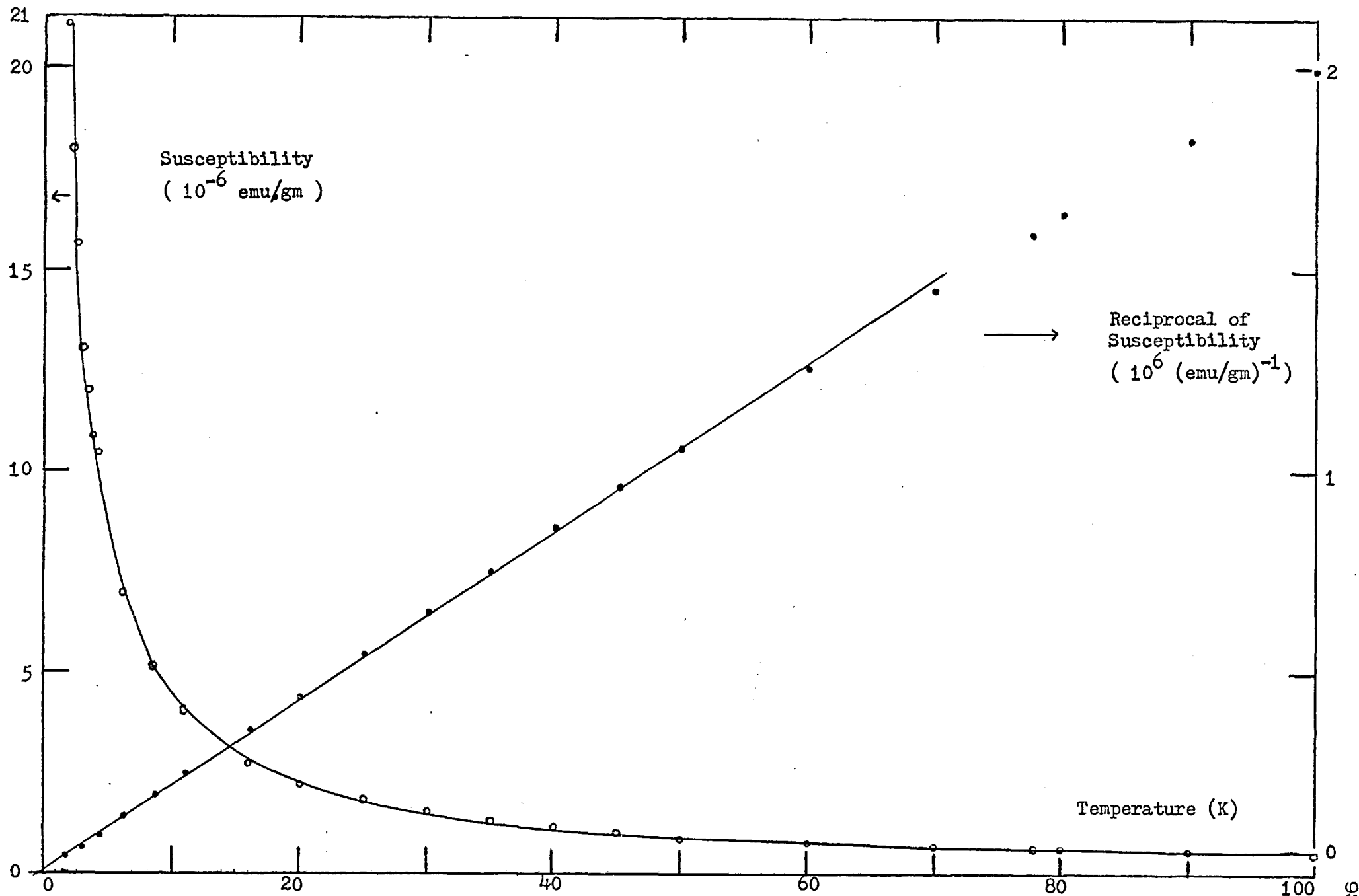
Fig.25 Susceptibility and Reciprocal of Susceptibility versus Temperature for AgMn (1370 ppm Mn) Impurity

The magnetic isotherms M taken at temperature T = 1.8, 3, and 4.2K versus field H of the Mn solute of these three alloys have been plotted in Fig. 26-28.

The RKKY impurity-impurity interaction and the single-impurity Kondo effect will both reduce the magnetization below the Brillouin function appropriate for free spins and, also, inhibit the approach to saturation of magnetization (39). A characteristic feature of magnetic interaction which arises from the RKKY interaction is that the magnetization per impurity atom, at a given field H and temperature T, decreases as the impurity concentration increases. This characteristic feature can be seen (and is compared with the Brillouin functions) in Fig. 29-31.

From the geometrically decreasing with the cube of distance (r^3) nature of the RKKY interaction, scaling laws (85) $(M/n) = F_1(T/n, H/n)$ and $X = F_2(T/n)$ were derived, where the impurity concentration n acted as the scaling parameter. The (M/n) versus (H/n) behaviour has been plotted in Fig. 32 for the three alloys by fixing the "reduced temperature" $T/n = 3.0 \times 10^{-3}$ K/ppm Mn and X versus (T/n) in Fig. 33 for the 630 and 1370 ppm alloys. The experimental results follow the scaling laws well. Thus, the r^3 decreasing characteristic of the RKKY interaction is verified.

The above evidence also suggests that the RKKY interaction, rather than the single-impurity Kondo effect or crystal field splitting, dominates the magnetic behaviour of the alloys measured.

By using a virial expansion of the free energy in a power series of the concentration of magnetic impurities to investigate the effect of the RKKY interaction on the thermodynamic function of "dilute" magnetic alloys,
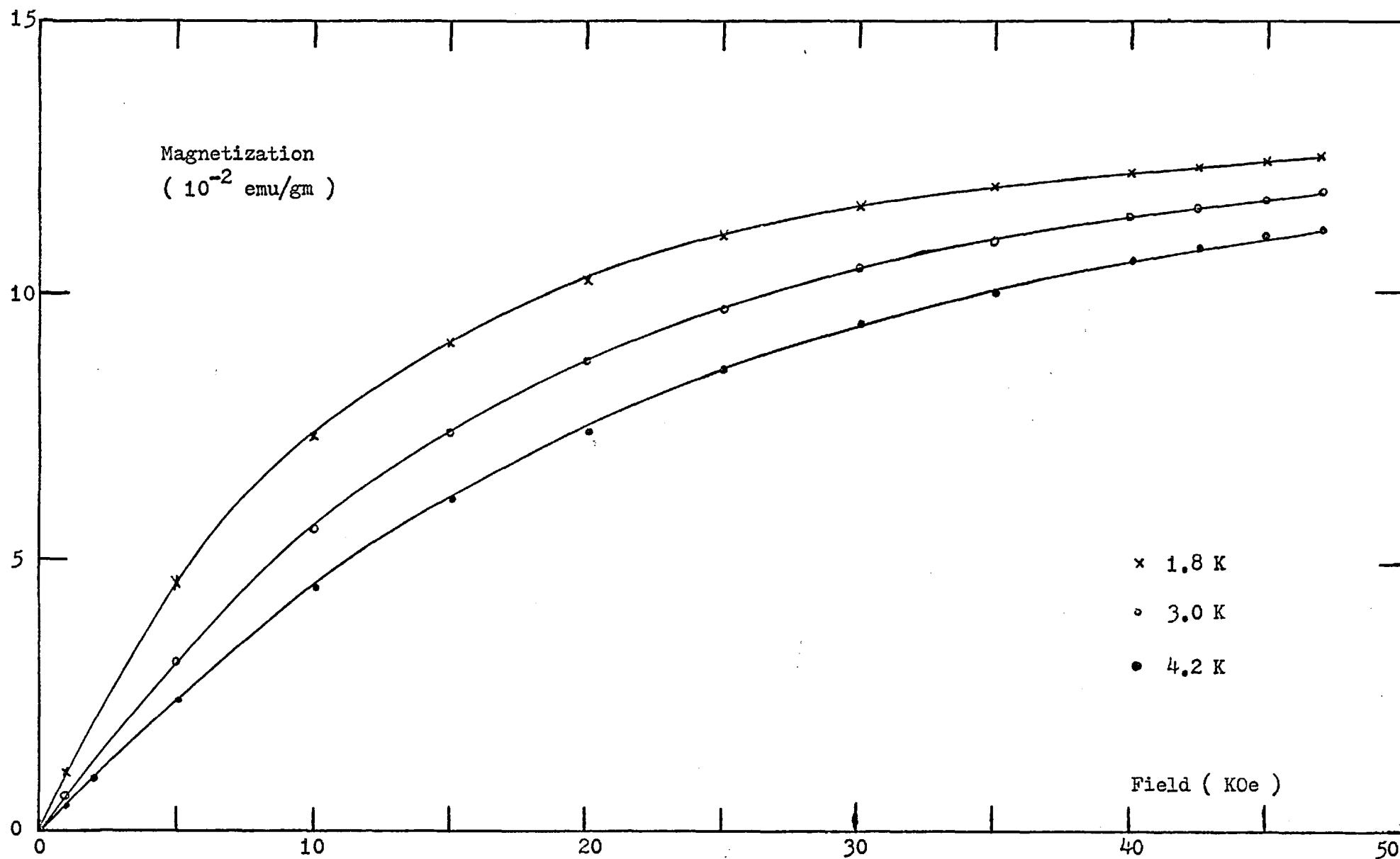
Fig. 26 Magnetization versus Field for AgMn (630 ppm Mn) Impurity
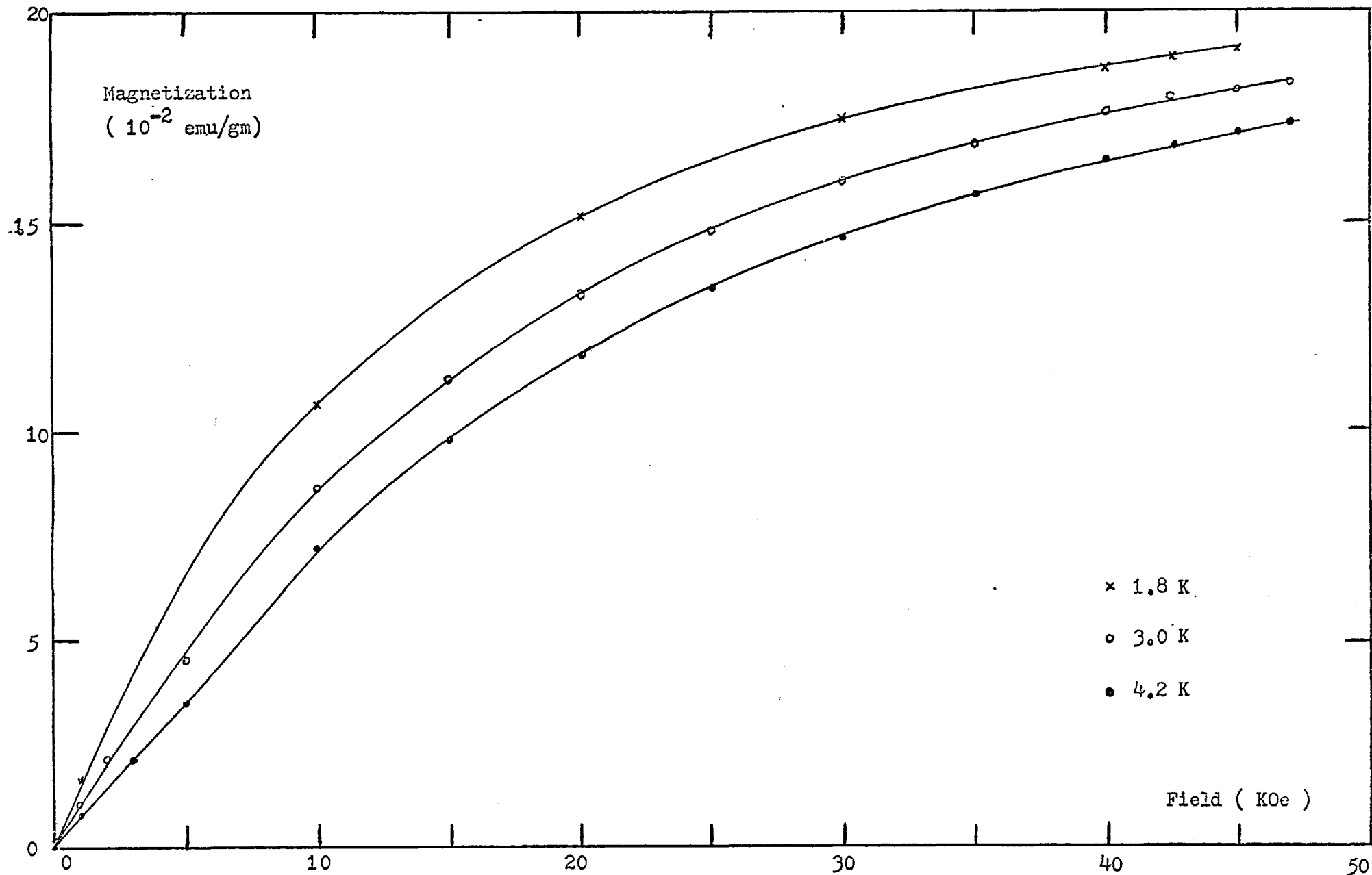
Fig. 27 Magnetization versus Field for AgMn (1000 ppm Mn) Impurity
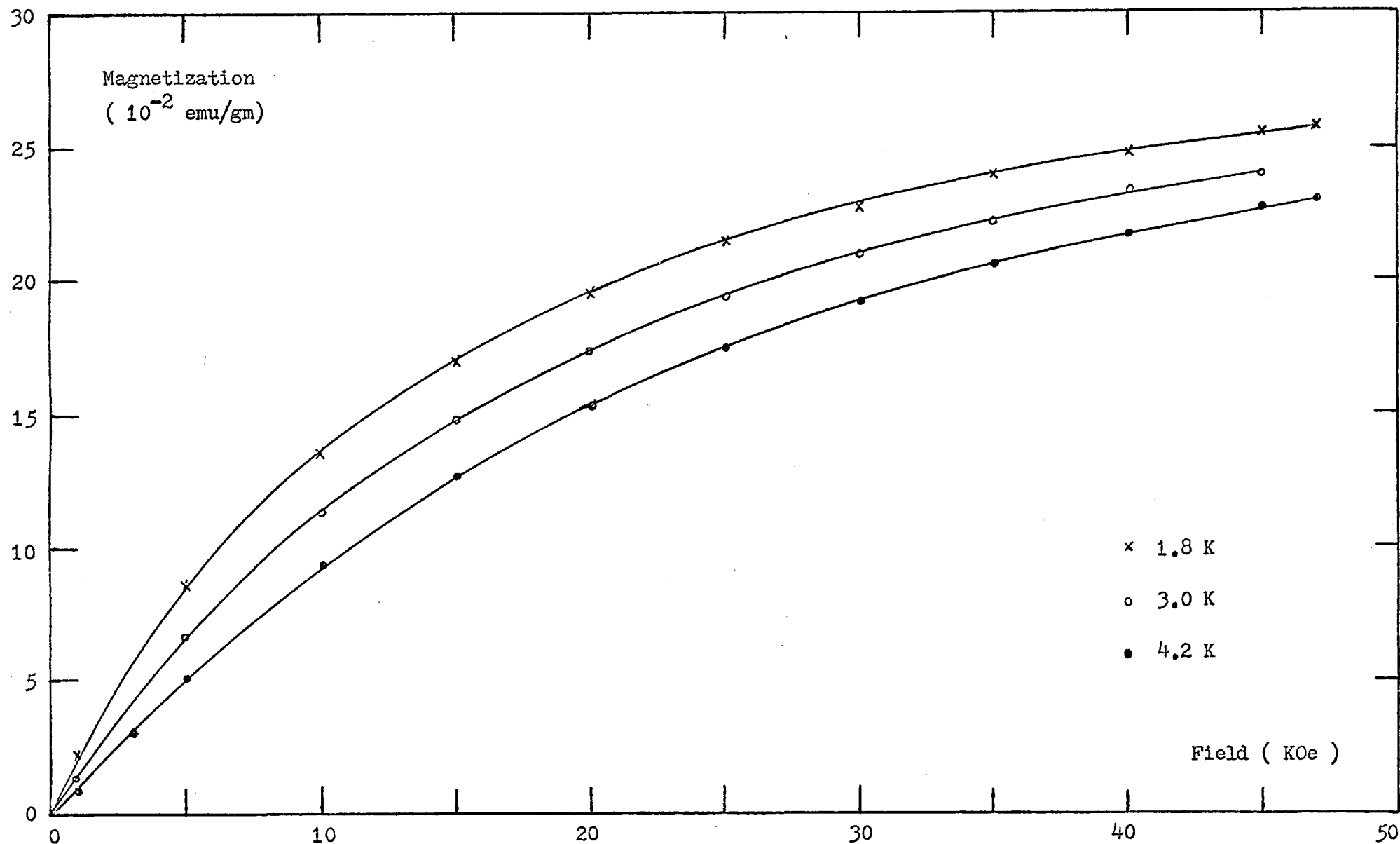
Fig. 28 Magnetization versus Field for AgMn (1370 ppm Mn) Impurity

97
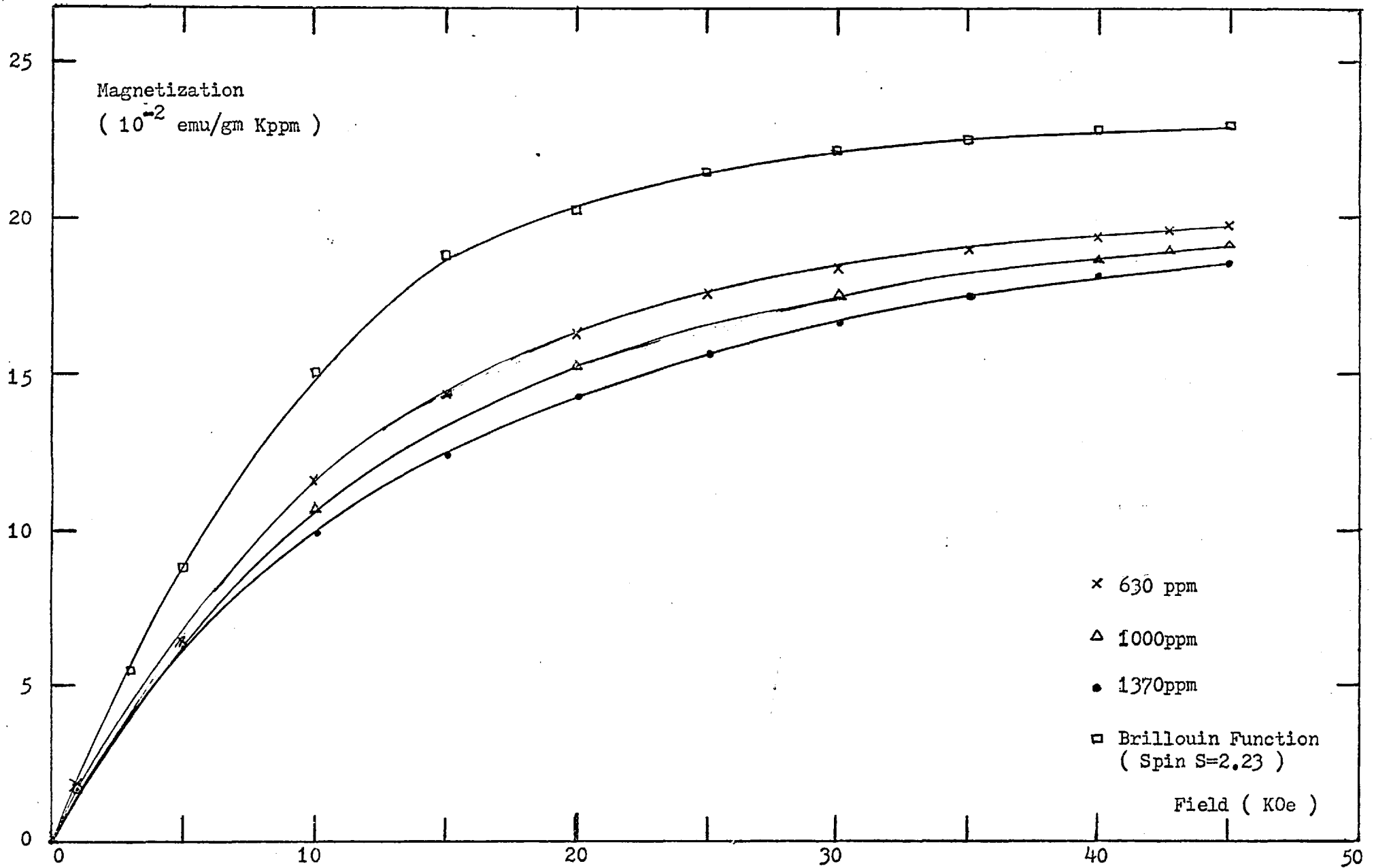
Fig.29 Magnetization versus Field for AgMn Impurity at 1.8K
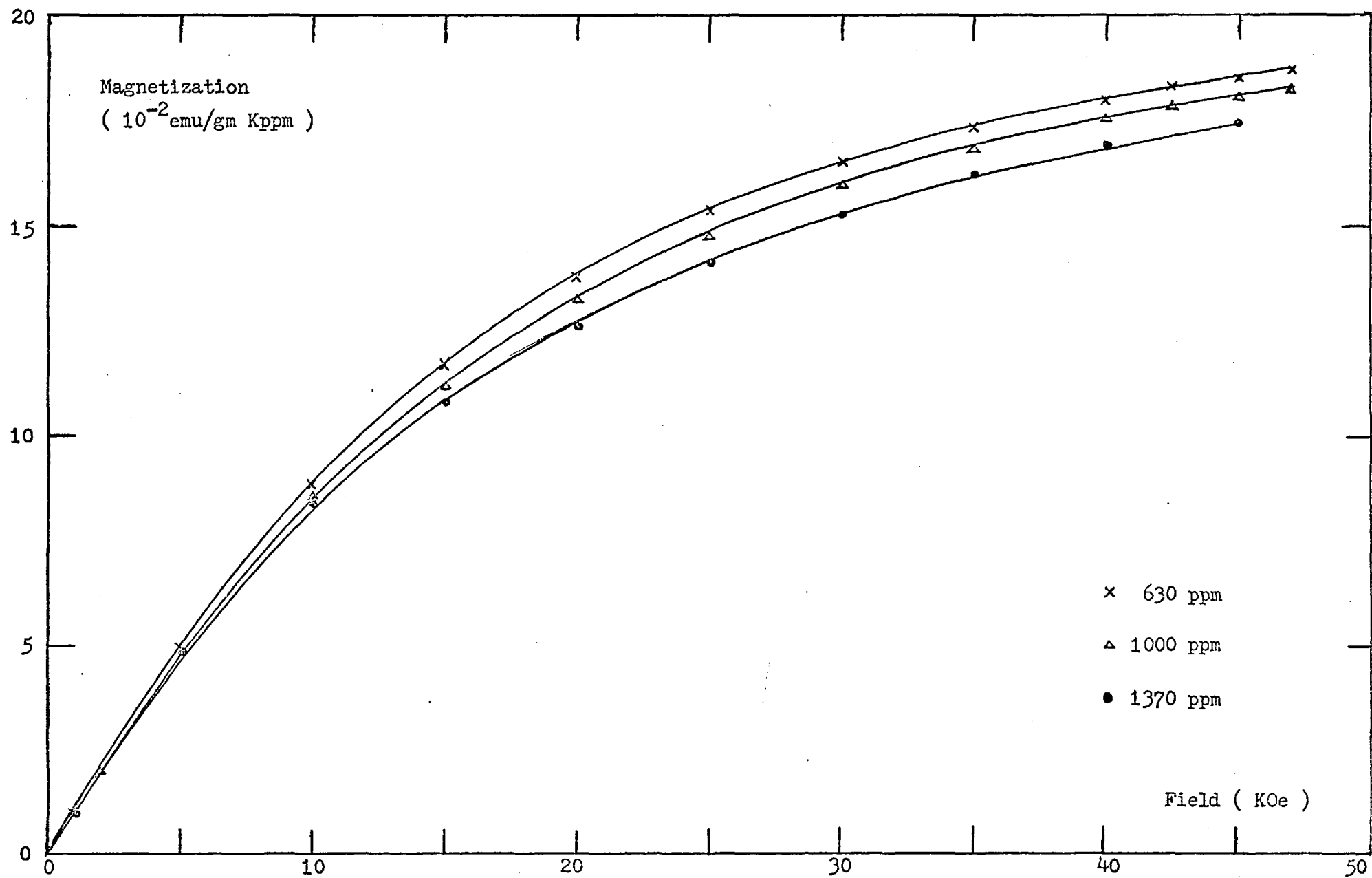
Fig.30 Magnetization versus Field for AgMn Impurity at 3.0K
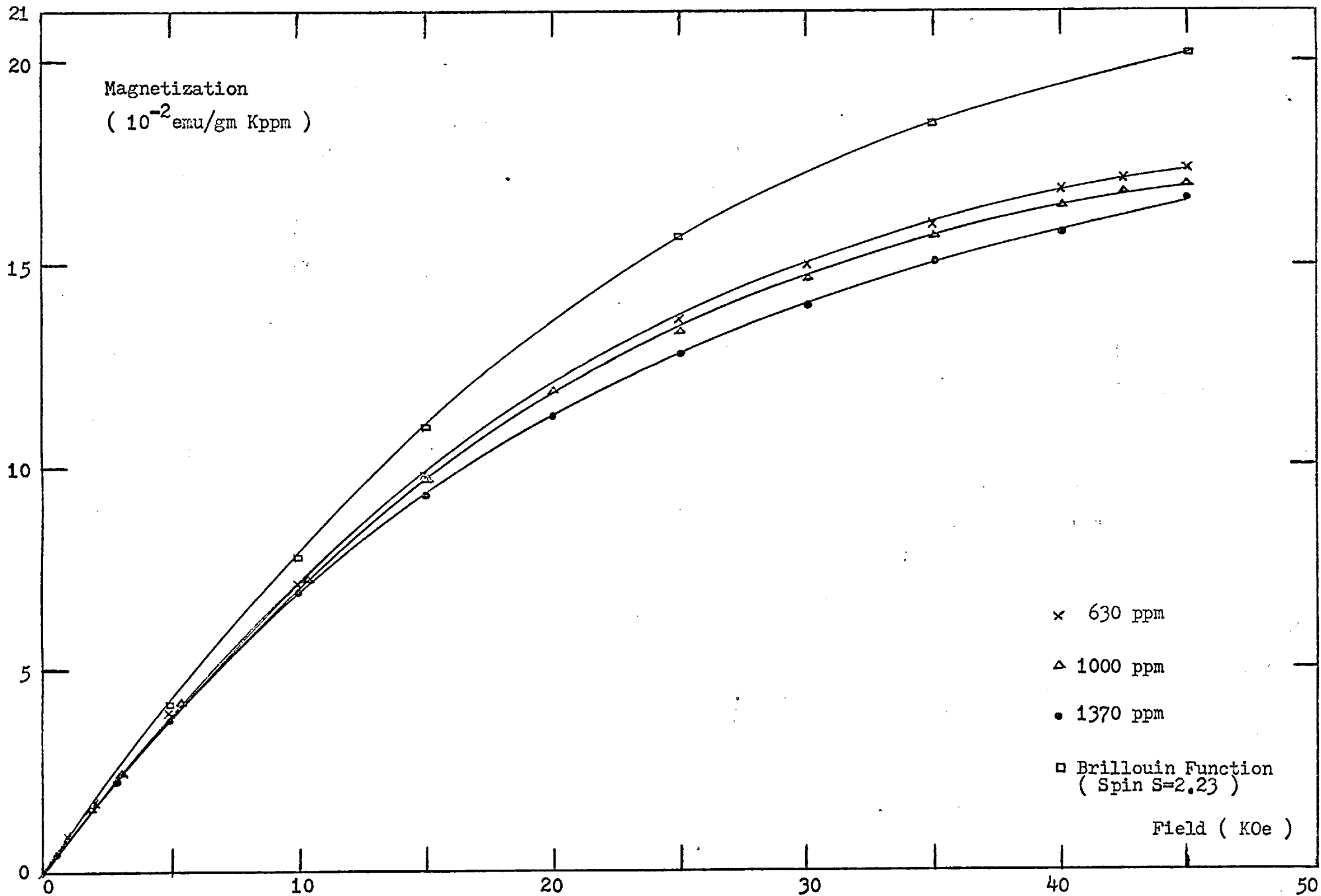
Fig. 31 Magnetization versus Field for AgMn Impurity at 4.2K
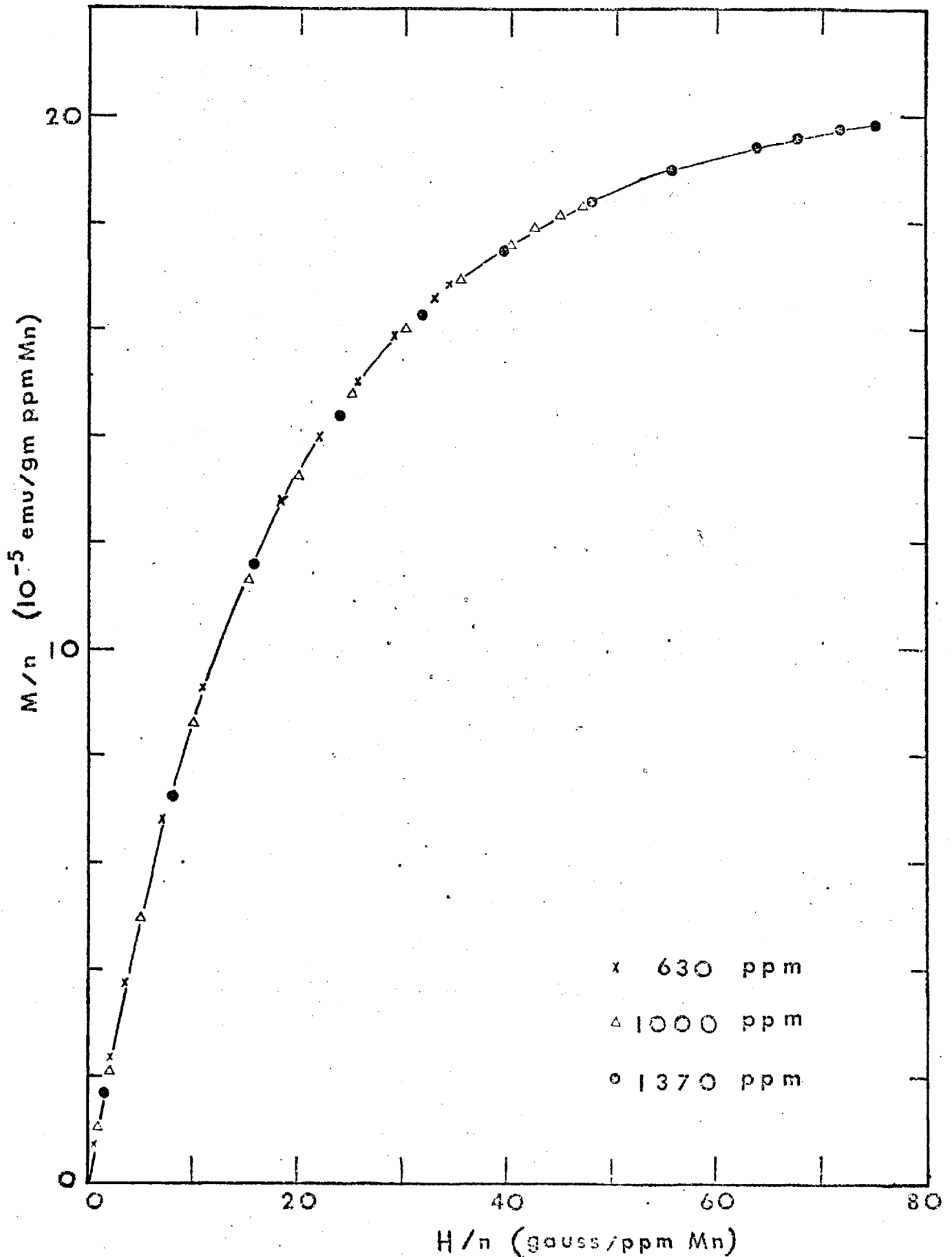
Fig. 32 Impurity magnetization M divided by concentration n as a function of magnetic field H divided by n at the fixed "reduced temperarure" (T/n) = 3.0 x 10^{-3} K/ppm Mn for 630, 1000 and 1370 ppm Mn _AgMn_ alloys.
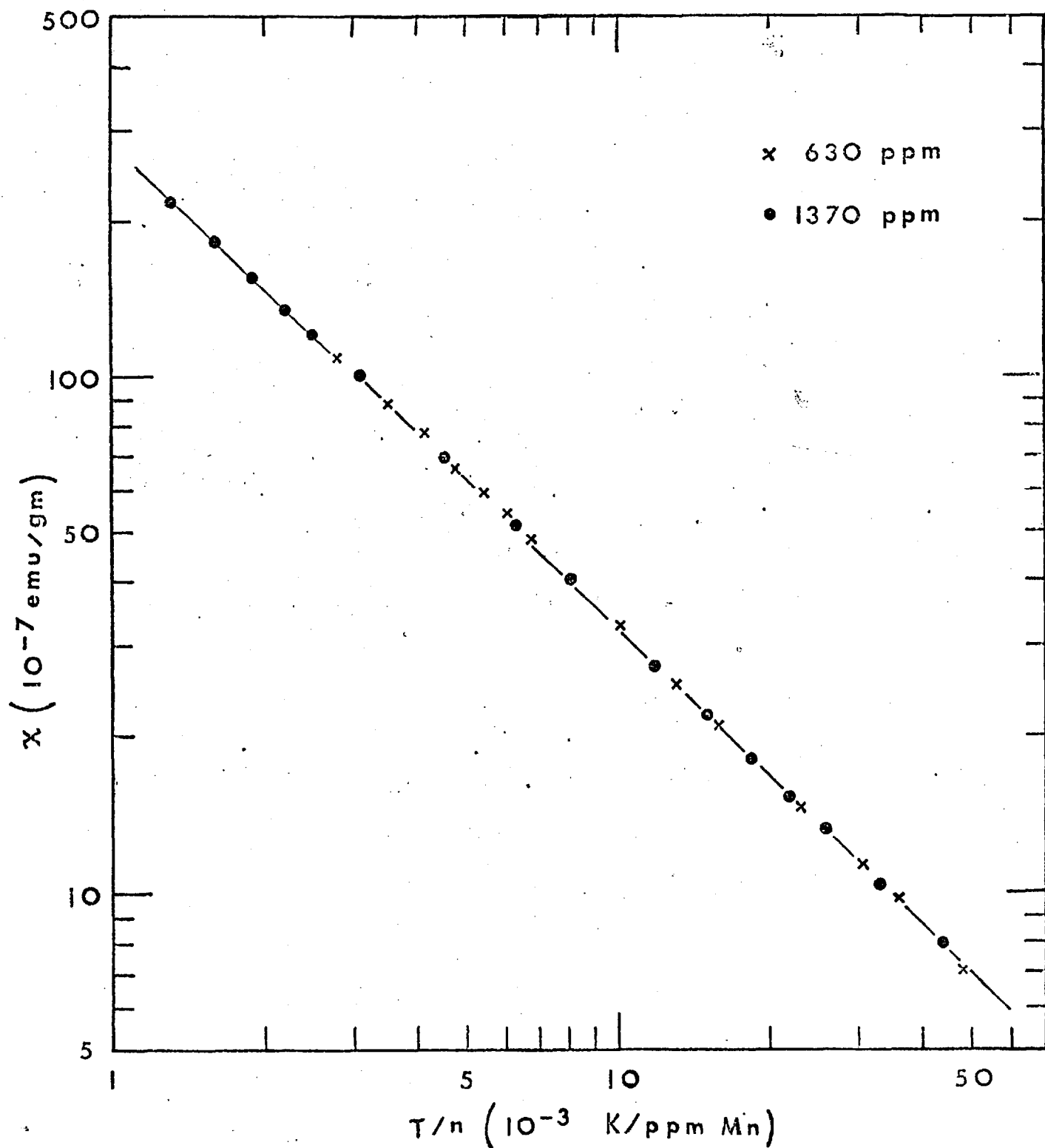
Fig. 33 Impurity magnetic susceptibility χ as a function of "reduced temperature" (T/n) for 630 and 1370 ppm Mn AgMn alloys.

Larkin and Khmel'nitskii (87) derived the following temperature-independent expression for magnetization M at the $k_B T \ll \mu_B H$ limit:

$$M = g \mu_B \bar{S} n [1 - 2(2\bar{S} + 1)n V_0 / 3g \mu_B H]$$

where $\bar{S} = (S(S + 1))^{1/2}$ and effective moment $\mu_{eff} = g \mu_B \bar{S}$.

The fractional deviation of magnetization M (taken at field H = 45KOe) from the saturation magnetization, assuming this to be n $\mu_{eff} = ng \mu_B \bar{S}$, has been plotted as $(1 - M/g \mu_B \bar{S} n)$ versus n in Fig. 34, and a linear relation between the $(1 - M/g \mu_B \bar{S} n)$ and n at a fixed T can be seen.

This inequivalence of the slopes of different temperatures suggests that under practical laboratory conditions (say H $=$ 45KOe) the $k_B T \ll \mu_B H$ limit might be difficult to achieve, and the effect of temperature should be considered as well. This can be done, as Larkin and Khmel'nitskii (87) suggested, by introducing the free energy in second order $F^{(2)} =$ $-(2/3)n^2 V_0 Re \; \psi \, [1/2 - (i/2\pi) \ln(1 + 2ch(g \mu_B H/k_B T))]$, where ψ is the logarithmic derivative of the Γ function. We obtained the following temperature-dependent expression for the small $(k_B T / \mu_B H)$ case:

$$M = g \mu_B \bar{S} n \left\{ 1 - 2(2\bar{S} + 1)(n V_0 / 3g \mu_B H) [1 + (1/3)(\pi k_B/g \mu_B H)^2 T^2] \right\}$$

The $(1 - M/g \mu_B \bar{S} n)$ versus T^2 relation has been plotted in Fig. 35, and a T^2 dependence is observed clearly.

From the intercepts at $T^2 = 0$ of the straight lines, the strength of the RKKY interaction between two Mn atoms in AgMn, $V_0 = (3.9 \pm 1) \times 10^{-25} eVcm^3$ has been determined, where 1-ppm Mn = 5.91 × 10^{16} Mn atoms/cm^3 (1).
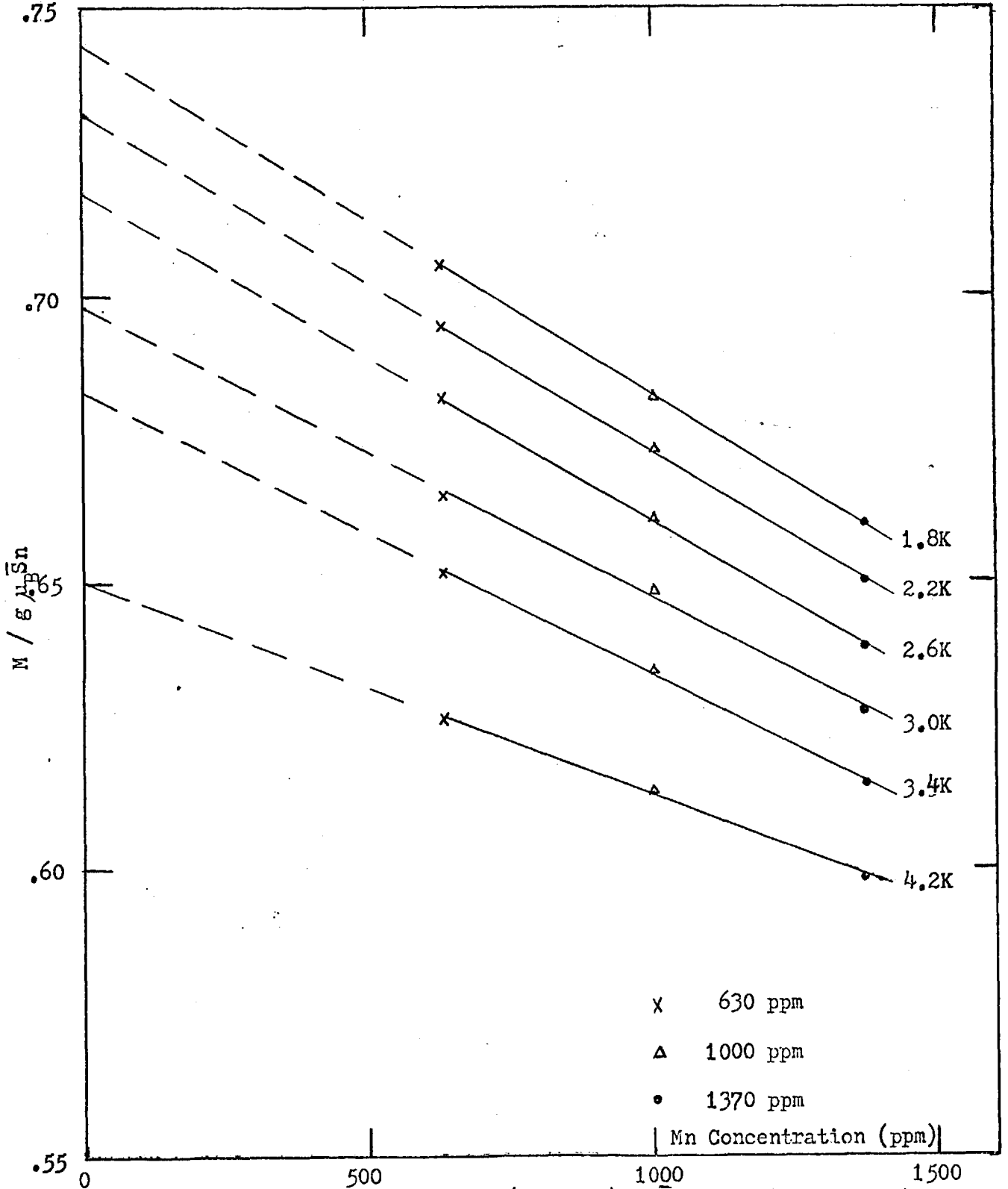
Fig. 34 Fractional Magnetization $M/n\mu_{eff} = M/ng\mu_B\bar{S}$, taken at field = 45 KOe, versus Mn concentration for 630, 1000 and 1370 ppm Mn AgMn alloys.
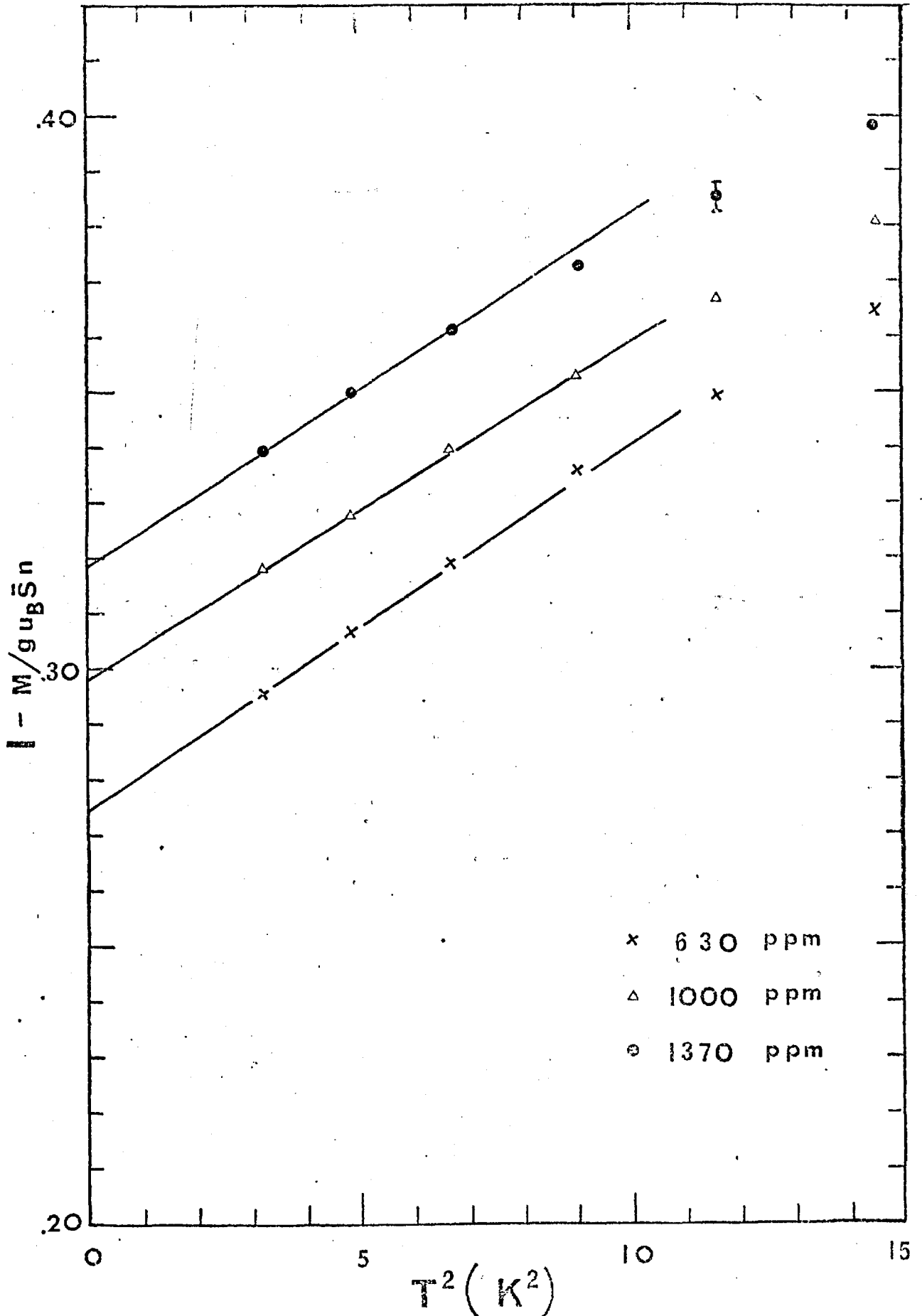
Fig. 35 Fractional deviation of Impurity Magnetization M, taken at field = 45 KOe, from the saturation magnetization $n\mu_{eff}=g\mu_B\bar{S}n$, $(1-M/g\mu_B\bar{S}n)$ as a function of T^2 for 630, 1000 and 1370 ppmMn AgMn alloys.

The effective $|J|$ value of the s-d exchange interaction $V_{sd} = -J \underset{\sim}{S} \cdot \underset{\sim}{s}$

between the spin operators $\underset{\sim}{S}$ and $\underset{\sim}{s}$ for the spin momenta of Mn and con-

duction electron of Ag can be estimated by putting the above obtained

values of V_O and S into the following equation (60):

$$V_O/2 = 9 \, \pi^2 J^2 S (S + 1)/64 \, \sqrt{2} \, E_F K_F^3$$

where the 1/2 factor at left appears because V_O is the strength defined

between two impurities, with $E_F = 5.48$ eV and $K_F = 1.2 \times 10^8$ cm^{-1}

(136). The effective $|J|$ value of (0.9 ± 0.1)eV has been determined

and is between that of 1.1 eV obtained by Mizuno (134) from NMR studies

and the value of 0.22 eV derived by Flouquet (135) from γ-ray

anisotropic measurements.

An alternative approach can be used to estimate roughly the order

of magnitude of the effective $|J|$ value from V_O as follows: the results

for AgMn alloys show that in this system when impurity concentration

n lies between 630 and 1370 ppm Mn, the RKKY interaction dominates.

From the ESR results for dilute AgMn alloys by Davidov et al (137),

we estimate by the behaviour of the g value that the $nV_O \sim k_B T_K$

condition holds when $n \sim 200$ ppm. Using the above V_O value, the AgMn

Kondo temperature $T_K = 55 \pm 10$ mK has been estimated and is close to

the value 40 mK obtained by Flouquet (135).

This value of T_K gives the effective $|J| \approx (0.27 \pm 0.02)$eV from

$T_K \approx T_F \exp(-1/2 \, |J| N(o))$ (30-34), with $T_F = 6.39 \times 10^4$K and

$N(o) = 0.137$ eV^{-1} (136), which is of the same order as the above

calculated $|J|$ value.

In order to compare the strength V_O of the RKKY interaction of one

kind of magnetic impurity, Mn in this case, in different hosts, the value

of V_O of $\underline{Cu}$Mn, $\underline{Zn}$Mn, and $\underline{Au}$Mn from susceptibility measurements and

of $\underline{Ag}$Mn from this work, along with their effective moment μ_{eff} values

of the Mn atom have been listed in Table 4. Note that where the μ_{eff}

value of $\underline{Zn}$Mn varies widely from different publications. From the general

tendency shown, we conclude that the strength V_O of the RKKY interaction

between two magnetic impurity atoms (Mn) in different hosts increases

as the μ_{eff} decreases. This phenomena can be seen because the

smaller the μ_{eff} of Mn indicates that the stronger interaction exists

between impurity Mn and host electrons, via which the RKKY interaction

acts and, thus, leads to a stronger impurity-impurity interaction.

TABLE 4

Comparison table of the strength of the RKKY interaction V_o

between two Mn atoms and the effective moment μ_{eff} per

Mn atom when Mn is the impurity in alloys of different hosts

Alloy	V_o (RKKY) (erg cm^3)	μ_{eff}(per Mn) (μ_B)
AuMn	2.2×10^{-37} [a]	5.3 [d]
AgMn	6.2×10^{-37} [b]	5.2 [b]
ZnMn	2.2×10^{-36} [c]	$3.6 \sim 4.7$ [e]
CuMn	5×10^{-36} [a]	4.4 [f]

(a) see Ref. 138   (d) see Ref. 139, 140

(b) from this work   (e) see Ref. 5, 141, 142

(c) see Ref. 5   (f) see Ref. 88, 139, 140

Section II. Magnetic Measurements on Some "Dilute" Al-3d Alloys

II-1. Introduction

In the research of dilute alloys, the Anderson model (17) and the s-d

model (7) are well-known and recognized. The magnetic properties of

the dilute alloys will depend on the value of the significant argument:

$\frac{U + 4J}{\pi \Delta}$, later written as $\frac{U}{\pi \Delta}$, where U is the Coulomb interaction

energy of two d electrons on the impurity atom with opposite spin, J is

the intra-atomic exchange integral, and Δ is the width of the virtual

bound energy. The similarity between these two models at the extreme

limits, magnetic (21,45) and non-magnetic, has been observed.

According to the Anderson model, there is a sharp transition between

the magnetic and the non-magnetic states of dilute alloys, and it occurs

at $\frac{U}{\pi \Delta} \approx 1$; but, as pointed out by many authors (46-49), if such a

"phase transition" exists, it cannot be a sharp one, because only a finite,

probably small, number of degrees of freedom will be involved. Doubts

about the adequacy of the Hartree-Fock treatment of Anderson Hamiltonian

have been raised (53), as when the impurity is nearly magnetic the many-

body effects (d-d electron correlation) must be taken into account. A

dynamic extension of the non-magnetic limit of the Anderson model is

suggested by the local spin fluctuation theory which allows for the probability

of a temporary moment occurring even when $\frac{U}{\pi \Delta} < 1$ (41).

In order to investigate this "sharp or smooth" transition between the

magnetic and the non-magnetic states of dilute alloys, the most straight-

forward treatment will be to study a dilute alloy system which is somewhere

in the transition region. The $\underline{Al}$-based alloys are the typical system which belongs to the magnetic limit. For example, the value of $\dfrac{U}{\pi\Delta}$ for $\underline{Al}$Mn is 0.7 (56) to 1.5 (57). Since the basic assumption of the s-d model is on one side (assuming the impurity is magnetic), and the local spin fluctuation theory on the other side, $\underline{Al}$-3d alloys represent a typical case of near magnetism where both approaches should join.

The preliminary observation on the $\underline{Al}$-3d alloy system is the single-peaked behaviour of the impurity resistivity ρ versus the impurity atomic number N_I at 4.2K. This behaviour can be fitted to $\rho \sim \sin^2 \dfrac{N_I \pi}{10}$ derived from the Hartree-Fock approximation of the Anderson model in the non-magnetic limit (143); therefore, usually the $\underline{Al}$-3d alloys are considered to be non-magnetic. The amplitude of the charge pertur- bation around the impurities in Al versus N_I at temperature $T \to 0K$ also possesses a single-peaked distribution, similar to that of the impurity resistivity at $T \to 0K$; however, the impurity resistivity measurements extrapolated to $T \to 0K$ for the well-recognized magnetic $\underline{Cu}$-3d alloy system, for example, have recently been realized to also show a single peaked behaviour (38).

At high temperatures, say 420K, due to the relatively strong temperature-dependence of the impurity resistivity and the charge perturbation of Mn and somewhat smaller of Cr in Al, the behaviours of the impurity resistivity versus N_I become doubly peaked (144-147). This behaviour was regarded as the basic evidence of a spin-split virtual bound state in the Hartree-Fock approximation of the Anderson model when the impurities are magnetic and is displayed in the magnetic, noble metal-3d alloys.

The s-d model provides a reasonable description of the alloys' proper-

ties at temperature T > Kondo temperature T_K, but the available approach

breaks down as T goes lower. The impurity resistivity of Al-3d alloys

at low temperatures can be described by the spin fluctuation theory and

gives a higher Kondo temperature, for example, 530K for AlMn and

1200K for AlCr (148,145). The high temperature results thus suggest

the non-magnetic behaviour at low temperature of Al-based alloys might

be the end-product of the cause of the high Kondo temperatures. In order

to approach this problem, perhaps the best way is to make the magnetic

measurements on the Al-3d alloys for a wide temperature range.

The previous results of the magnetic measurements of the Al-3d alloy

system are rather inconclusive. Aoki and Ohtsuka (149) reported that,

although the susceptibilities of the AlMn, AlCr, and AlV alloys showed a

slight temperature dependence from 1.3K to room temperature, no

significant temperature dependence was observed for the difference in

the susceptibilities between the alloys and the reference Al samples.

Hedgcock and Li (56), on the other hand, reported that from their

susceptibility measurements of AlMn alloys between 2 and 300K,

the impurity susceptibility X(T) can be characterized by the equation

$X(T)/n$ emu/cc at.% Mn $= 13.8 \pm 0.8 \times 10^{-7} - (14 \pm 3 \times 10^{-13})T^2$, where

n is the Mn impurity concentration, and T is the temperature. This will

give a value of T_K in fairly good agreement with the value from resistivity

measurements; however, the susceptibility measurements on AlMn and

AlCr in the liquid state at higher temperatures from 800 to 1150K by

Flynn et al (150) did not show a Curie-Weiss law behaviour.

The above quite diverse results probably occur because of the relatively strong effects from other origins, such as, for example, the susceptibility of the Al host and the crystal field effect; therefore, it makes the evaluation of the contribution from the impurity somewhat ambiguous.

It will be interesting to make a careful measurement of the Al-3d alloys with a wide temperature range, say from 1.4K to the order of room temperature, and compare it with the previous experimental data and different theoretical models; therefore, a series of Al-3d alloys, AlMn, AlCr, and AlV, has been studied through the magnetic measurements and is presented here.

II-2. Experimental Procedures

Two AlMn alloys with respective nominal concentrations n of 700 and 3100 ppm Mn, one AlCr with n of 4000 ppm Cr, and one AlV alloy with n of 600 ppm V were examined. The alloys belong to the FCC structure. All the samples were obtained from Gruner (119) (Hungarian Academy of Sciences) and were in the form of cylinders of about 3mm diameter and 1.5cm long. All samples were cleaned by a solution of 30% HNO_3 and homogenized at 600°C for one hour, then quenched in cold water before measuring.

Since the samples were made outside, the impurity concentrations of the AlMn alloys were checked for reference. The composition of the alloys was monitored by measuring the residual resistance ratio by an apparatus described in Chapter 2. The concentrations of the AlMn alloys have been determined to be 3110 and 705 ppm Mn, which are very close

to the given values of 3100 and 700 ppm Mn. It is thus suggested that the given values of the impurity concentrations of these alloys are reliable.

Measurements were carried out by a force (Faraday) method using a superconducting solenoid (0-50KOe) with separate superconducting gradient field coils in a B.O.C. cryostat; the forces were measured with a Beckman microbalance LM-600. Temperatures were derived from the helium vapour pressure with reference to the standard table from 1.4 to 4.2K, from the reading of an $\underline{Au}$Fe versus chromel thermocouple with a reference junction in liquid helium from 4.2 to 20K and, at higher temperatures, from the reading of a copper-constantan thermocouple with a reference junction in liquid nitrogen.

II-3. Experimental Results and Discussion

Two $\underline{Al}$Mn alloys with respective nominal concentrations n of 700 and 3100 ppm Mn, one $\underline{Al}$Cr alloy with n of 4000 ppm Cr, and one $\underline{Al}$V alloy with n of 600 ppm V were examined. The alloy magnetic isotherms M_{alloy} at several temperatures and the alloy magnetic susceptibilities X_{alloy} from 1.4 to a maximum of 200K have been measured and are plotted in Fig. 36-43. The magnetic isotherm of an Al sample has been also measured at 72K and is plotted in Fig. 44.

The general behaviour of the susceptibilities for these $\underline{Al}$-3d alloys are, as expected, very close to that of Al, X_{Al}, itself (56). The differences between them are just what we are interested in; however, the susceptibilities of the impurities along cannot be obtained by simply subtracting the X_{Al} out of the measured X_{alloy}. There might be
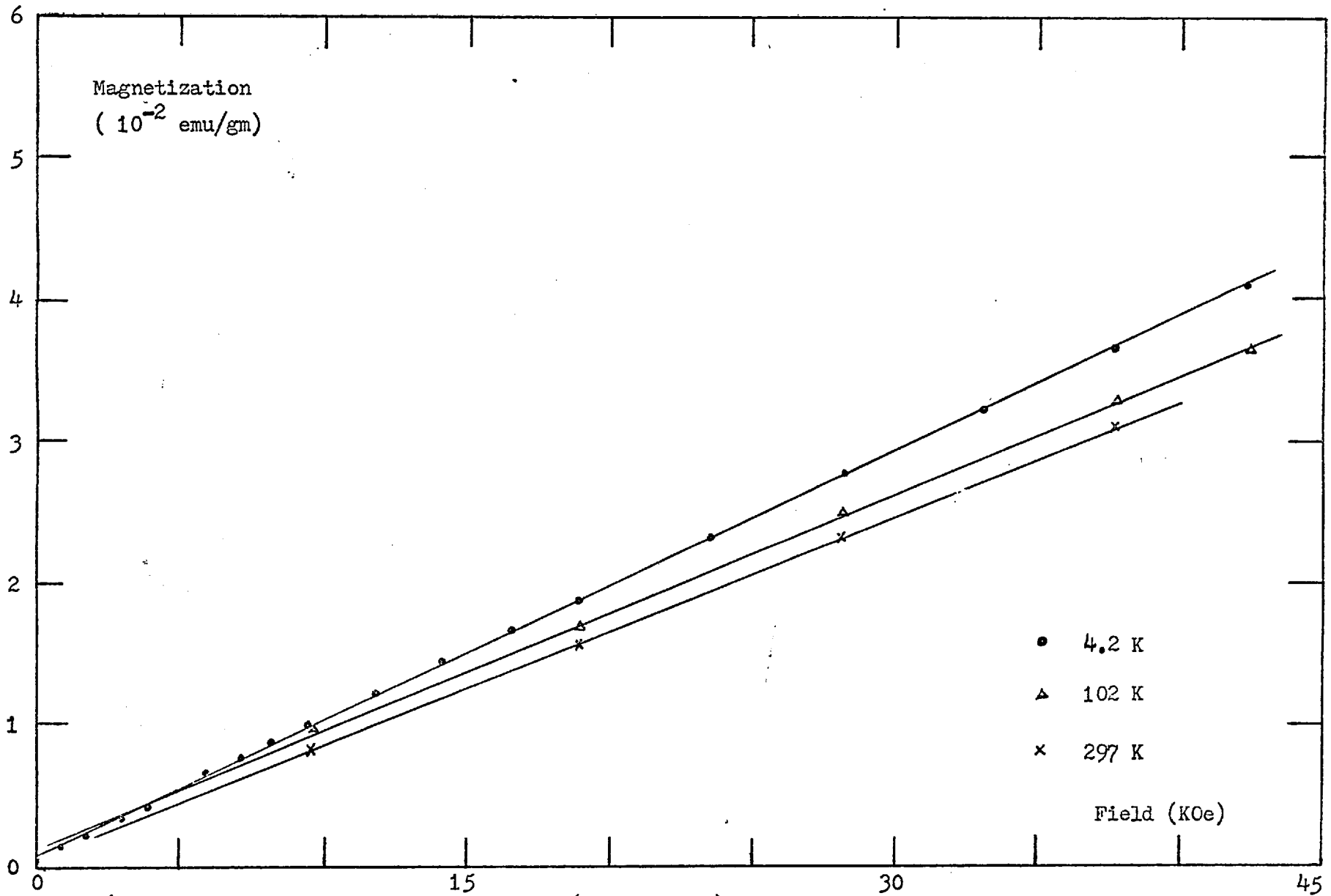
Fig. 36 Magnetization versus Field for AlMn (3100 ppm Mn) alloy
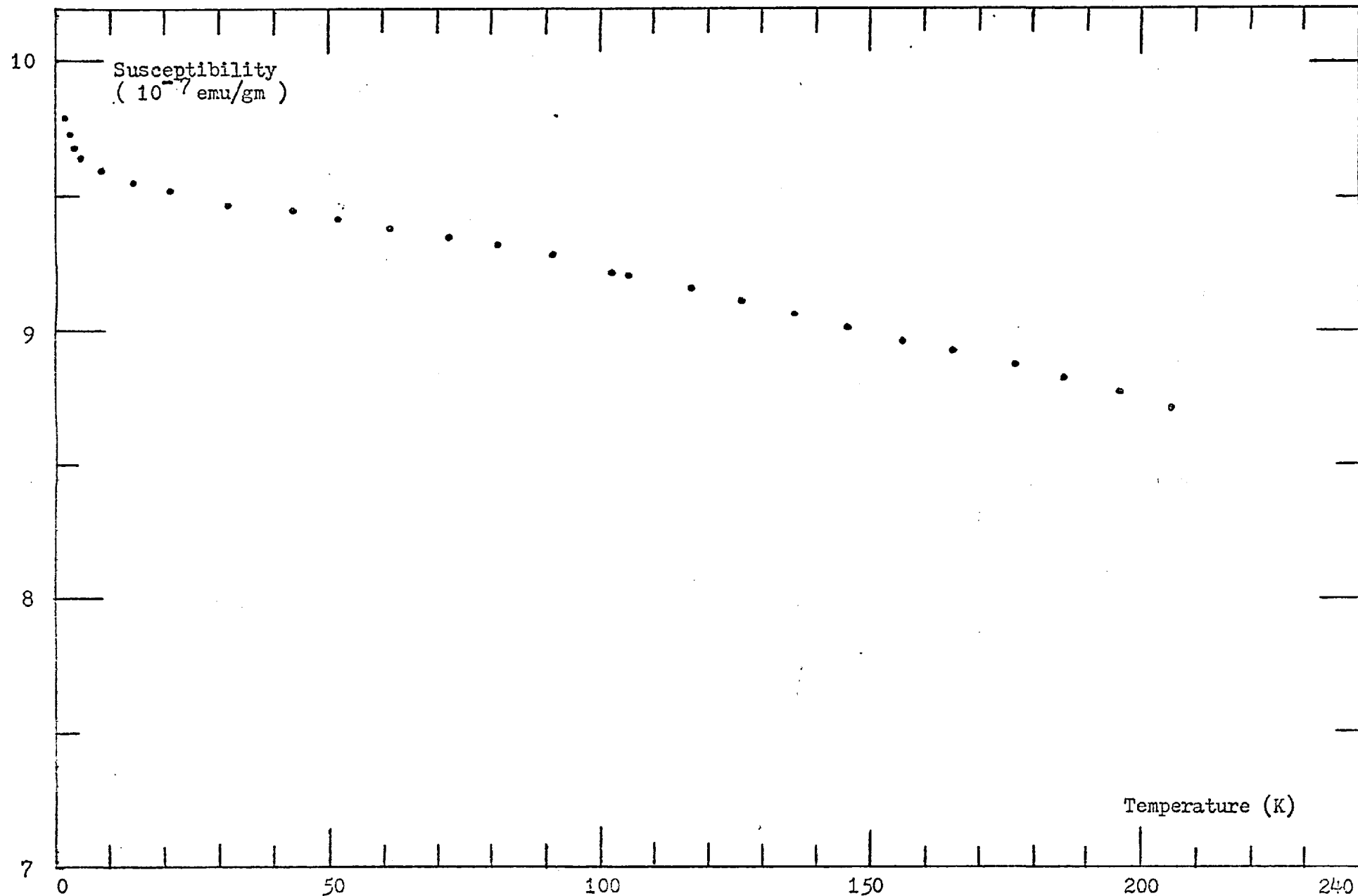
Fig. 37 Susceptibility versus Temperature for A̲l̲Mn (3100 ppm Mn) alloy
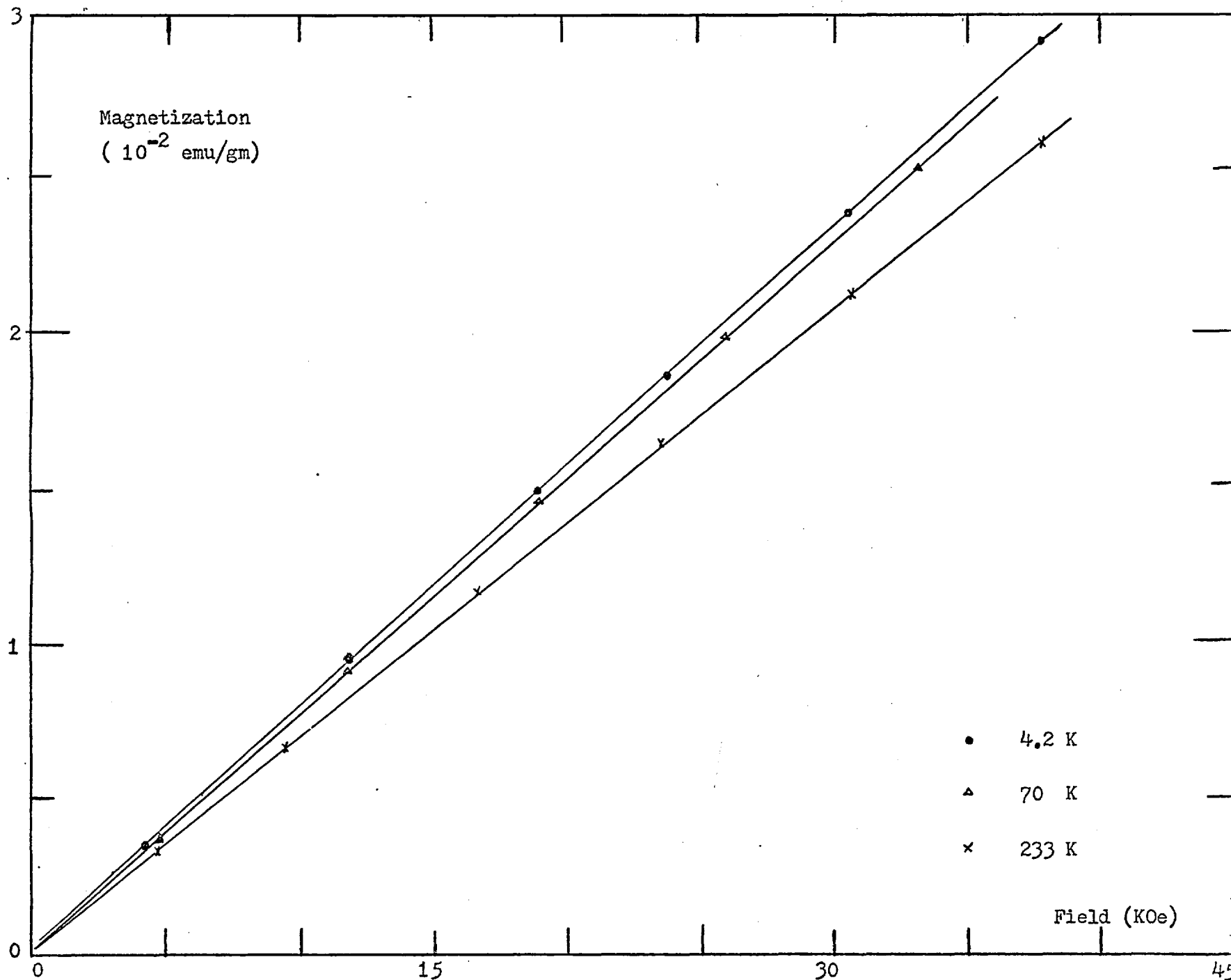
Fig. 38 Magnetization versus Field for AlMn (700 ppm Mn) alloy

Susceptibility (10^{-7} emu/gm)
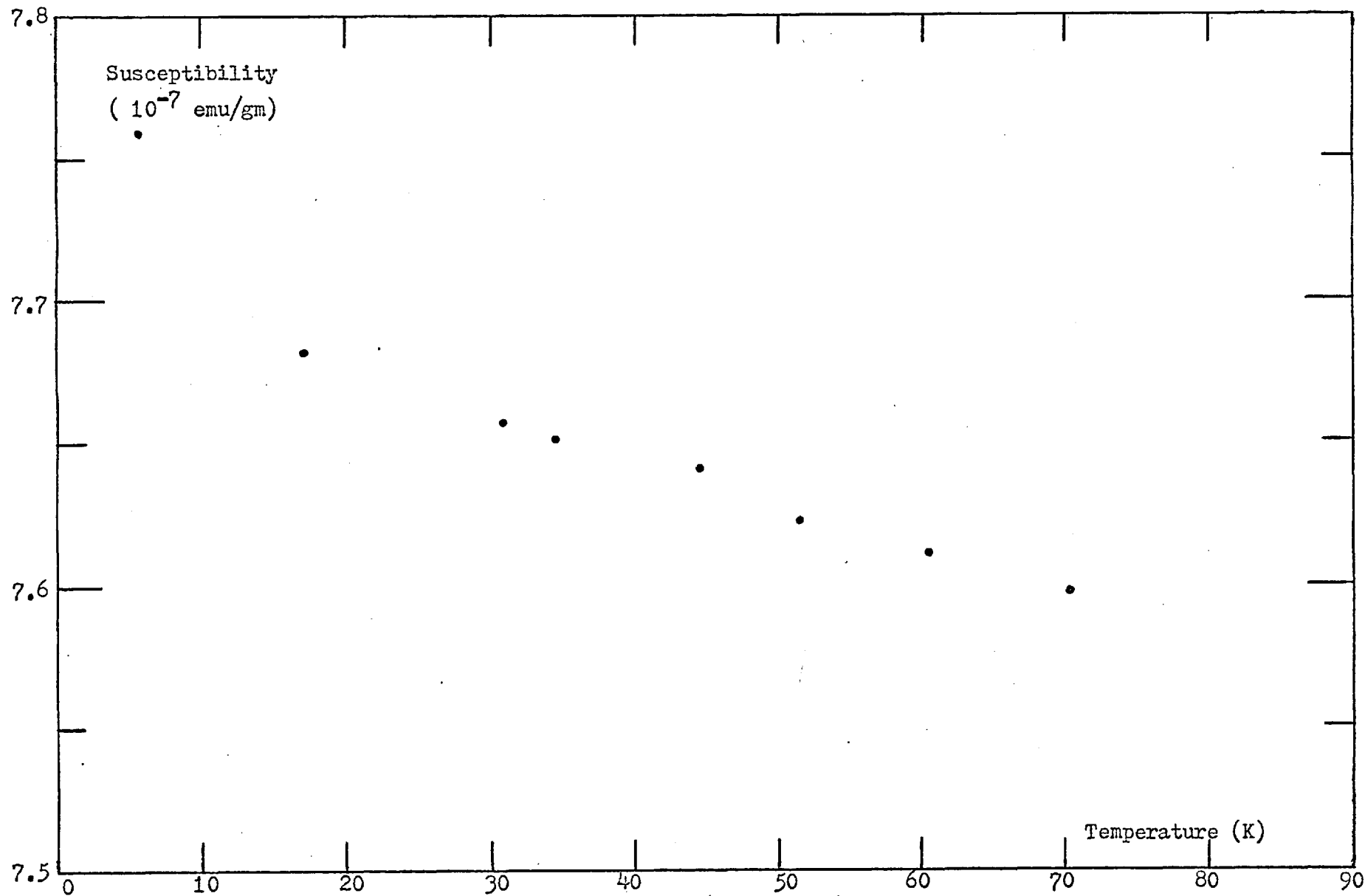
Temperature (K)

Fig. 39 Susceptibility versus Temperature for $\underline{Al}$Mn (700 ppm Mn) alloy
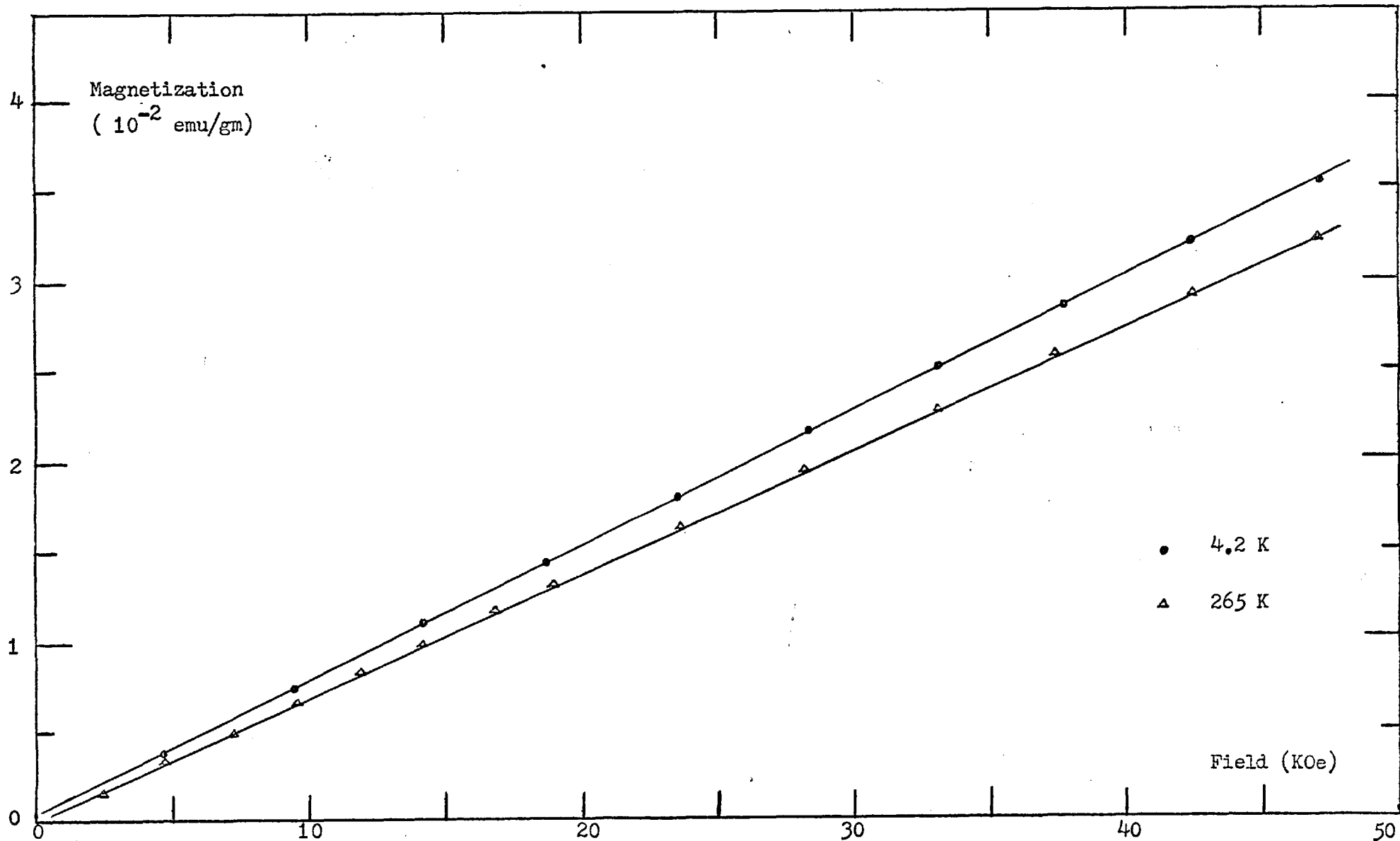
Fig. 40 Magnetization versus Field for AlCr (4000 ppm Cr) alloy
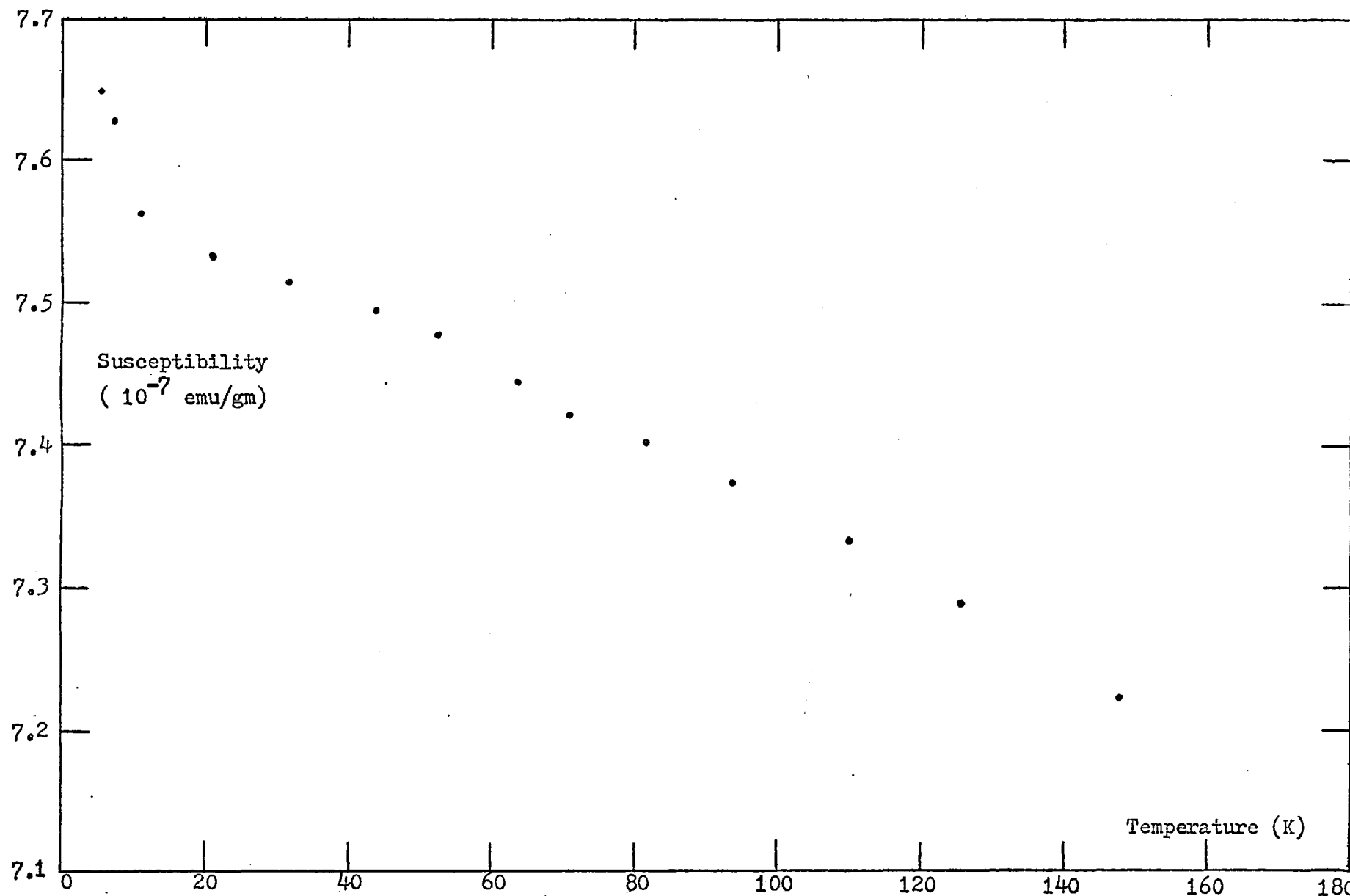
Fig. 41   Susceptibility versus Temperature for AlCr (4000 ppm Cr) alloy
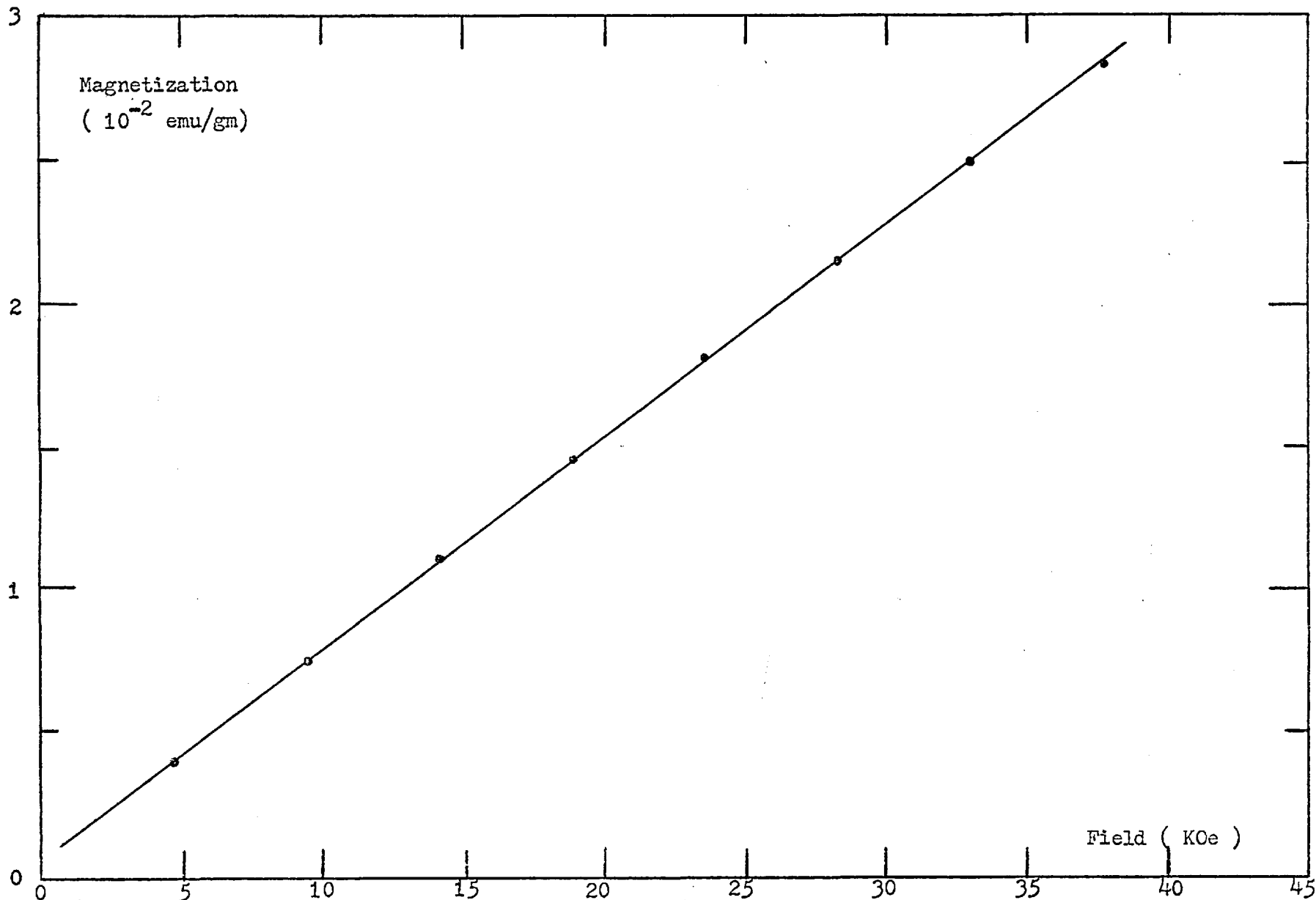
Fig. 42 Magnetization versus Field for <u>Al</u>V (600 ppm V) alloy at 4.2K
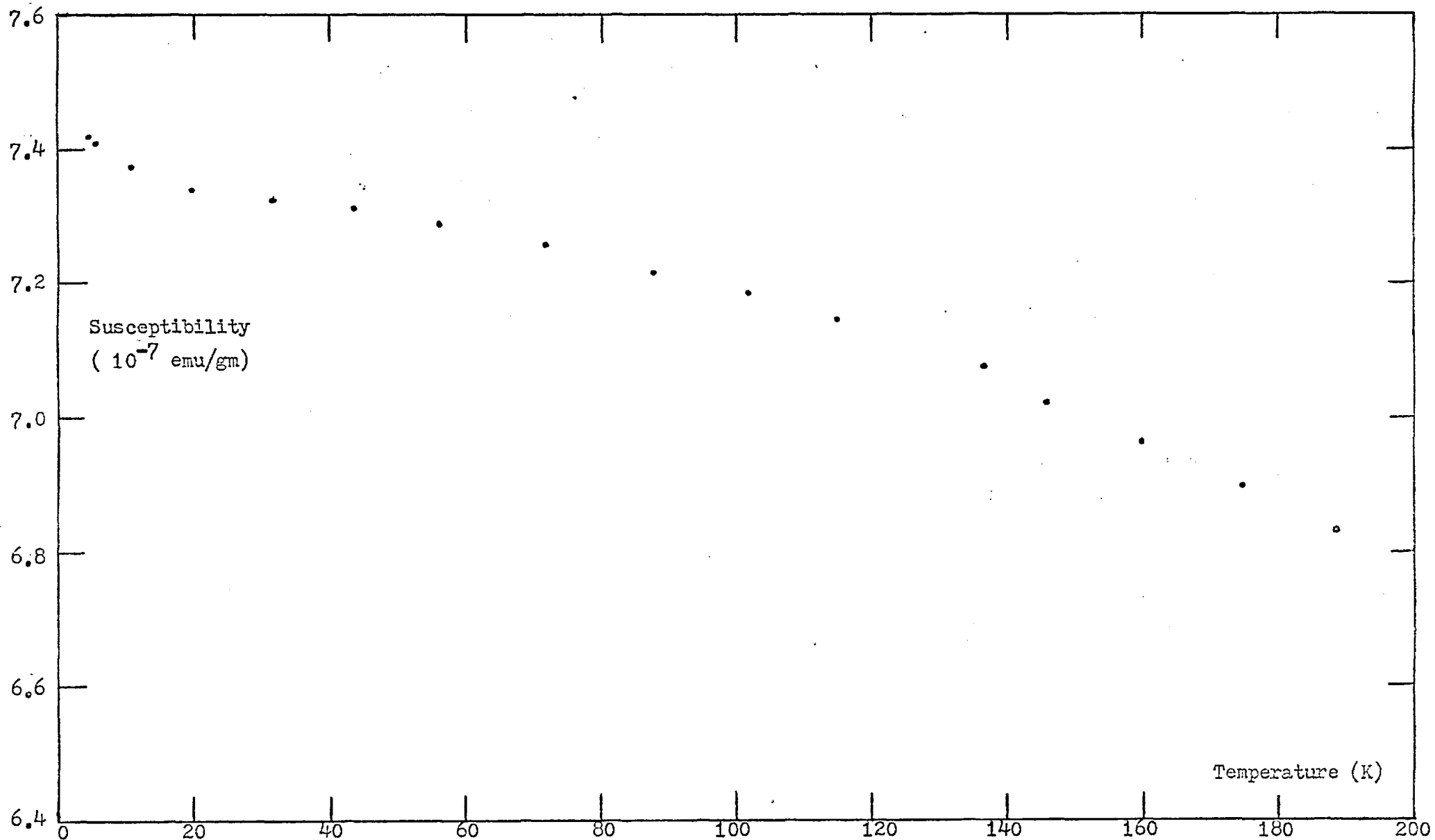
Fig. 43 Susceptibility versus Temperature for $\underline{Al}V$ (600 ppm V) alloy
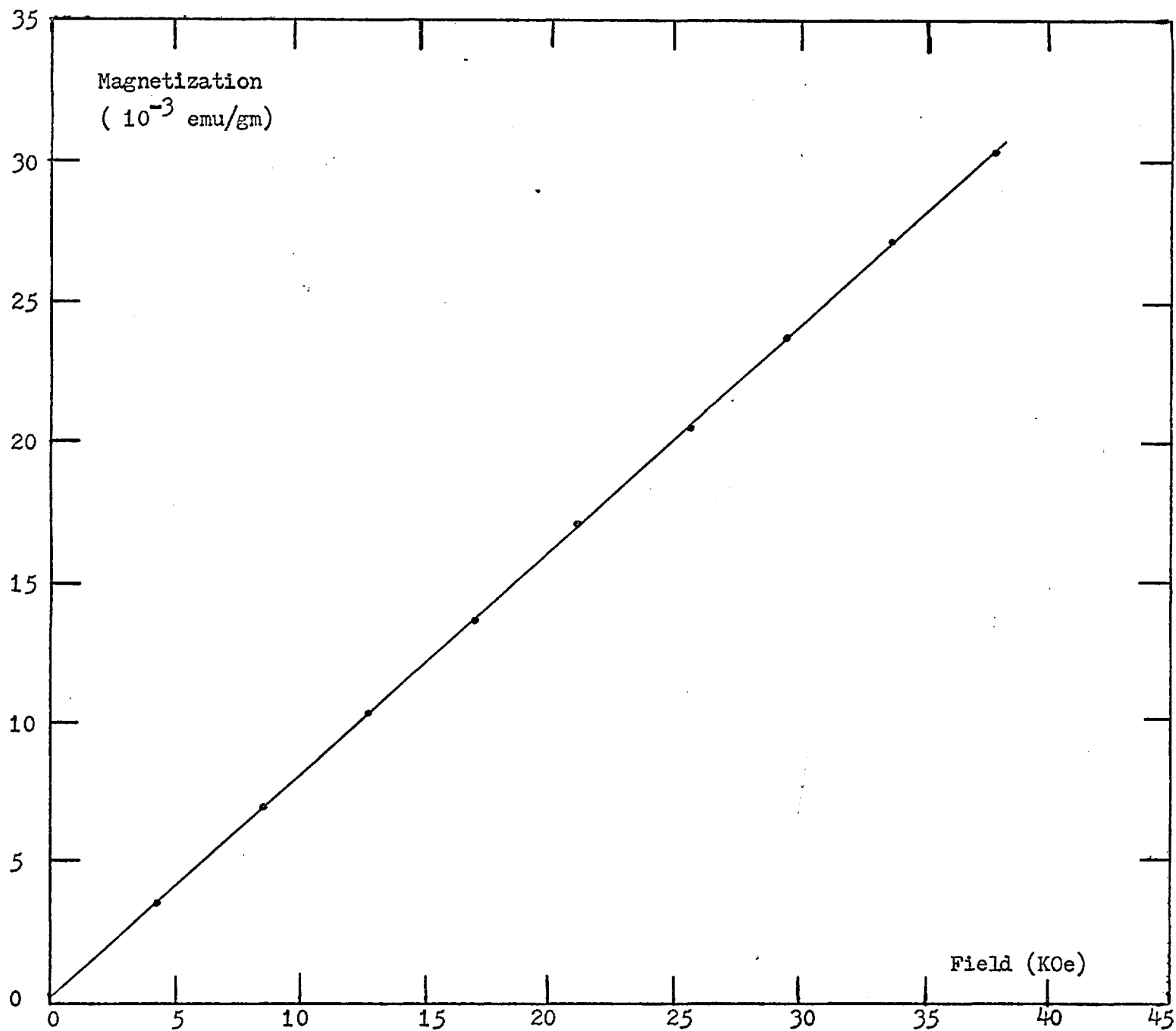
Fig. 44 Magnetization versus Field for Al at 72K

several different reasons, but the first to consider is that the significance of this measured X_{alloy} is still an open question.

The question arises from the appearances of the curvature on all the magnetic isotherms taken at all the temperatures and of all the alloys being considered. Because the effect of the impurities in the Al-based alloys is small itself, this curvature of the magnetic isotherm will affect severely the significance of the results.

The source of this curvature might come from the ferro-impurities contamination in the samples, since even the materials of the alloys to start with are not one-hundred percent pure, and there are some possible surface effects; therefore, an experiment was designed wherein the magnetic isotherm was taken to "high fields" (say 45KOe), so that the possible contaminated ferro-impurities and surface effects will be saturated earlier and will not affect the slope of the magnetic isotherm at "high field" (the Curie temperature of Fe, for example, is at the order of one thousand degrees K); thus, a more reliable value of susceptibility X_{alloy} can be determined from this slope. By proceeding the same way at different temperatures, a set of values of X_{alloy} can be obtained, and the general tendency of the behaviour of the X_{alloy} in relation to temperature will be achieved.

This experimental technique has been applied on the AlMn alloy with n of 3100 ppm Mn. The magnetic isotherms versus field H have been taken at temperatures 1.4, 4.2, 77.4, 150, 219, and 302K and are plotted in Fig. 45 and 46. The curvature on the magnetic isotherm has been reduced as the field increases, but it still persists up to the highest field (45KOe) being applied.
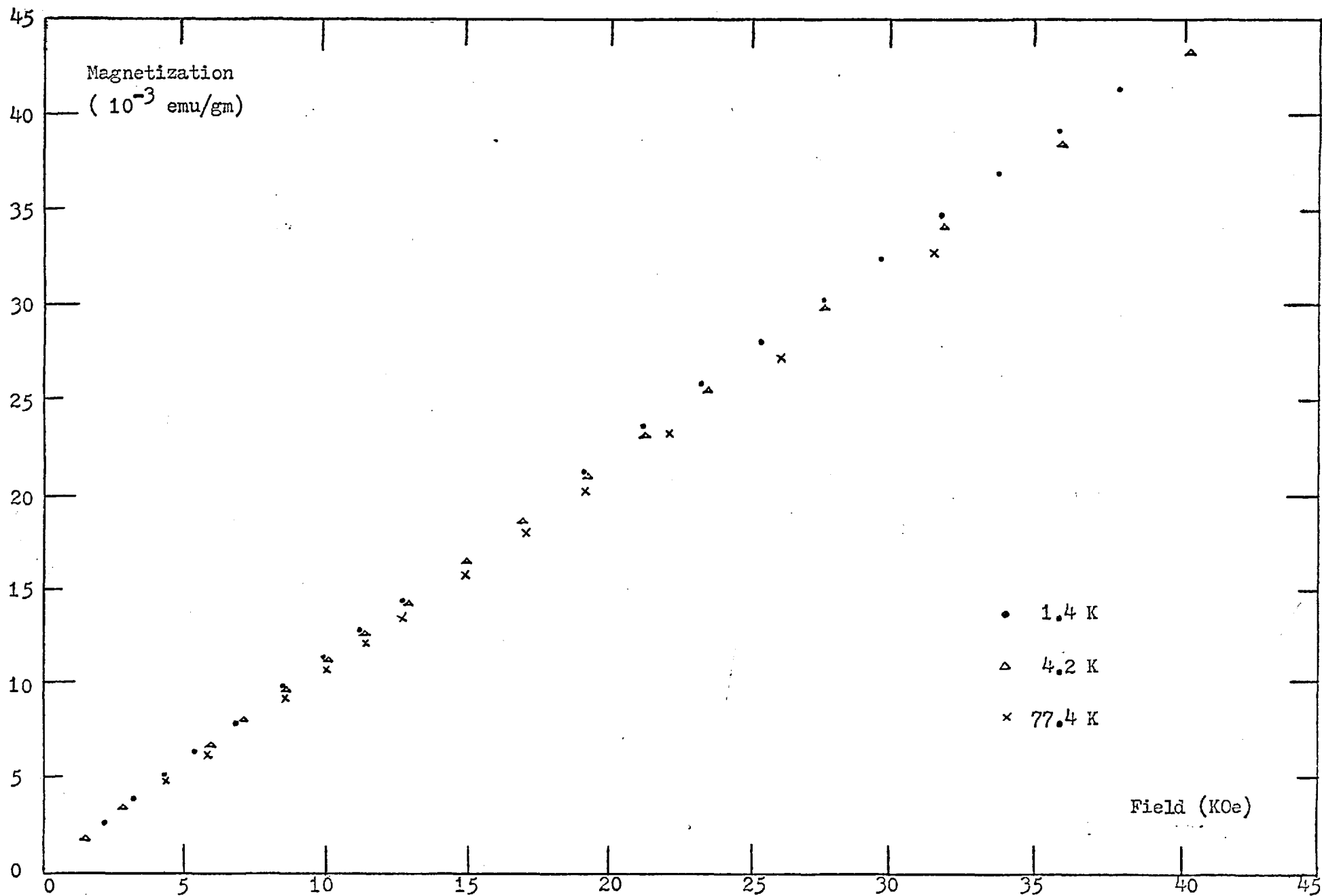
Fig. 45 Magnetization versus Field for AlMn (3100 ppm Mn) alloy at 1.4, 4.2 and 77.4K
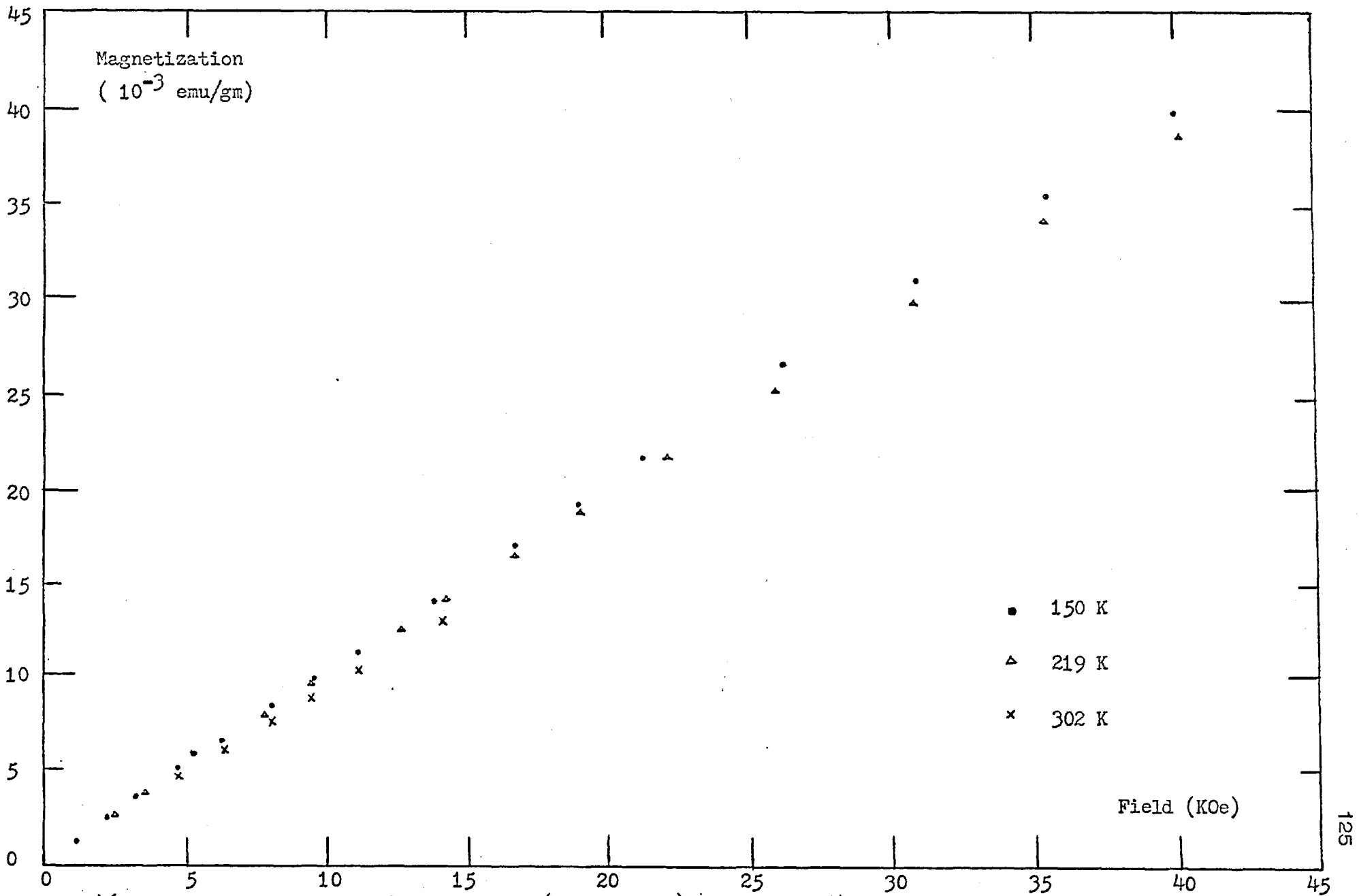
Fig. 46   Magnetization versus Field for AlMn (3100 ppm Mn) alloy at 150, 219 and 302K

The magnetic isotherms versus field of the Al sample is a straight line at "high field" within the experimental range, as has been shown in Fig. 44, where the low field deviations are considered to have come from the ferro-impurities contamination and to have been saturated clearly when the field is over just a few KOe.

If one assumes that the local magnetic moment does exist on the isolated impurity sites of the dilute Al-based alloys within our experimental region, it must be a rather small magnetic moment. Even if we take a possible higher bound of this moment, say $\mu_{eff} = 1 \mu_B$, the magnetic isotherm will deviate from a straight line at our experimental conditions, (say at 150K and 45KOe) to less than one part in ten-thousand, according to the free spin Brillouin function. Such a small deviation from a straight line will be within our experimental uncertainty and cannot be recognized. Therefore, the magnetization of the alloy, which is assumed to be the addition of the Al host and the possible small magnetic moment of the Mn solute atoms should also be a straight line after the possible ferro-impurities and surface effects have been saturated at "high field." But, the curvature of the magnetic isotherm still persists even at a field and a temperature as high as 45KOe and 219K respectively.

These unexpected results have been approached experimentally and also theoretically. Experimentally, any part(s) of the whole series of the experimental apparatus, if it has a defect, will result in misleading collected data; therefore, a list of check-ups from the D.V.M. to the power suppliers was carried out. However, no defect was found. Conclusively, the magnetic isotherms of Al sample and that of the previously

presented Ag sample are all straight lines at "high fields." Therefore,

we would not expcet that the curvature problem of the magnetic isotherms

of Al-based alloys was mainly caused by any defect of the apparatus.

Theoretically, we believe this behaviour might be a result arising

from the impurity-impurity interactions, which will cause the magnetic

isotherm to deviate from the ideal free spin Brillouin function. The

expectation of the straight line of magnetic isotherms under this experi-

mental condition was based on the Brillouin function. Suhl (67) has

shown that the impurity interaction will persist even at very low

concentrations ($T_I < T_K$, where T_I is the measure of average interaction

between solute atoms, and T_K is the Kondo temperature). Our results

might be experimental evidence for this persistency of impurity

interaction.

In order to minimize the effect of the curvatures of the magnetic

isotherms, the extrapolating technique was adapted to find the suscepti-

bilities. The plots of ($\Delta M_{alloy} / \Delta H$) versus (1/H) are shown in

Fig. 47 and 48, for the magnetic isotherms taken at temperatures T =

4.2, 77.4, 150, 209, and 302K. The data points were rather scattered,

and the least square fit technique was used. From the intercepts at

1/H = 0, the alloy susceptibilities X_{alloy} at these temperatures were thus

obtained; and the susceptibility X of the Mn impurity can be obtained by

assuming X to be ($X_{alloy} - X_{Al}$).

In Fig. 49 and 50, the susceptibility X of the Mn impurity versus T and

T^2 have been plotted respectively. The results at the low temperature

range are more ambiguous because of the rapid change of susceptibility

of the Al host; however, at the intermediate temperature, a T^2 dependence
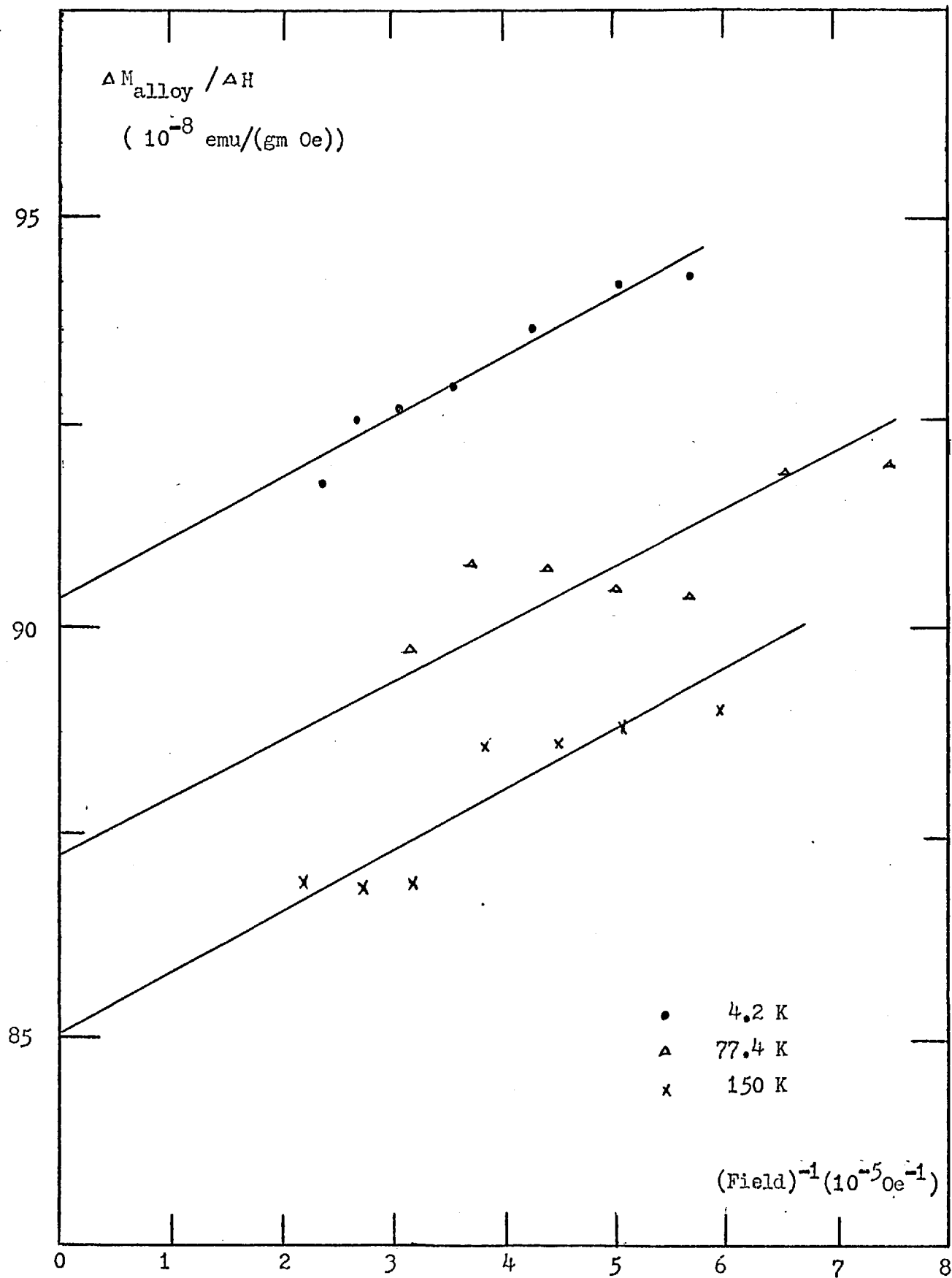
Fig. 47 $\Delta M_{alloy} / \Delta H$ versus (1/H) for $\underline{Al}$Mn (3100 ppm Mn) alloy

Fig. 48 $\Delta M_{alloy} / \Delta H$ versus (1/H) for AlMn (3100 ppm Mn) alloy

Axis label (left): $\Delta M_{alloy} / \Delta H$ (10^{-8} emu/(gm Ce))

Axis label (right): (Field)$^{-1}$(10^{-5}Oe^{-1})

Legend:
● 219 K
△ 302 K
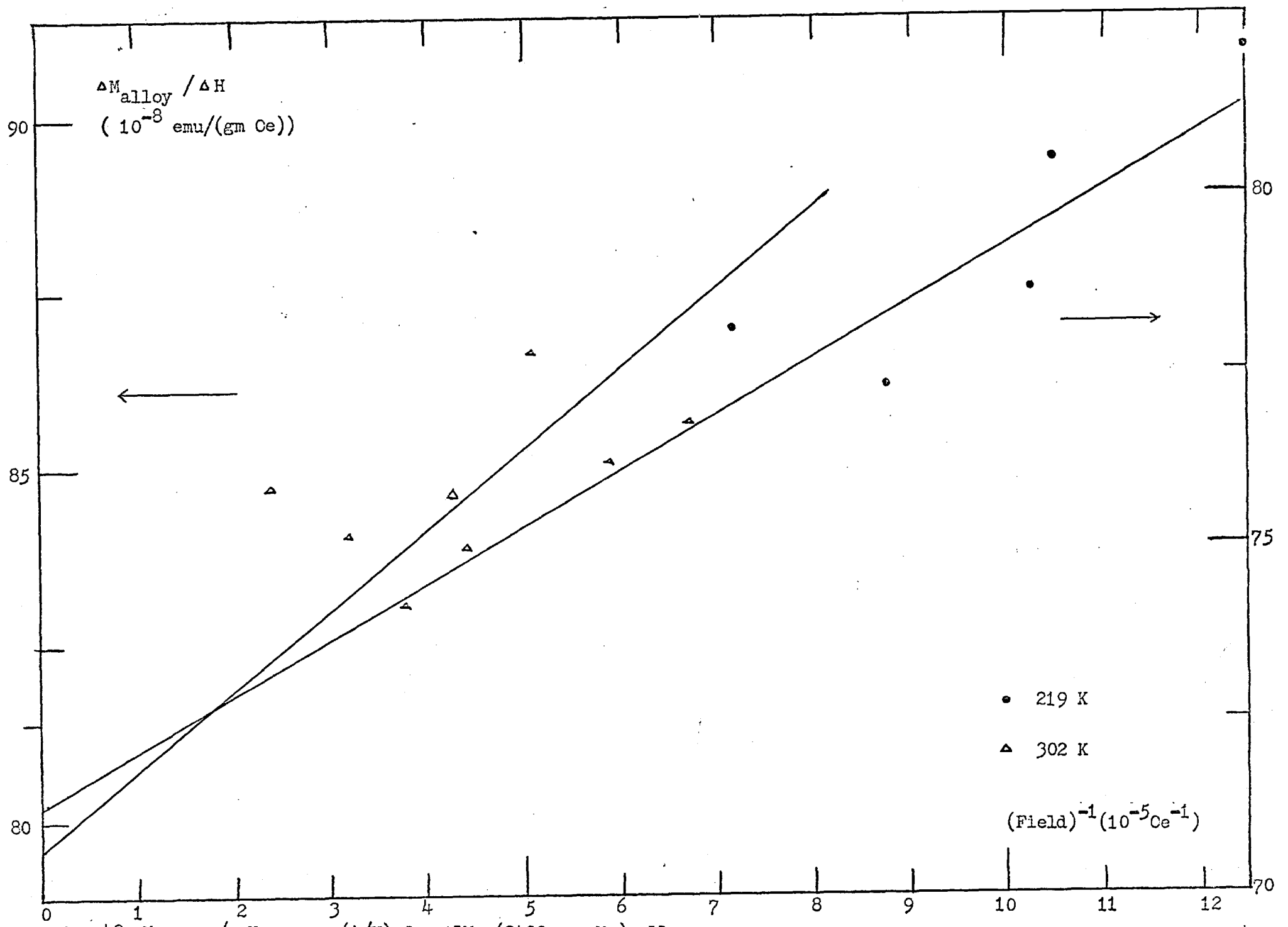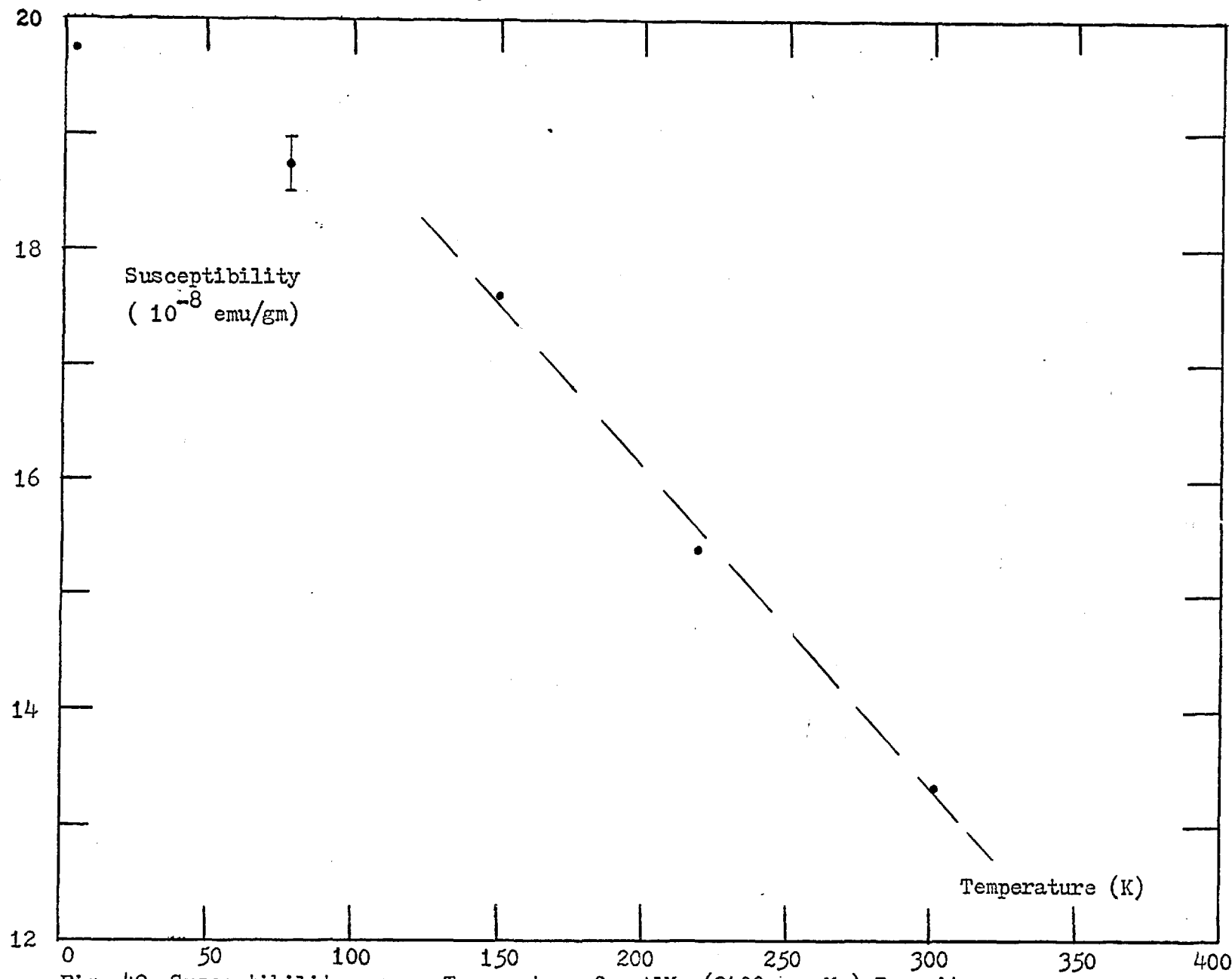
Fig. 49 Susceptibility versus Temperature for AlMn (3100 ppm Mn) Impurity
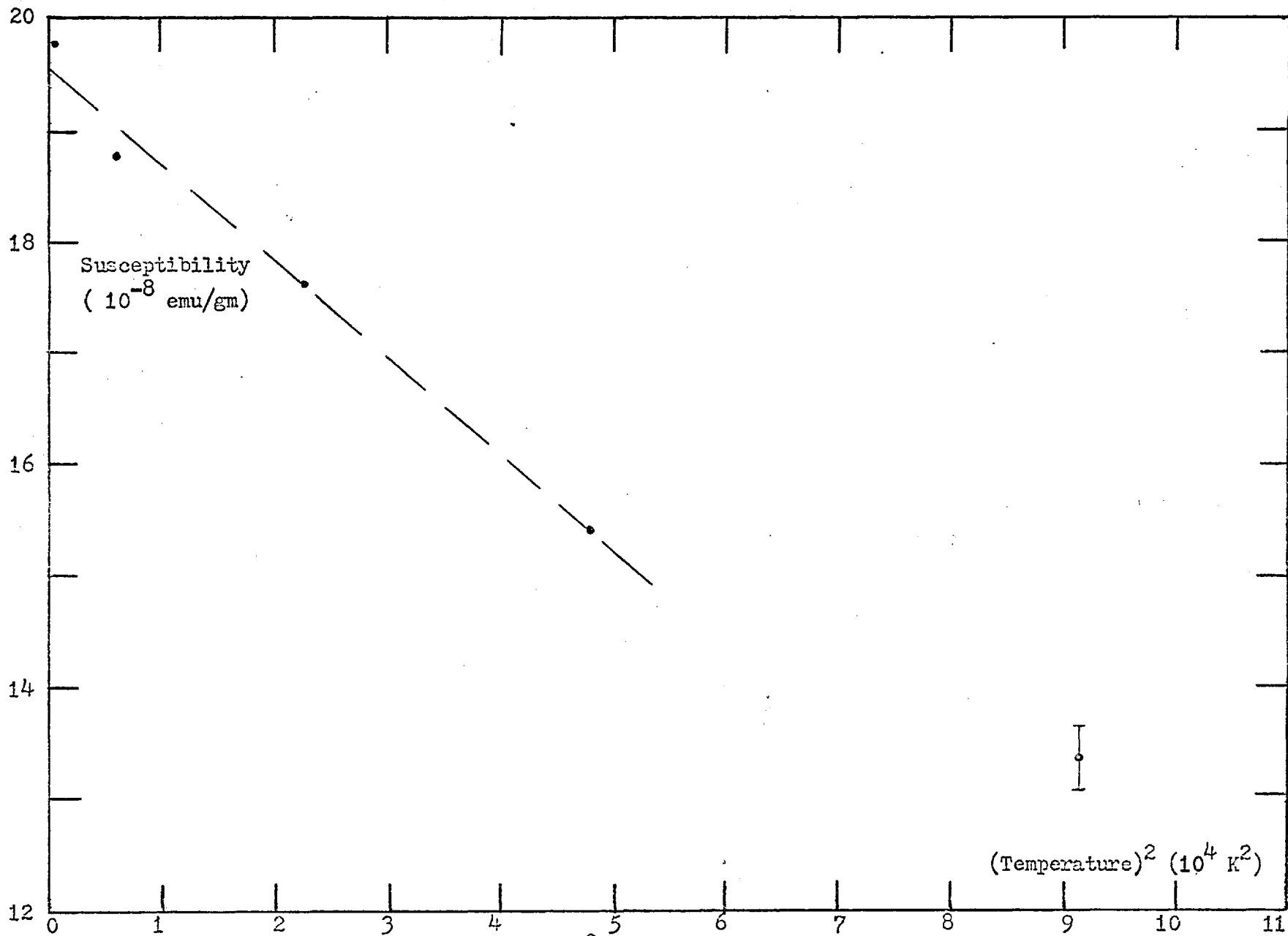
Fig. 50 Susceptibility versus (Temperature)^2 for AlMn (3100 ppm Mn) Impurity

can be found. The reciprocal of the susceptibility (1/X) versus T is plotted in Fig. 51. The curve shows a Curie-Weiss like behaviour at high temperatures and bends upward compared to the Curie-Weiss law as temperatures lower. This is to be expected according to the local spin fluctuation theory. This high-temperature Curie-Weiss behaviour gives a Weiss temperature of $\theta \sim$ 340K and effective moment of 1.1 $\pm$ 0.2 μ_B on each Mn solute atom. This value of moment is, it seems, a little higher than it might be.
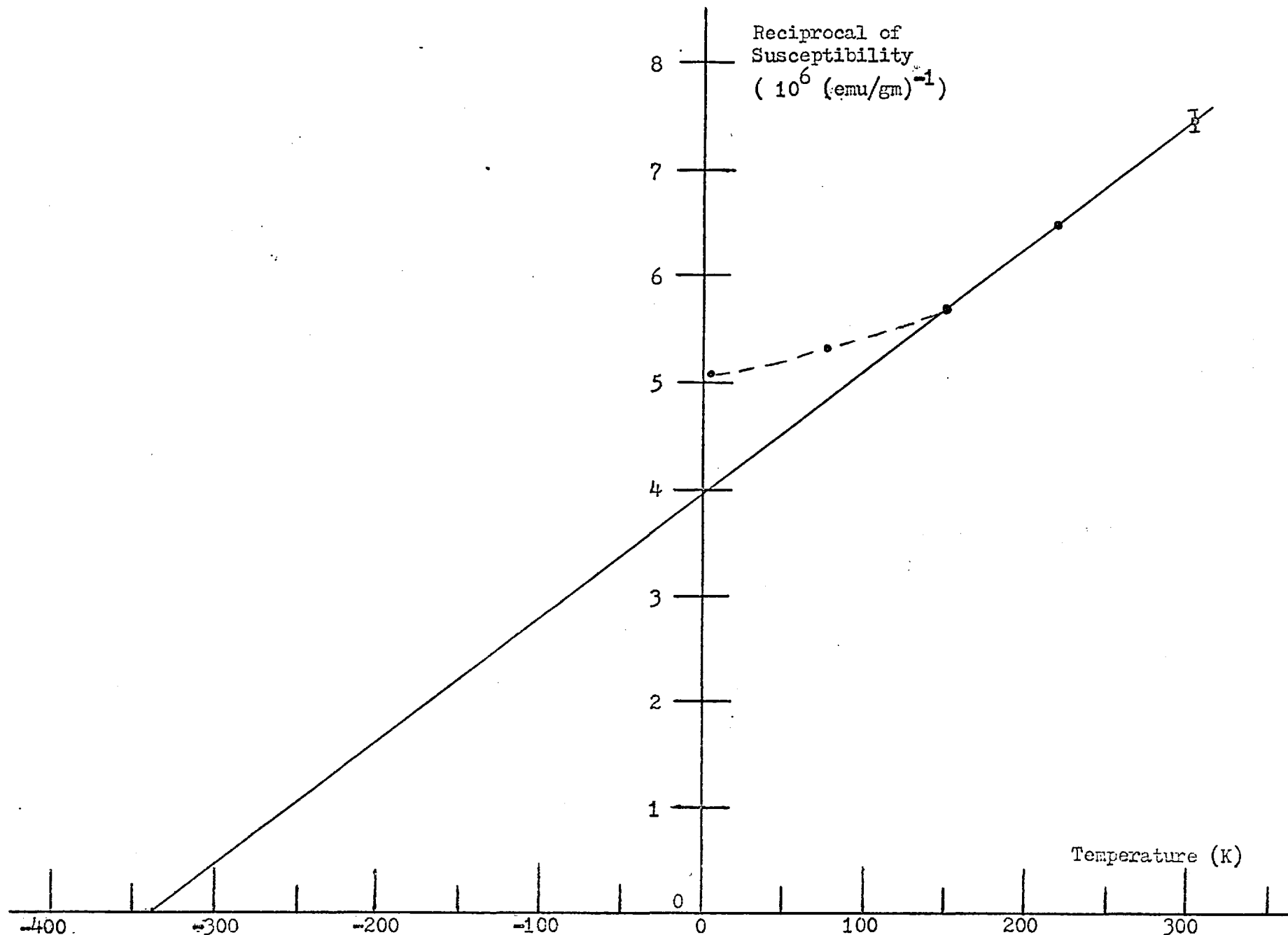
Fig. 51   Reciprocal of Susceptibility versus Temperature for AlMn (3100 ppm Mn) Impurity

CHAPTER 4 MAGNETIC ORDERING IN PtMn AND PtCr ALLOY SYSTEMS

Abstract

A series of PtMn alloys with respective nominal concentrations of 0.09, 2, 3, 5.4, 8, 11, and 12 at.% Mn has been examined magnetically from 1.4 to 70K. The behaviour of the most dilute alloy (0.09 at.% Mn) approximates a free spin system. For other alloys, the paramagnetic-superparamagnetic-magnetic spin glass state transitions have been observed. The temperature T_{max} of the susceptibility maximum follows a linear relation of the impurity concentration n. For alloys of n from 2 to 8 at.% Mn, the Weiss temperature θ follows a linear relation of n, and susceptibility follows the same power law of the reduced temperature (T/n) at high temperatures. The PtMn alloy system is found to have a "region" transition at a critical impurity concentration $n = n_c \sim 9$ at.% Mn. In the $n < n_c$ region, the system is dominated by the indirect RKKY interaction, and when $n_c < n$, the direct impurity interactions become more important. The magnetic phase diagram of the PtMn alloy system has been established.

A series of PtCr alloys with respective nominal concentrations of 7, 10, 14.1, and 17 at.% Cr has been studied. The three alloys with higher impurity concentrations n have been examined by magnetic measurements from 1.4 to 70K. The two PtCr alloys of n = 7 and 10 at.% Cr have been examined by resistivity measurement from 2 to 4.2K, as have the other two PtCr alloys of n = 14.1 and 17 at.% Cr from 1.7 to 150K. A magnetic spin glass state is seen for alloys of n = 14.1 and 17 at.% Cr, and the

giant moments have been observed. The magnetic spin glass state in the

PtCr alloy system is found to begin to stabilize at n ~ 11 at.% Cr.

The magnetic phase diagram of the PtCr alloy system has been

established.

From the results of PtMn and PtCr alloy systems in combination

with the data of Co and Fe as impurities in a Pt host, a comprehensive

magnetic phase diagram of the Pt-3d alloy systems has been

established.

Section I. Introduction

In the extremely dilute alloys, the impurities are mainly non-interacting, and the single-impurity Kondo effect (7) dominates. As the impurity concentration increases, the long-range indirect Ruderman-Kittel-Kasuya-Yosida (RKKY) interaction (24-26) between impurities will begin to dominate. Even as the temperature is lowered in zero external field, the impurity spins "freeze out" or become "locked" in random directions with no long-range magnetic ordering. The freezing occurs in a certain kind of alloy, at a well-defined impurity concentration n dependent temperature $T_0(n)$. Above this T_0, the alloy behaviour approximates the Curie-Weiss law. For this region, the thermodynamic parameters will scale as universal functions of (T/n) and (H/n), where T is the temperature, and H is the field, and the freezing temperature is a function of n (85). If the impurity concentration increases further, the scaling laws will be broken down. Because the short range correlations are becoming more important;and the interaction between the spin oscillates in sign according to distance, there will be a ground state with the spins aligned in definite directions, even if these directions appear to be at random, these non-dilute alloys, when there is a random freezing at a distinct temperature of impurity moments, give rise to a sharp peak in the low field susceptibility and a sudden splitting of the Mössbauer spectrum, along with remanence, irreversibility and relaxation. These phenomena happened at the critical temperature because the existence of these preferred directions affect the orientation of the spins (151-153). These states of the non-dilute alloys are termed as magnetic spin glass (90) and/or mictomagnetic (91) state.

In order to study the wide variety of properties of the magnetic spin glass/mictomagnetic systems, it is natural to start with the less-complicated alloys of simple host materials with no partly-filled d or f shells. The alloys belonging to this category, such as $\underline{Au}Cr$, $\underline{Au}Mn$, $\underline{Au}Fe$, $\underline{Ag}Mn$, and $\underline{Cu}Mn$ have been studied extensively.

Alloys of binary combinations of transition metals can be classified as simple and enhanced transition hosts. In simple transition hosts, where there is no evidence for significant exchange enhancement, alloys in such simple transition hosts such as in Rh (97-99), for example, require a sufficiently large concentration of magnetic impurity before magnetic spin glass behaviour manifests itself. Below this impurity concentration the paramagnetic spin fluctuations are present without any evidence of a region where ferromagnetism is stabilized, and the Rh-3d alloy system has been studied extensively.

In enhanced transition host Pd, for example, where the low field susceptibility of alloys is significantly different from what has been estimated from the electronic specific heat (101),NMR (102), and Mössbauer techniques (103), sometimes a strong tendency towards "giant moment" exists even at low impurity concentrations (100). The implication of this is that clearly the giant moment arises from a long-range polarization of the host metal, and this has been verified by the direct neutron diffraction experiments on $\underline{Pd}Fe$ (104). If Mn, Fe, Co, or Ni as the impurity is dissolved in Pd, the room temperature susceptibility of the alloy is larger than that of pure Pd, while most other elements of solute, including Cr, bring about a smaller susceptibility. From this observation,

Gerstenberg (154) proposed that Mn, Fe, Co, and Ni retain their d

electrons, while the other elements lose their electrons (or at least

partly so) when dissolved in Pd. But, the latter effect (a decrease of the

susceptibility) is not caused by a decrease in electron density at Fermi

level $n(E_F)$, as the Pd d-band is filled by these electrons, because

the specific heat increases by alloying Pd with Cr (155); it might be

caused by a negative polarization of the Pd atoms surrounding the Cr

atoms (68). At low temperatures the difference between Mn, Fe, Co,

Ni, and Cr becomes more pronounced. PdFe alloys are long-range

ferromagnetically ordered, even at quite low concentrations (at very low

Fe concentrations there is evidence for the usual magnetic spin glass

phase of good moment systems (118), like CuMn and AuFe) featuring

"giant moments" due to the strong exchange enhancement of the host

and the consequent positive polarization of the conduction band. At

higher Fe concentrations the contribution of the Pd d-band polarization

to the moment per ion atom falls, but the d-d coupling of Fe nearest

neighbors remains ferromagnetic to more than 50% Fe. Qualitatively,

PdCo alloys have behaviour similar to PdFe alloys. In contrast, PdMn

is also giant moment ferromagnetically ordered at low concentrations,

but on raising the Mn concentration (more than about 5 at.% Mn) as

Mn-Mn nearest neighbor antiferromagnetic couplings (68) become more

important, the alloy behaves as magnetic spin glass (69); and, in PdMn

the strong interaction between the impurities via the strong polarized Pd-

4d band lead to higher ordering temperatures for low concentrations. This

behaviour of PdMn is shown in its magnetic phase diagram, Fig. 16.

Qualitatively, the properties of dilute PdCr alloys are very similar to

those of dilute $\underline{Pd}Ni$ alloys, both show an enhanced Pauli paramagnetism.

For concentrations below 2.3 at.% Ni, the $\underline{Pd}Ni$ alloys show the tendency

of local moment behaviour, and the temperature dependence becomes

larger. Above 2.3 at.% Ni, the $\underline{Pd}Ni$ alloys are ferromagnetically

ordered (156, 157). For $\underline{Pd}Cr$ alloys, where the concentrations need to

be higher than 7 at.% Cr, a magnetic ordering occurs similar to the

$\underline{Cu}Mn$ alloys (158,159). For dilute n ∿ 1 at.%, heavy rare-earth alloys

of the $\underline{Pd}R$ system where R = Ce, Pr, Nd, Sm, Eu, Gd, Tb, Dy, Ho, Er,

Tm, Yb, Lu, or Y, the magnetic moment of the rare-earth ion is found

to be close to its free-ion value. The susceptibility can be fitted to a

Curie-Weiss law with a Weiss temperature of less than $\pm$ 3K (160). The

magnetic phase diagram of Pd alloys with 3 d transition impurities is

plotted in Fig. 52.

The transition metal host Pt, in respect to the magnitude of the

exchange enhancement, can be classified as intermediate, for example,

between Rh and Pd, the exchange enhancement factor is about 3.8 for Pt

as compared to 9.4 for Pd (112,163). The $\underline{Pt}Fe$ alloys (82) appear to

show similar behaviour as that of $\underline{Pd}Fe$ alloys with a value of T_K ∿ 0.4K;

in the case for the dilute limit, magnetic spin glass behaviour is then

stabilized over a fairly narrow impurity concentration region before the

onset of the long range ferromagnetism. The magnetic moment per

dissolved atom as been found to be very large at very low concentrations.

This giant moment is also considered to be induced in the surrounding

matrix as in a Pd host (164). The $\underline{Pt}Co$ alloys are also ferromagnetic

down to a very low concentration (0.06 ∿ 0.8 at.% Co) (96,165) with a

similar behaviour to the $\underline{Pt}Fe$ alloy.
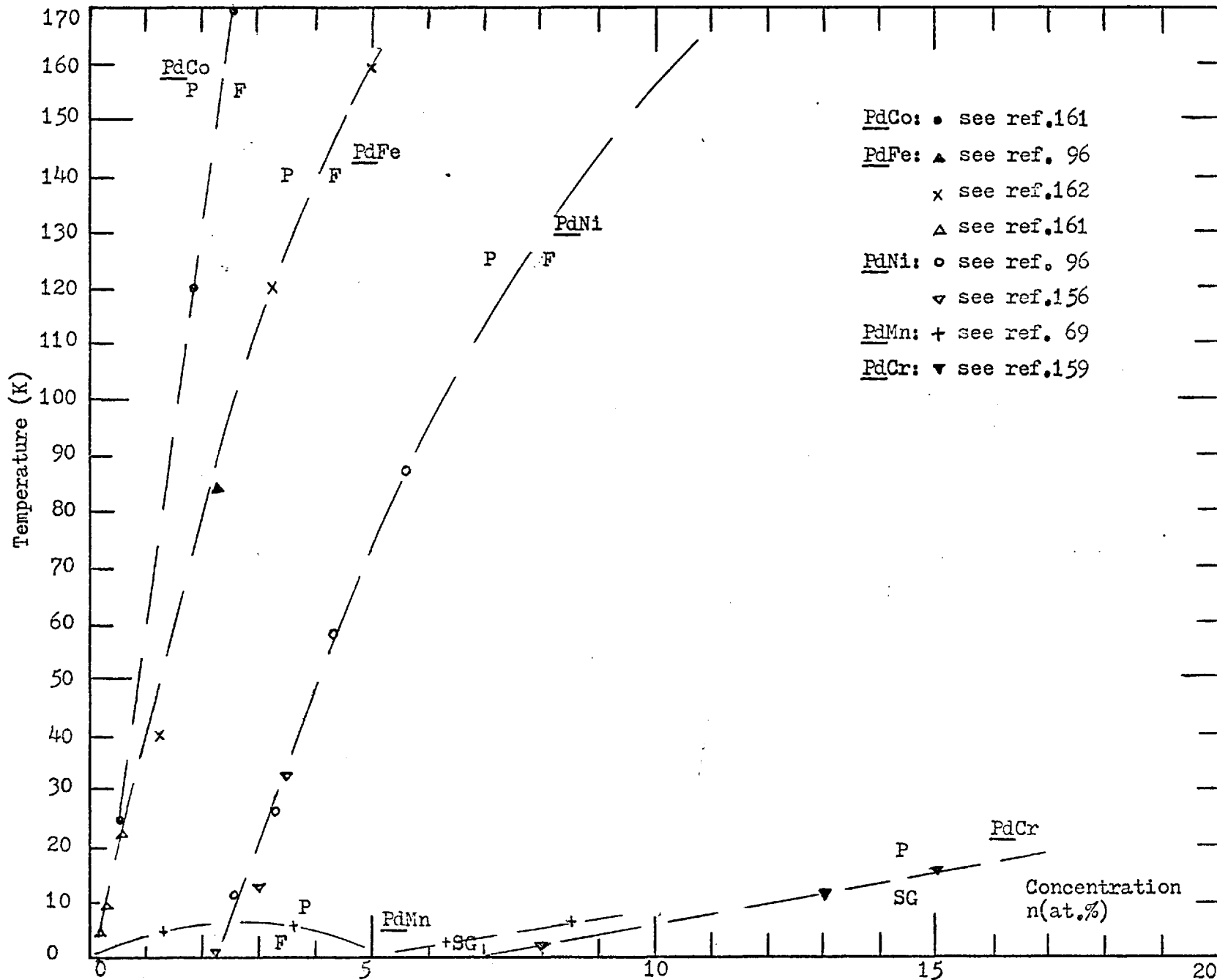
Fig. 52 Magnetic Phase Diagram for Pd-3d alloy systems; P:Paramagnetic, F:Ferromagnetic,
SG:S in G ass ⁺ te

The significantly different behaviours of the Mn atoms as an impurity in the simple transition host Rh, for example, and in the strongly enhanced transition host Pd, for example, interested us in making a detailed investigation of the PtMn alloy system, since the exchange enhancement of Pt lies in between that of Rh and Pd. The pronounced behaviour of PdMn alloys in the strong interaction between the impurities via the strongly polarized Pd 4d band leads to higher ordering temperatures for low concentrations; and, as raising the Mn concentration as the Mn-Mn nearest neighbor antiferromagnetic couplings becomes more important, the alloy behaves as magnetic spin glass.

In order to study the PtMn alloy system, first of all we should examine the interaction between Mn atoms in a Pt host. Some information can be obtained from the data on ordered intermetallic compounds, Mn_3Pt, $MnPt$, and $MnPt_3$ by Kren et al (166) through diffraction methods. The $MnPt_3$ compound is ferromagnetic with a Curie temperature at about 425K (166,167). The MnPt compound is antiferromagnetic with a Neel temperature at about 975K (166); and the Mn_3Pt compound is also anti-ferromagnetic of triangular and collinear structures with a Neel temperature at about 475K (166,168). The simple antiferromagnetic and ferromagnetic structures are produced by the nearest and next-nearest neighbor Mn-Mn interactions, which are sensitive to the inter-atomic distances. The nearest neighbor interaction constant J_1 is negative, while the next nearest neighbor interaction constant J_2 is positive or negative, depending on the interatomic separation. The triangular and collinear phase structures of the Mn_3Pt undergo a first-order transformation to each other at an initial value of the lattice

parameter a, at which J_2 changes sign, i.e. for a < a(critical), J_2 > 0

and for a > a(critical), J_2 < 0 (166).

By comparing the above results of the ordered phases of Mn-Pt

systems with the totally ferromagnetic phase of Fe_3Pt, FePt, CoPt,

and $CoPt_3$ ordered compounds (169) at low temperatures, the possibility

of the disordered PtMn alloy system having a magnetic spin glass state

is foreseen.

The most comprehensive work carried out previously is that by

Miyako, Morishita, and Watanabe (170). They measured the PtMn alloys

with concentrations of 0.47, 1.58, 6.07, and 12.6 at.% Mn and from 1.5

to 300K; however, they did not draw any conclusive statement outside

of presenting the experimental data. Hence, in order to clarify the

behaviours of the PtMn alloy system, an extensive study has been carried

out on this system and is presented here.

In order to study the behaviour of the PtCr alloy system, the data

of the ordered intermetallic compounds will be looked at first. The

ordered intermetallic compound of CrPt is antiferromagnetic, and that

of $CrPt_3$ is ferromagnetic at low temperatures (171); therefore, this

result suggests that the possibility of a magnetic spin glass state in the

disordered PtCr alloy system might exist. The previous works on PtCr

alloys by Nagasawa (172) (0.5 to 3.5 at.% Cr), Van Dam (159) (0.5 to

0.9 at.% Cr), Stan et al (173) (0.5 to 3 at.% Cr), and Roshko and Williams

(174) (5 to 12 at.% Cr) all draw the same conclusion---there is no evidence

of the magnetic spin glass state existing in the PtCr alloy system down

to 1.5K.

The results on ordered intermetallic compounds of CrPt suggest the possibility of a magnetic spin glass state existing, and the results of the similar alloy system, PdCr, offer the hint that if a magnetic spin glass state does exist in the PtCr alloy system, it should start at a rather high concentration of Cr. Since the solubility of Cr in a Pt host forming disordered PtCr alloys is about 19 at.% Cr (121,122) despite the previous results on PtCr alloys up to 12 at.% Cr which give no evidence of the magnetic spin glass state existing, there is still some room left to put more Cr into the Pt host to make a further investigation. Hence, a series of PtCr alloys with concentrations as high as 17 at.% Cr has been examined and is presented here.

A series of PtMn alloys with respective nominal concentrations of 0.09, 2, 3, 5.4, 8, 11, and 12 at.% Mn were made. Another series of PtCr alloys with respective nominal concentrations of 7, 10, 14.1, and 17 at.% Cr were made. Both the PtMn and the PtCr alloys belong to the FCC structure. The starting materials were 99.99% pure Pt from Johnson Matthey Ltd. and 99.99% pure Mn and 99.99% pure Cr from Koch-Light Labs. Ltd. The solubilities when putting Mn and Cr into Pt to form disordered alloys are about 17 and 19 at.% respectively (121,122) ; therefore, no special technique is needed to make the samples. All samples were made in an arc furnace within which was a circular cavity on a water cooled copper hearth filled with two-thirds atmosphere argon. The alloys were melted, turned over, and remelted several times, and then formed into short cylinders of about 3 mm diameter for magnetic measurements, and into thin long wires of about 0.8mm diameter for electrical resistivity measurements, either by the casting method or by stretching through iron-free tools. All samples were cleaned by an aqua regia solution and homogenized in a vacuum at 1000°C for about five hours, then quenched in cold water before measuring.

Magnetic measurements were carried out by a force (Faraday) method using a superconducting solenoid (0-50KOe) with separate superconducting gradient field coils in a B.O.C. cryostat; the forces were measured with a Beckman microbalance LM-600. Temperatures were derived from the helium vapour pressure with reference to the standard table from 1.4 to 4.2K, from the resistance of an Allen Bradley carbon resistor from 4.2 to 25K and at higher temperatures from the readings of a copper-constantan thermocouple with a reference junction in liquid nitrogen.

Electrical resistivity measurements were made using an apparatus

utilizing the standard four-terminal D.C. technique and set in the standard

two-layer glass dewar (130). The sample(s) and a standard resistor are

connected in series; by switching back and forth, the effect of drifting

currents and thermal emf's could be reduced. The current is supplied

by a Tinsley regulated current supply 5753, and is obtained by the

potential drop across the standard resistor. The potential drops across

the standard resistor, and the sample(s) are measured by a potentiometer.

Temperatures were derived from the helium vapour pressure with

reference to the standard table from 1.6 to 4.2K; from the reading of

an AuFe-chromel thermocouple with a reference junction in liquid helium

and,(at higher temperatures), from the reading of a copper-constantan

thermocouple with a reference junction in liquid nitrogen.

Section III.   Results and Discussion

A. The PtMn Alloy System

A series of PtMn alloys with respective nominal concentrations of

0.09, 2, 3, 5.4, 8, 11, and 12 at.% Mn has been examined magnetically

from 1.4 to 70K.

The magnetization M and the magnetic susceptibility X of the Mn

solute are assumed to be $(M_{alloy} - M_{Pt})$ and $(X_{alloy} - X_{Pt})$ respectively,

where M_{alloy} and X_{alloy} are respectively the magnetization and the

susceptibility of the alloy, and M_{Pt} and X_{Pt} are that of the host Pt. The

numerical values of X_{Pt} are taken from that of Van Dam (159).

For the most dilute PtMn alloy with impurity concentration n of 0.09

at.% Mn, the magnetic isotherms M taken at temperatures T = 1.4 and

4.2K of the Mn solute versus field H, and the initial susceptibility X and

the reciprocal of the susceptibility (1/X) versus temperature T have

been plotted in Fig. 53 and 54, respectively.

These two magnetic isotherms M taken at different temperatures and

a comparable Brillouin function appropriate for the free spin system are

plotted versus "field over temperature" (H/T) in Fig. 55. The close

representations among them thus suggest that the behaviour of the most

dilute PtMn (0.09 at.% Mn) alloy approximates a free spin system in

this experimental region.

The susceptibility follows the Curie-Weiss law well with a small

Weiss temperature $\theta \approx -(0.4 \pm 0.2K)$. From the Curie constant,

$C = n \, \mu_{eff}^{2}/3k_{B}$, where k_{B} is the Boltzmann constant, the effective

magnetic moment $\mu_{eff} = (7.4 \pm 0.1) \, \mu_{B}$ (Bohr Magneton) per Mn
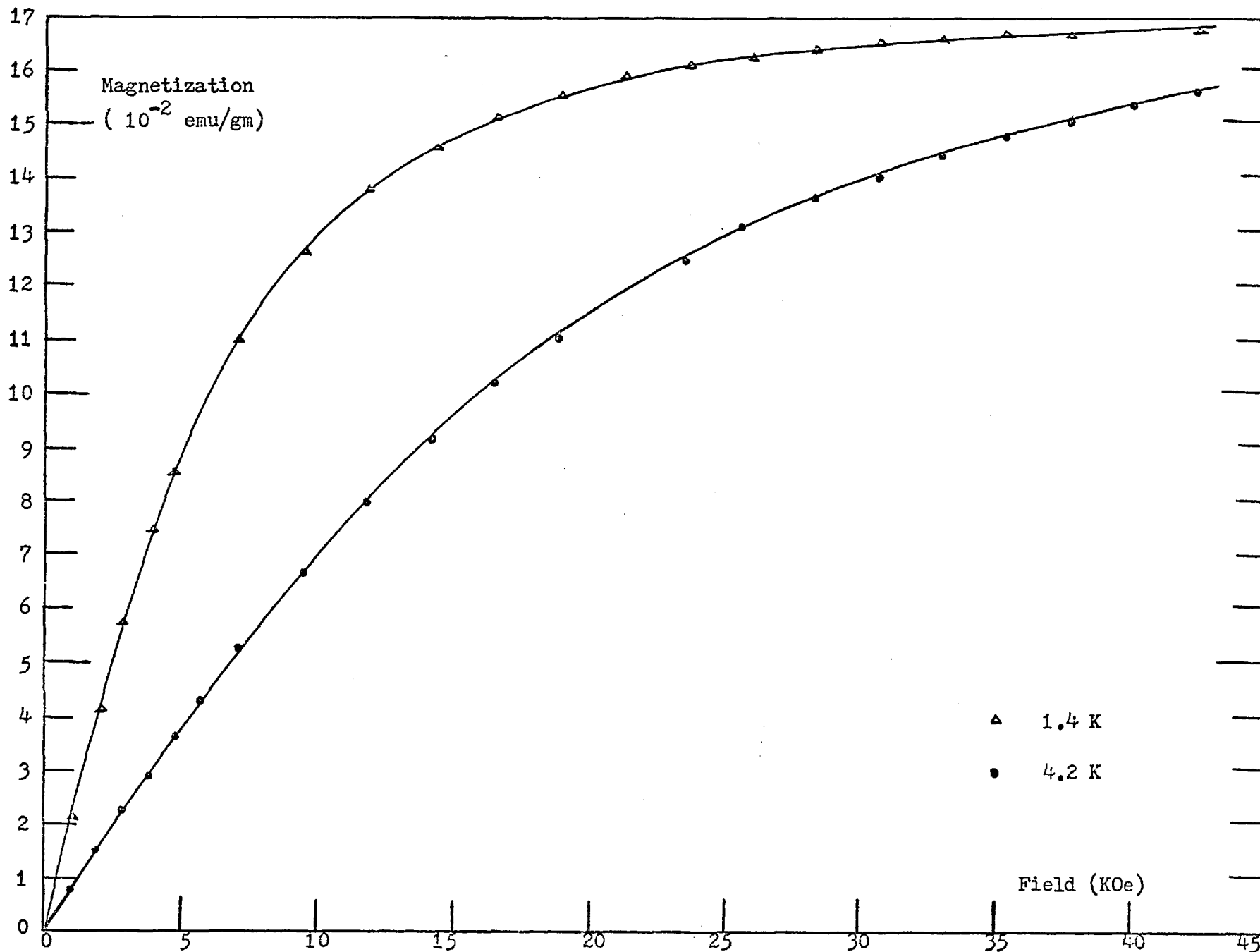
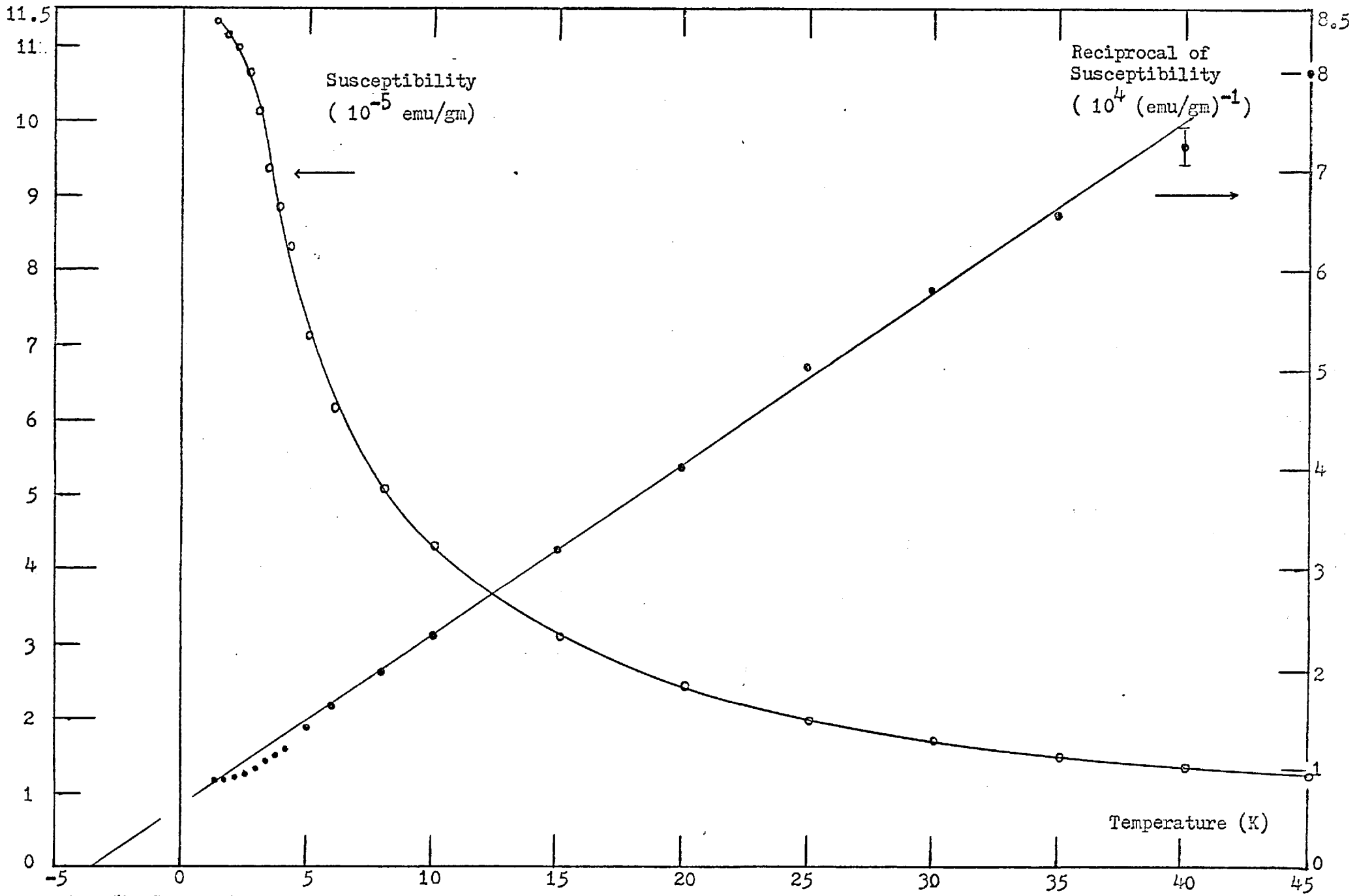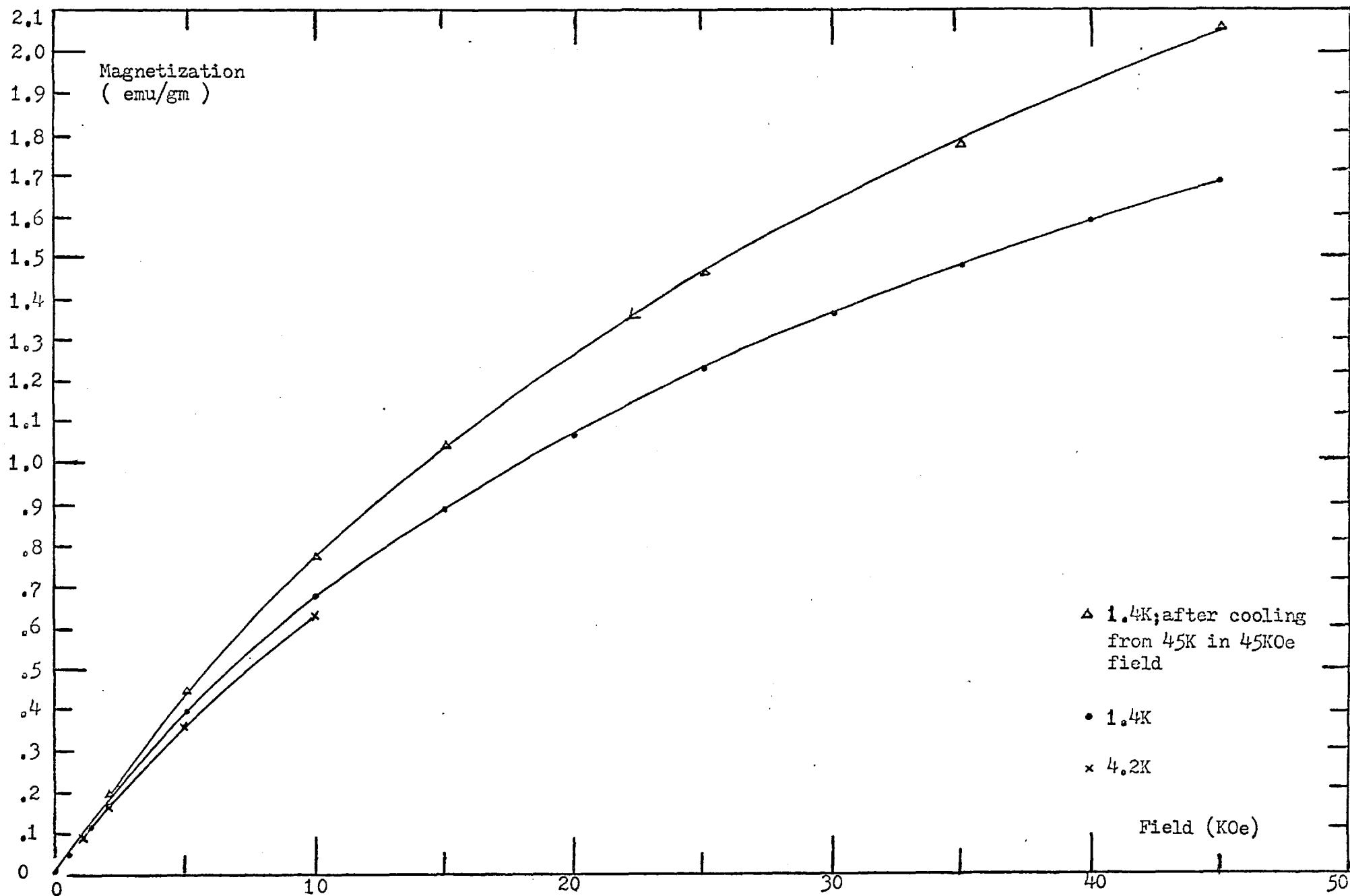Fig. 53 Magnetization versus Field for PtMn (0.09 at.% Mn) Impurity
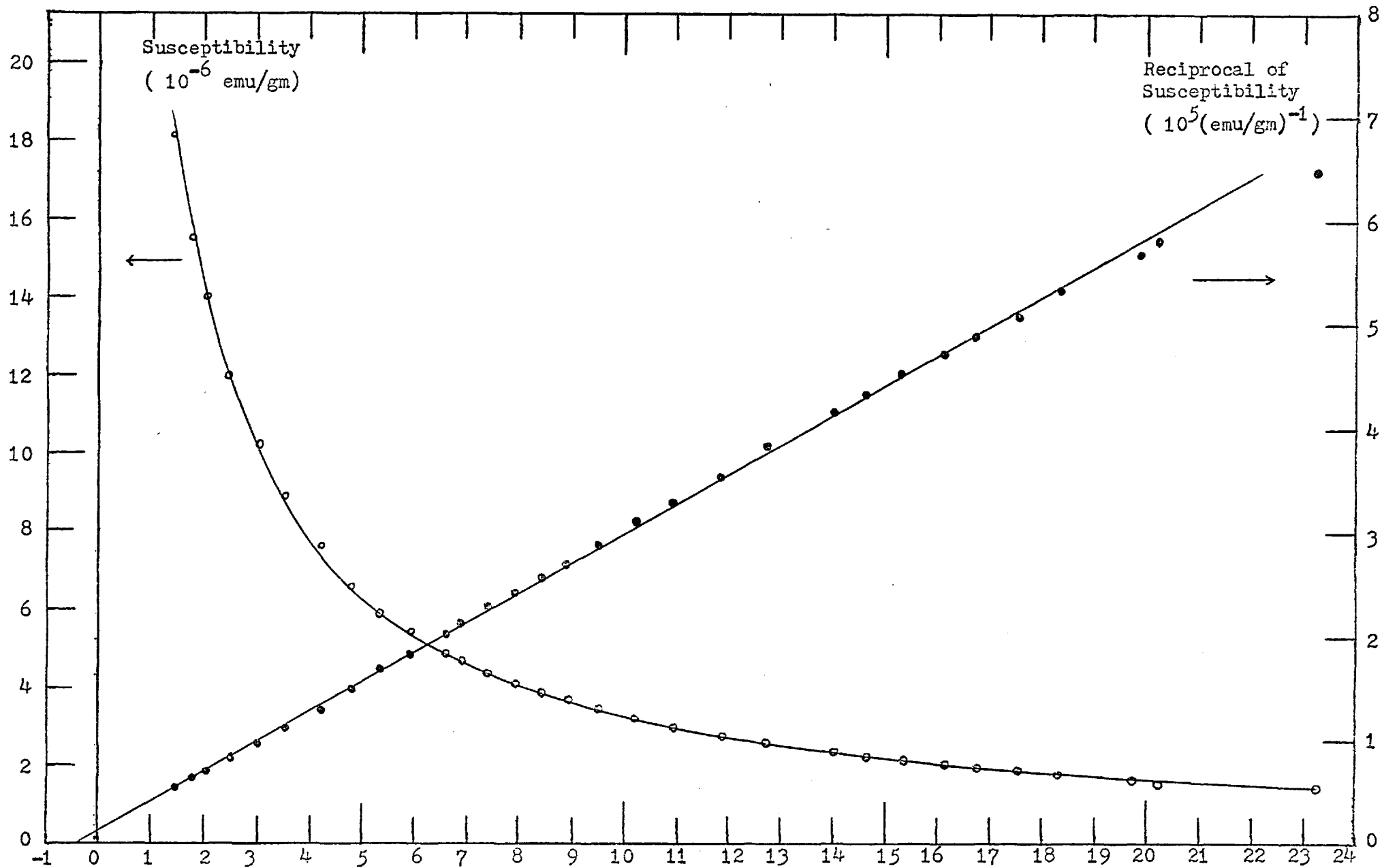
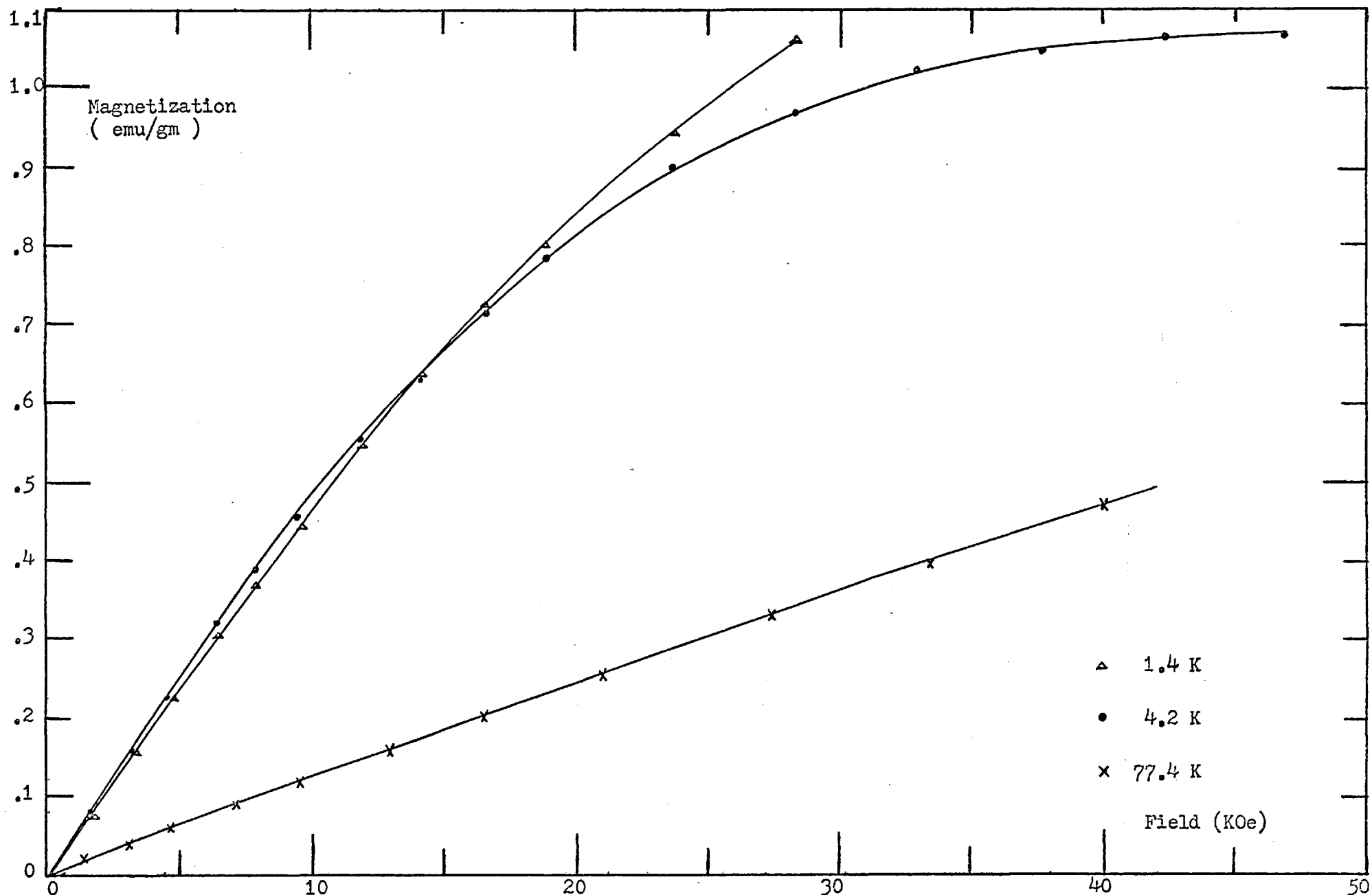Fig. 54 Susceptibility and Reciprocal of Susceptibility for PtMn (0.09 at.% Mn) Impurity.
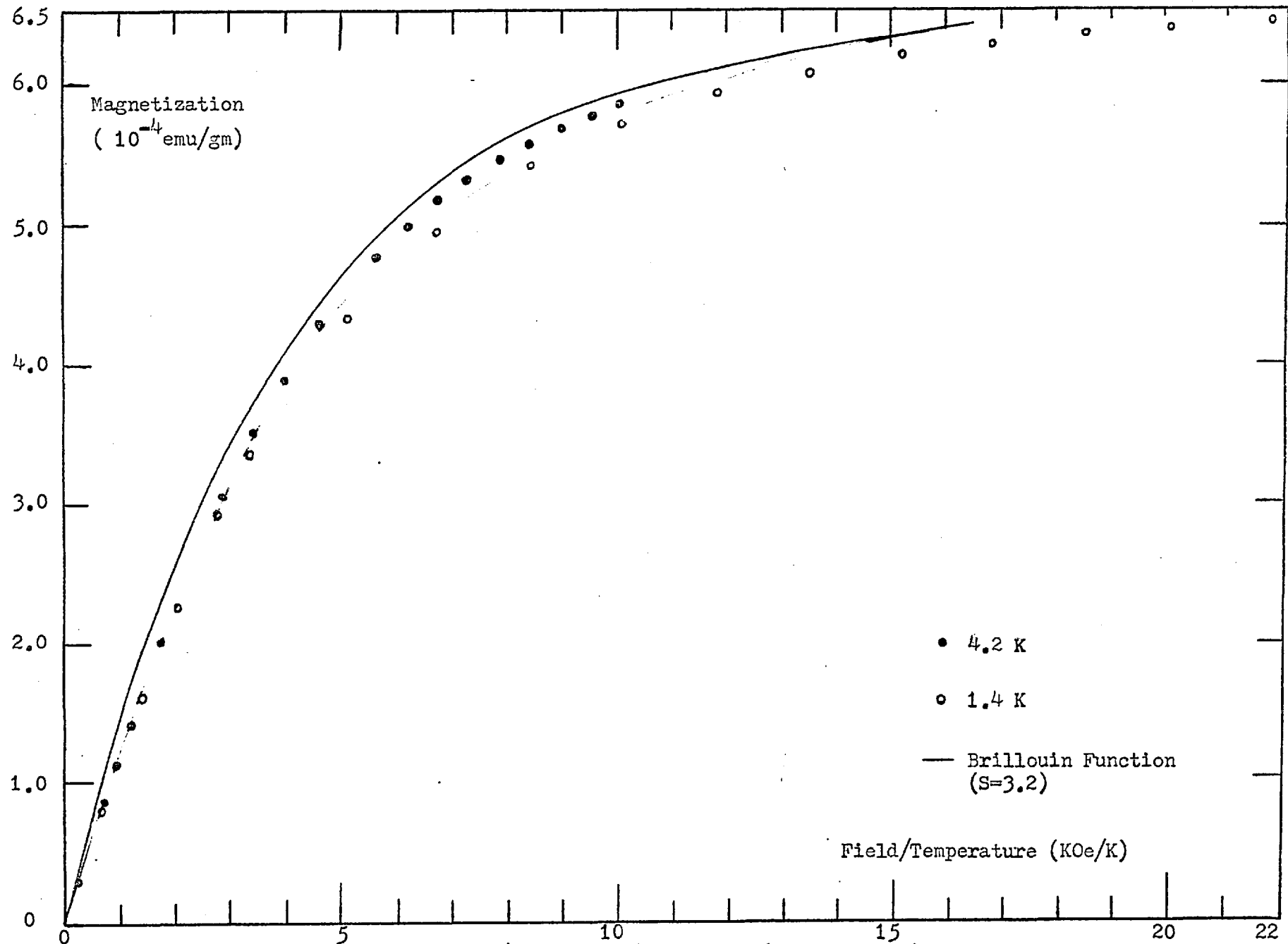
Fig. 55 Magnetization versus (Field/Temperature) for PtMn (0.09 at.% Mn) Impurity

atom has been determined. This value of $\mathcal{U}_{eff}$ is a little larger than

that of 6.0 $\mathcal{U}_B$ determined magnetically by Miyoko et al (170)

(n = 0.47 at.% Mn) and is smaller than that of 7.8 $\mathcal{U}_B$ of PdMn (0.08

at.% Mn) alloys (175); it is larger than the value of 2.6 $\mathcal{U}_B$ per Mn

atom of PtMn (0.36 at.% Mn) alloy obtained through specific heat

measurement (165). This giant moment of the Mn atom in a PtMn alloy

derived from susceptibility measurements is considered to have been

induced in the surrounding matrix of Mn impurity atom, and the existence

of such giant moments is evidence of the large exchange enhancement of

the Pt host. The smaller $\mathcal{U}_{eff}$ value of Mn atoms in a Pt host compared

to that in a Pd host implies the exchange enhancement of the Pt host is

less than that of the Pd host.

The behaviours of the PtMn alloys with higher concentrations

(n = 2, 3, 5.4, 8, 11, and 12 at.% Mn) belong to another category. The

magnetizations M of the Mn solute versus field H and the low-field

magnetic susceptibility X and the reciprocal of the susceptibility (1/X)

of the Mn solute versus temperature T of these alloys are plotted in

Fig. 56 to 68.

It is obvious that the magnetic isotherms do not approximate the

characteristics of the Brillouin function. Hence, the behaviour of

these alloys does not belong to a free spin system. Another interesting

point is the cross of the magnetic isotherms taken at different tempera-

tures, for example, see the alloys with n = 5.4 at.% Mn in Fig. 60.

This behaviour has not been observed in the previous dilute PtMn

(0.09 at.% Mn) alloy , and it represents the relative weights and
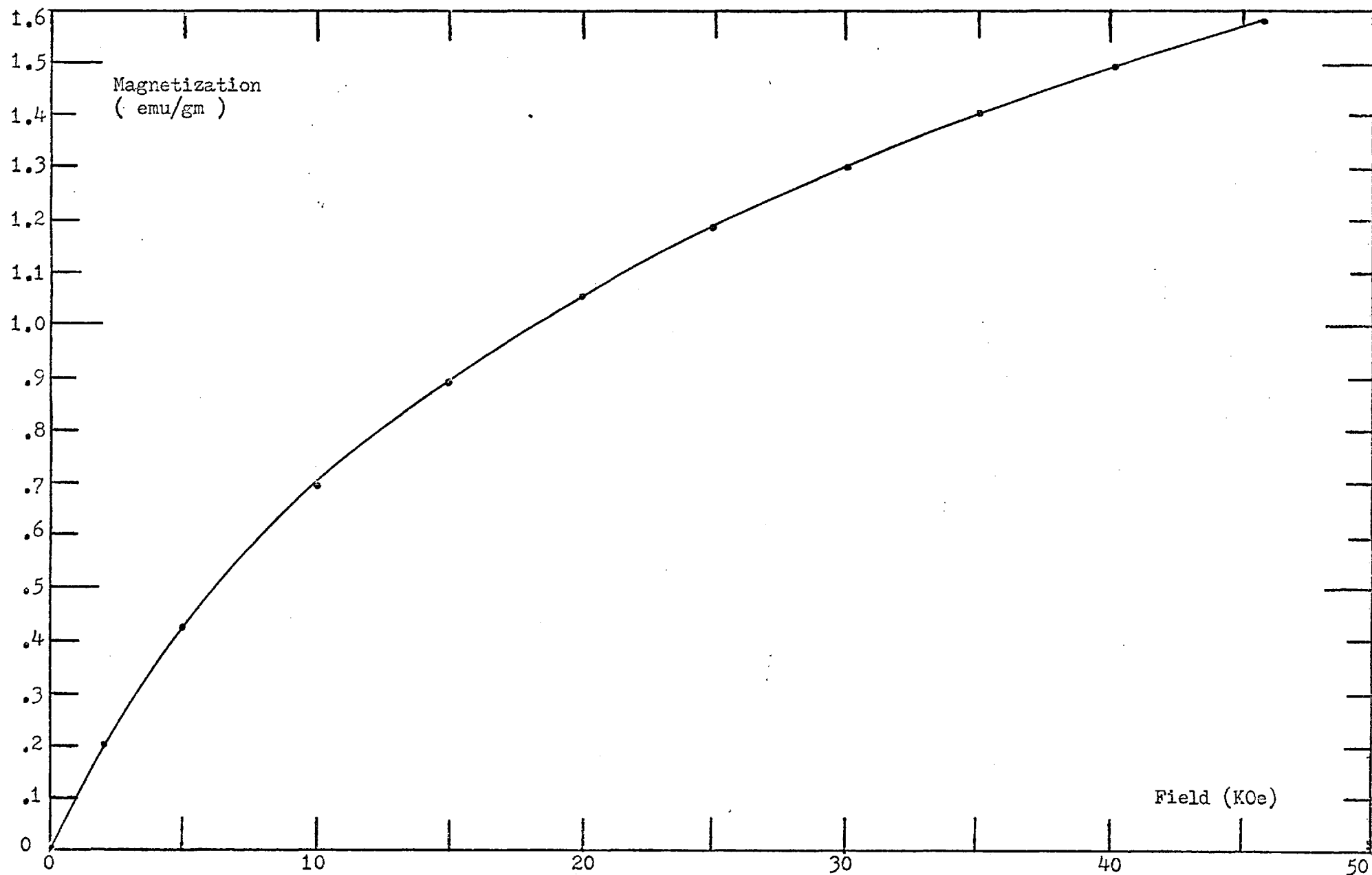
Fig. 56 Magnetization versus Field for PtMn (2 at.% Mn) Impurity at 1.4K after cooling from 50K in 45KOe field

Fig. 57 Susceptibility and Reciprocal of Susceptibility versus Temperature for P̲t̲Mn (2 at.% Mn) Impurity
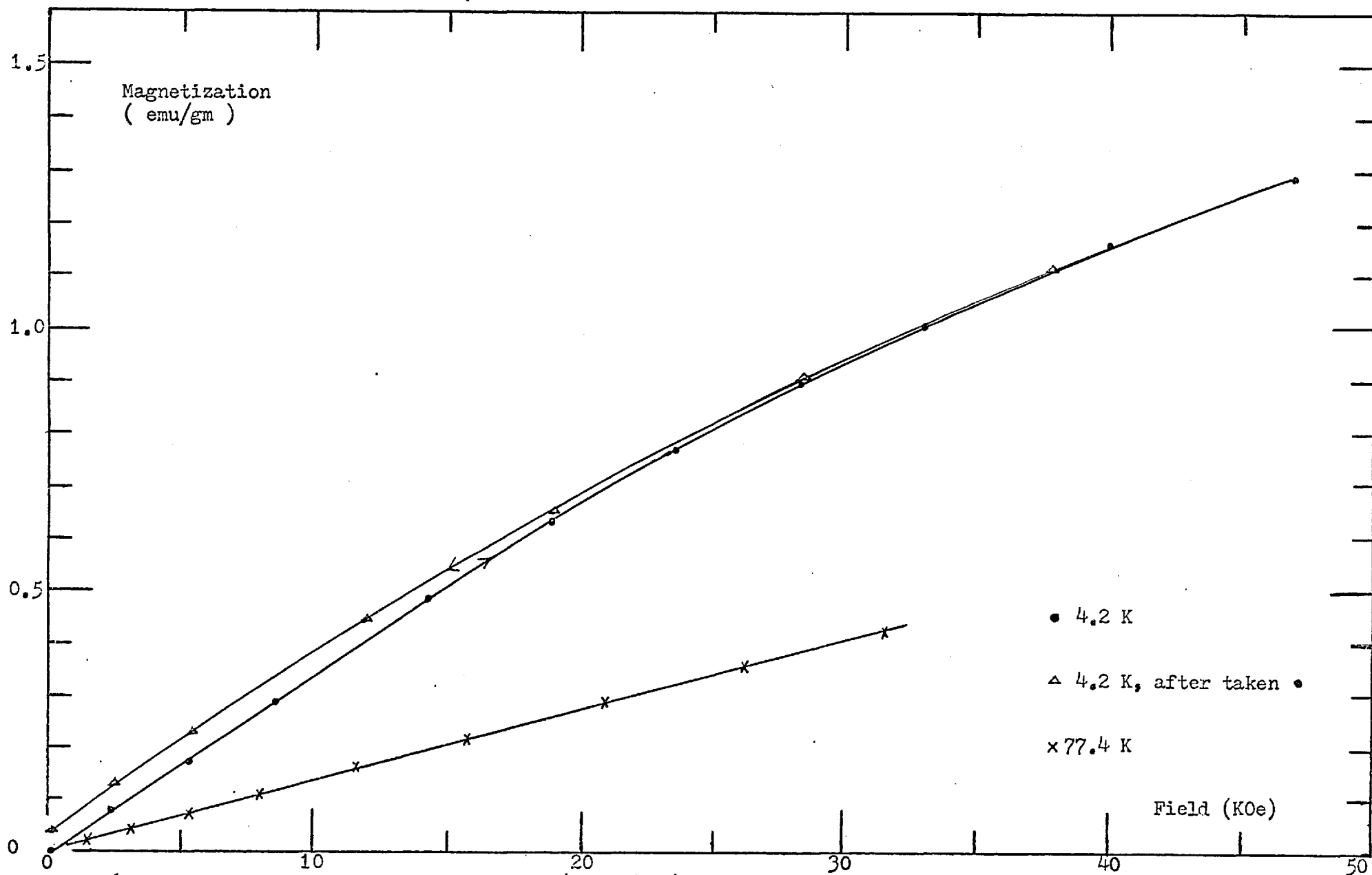
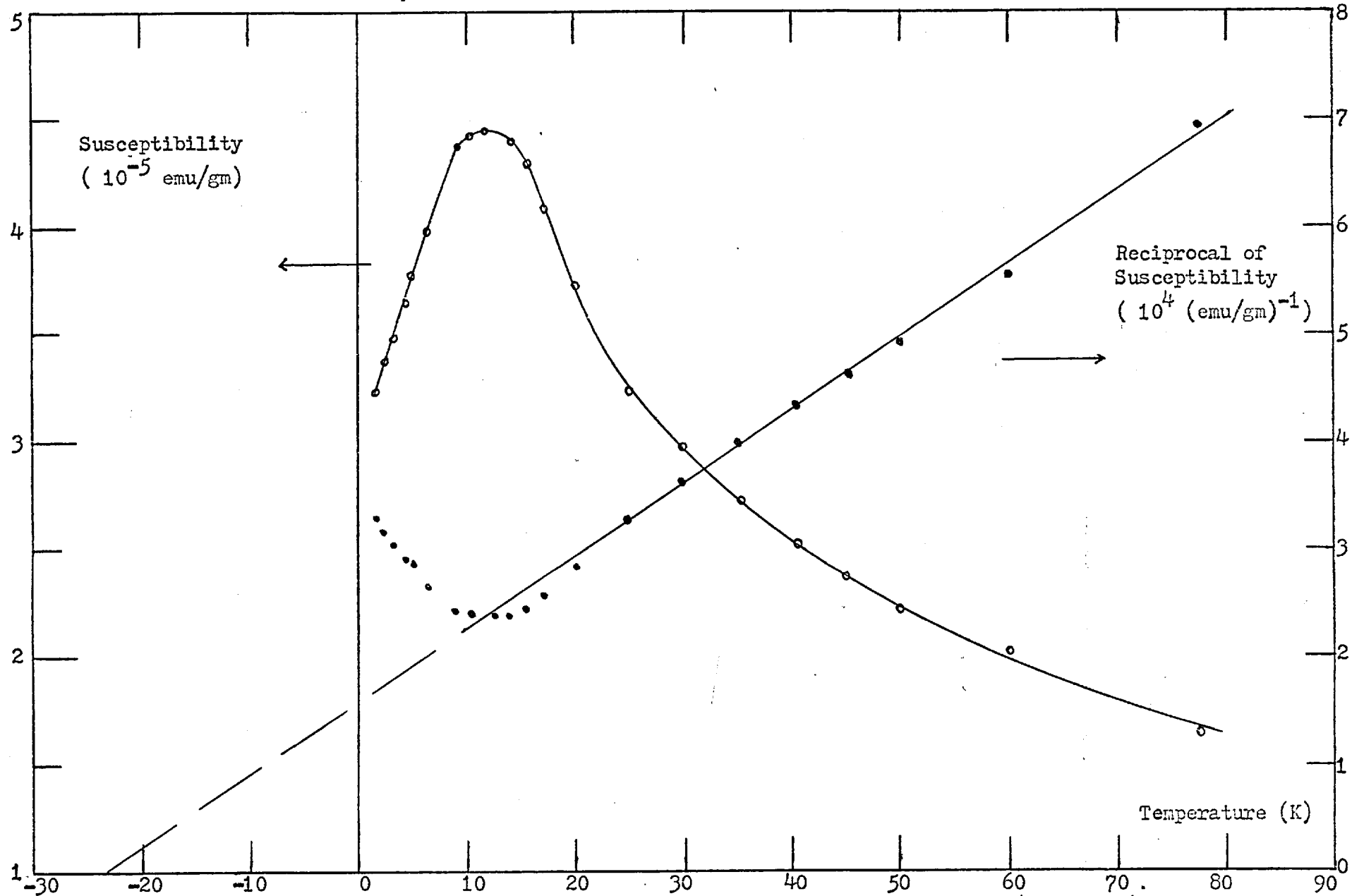Fig. 58 Magnetization versus Field for PtMn (3 at.% Mn) Impurity
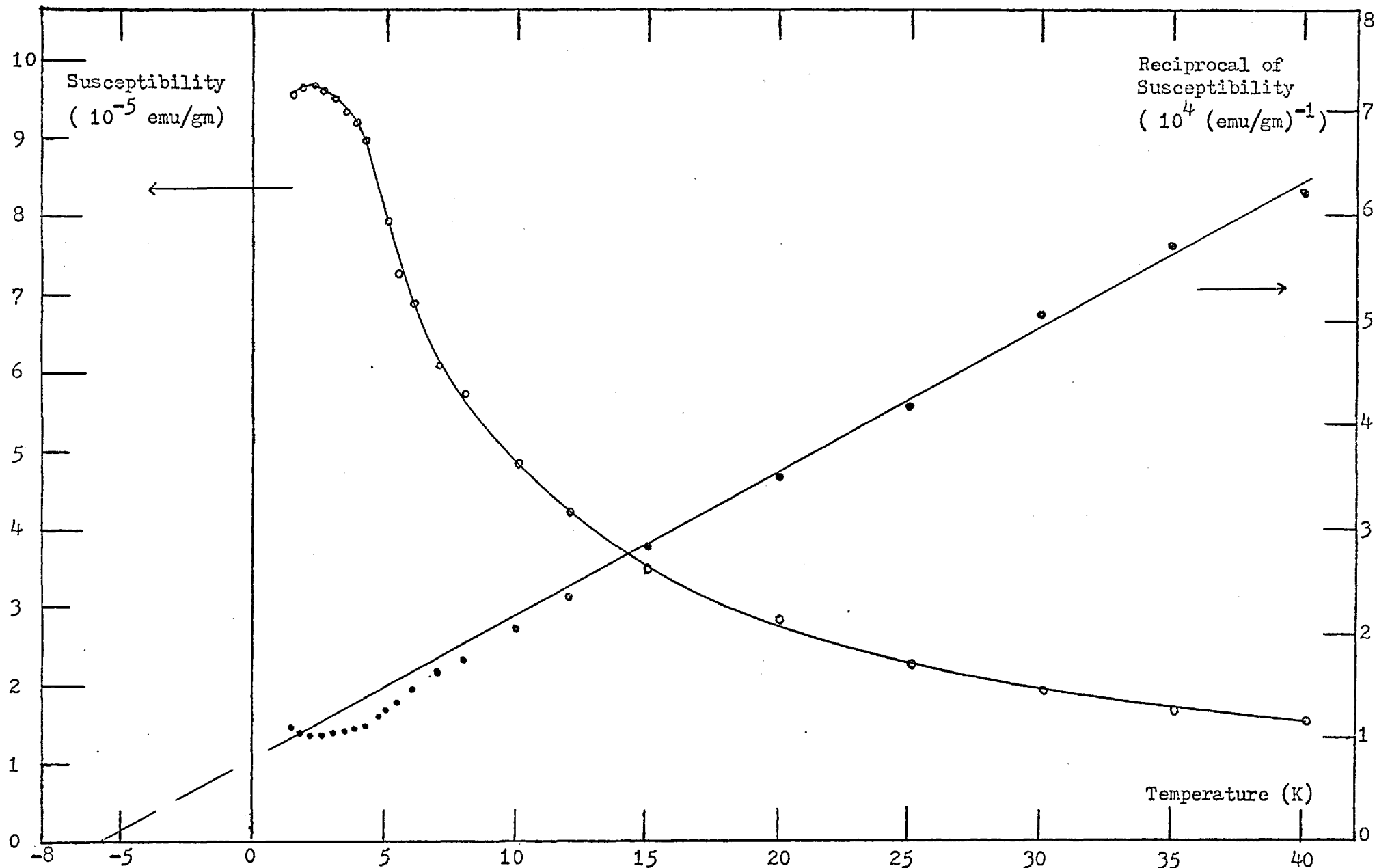
Fig. 59 Susceptibility and Reciprocal of Susceptibility versus Temperature for PtMn (3 at.% Mn) Impurity
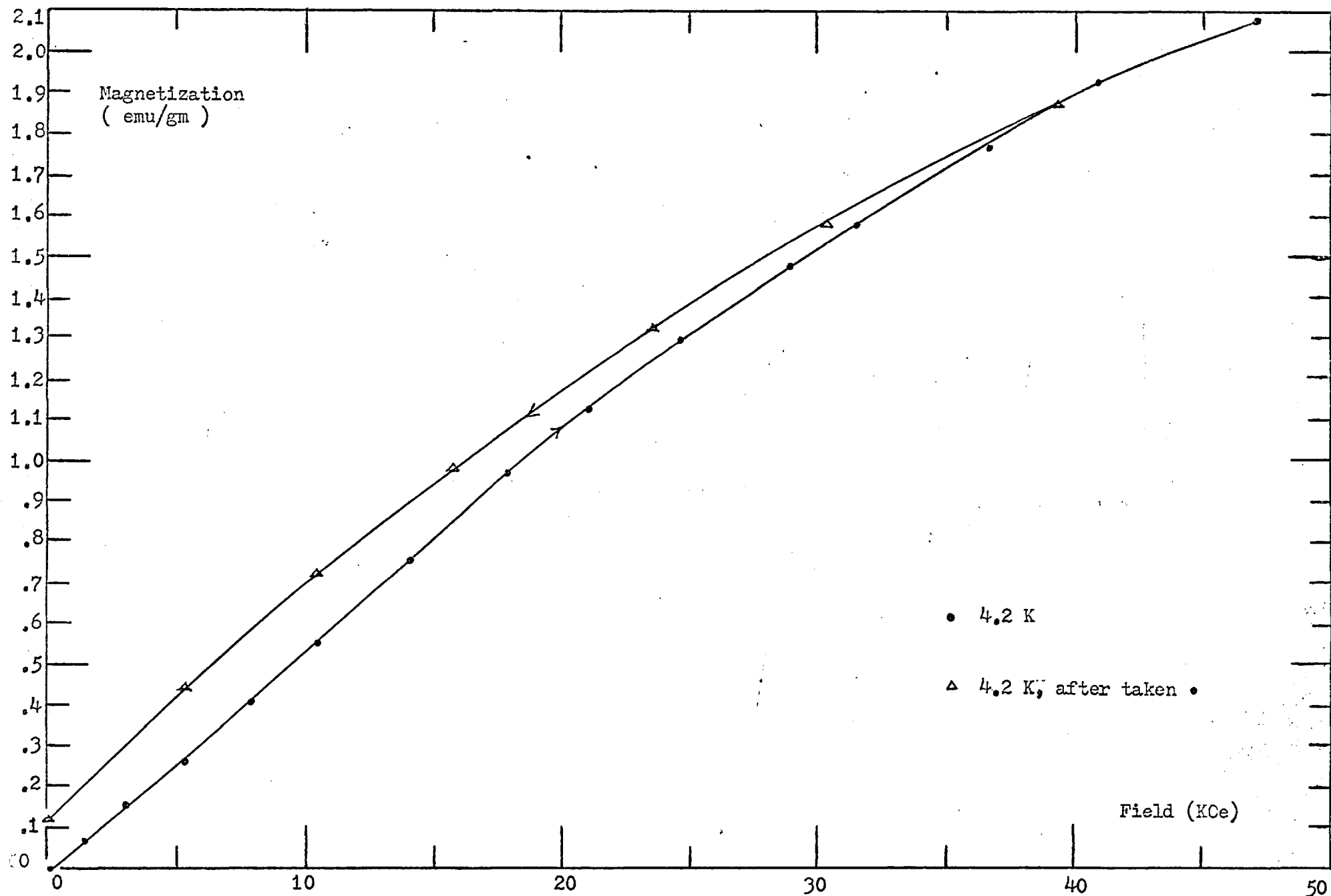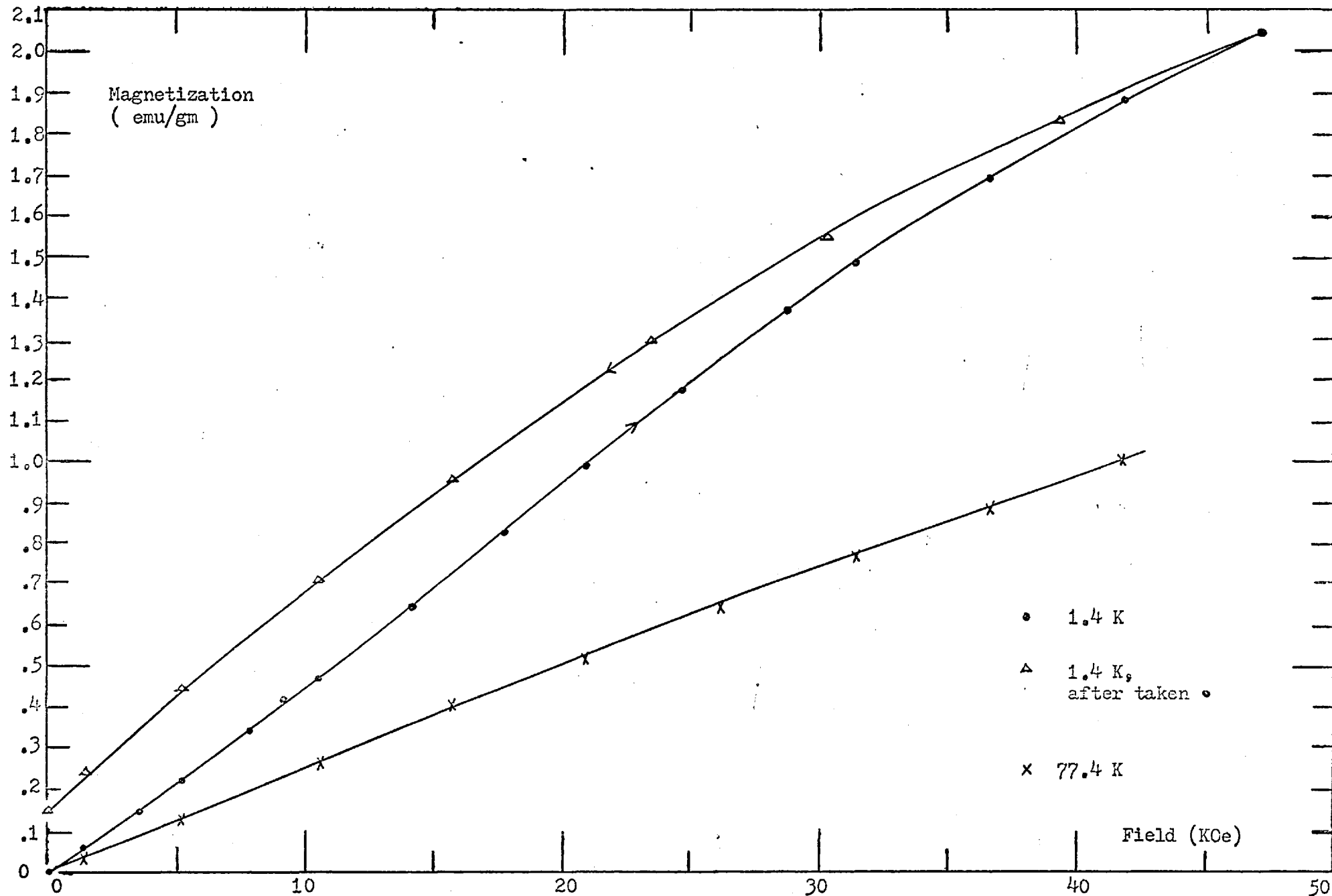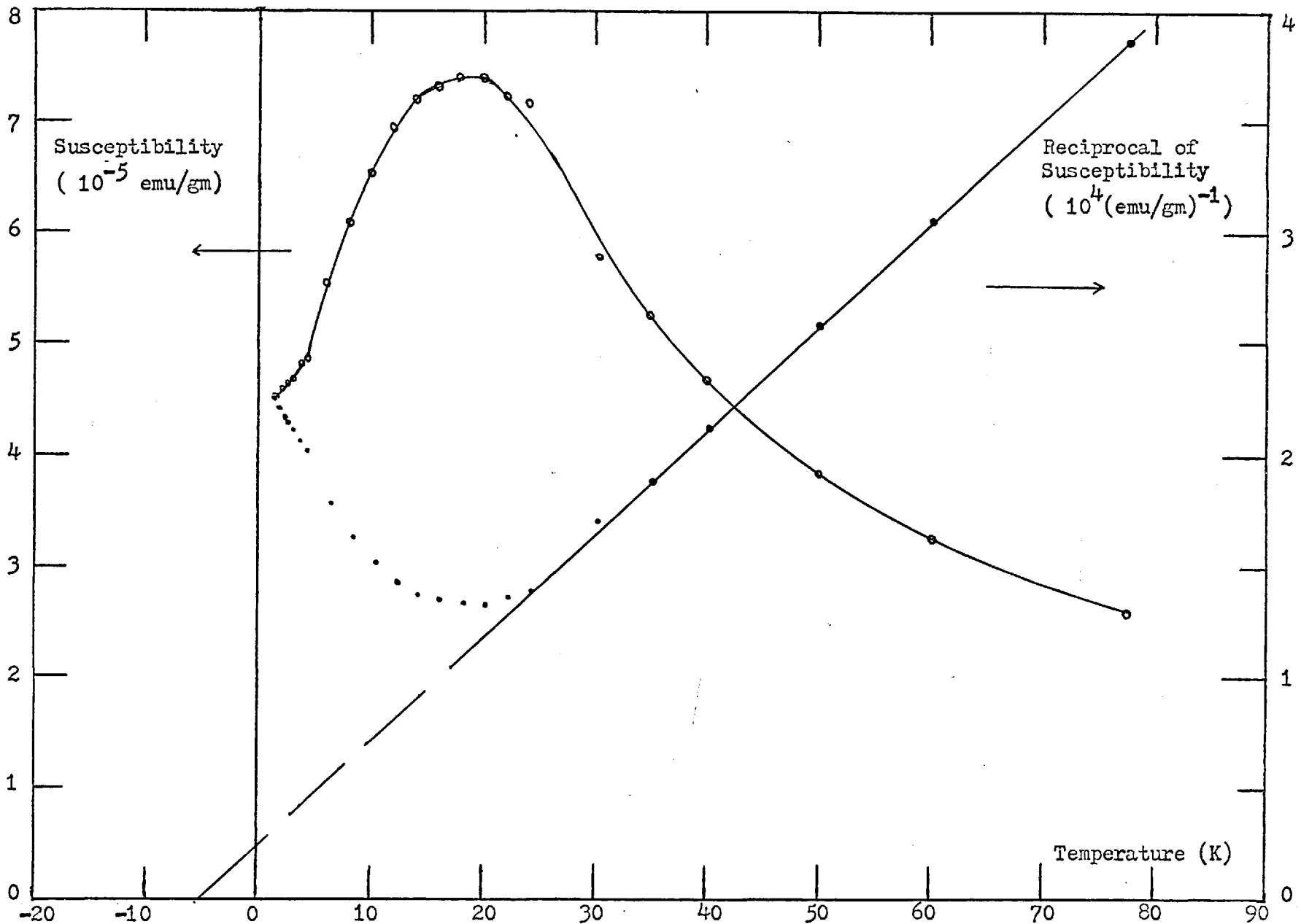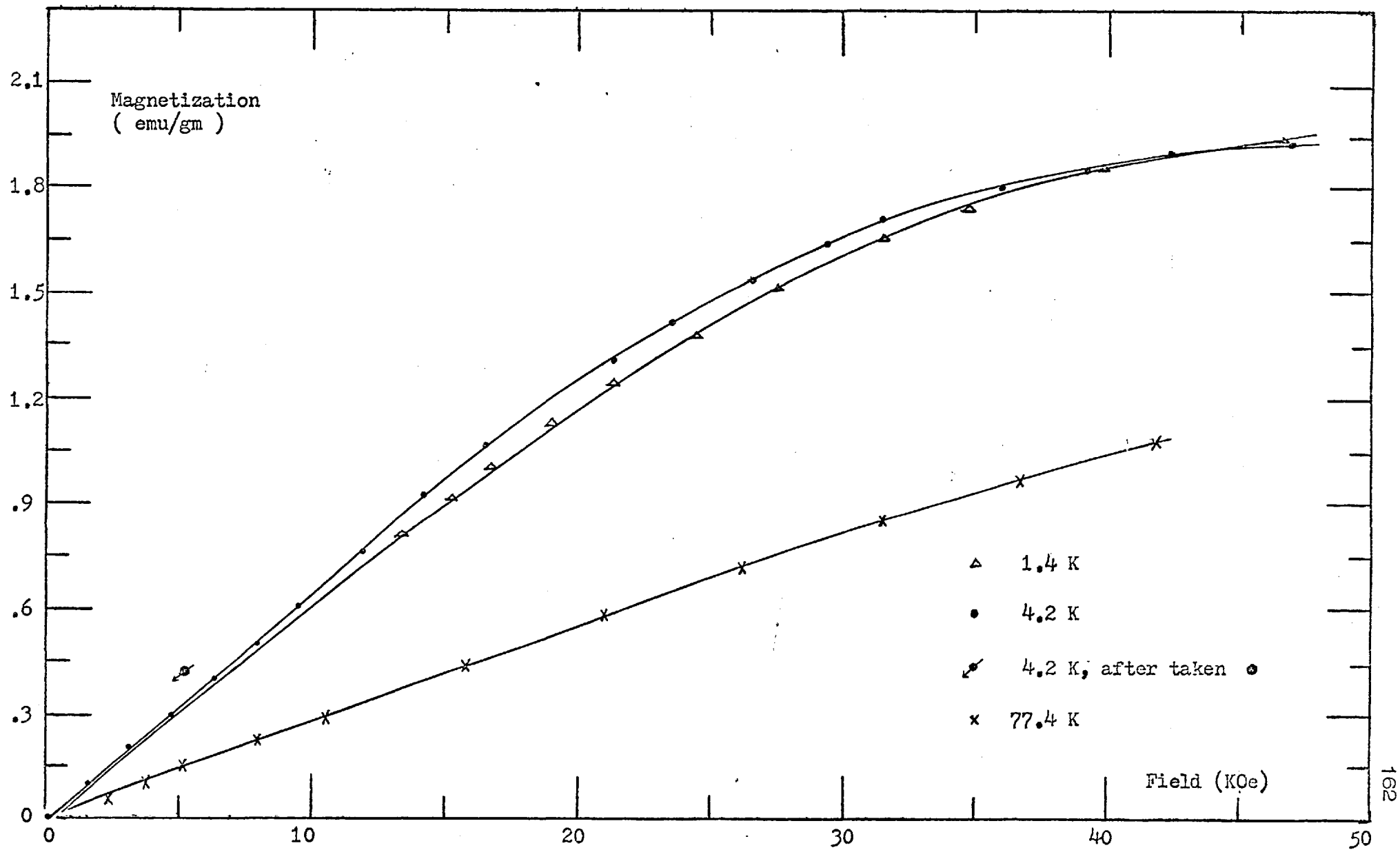
Fig. 60 Magnetization versus Field for PtMn (5.4 at.% Mn) Impurity

155
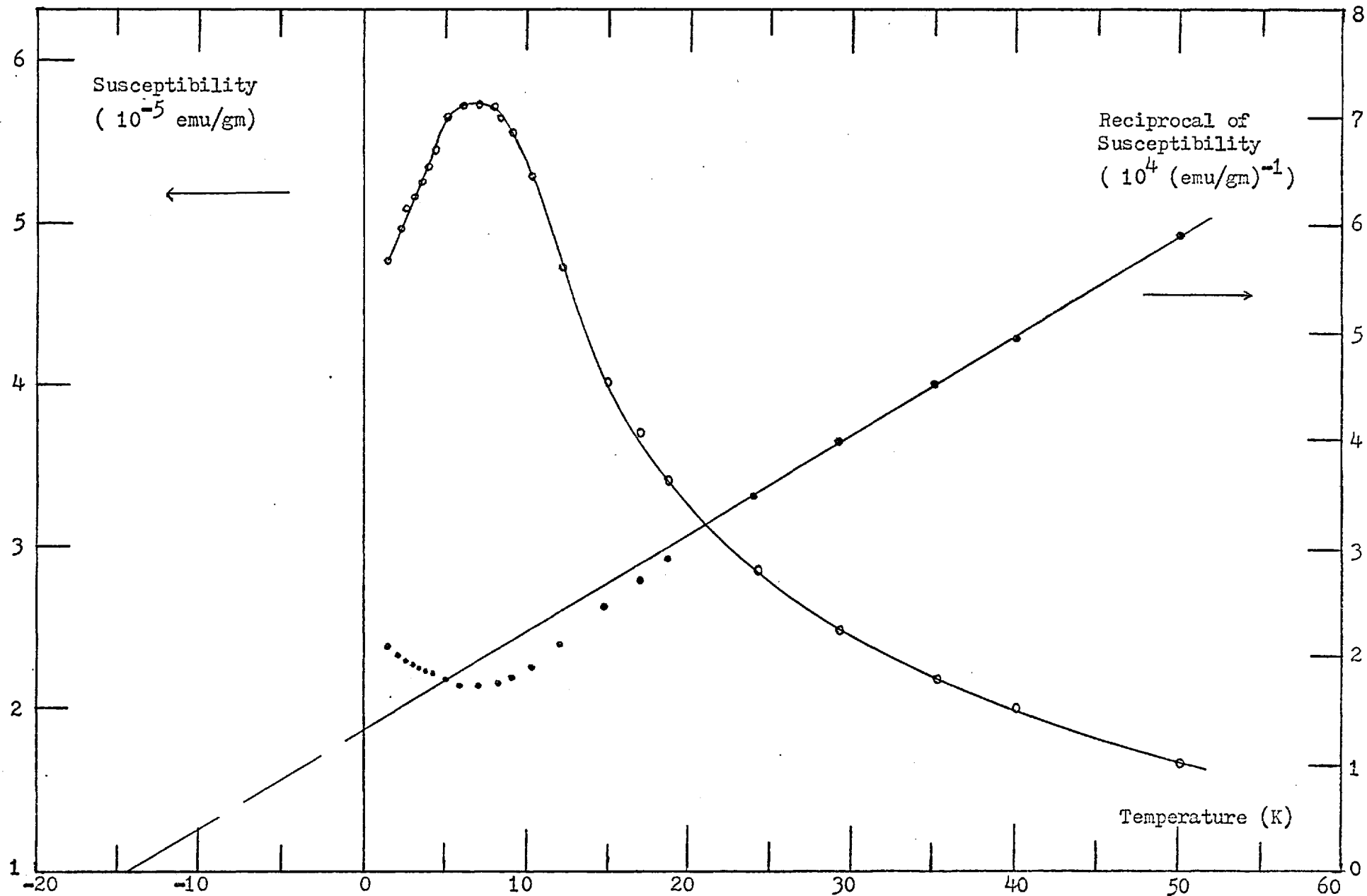
Fig. 61 Susceptobility and Reciprocal of Susceptibility versus Temperature for PtMn (5.4 at.% Mn) Impurity

Fig. 62 Magnetization versus Field for PtMn (8 at.% Mn) Impurity

Fig. 63 Susceptibility and Reciprocal of Susceptibility versus Temperature for PtMn (8 at.% Mn) Impurity

Fig. 64 Magnetization versus Field for PtMn (11 at.% Mn) Impurity at 4.2K

Fig. 65 Magnetization versus Field for PtMn (11 at.% Mn) Impurity at 1.4 and 77.4K

Fig. 66 Susceptibility and Reciprocal of Susceptibility versus Temperature for PtMn (11 at.% Mn) Impurity

Fig. 67 Magnetization versus Field for $\underline{Pt}Mn$ (12 at.% Mn) Impurity
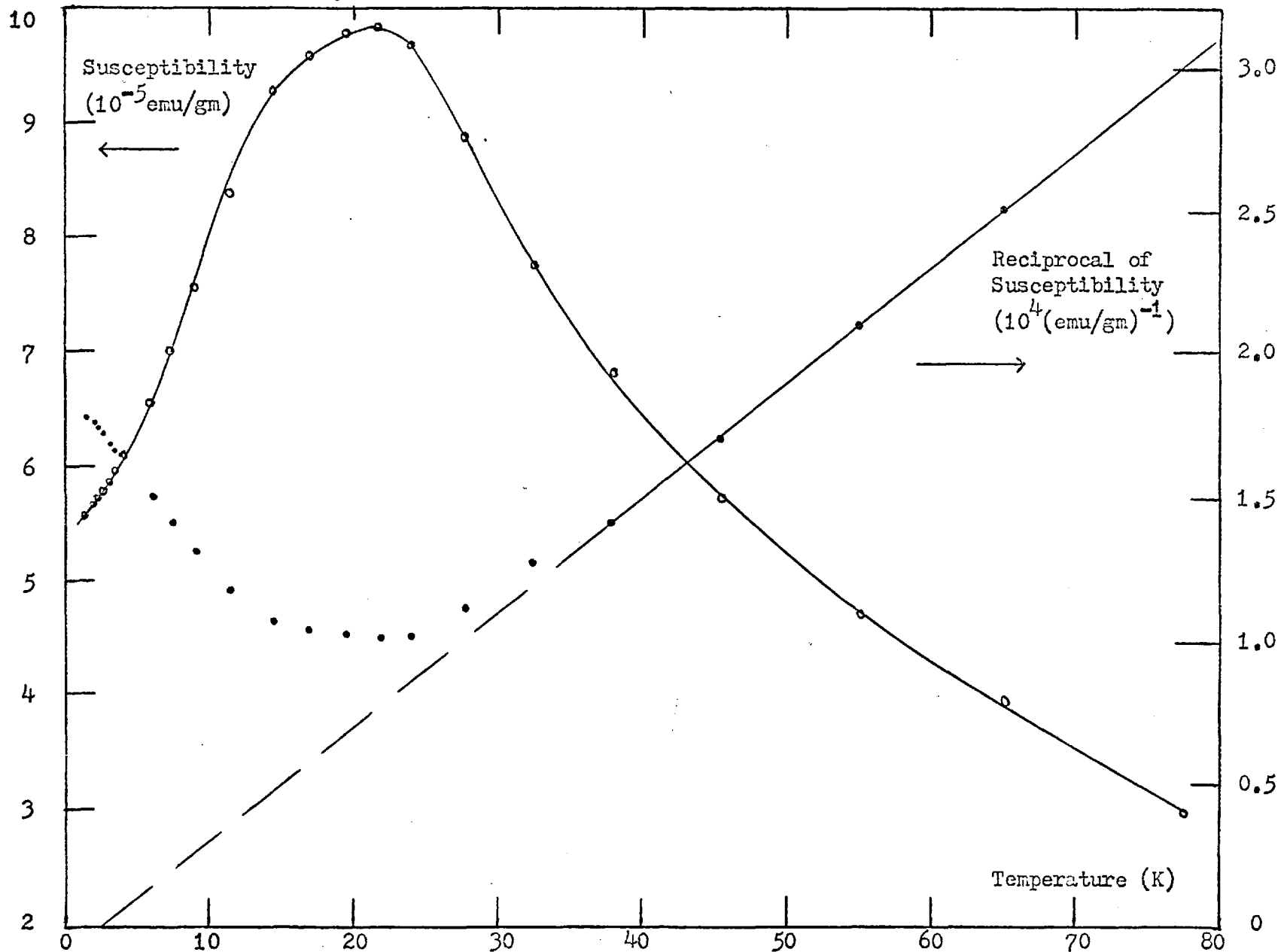
Fig. 68 Susceptibility and Reciprocal of Susceptibility versus Temperature for $\underline{Pt}$Mn (12at.%Mn) Impurity

competitions among the effects of the temperature, the external field, and the strong impurity interactions.

The magnetization $M(H, T, I)$ is a function of the external field H, temperature T, and the impurity interaction I. In an ideal free spin system, the impurity interaction, which includes the interactions between the host conductor electron and the impurity spin and the interactions between impurities, is zero. The magnetization will be a function of H and T only and can be described by the Brillouin function, which is a function of the argument (H/T). If the temperature is kept constant and the field increases, magnetization will increase along the Brillouin curve and toward saturation. If the field is kept constant and the temperature increases, the thermal fluctuation will increase and, thus, reduce the magnetization further from saturation. The initial susceptibility is referred to the zero field limit, in which case the effect of the saturation of spins could be negligible, the magnetization versus field follows a linear relation, and the initial susceptibility of an ideal free spin system will follow the Curie law. If both the field and temperature are variables, the magnetization can be plotted versus (H/T), and all the magnetic isotherms taken at different temperatures will fall on the single spin dependent Brillouin curve and coincide with one another.

If the impurity interactions are also taken into consideration, the magnetization will usually fall below the Brillouin curve for paramagnetic systems. In the paramagnetic region, generally, the impurity interaction can be treated by the molecular field approach. Each spin and its surroundings can still be considered as an independent group, and the

susceptibility can be described by a Curie-Weiss law; however, in the

magnetic spin glass region, the spin freezing effect will dominate the

system. Therefore, the low field susceptibility taken at temperatures

farther away from the characteristic temperature T_{max} of the suscepti-

bility maximum will have values less than those taken at temperatures

closer to T_{max}, and the Curie-Weiss law is no longer suitable to

describe the system in this region. This effect is shown clearly in the

susceptibility as well as on the slope of the magnetic isotherms taken at

1.4 and 4.2K and at low fields of the PtMn (5.4 at.% Mn) alloy, for which

the T_{max} is 7K.

When the external field is applied, it will compete with the internal

field which caused the spin freezing and will align the spins to its

direction. As the external field increases to above a critical value, it

will dominate the system, and the magnetization will increase faster at

lower temperatures than at higher temperatures because of the smaller

thermal fluctuation effect; therefore, the magnetization curve taken at

lower temperatures, although it has smaller values than that taken at

higher temperatures at small external field, will become higher as the

external field increases, and then both approach saturation as the field

increases further. Hence, a cross between these two magnetic isotherms

appears.

The magnetic thermal remanence effect of the magnetic spin glass

state alloy can be seen clearly from the magnetization curves, for example,

see the PtMn (3 at.% Mn) alloy in Fig. 58. The magnetization has higher

value if the alloy is cooled down from a high temperature with a field

applied, in this case they are 45K and 45KOe respectively, than if the alloy

is cooled down without a field applied; and this magnetic thermal remanence is a time-dependent effect.

The magnetic isothermal remanence effect of the magnetic spin glass state alloy can also be seen clearly from the magnetization curves, for example, see the PtMn ($n = 8,11$ and 12 at.% Mn) alloys in Fig. 62, 64, 65, and 67. The magnetic isotherms have a time-dependent magnetic remanence if the field goes up first, then down to the set value.

The susceptibilities of all the alloys follow a Curie-Weiss law at high temperatures. As the temperature decreases, the susceptibilities deviate to above the Curie-Weiss law, indicating the onset of the super-paramagnetic state. They then fall below the Curie-Weiss law and form the cusp in the susceptibilities. This maximum in susceptibility and the field cooling magnetic remanence observed indicate the existence of a magnetic spin glass state, and the paramagnetic-superparamagnetic-magnetic spin glass states transitions have been observed for the PtMn alloys with concentrations from 2 to 12 at.% Mn.

From the behaviours of the susceptibility of the PtMn alloys, the values of the Weiss temperature θ, the temperature T_{max} of the suscep-tibility maximum, and the effective moment μ_{eff} per Mn atom from the Curie constant can thus be determined and are listed in Table 5.

TABLE 5

PtMn Alloy System Magnetic Measurements

Impurity Concentrations	Weiss Temperature	Susceptibility Maximum Temperature	Effective Moment per Mn Atom
at.% Mn	$\Theta(K)$	$T_{max}(K)$	$\mu_{eff}(\mu_B)$
0.09	0.4 ± 0.2	---	7.4 ± 0.2
2	3.2 ± 0.2	---	6.6 ± 0.2
3	6.4 ± 0.2	2.5 ± 0.4	6.1 ± 0.2
5.4	14.3 ± 0.2	7 ± 0.4	5.5 ± 0.2
8	23 ± 0.2	12 ± 0.4	5.2 ± 0.2
11	6 ± 0.2	18 ± 0.4	5.3 ± 0.2
12	-3 ± 0.2	20.5 ± 0.4	5.4 ± 0.2

The temperature T_{max} of the susceptibility maximum follows a linear relation of the impurity concentration n and is plotted in Fig. 69. This linear relation agrees with the proposals calculated from the molecular field theory (74,77).

The susceptibility versus the "reduced temperature" (T/n) has been plotted in Fig. 70. The high temperature susceptibility, above T_{max}, of the PtMn alloys with n from 2 to 8 at.% Mn, form a series of ordered parallel straight lines. It indicates that the susceptibility follows the same power law of the "reduced temperature." This is different from the single coinciding line of the "dilute" AgMn alloys, as has been presented in Chapter 3. Possibly, when a significant amount of impurity
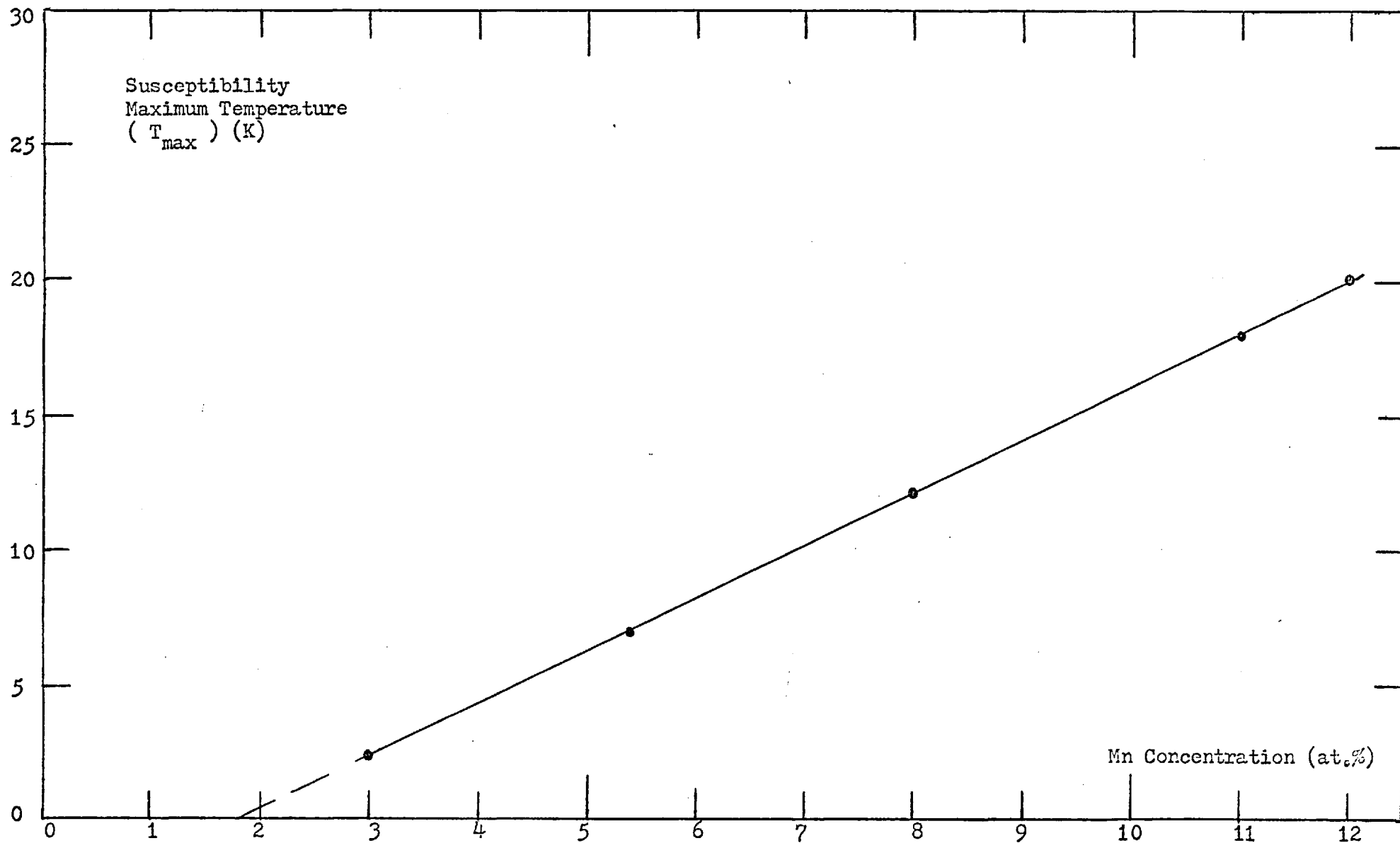
Fig. 69 Susceptibility Maximum Temperature versus Mn Concentration for PtMn alloy system
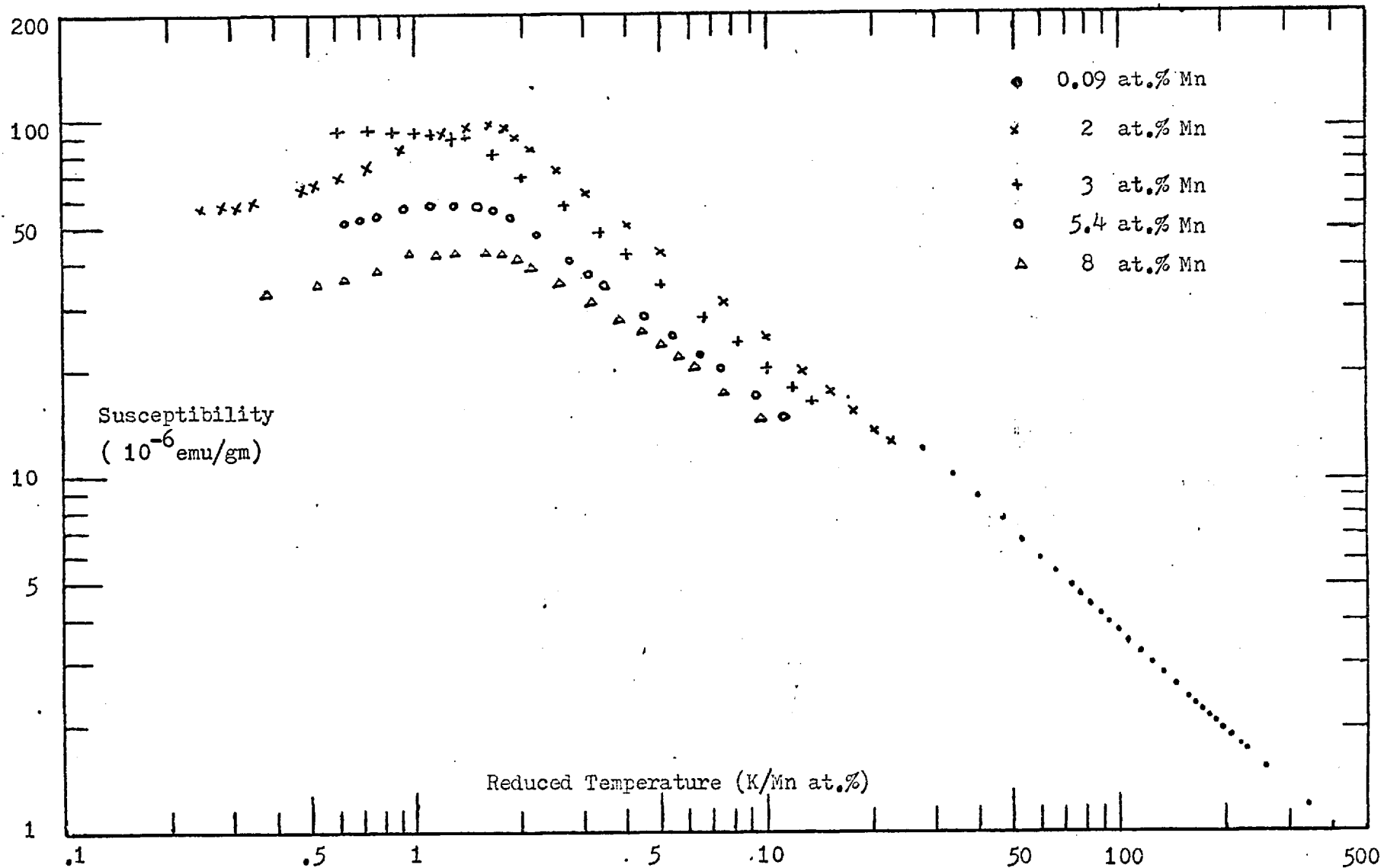
Fig. 70 Susceptibility versus Reduced Temperature for Pt̲Mn alloy system

atoms is added to an enhanced host matrix, it might cause a change in the band structure and, hence, modify the susceptibility.

The Weiss temperature θ versus impurity concentration n of all the alloys has been plotted in Fig. 71. For the $\underline{Pt}Mn$ alloys with n from 2 to 8 at.% Mn, the θ follows a linear relation with n. This scaling of θ might indicate that indirect impurity interactions dominate the system. From the Larkin and Khmel'nitskii theory (87), the strength V_O of the indirect interaction between two impurity atoms can be obtained from the formula $nV_O = C_S k_B \theta$, where C_S is a spin-dependent proportional constant of order unity. Hence, the value of the strength V_O of the indirect inter- action between two Mn atoms in $\underline{Pt}Mn$ alloys can be estimated and is $(5.6 \pm 0.2) \times 10^{-37}$ erg cm^3. For the $\underline{Pt}Mn$ alloys with n equal to 11 and 12 at.% Mn, the susceptibility and Weiss temperature θ are completely out of the scaling picture. The effective moment μ_{eff} per Mn atom versus Mn concentration n has been plotted in Fig. 72. The μ_{eff} decreases as the Mn concentration n increases until the n = 8 at.% Mn data point; for n = 11 and 12 at.% Mn, the μ_{eff} increases as the Mn concentration increases.

This common division of behaviour of the Weiss temperature and the effective moment, thus, suggests the $\underline{Pt}Mn$ alloy system undergoes a "region" transition at a critical impurity concentration n_c which lies in between 8 and 11 at.% Mn, of value about 9 at.% Mn. In the n < n_c region, the indirect RKKY impurity interaction dominates when the Mn concentration decreases, then each Mn atom can act more freely with its surrounding local polarization cloud in response to any external field as a giant moment; this effect will result in a decrease of Weiss temperature
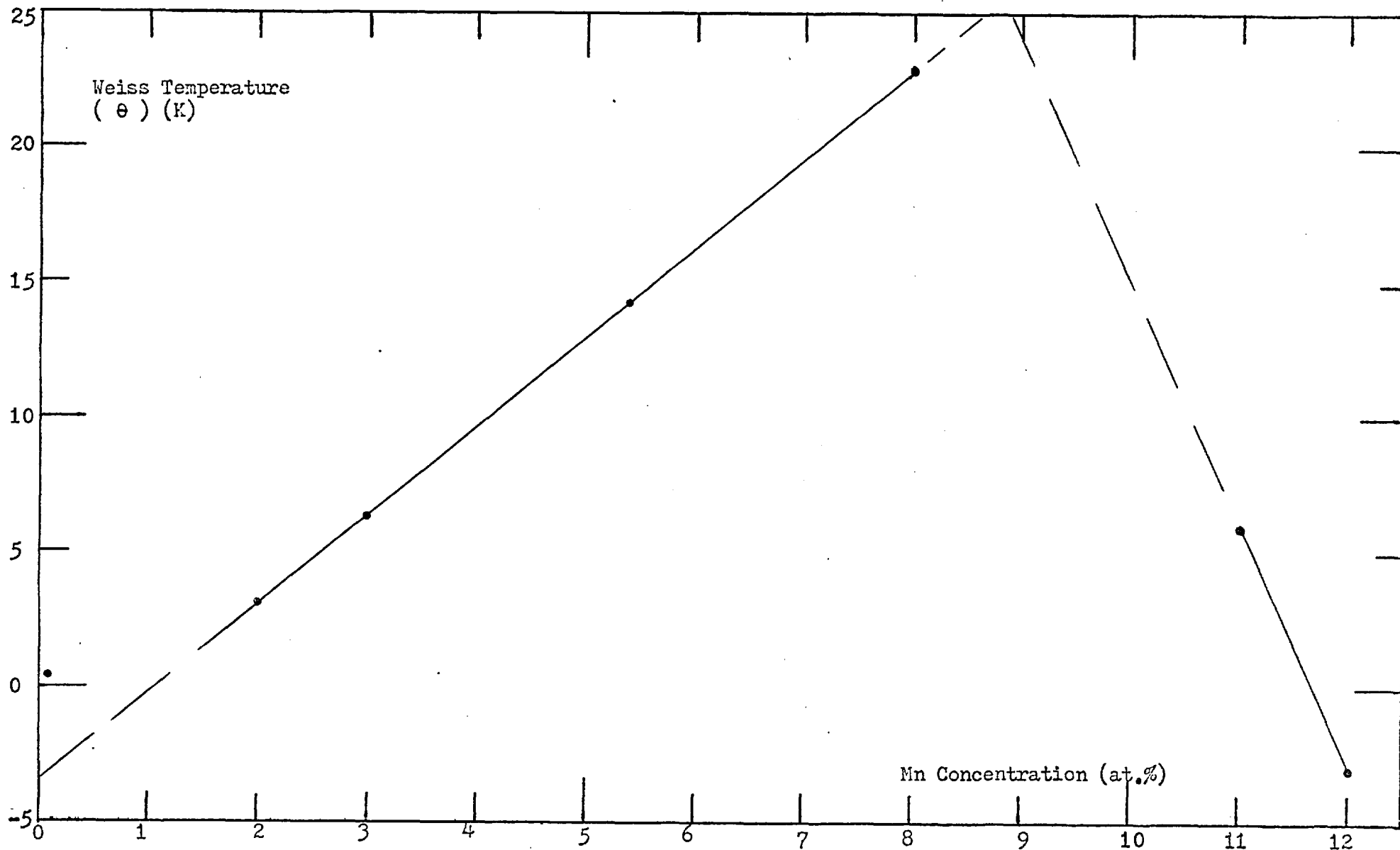
Fig. 71 Paramagnetic Weiss Temperature versus Mn Concentration for P̲t̲Mn alloy system
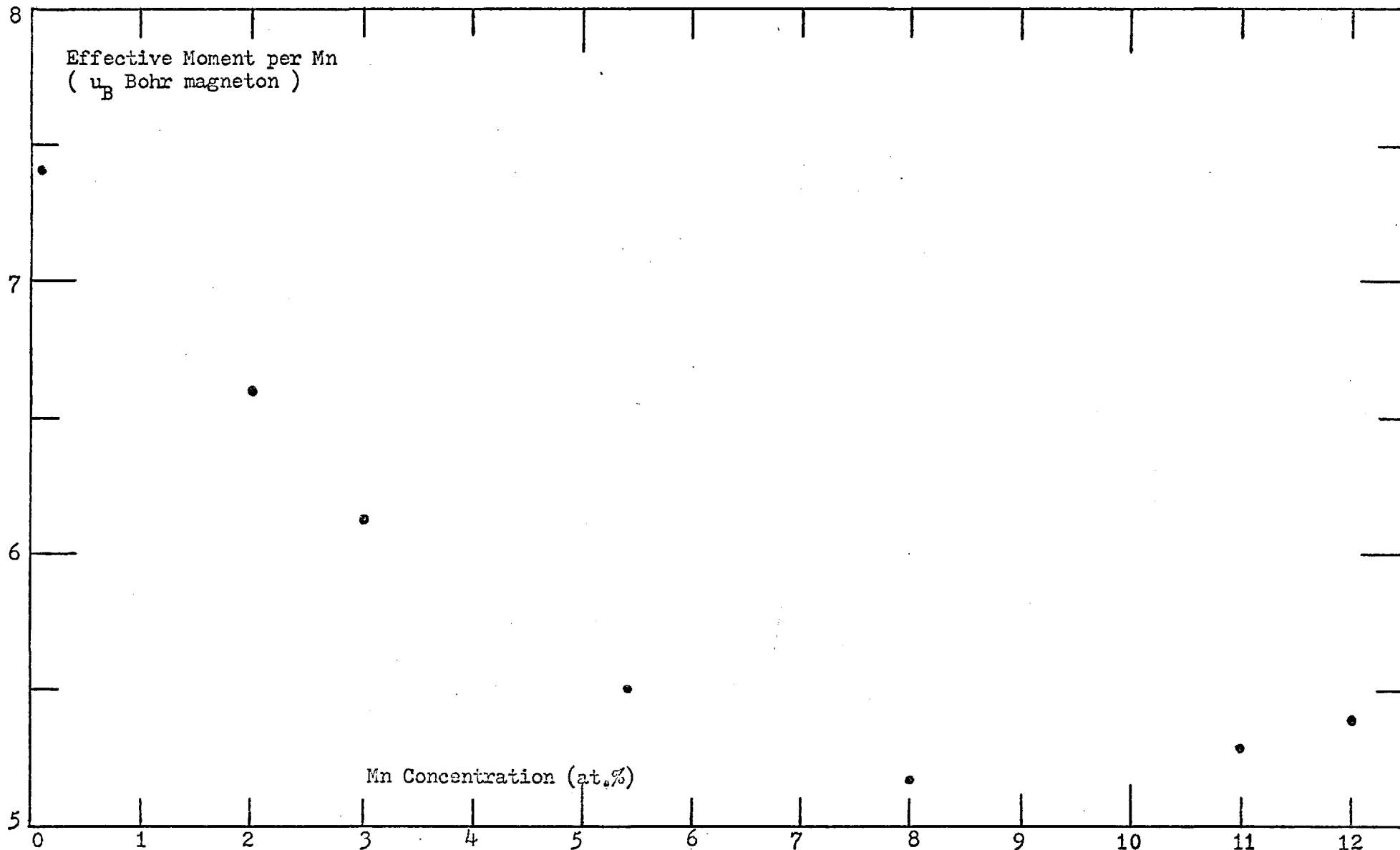
Fig. 72 Effective Magnetic Moment per Mn Atom versus Mn Concentration for PtMn alloy system

and an increase of effective moment from the bulk susceptibility measure-

ments. In the $n > n_c$ region, on the other hand, the direct impurity

interactions become more important, and its effect will increase as n

increases; hence, the collective results between impurities from the

increasing probability of overlapping of polarization clouds will make the

alloy more "magnetic" and a lower Weiss temperature and a larger

effective moment will be seen.

Therefore, the PtMn alloys being examined have covered these

different regions:

(1) the dilute, single-impurity effects dominate region   (n = 0.09

at.% Mn),

(2) the indirect impurity-interactions dominate region (n = 2 to 8

at.% Mn), and

(3) the direct-indirect impurity interactions dominate region

(n = 11 and 12 at.% Mn).

If the temperature T_{max} of the susceptibility maximum represents

the dividing temperature between the magnetic spin glass region and the

paramagnetic region, the magnetic phase diagram of the PtMn alloy

system can thus be established and is shown in Fig. 73.
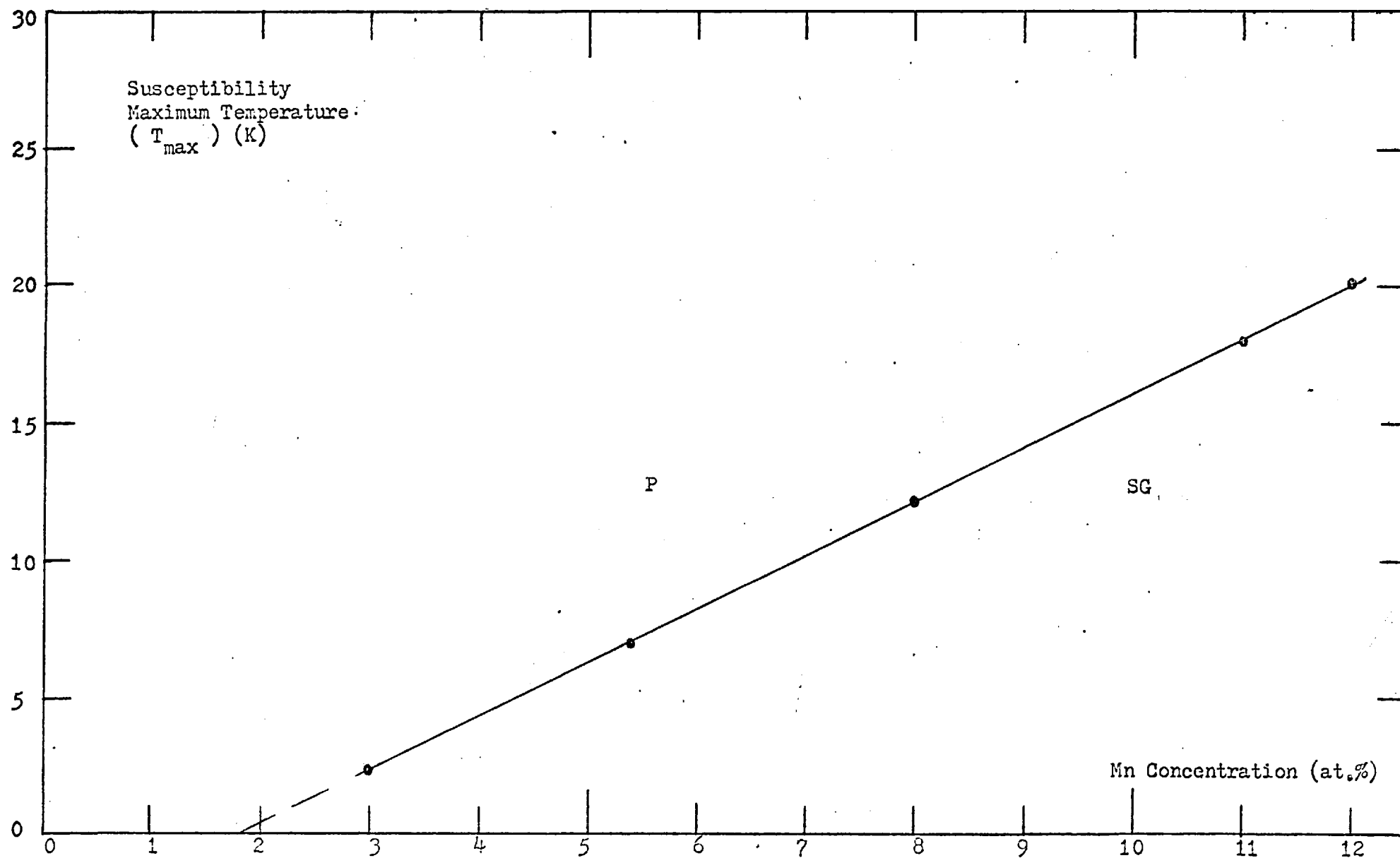
Fig. 73 Susceptibility Maximum Temperature versus Mn Concentration for PtMn alloy system
Magnetic Phase: P:Paramagnetism, SG:Spin Glass

A series of PtCr alloys with respective nominal concentrations n of

7, 10, 14.1, and 17 at.% Cr has been studied. The three alloys with

higher impurity concentrations have been examined by magnetic measure-

ments from 1.4 to 70K and by resistivity measurements from 2 to 4.2K

for the alloy with n = 10 at.% Cr and from 1.7 to 150K for the alloys with

n = 14.1 and 17 at.% Cr. The PtCr (7 at.% Cr) alloy has been examined

by resistivity measurements from 2 to 4.2K.

The magnetization M and the magnetic susceptibility X of the Cr solute

are assumed to be ($M_{alloy} - M_{Pt}$) and ($X_{alloy} - X_{Pt}$) respectively, where

M_{alloy} and X_{alloy} are the magnetization and the susceptibility respectively

of the alloy and M_{Pt} and X_{Pt} are that of the host Pt. The numerical

values of X_{Pt} are taken from that of Van Dam (159). For the three PtCr

alloys (n = 10, 14.1, and 17 at.% Cr) being measured magnetically, the

magnetic isotherms M of the Cr solute versus field H, the low field

susceptibility X, and the reciprocal of the susceptibility ($1/X$) versus

temperature T have been plotted in Fig. 74-78.

From the behaviour of the magnetic isotherms, it is obvious that

these three PtCr alloys do not belong to the free spin systems. There

is no magnetic isothermal remanence after going to high field, 45KOe,

observed in the PtCr (10 at.% Cr) alloy. The susceptibilities of these

three alloys follow a Curie-Weiss law at temperatures above 30K. As

the temperature decreases, the susceptibilities deviate to above the

Curie-Weiss law, which indicates the onset of the superparamagnetic

state. A frozen-in component of the magnetization, when cooled down

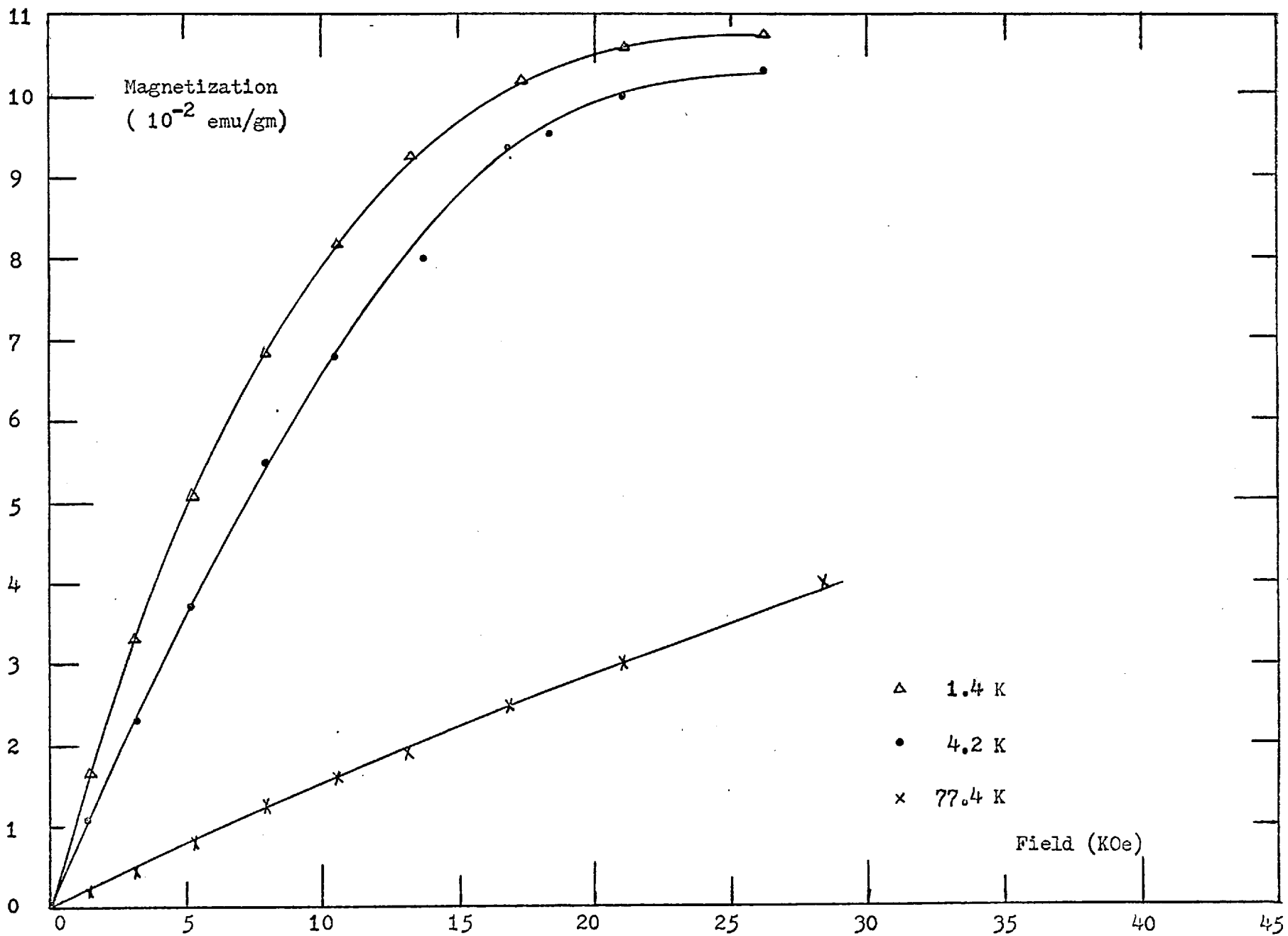in an applied field, magnetic isothermal remanence after going to high

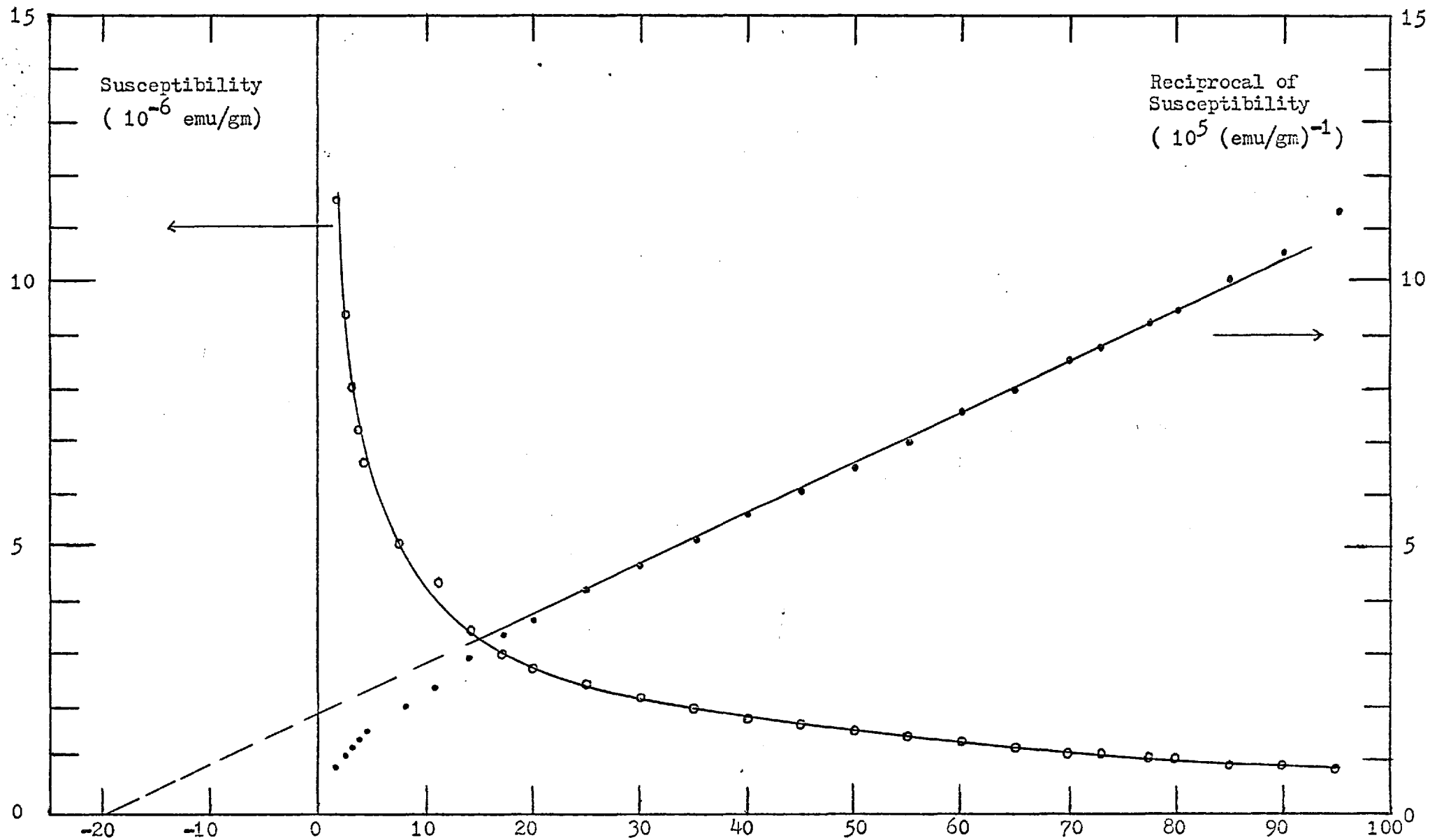Fig. 74 Magnetization versus Field for PtCr (10 at.% Cr) Impurity

176

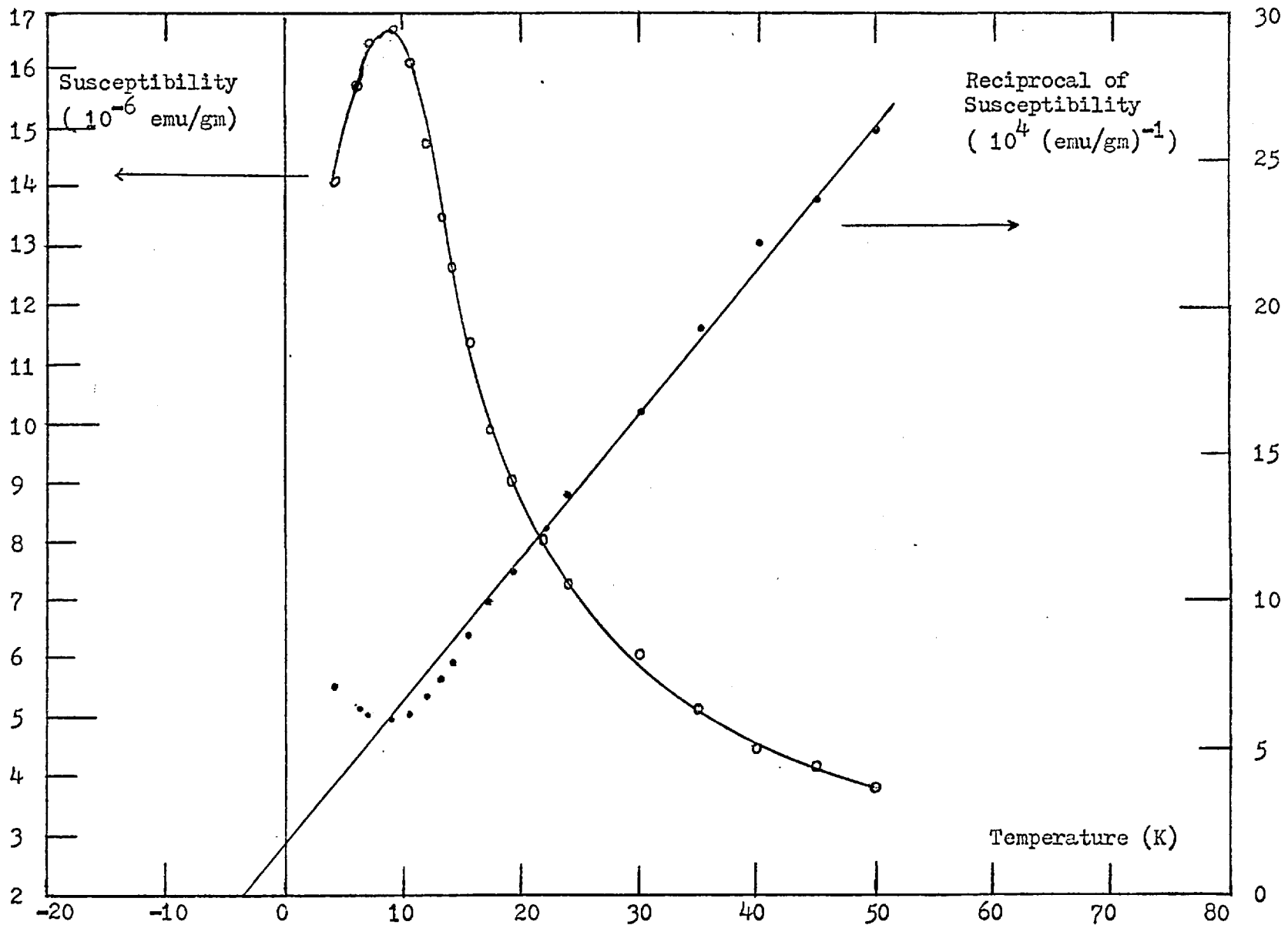Fig. 75 Susceptibility and Reciprocal of Susceptibility for PtCr (10 at.% Cr) Impurity

Fig. 76 Susceptibility and Reciprocal Susceptibility for PtCr (14.1 at.% Cr) Impurity
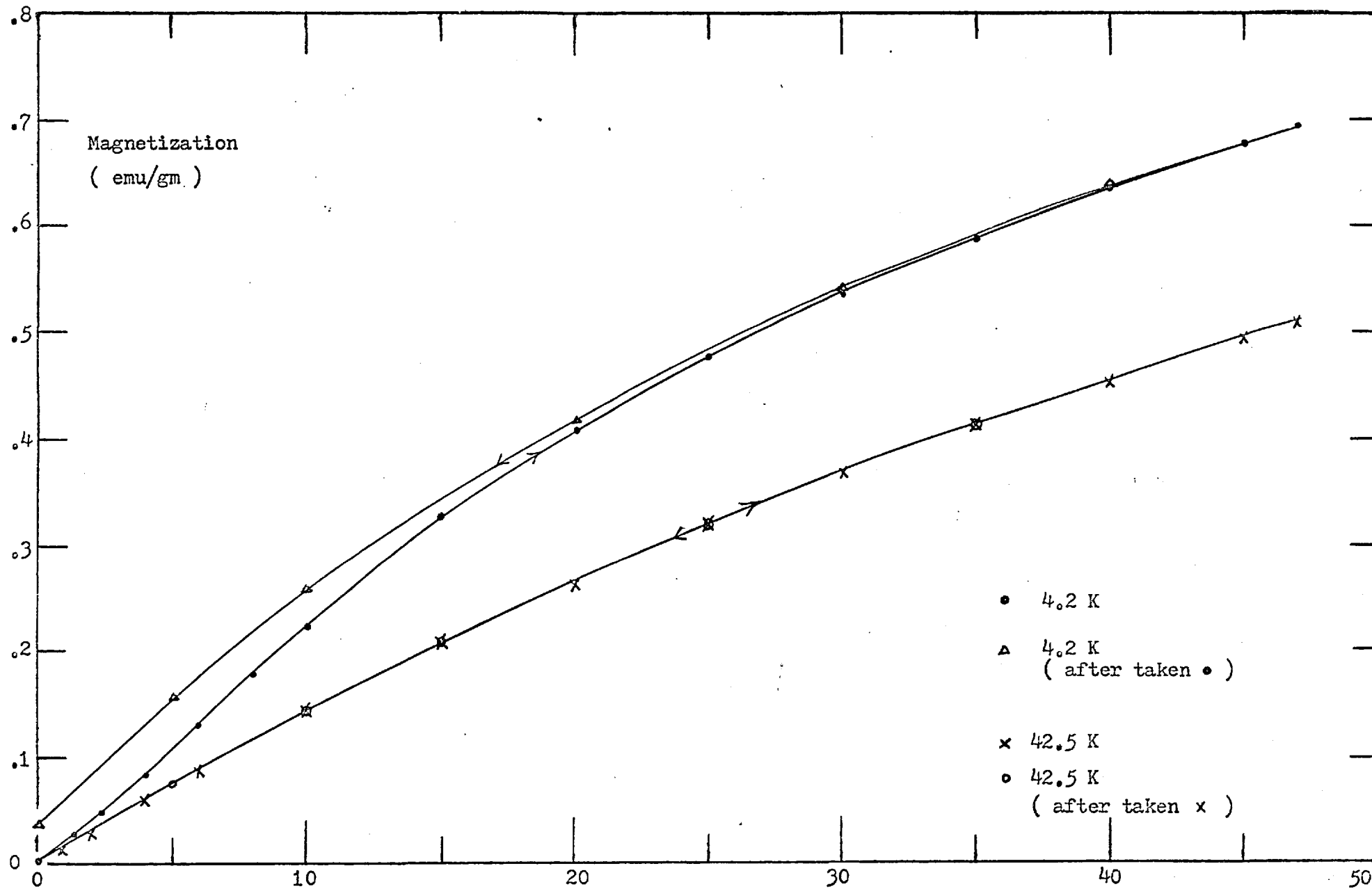
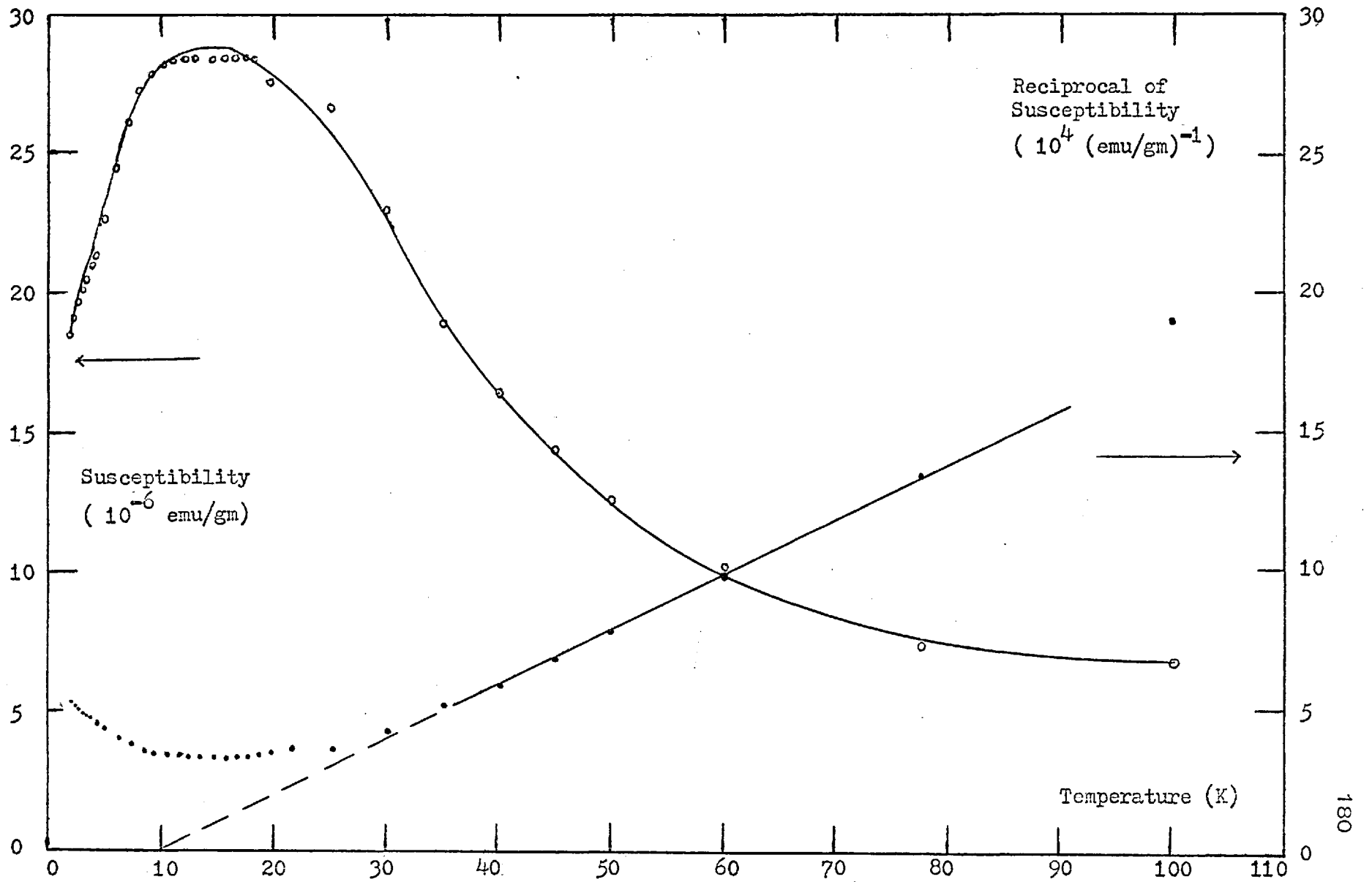Fig. 77 Magnetization versus Field for PtCr (17 at.% Cr) Impurity

Fig. 78 Susceptibility and Reciprocal of Susceptibility for PtCr (17 at.% Cr) Impurity

field, and a maximum on each of the susceptibility curves of the PtCr

alloys with n = 14.1 and 17 at.% Cr at distinct temperature T_{max} = 8.5

and 16K respectively have been observed. It is clear evidence that the

magnetic spin glass state exists in these two alloys within the experimental

range.

From the high temperature susceptibility data of these three PtCr

alloys, the Weiss temperature θ and the effective moment μ_{eff} per Cr

atom have been determined. The values of θ, μ_{eff} and T_{max} of this

experiment and some previous data versus Cr concentration n are listed

in Table 6.

TABLE 6

Magnetic Measurements of PtCr Alloys

Impurity Concentration n	Weiss Temperature θ	Effective Moment μ_{eff}	Susceptibility Maximum Temp. T_{max}	Remark
17 at.% Cr	10 ± 1K	2.0 ± 0.1 μ_B	16.5 ± 1K	Ref. 1
14.1	-4 ± 1	1.45 ± 0.1	8.5 ± 1	Ref. 1
10	-20 ± 1	1.14 ± 0.1	---	Ref. 1
3.5	-55 ± 10	1.2 ± 0.1	---	Ref. 172
1.8	-55 ± 10	1.2 ± 0.1	---	Ref. 172
0.89	-60	1.3	---	Ref. 159
0.8	-55 ± 10	1.2 ± 0.1	---	Ref. 172
0.5	-55 ± 10	1.2 ± 0.1	---	Ref. 172
0.48	-47	1.0	---	Ref. 159

The Weiss temperature θ versus the impurity concentration n has been plotted in Fig. 79. Hence, a scaling relation is observed. The strength V_O of the indirect interaction between two impurity atoms can be estimated through the Larkin and Khmel'nitskii theory (87) $nV_O = C_S k_B \theta$, where C_S is a spin dependent proportional constant of the order unity, and k_B is the Boltzmann constant; therefore, the value of the strength V_O of the indirect interactions between two Cr atoms has been estimated to be $(1.1 \pm 0.1) \times 10^{-37}$ erg cm^3 for PtCr (17 at.% Cr) alloy. This value of V_O is less than that of Mn impurity atoms $(5.6 \times 10^{-37}$ erg cm$^3)$ in the same Pt host as obtained in a previous section.

If the temperature T_{max} of the susceptibility maximum represents the division between the magnetic spin glass region and the paramagnetic state, from the experiences from other similar alloy systems such as PtMn (1) (similar impurity in same host) and PdCr (159) (same impurity in similar host), we may propose that the division between the magnetic spin glass region and paramagnetic state is a straight line connecting the data points of T_{max} on the temperature T versus impurity concentration n plot. Hence, a magnetic phase diagram of the PtCr alloy system can be established and is shown in Fig. 80.

From this magnetic phase diagram, the magnetic spin glass state does not appear in the PtCr alloy system until the impurity concentration is above about 11 at.% Cr. This conclusion is consistent with our experimental results of the PtCr (10 at.% Cr) alloy, i.e. no magnetic spin glass state being observed within the experimental range. It is also consistent with the magnetic measurements by Inoue and Nagasawa (n = 0.05 to 2 at.% Cr) (176) and by Van Dam (n = 0.5 to 0.9 at.% Cr) (159) and with
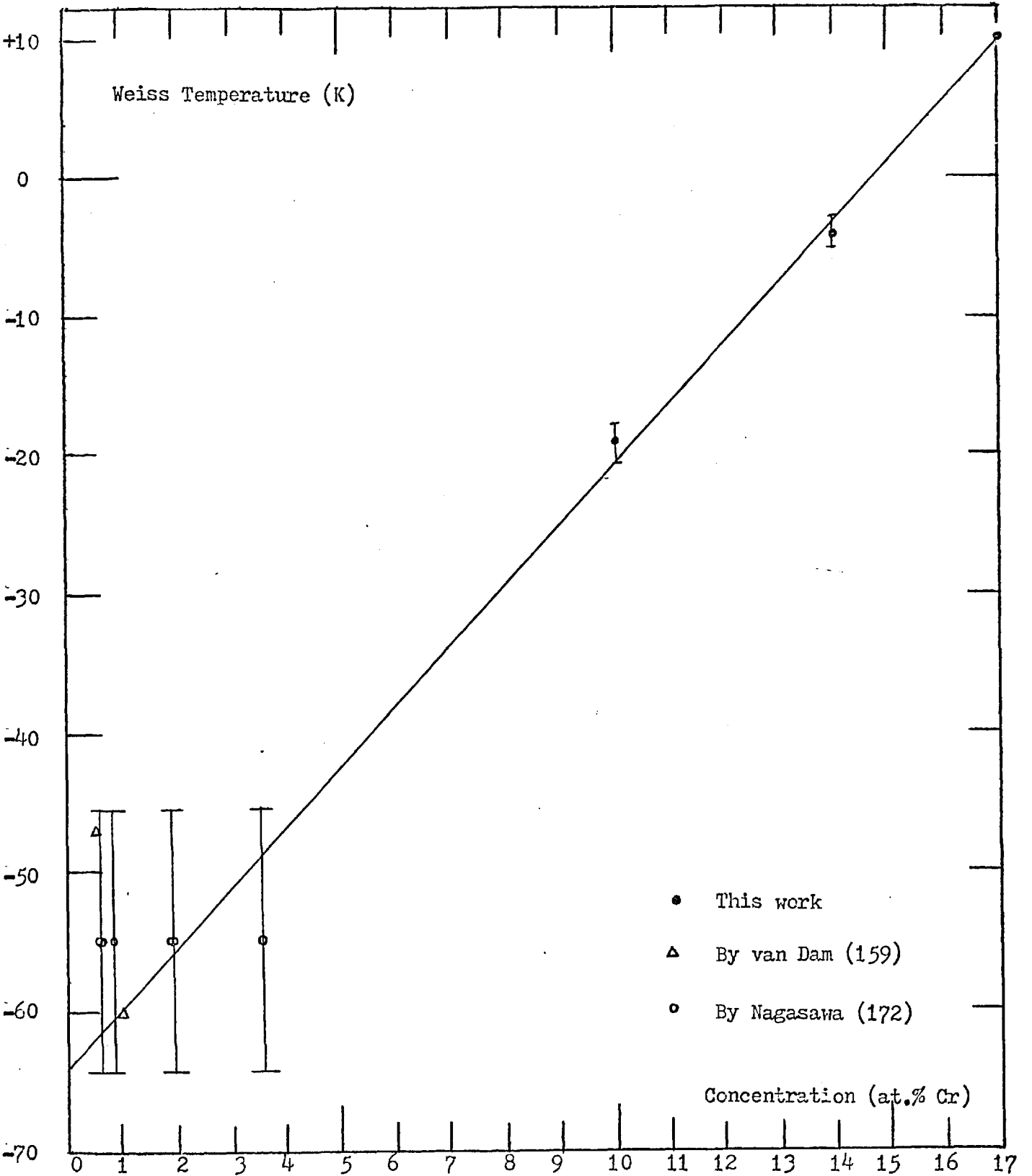
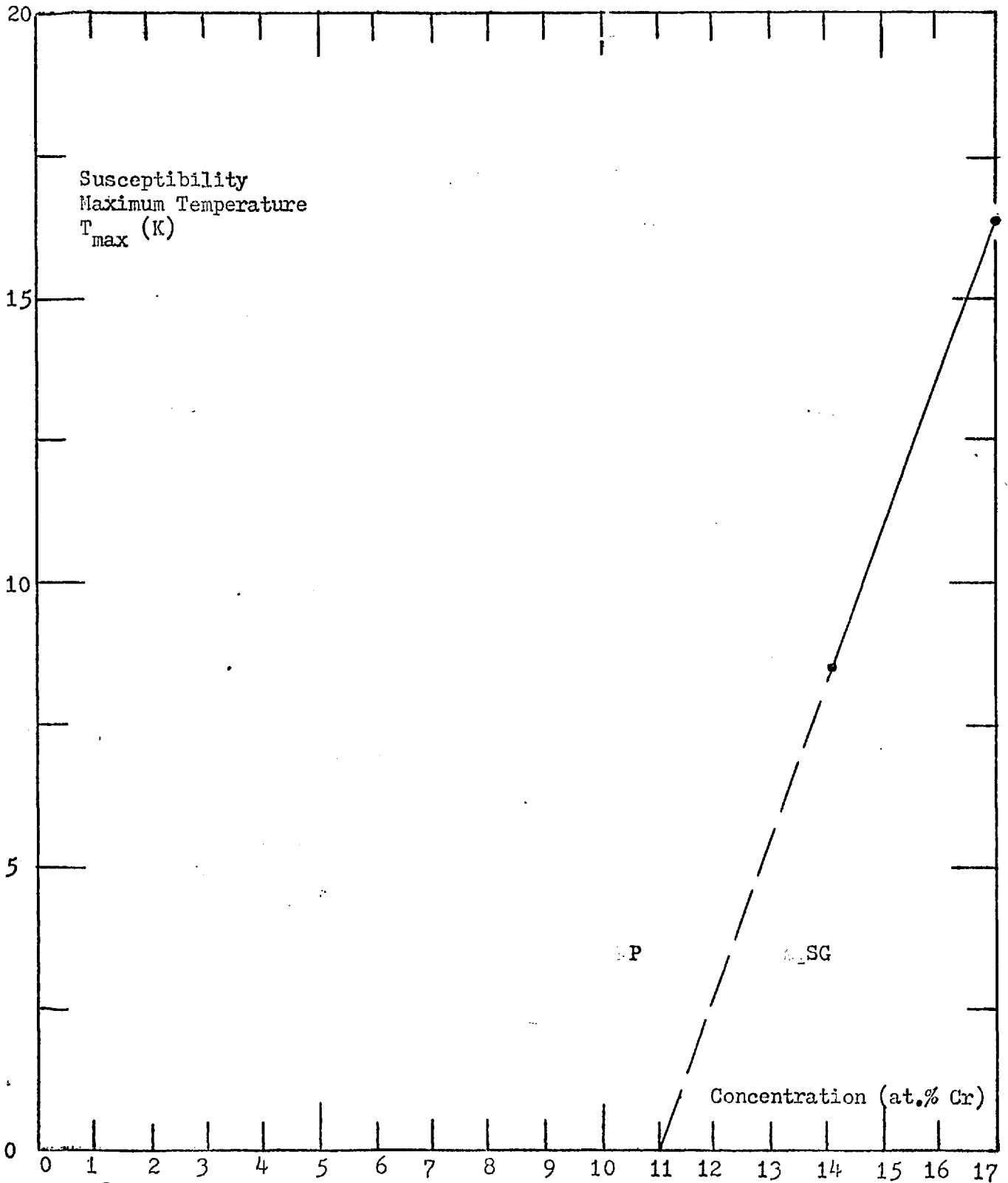Fig. 79 Weiss Temperature versus Concentration for PtCr alloy

Fig. 80 Susceptibility Maximum Temperature versus Concentration for PtCr alloy
Magnetic Phase: P:Paramagnetism, SG:Spin Glass

the resistivity measurements by Star et al (n = 0.5 to 3 at.% Cr) (173),

in which they did not observe any sign of the magnetic spin glass behaviour.

Another early susceptibility data measured by Nagasawa (n = 0.5 to 3.5

at.% Cr) (172,177) has a strong temperature-dependent behaviour at low

temperatures. We believe, as suggested by Van Dam (159), that this

anomalous behaviour is due to a large amount of magnetic contamination.

Recently, Roshko and Williams (174) claimed that the magnetic

ordering does not exist above 1.4K in the PtCr alloy system even in their

highest concentration sample, n = 12 at.% Cr. Their claim is based on

the fact that "there is no maximum" in their incremental resistivity

measurements. This seems to challenge our conclusion at first glance;

however, we cannot agree with them. It might be because the PtCr

(12 at.% Cr) alloy, which is located at the near margin of the possible

magnetic spin glass state, merely begins to stabilize, and this will probably

affect the significance of the results at the boundary of their experimental

range. Our main objection is that the existence of a magnetic spin glass

state does not necessarily imply the existence of an incremental

resistivity maximum.

In order to prove our arguments, we chose two PtCr alloys of n =

14.1 and 17 at.% Cr, with well-established behaviours of the magnetic

spin glass state, i.e. with a maximum in the susceptibility and the field

cooling and the isothermal magnetic remanence effects and measured

their resistivities from 1.7 to 150K. The incremental resistivity ρ ,

assumed to be $\rho_{alloy} - \rho_{host}$ where ρ_{alloy} is the resistivity of

the alloy and ρ_{host} is that of the host, of these two alloys versus

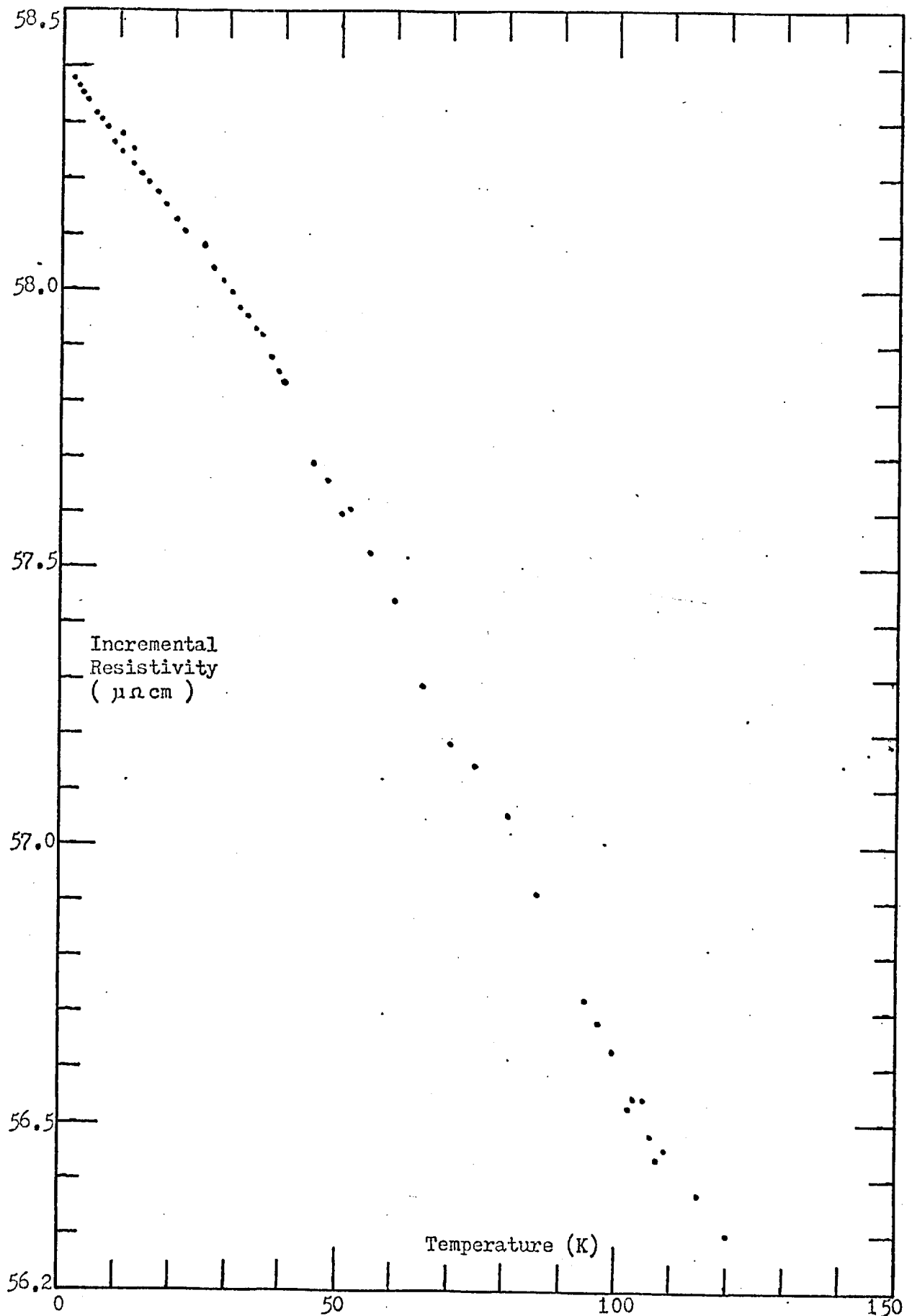temperature T, are plotted in Fig. 81 and 82. There is no maximum

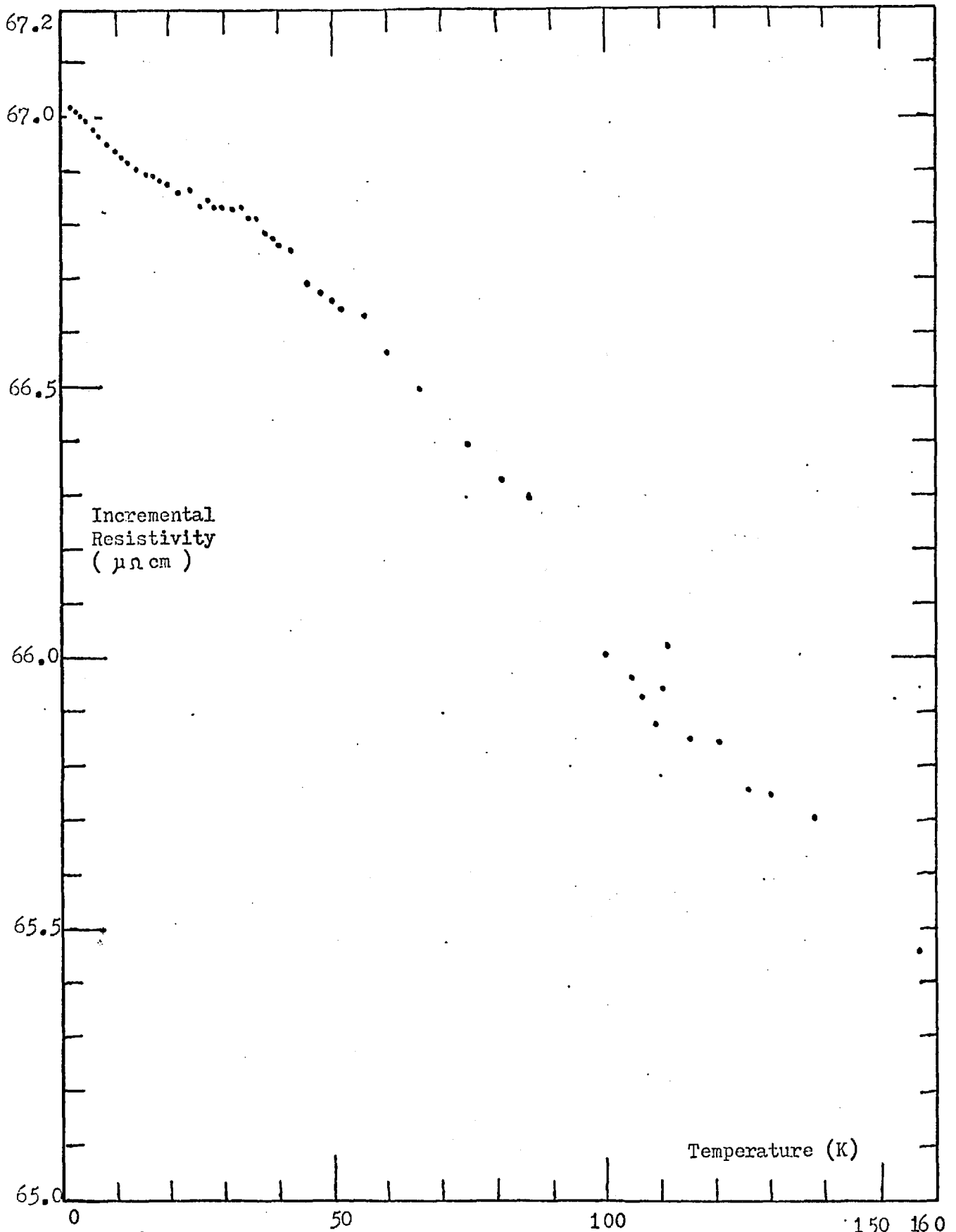Fig. 81 Incremental Resistivity versus Temperature for PtCr (14.1at.% Cr)

Fig. 82 Incremental Resistivity versus Temperature for PtCr (17at.% Cr)

being observed in the incremental resistivity of these two PtCr alloys

above 1.7K. Hence, our argument has been experimentally verified,

and we believe the magnetic spin glass state of the PtCr alloys will start

to stabilize from the impurity concentration at about 11 at.% Cr.

The low temperature incremental resistivity ρ of all the measured

PtCr alloys with impurity concentrations of 7, 10, 14.1, and 17 at.% Cr

versus temperature T and temperature square T^2 are plotted in Fig. 83

and 84, respectively. The low temperature incremental resistivity

of the two PtCr alloys with higher impurity concentrations (14.1 and 17

at.% Cr) have also been plotted versus $T^{3/2}$ in Fig. 85.

The incremental resistivity ρ of the two PtCr (7 and 10 at.%

Cr) alloys both decrease as the temperature increases and are a function

of T^2 at low temperature as this behaviour has been shown in Fig. 84.

The incremental resistivity ρ can be expressed by (174):

$$\rho = A + B \ln ((T^2 + \theta_o^2)^{1/2})$$

where A and B are impurity concentration dependent constants, and θ_o

measures the local spin fluctuation lifetime, $T_{sf} \simeq h/k_B\theta$. As the

temperature increases, ρ will vary with T^2, T, and then lnT. The

constant B can be expressed as:

$$B \propto \sin^2 (\pi S/(2l + 1)) \cos (\pi Z/(2l + 1))$$

where S is the impurity spin, (2l + 1) accounts for the orbital degeneracy

of the impurity, and Z is the host-impurity change difference. For the

PtCr alloy system, using s = 5/2 and Z = -4 yields a negative sign for

B (82). It is thus suggested that these two PtCr alloys belong to the Kondo-
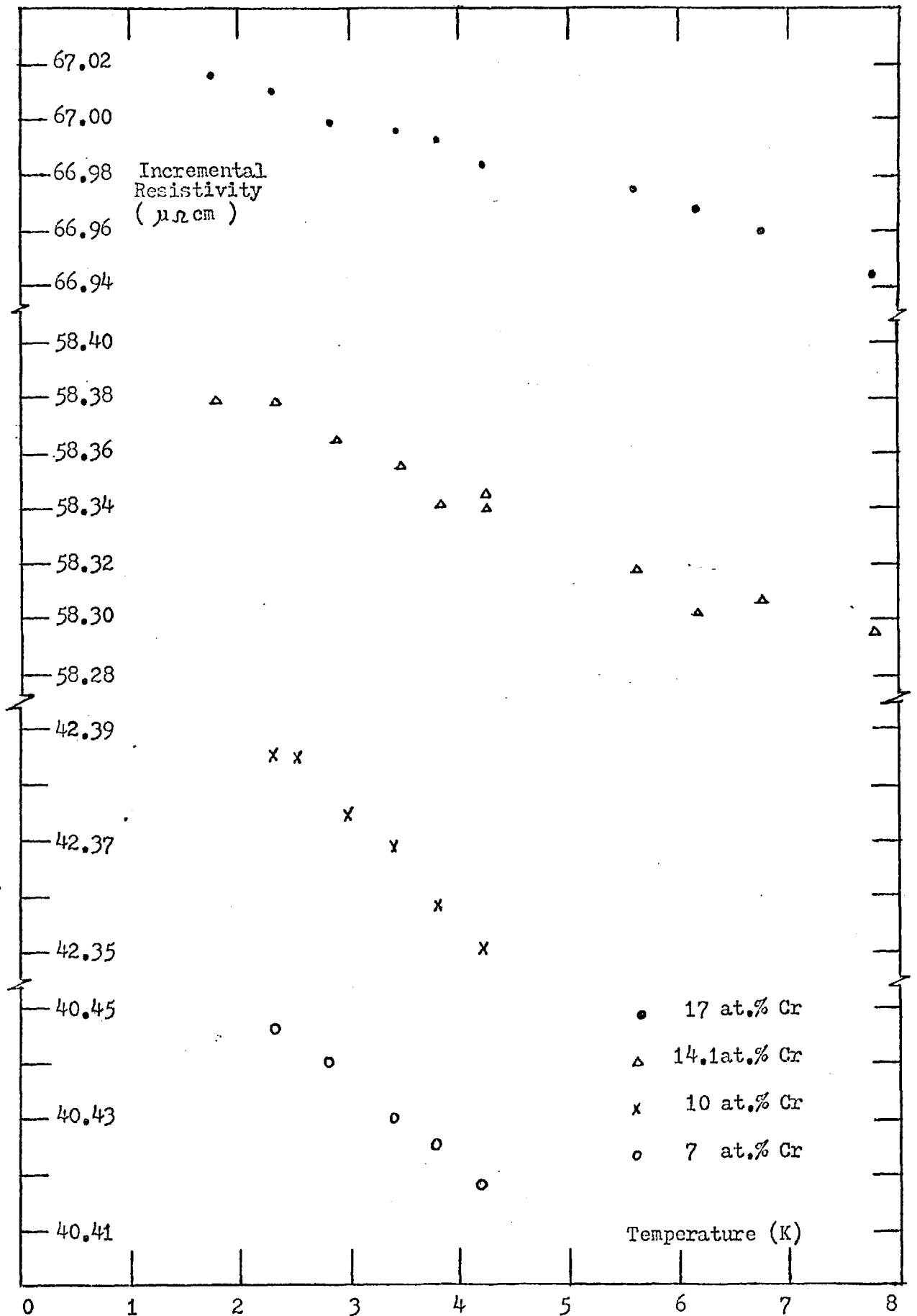
like spin fluctuation alloys.

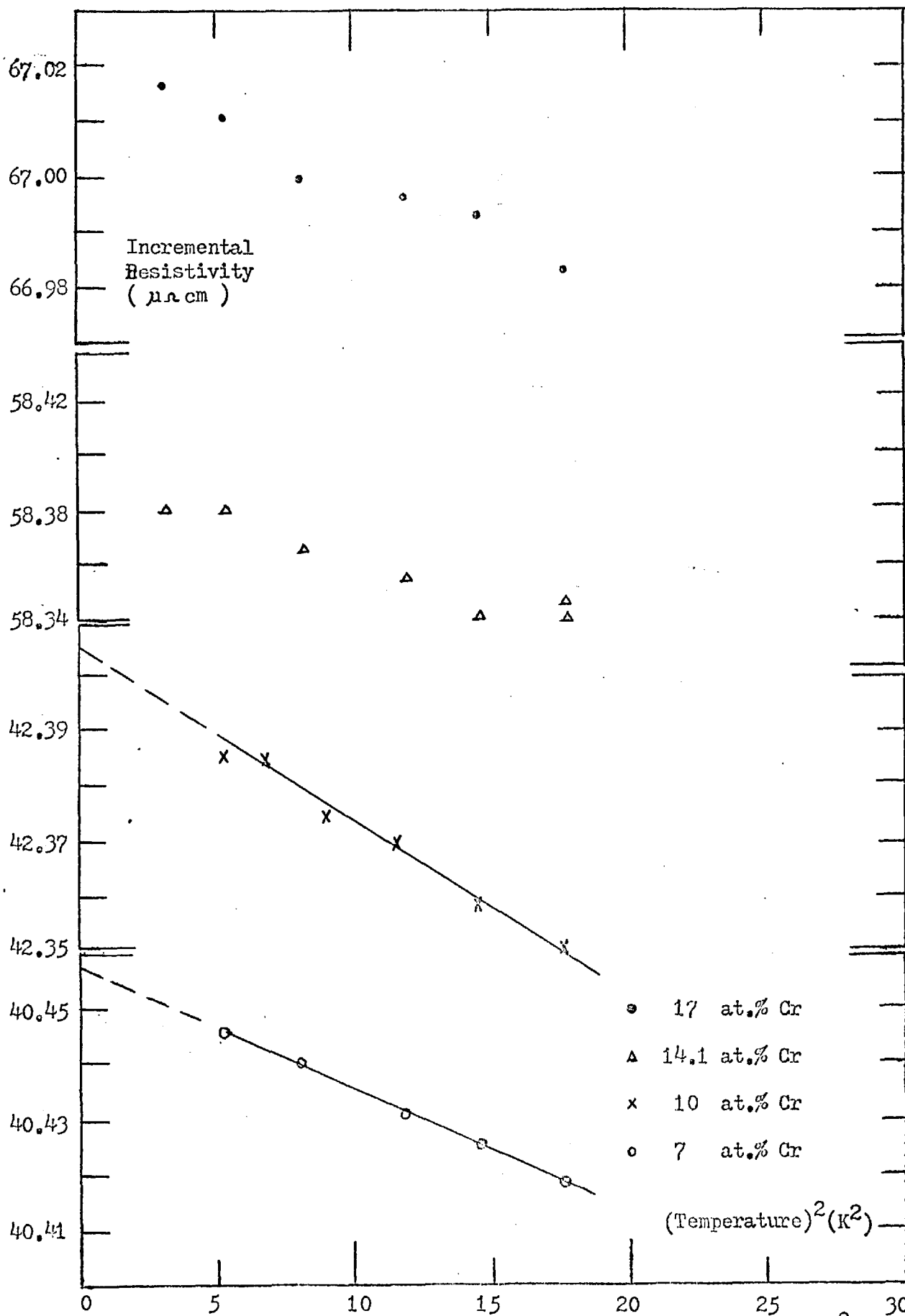Fig. 83 Incremental Resistivity $\rho_a - \rho_{host}$ versus Temperature for PtCr alloy

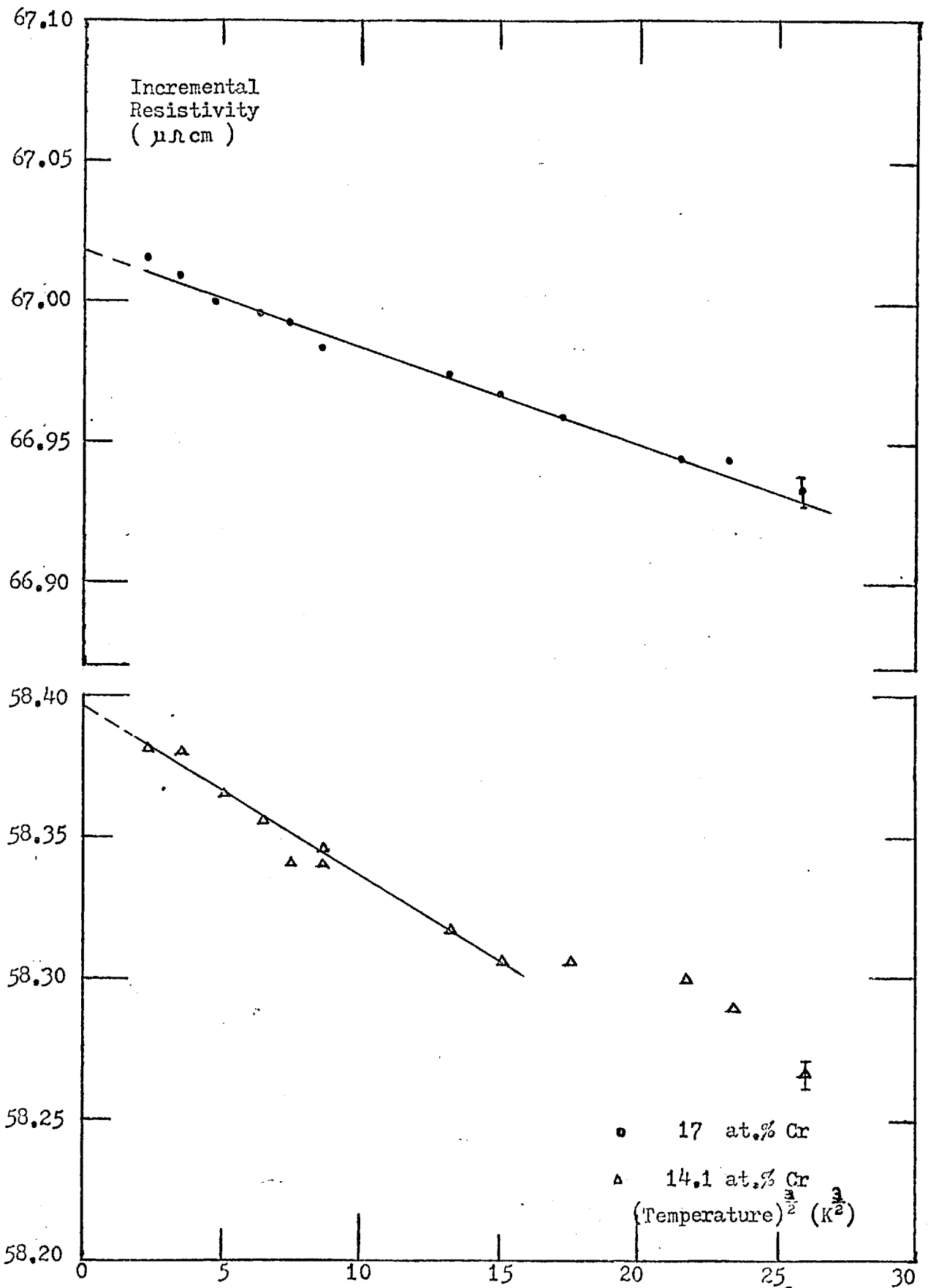Fig. 84   Incremental Resistivity $\rho_{alloy} - \rho_{host}$ versus (Temperature)^2 for PtCr

Fig. 85 Incremental Resistivity $\rho_{alloy} - \rho_{host}$ versus (Temperature)$^{\frac{3}{2}}$ for PtCr

The incremental resistivity ρ of the two PtCr (14.1 and 17 at.%

Cr) alloys both fall as the temperature increases and are a function of

$T^{3/2}$ at low temperatures. This behaviour has been shown in Fig. 85.

It is, thus, suggested that these two PtCr alloys belong to the magnetic

spin glass category, and this agrees with the magnetic measurements. A

linear relation between ρ and temperature T can be seen at higher

temperatures in Fig. 83 and 84. The above experimental results of

resistivity measurements provide further support to our magnetic

results and the magnetic phase diagram in Fig. 80.

The experimental results which have been presented in this chapter

provide the magnetic phase diagrams of the PtMn and the PtCr alloy

systems. A comprehensive magnetic phase diagram of the Pt-3d

alloy systems can thus be established and is plotted in Fig. 86. The

magnetic phase diagram of the Pd-3d alloy system has been already
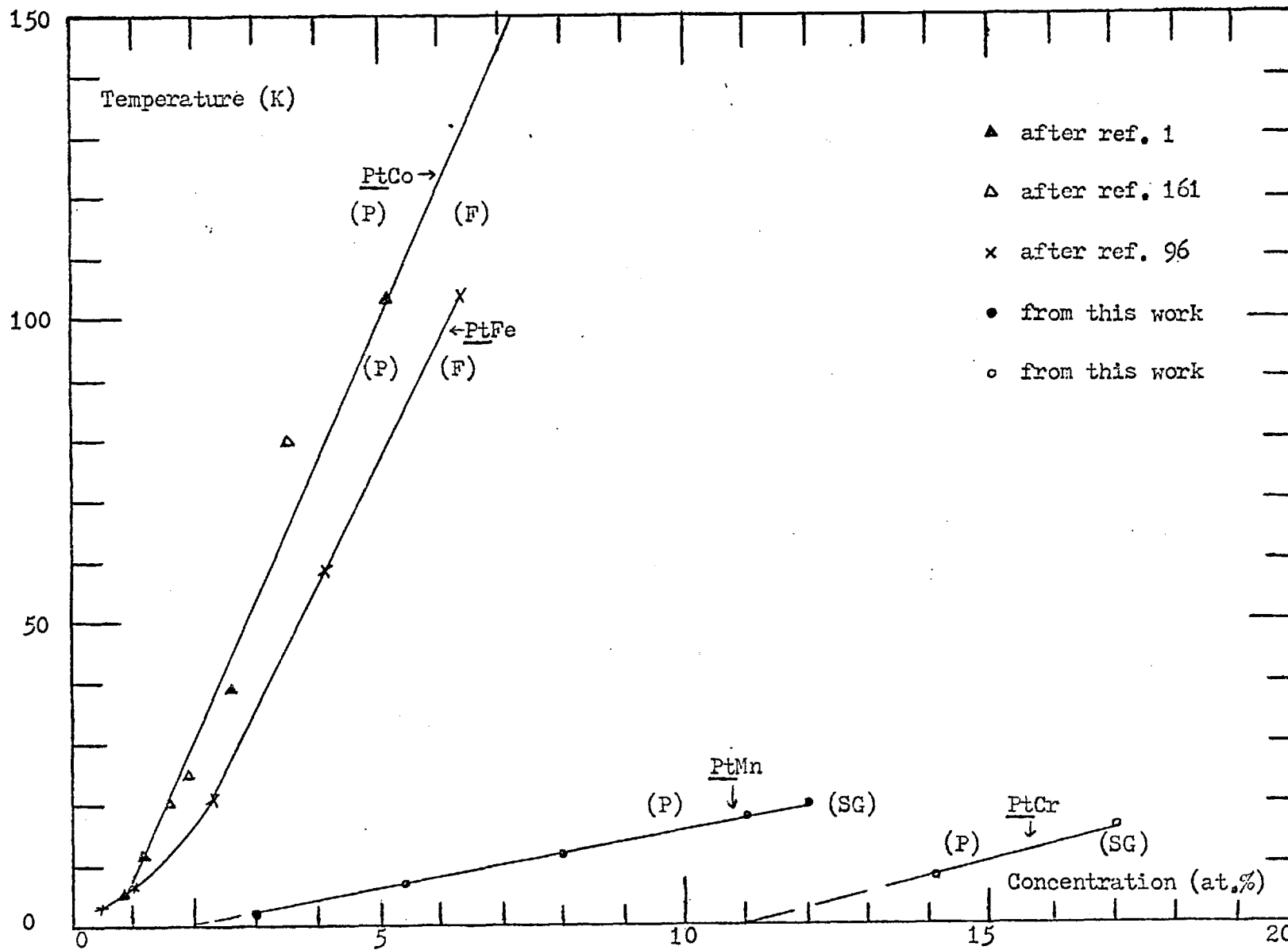
plotted in Fig. 52 for reference.

Fig. 86 Magnetic Phase Diagram for Pt-3d Alloy System, paramagnetic:(P), Ferromagnetic:(F), Spin Glass State:(SG); PtMn and PtCr data points from susceptibility maximum points

CHAPTER 5   MAGNETIC ENVIRONMENTAL EFFECTS IN

Pd-PtMn ALLOYS

Abstract

When 3d transition metal is dissolved as the impurity in the 4d and/or 5d transition metal host to form disordered alloys, the magnetic properties of such alloys provide a wide variety of characteristics.

Because of the large exchange enhancement factors of Pd and Pt, the Pd-3d and the Pt-3d alloys are of particular interest. When a small amount of Mn, say 3 at.% Mn, is dissolved in Pd or Pt, at low temperature, PdMn is ferromagnetic, and PtMn is of magnetic spin glass state. The striking difference between them can be interpreted by the wide difference between their exchange enhancement factors. In the case that the environment of the Mn impurity changes continuously from Pd to $Pd_{1-x}Pt_x$ to Pt by alloying, the behaviours of the alloys should also change accordingly.

The $Pd_{1-x}Pt_x$Mn alloy system has been studied mainly by magnetic measurements from 1.4 to 20K and also by some resistivity measurements. The magnetic phase diagram of paramagnetic-ferromagnetic-magnetic spin glass state has been established. For $Pd_{1-x}Pt_x$Mn alloys containing 3 at.% Mn, the ferromagnetism dominates for $x < (0.10 \pm 0.02)$, and the magnetic spin glass state is observed for higher x alloys.

Section I. Introduction

When 3d transition metal is dissolved as the impurity in the 4d and/or

5d transition metal host to form disordered alloys, the magnetic properties

of such alloys provide a wide variety of characteristics.

For the dilute alloys, because of the relatively small number of

parameters involved, a model could almost be deduced from the experi-

mental results; however, for the more concentrated alloys, the number

of parameters is much larger, and the behaviours are much more involved.

In the present state of experiments, a model must be chosen a priori.

The magnetic environmental effects in alloys provide a brief description

for the causes of these wide behaviours.

The investigation of the environmental effects in alloys has naturally

been approached through two models of opposing directions: the local

environmental effect (106) and the cooperative effect (110).

The model of the local environmental effect on magnetic moment

formation assumes that the alloy is random and perfectly disordered,

and a well-defined magnetic moment is assigned to each solute atom with

a certain number of atoms within a critical range (106-108) of one of the

constituents of the matrix host.. The magnetization process may be

essentially a discontinuous one, the moment being either zero or some

well-defined value on a solute atom. This model has successfully

interpreted the behaviours of alloys of, for example, Nb-MoFe, Rh-PdCo

(106), Ir-PtFe and Os-Ir-PtFe (109).

The model of the cooperative effect, on the other hand, suggests

a gradual variation in the magnitude of the moment with the size of a

cluster above some critical value. The idea of giant moments can be

verified by, for example, the neutron scattering experiment (104,178) and by comparing the difference between the measurements of the local and bulk properties (100-103). The existence of such giant moments suggests that magnetic atoms are in clouds of host spins within which they are strongly coupled; these clouds are more or less independent in the paramagnetic range and give rise to superparamagnetism.

In comparing the different behaviours of 3d transition metal impurities in Pd or Pt host, the main reason there is a wide variety of characteristics possible is the large values but with a wide difference of the exchange enhancement factor D; the values of D have been estimated to be 9.4 and 3.8 for Pd and Pt respectively (112,163).

For these large exchange enhancements of Pd and Pt, we can reach the interpretation that when the ferromagnetic transition element Fe, for instance, is dissolved in a matrix of Pd or Pt, the long range magnetic coupling results from the overlapping of strong spin polarization of the matrix, which aligns itself in the direction of and centered on the magnetic moment of the solute atoms. The Curie temperature rises rapidly with solute content and only at very low Fe concentration in Pd (118) and Pt (82) is there evidence for the usual magnetic spin glass phase of good moment system. The behaviours of Co dissolved in Pd or Pt are similar to that of the Fe alloys.

In the PdMn alloy system, for example, the behaviours are different. PdMn for concentrations up to about 3 at.% Mn resembles PdFe (but with Curie temperatures almost a factor of 10 smaller). At concentrations above 5 at.% Mn, the ferromagnetism disappears, and an enfeebled version of the CuMn magnetic spin glass appears. This behaviour has been shown

clearly in the magnetic phase diagram of the Pd-3d alloy system as in

Fig. 52. The difference between Fe and Mn is due to a difference in sign

of the nearest neighbors Fe-Fe (ferromagnetic) and Mn-Mn (antiferro-

magnetic) interactions (68) which becomes important as the impurity

concentration increases (69).

The PtMn alloys, on the other hand, show a magnetic spin glass

phase behaviour and no observation of ferromagnetic phase at low

concentrations (1). This behaviour has been shown clearly in the magnetic

phase diagram of the Pt-3d alloy system in Fig. 86.

This difference in behaviours between PdMn and PtMn must be due to

the difference of the exchange enhancements of the hosts Pd and Pt. In

the "dilute" PdMn alloys, although the Mn atoms are rather far apart

from each other, the long range magnetic coupling resulting from the

strong spins polarization clouds centered at Mn atoms are overlapping

and cause ferromagnetism. But, for the "dilute" PtMn alloys, the less

strong spin polarization clouds centered at Mn atoms are not overlapping

yet and cause only superparamagnetism. As the Mn concentration

increases, the nearest neighbor Mn antiferromagnetic interaction becomes

important. There is a keen competition between this antiferromagnetic

interaction and long range ordering, and a magnetic spin glass phase

appears.

The striking difference between the low concentration of Mn impurity

in Pd and Pt hosts has been, thus, well interpreted. The next question

to ask in research will be what will happen if we add a small amount of Mn

as an impurity into the $Pd_{1-x}Pt_x$ binary matrix host? For a low concen-

tration of Mn impurity, say 3 at.% Mn, in the $Pd_{1-x}Pt_x$ binary matrix

at low temperature, on one hand, $\underline{Pt}Mn$ ($x = 1$) is of magnetic spin glass

state, and on the other hand, $\underline{Pd}Mn$ ($x = 0$) is of ferromagnetic state.

Where and how will these two states meet each other? To determine this,

a study on the $\underline{Pd_{1-x}Pt_x Mn}$ alloy system has been carried out and is

presented here.

The alloys with 3 at.% Mn impurity in $Pd_{1-x}Pt_x$ binary matrix with

$x = 0.02, 0.05, 0.15, 0.25, 0.35, 0.50, 0.75,$ and 1.00 and other alloys

of $\underline{Pd_{.75}Pt_{.25}}Mn$ (4 at.% Mn) and $\underline{Pd_{.98}Pt_{.02}}Mn$ (1.5 at.% Mn) have been

examined.

The impurity concentration of 3 at.% Mn was chosen because $\underline{Pd_0 Pt_1 Mn}$

(3 at.% Mn) alloy (which has been studied in Chapter 4) belongs to magnetic

spin glass state at low temperatures with a well-defined susceptibility

maximum at temperature $T_{max} = 2.5 \pm 0.5K$ (1) and, on the other end

of the series $\underline{Pd_1 Pt_0 Mn}$ (3 at.% Mn) alloy is ferromagnetic at low tempera-

tures with a Curie temperature $T_c \approx 8 \pm 0.5K$ (179,180). This concen-

tration of impurity for $\underline{Pd}Mn$ alloy has the highest T_c on the magnetic phase

diagram. If the Mn concentration decreases, it will cause a decrease of

T_c, which means less ferromagnetic correlation; if the Mn concentration

increases, the T_c will also fall lower because the nearest neighbor Mn-Mn

antiferromagnetic couplings become more important, and the interactions

become more involved. Therefore, the 3 at.% Mn in Pd should be the

critical Mn concentration with clearest ferromagnetic correlation effect

but before the impurity interaction becomes too involved.

Some previous experiments have been carried out on Ir-Pt, Ir-Pd,

Pd-Pt, Rh-Pd, Ir-Rh, Ir-Pd-Rh, and Pb-Pd-Rh alloy systems (113), and

the smooth change of susceptibility versus electron density has been shown

in Fig. 17. This smooth change of Pd-Pt alloys gives us a preliminary

knowledge of the host of the $Pd_{1-x}Pt_xMn$ alloys.

The magnetic properties of the ordered single crystal of $Fe(Pd_xPt_{1-x})_3$

alloys have been investigated (181). $FePd_3 (x = 1)$ is ferromagnetic with

the Curie temperature $T_c = 540K$, and $FePt_3 (x = 0)$ is antiferromagnetic

with the Neel temperature $T_N = 170K$; and there is a ferromagnetic-

antiferromagnetic transition in the composition range $0.4 < x < 0.6$.

In the ferromagnetic state, the Curie temperature decreases monotonically

with decreasing x, and in all the antiferromagnetic ones, the Neel tempera-

ture is constant at 170K. In the narrow composition range $0.65 > x > 0.45$,

they are in a ferrimagnetic state at low temperatures and in ferromagnetic

state at the temperatures above T_t. The Weiss temperature θ decreases

monotonically with decreasing x and changes the sign in the vicinity of

$x = 0.2$. Both ferromagnetic and antiferromagnetic coexist for $x = 0.53$.

The magnetic phase diagram, the effective moment, and spontaneous

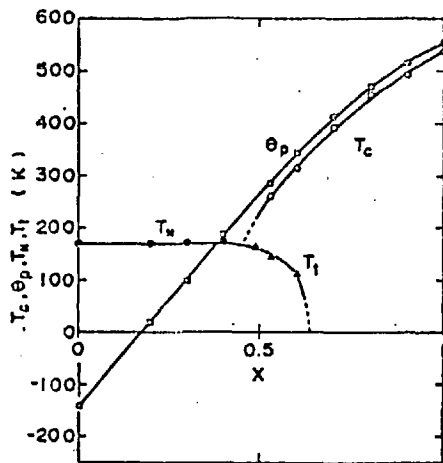magnetization at 4.2K versus x are shown in Fig. 87 and 88 respectively.

Fig. 87 Curie temperature T_c, Weiss
temperature θ, Neel tempera-
ture T_N, and ferrimagnetic-
ferromagnetic transition
temperature T_t versus
composition x of $Fe(Pd_xPt_{1-x})_3$
compounds (after Kadomatsu
(181)).

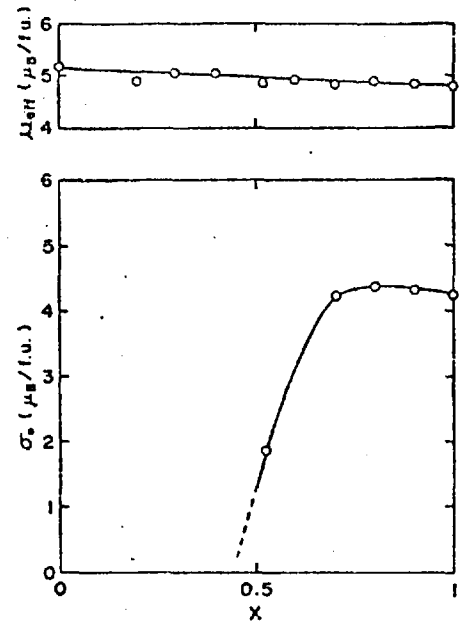Fig. 88 Effective moment $\mathcal{M}_{eff}$
and spontaneous magne-
tization per formula unit
at 4.2K versus composi-
tion x of $Fe(Pd_xPt_{1-x})_3$
compounds (after
Kadomatsu (181)).

For further references, the Weiss temperatures θ and the effective
moment $\mathcal{M}_{eff}$ versus host composition of the similar alloys of the
$\underline{Rh_xPd_{1-x}Fe}$ (1 at.% Fe) and the $\underline{Ir_xPt_{1-x}Fe}$ (1 at.% Fe) have been plotted
in Fig. 89 and 90 respectively.
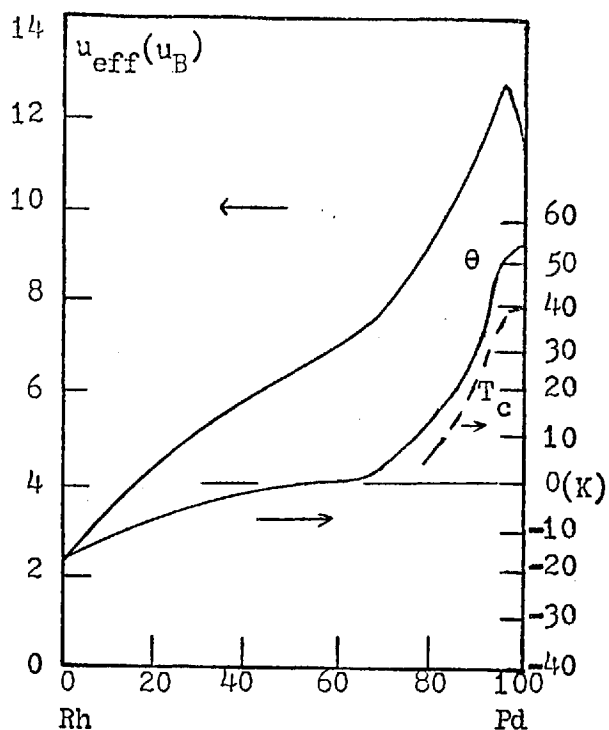
Fig. 89 Effective moment $\mathcal{U}_{eff}$, Curie

temperature T_c, and Weiss

temperature θ versus composi-

tion of Rh-PdFe (1 at.% Fe)

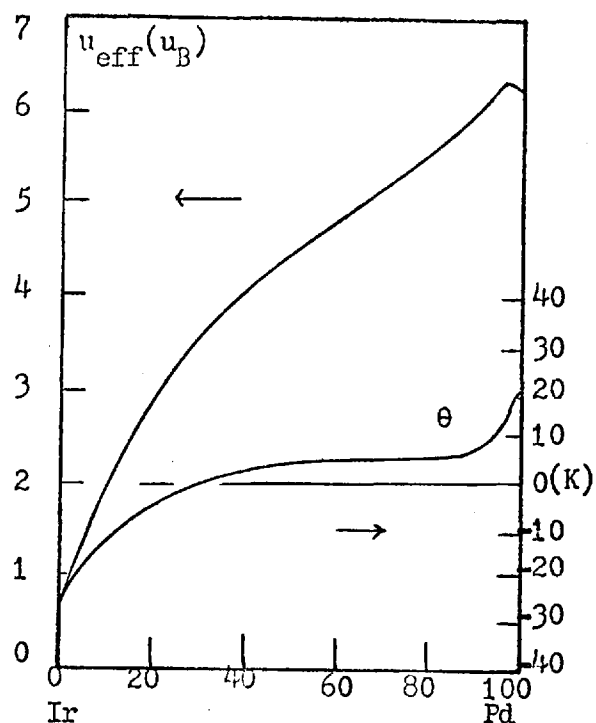alloy (after Clogston et al

(182) and Nagasawa (182a)).

Fig. 90 Effective moment $\mathcal{U}_{eff}$

and Weiss temperature

θ versus composition of

Ir-PtFe (1 at.% Fe)

alloy (after Geballe

et al (109)).

Section II. Experimental Procedures

A series of $Pd_{1-x}Pt_xMn$ alloys with 3 at.% Mn impurity in $Pd_{1-x}Pt_x$ binary matrix with x = 0.02, 0.05, 0.15, 0.25, 0.35, 0.50, 0.75, and 1.00 and other alloys of $Pd_{.75}Pt_{.25}Mn$ (4 at.% Mn) and $Pd_{.98}Pt_{.02}Mn$ (1.5 at.% Mn) were made. All the alloys belong to the FCC structure. The starting materials were 99.99% pure Pt and 99.999% "Specpure" Pd, both from Johnson Matthey Ltd., and 99.99% pure Mn from Koch-Light Labs. Ltd. All samples were made in ar. arc furnace within which was a circular cavity on a water cooled copper hearth filled with two-thirds atmosphere argon. The alloys were melted, turned over, and remelted several times, and then formed into short cylinders of about 3mm diameter for magnetic measurements, and into thin long wires of about 0.8mm diameter for electrical resistivity measurements. All samples were cleaned by an aqua regia solution and homogenized in a vacuum at $1000^\circ C$ for about five hours, then quenched in cold water before measuring.

Magnetic measurements were carried out by a force (Faraday) method using a superconducting solenoid (0-50KOe) with separate superconducting gradient field coils in a B.O.C. cryostat; the forces were measured with a Beckman microbalance LM-600. Temperatures were derived from the helium vapour pressure with reference to the standard table from 1.4 to 4.2K, from the resistance of an Allen Bradley carbon resistor from 4.2 to 20K and at higher temperatures from the readings of a copper-constantan thermocouple with a reference junction in liquid nitrogen.

Electrical resistivity measurements were made using an apparatus utilizing the standard four-terminal D.C. technique and set in the standard two-layer glass dewar (131). The sample(s) and a standard resistor are

connected in series; by switching back and forth, the effect of drifting currents and thermal emf's could be reduced. The current is supplied by a Tinsley regulated current supply 5753 and is obtained by the potential drop across the standard resistor. The potential drops across the standard resistor and the sample(s) are measured by a potentiometer. Temperatures were derived from the resistance of an Allen Bradley carbon resistor.

Section III.   Results and Discussion

A series of $Pd_{1-x}Pt_xMn$ binary matrix alloys has been studied. The alloys with 3 at.% Mn impurity in $Pd_{1-x}Pt_x$ binary matrix with x = 0.02, 0.05, 0.15, 0.25, 0.35, 0.50, 0.75, and 1.00 and another alloy with 4 at.% Mn impurity in $Pd_{.75}Pt_{.25}$ binary matrix have been examined magnetically from 1.4 to 20K. The alloys with 1.5 and 3 at.% Mn impurity in $Pd_{.98}Pt_{.02}$ binary matrix have been examined by resistivity measurements from 2.6 to 4.2K.

The $Pd_{1-x}Pt_xMn$ alloys being studied can be classified into two different categories. The two alloys with the highest compositions of Pd (x = 0.02 and 0.05) in the binary matrix with impurity concentration n of 3 at.% Mn and the $Pd_{.98}Pt_{.02}Mn$ (1.5 at.% Mn) alloy belong to the first category; there, a ferromagnetic-paramagnetic state transition occurs. This behaviour is similar to that of the PdMn (3 at.% Mn) alloy (179,180). The other alloys being studied belong to the second category, where a magnetic spin glass-superparamagnetic-paramagnetic state transition occurs. This behaviour is similar to that of the PtMn (3 at.% Mn) alloy (1).

The magnetization M and the magnetic susceptibility X of the Mn solute are assumed to be $(M_{alloy} - M_{host})$ and $(X_{alloy} - X_{host})$ respectively, where M_{alloy} and X_{alloy} are the magnetization and the susceptibility respectively of the alloy, and M_{host} and X_{host} are that of the binary matrix $Pd_{1-x}Pt_x$. The X_{host} is a function with a smooth variation of the composition argument x and has been experimentally measured by Andres and Jensen(113).

For the two alloys measured magnetically belonging to the first category, the low temperature magnetic isotherms M of the Mn solute versus field H and the low field susceptibility X and the reciprocal of the susceptibility (1/X) versus temperature T from 1.4 to 20K have been plotted in Fig. 91 to 94.

The susceptibility follows the Curie-Weiss law at temperatures above 8K. By extrapolating the reciprocal of the susceptibility between 8 and 20K, the Weiss temperatures Θ have been determined to be +5.3 $\pm$ 0.3 and +2.9 $\pm$ 0.3K for the $Pd_{.98}Pt_{.02}Mn$ (3 at.% Mn), (x = 0.02), and the $Pd_{.95}Pt_{.05}Mn$ (3 at.% Mn),(x = 0.05), alloys respectively. From the Curie constant, $C = n \, \mu_{eff}^2/3k_B$, where k_B is the Boltzmann constant, the effective magnetic moments μ_{eff} per Mn atom have been determined to be 4.6 $\pm$ 0.2 and 6.1 $\pm$ 0.2 μ_B (Bohr Magneton) for the (x = 0.02) and the (x = 0.05) alloys respectively. These two obtained values of effective moment per Mn atom are smaller, as expected, than that of the value 6.3 μ_B of the PdMn (3 at.% Mn) alloy (180).

In order to investigate the behaviours of the alloys at the temperature region near the Curie temperature T_c, the equation of state, derived from the basis of the Landau theory of phase transition (51), can be written as:

$$H/M = A + BM^2 + 0(M^4)$$

for T $\ll$ T_F, where T_F is the effective degeneracy temperature, and the coefficients A and B can be approximated to as:
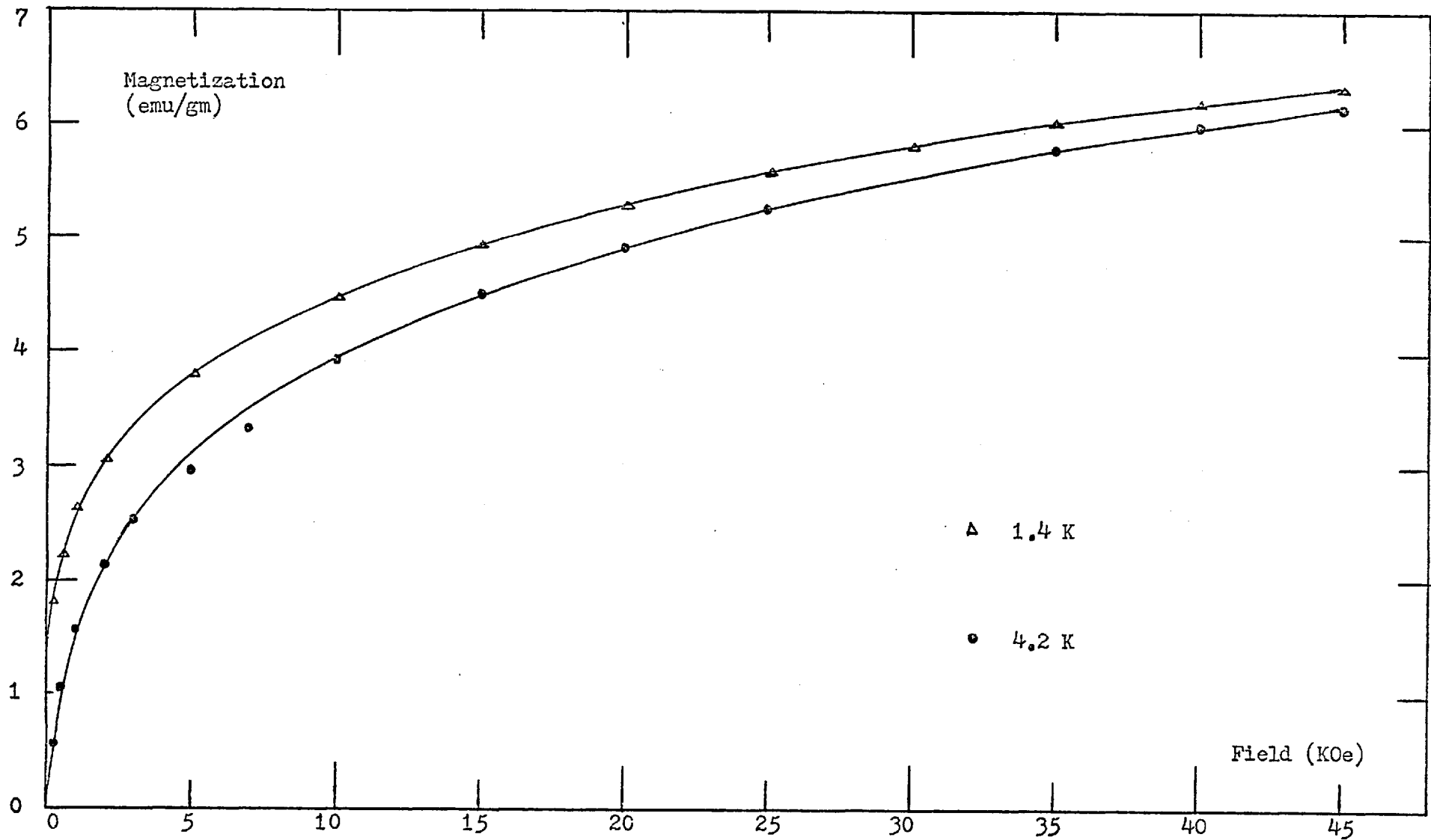
$$A = -\frac{1 - (T^2/T_c^2)}{2X_0}$$

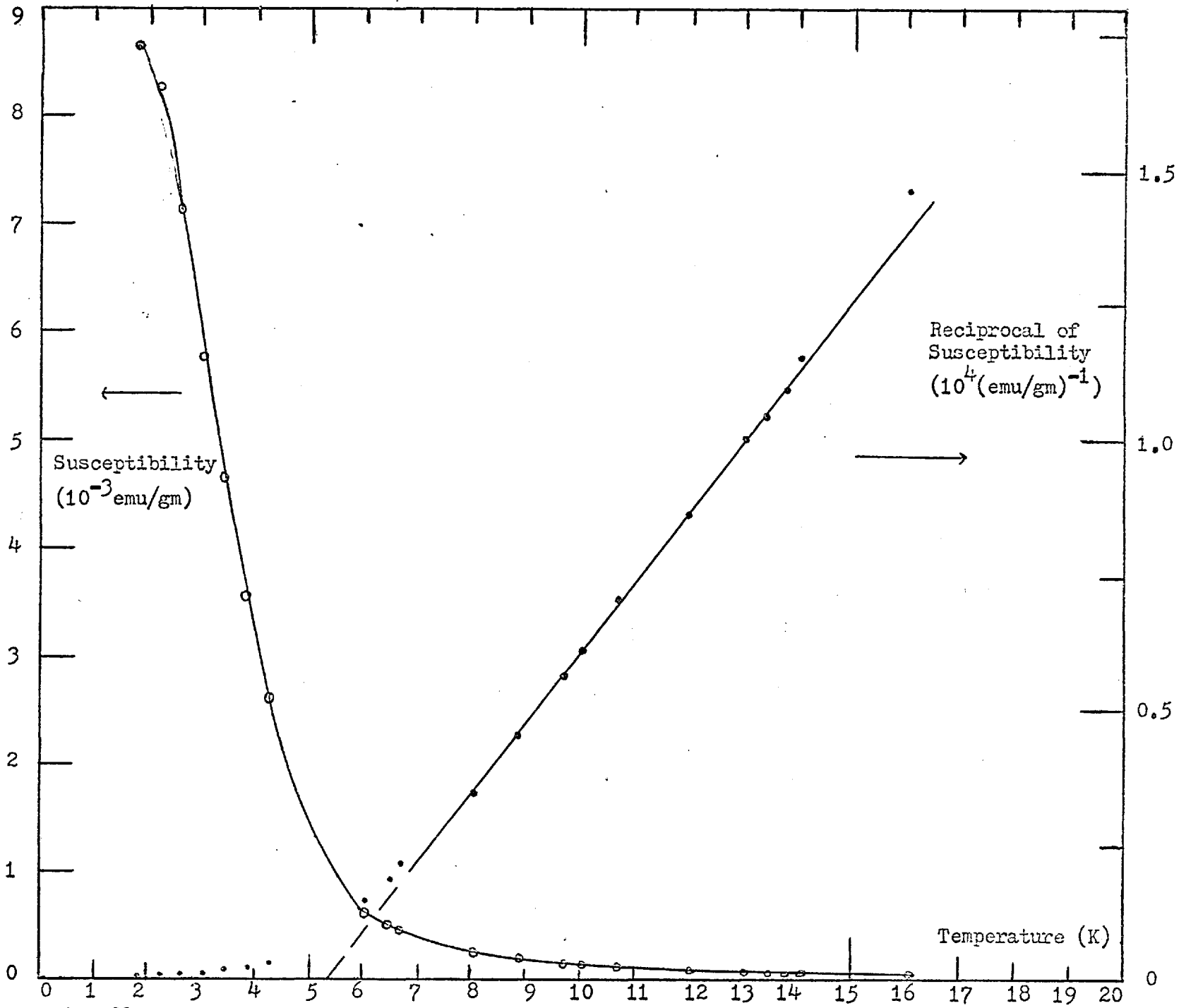Fig. 91 Magnetization versus Field for Pd$_{.98}$Pt$_{.02}$Mn (3at.% Mn) Impurity

Fig. 92 Susceptibility and Reciprocal of Susceptibility versus Temperature for $Pd_{.98}Pt_{.02}Mn$ (3at.% Mn) Impurity
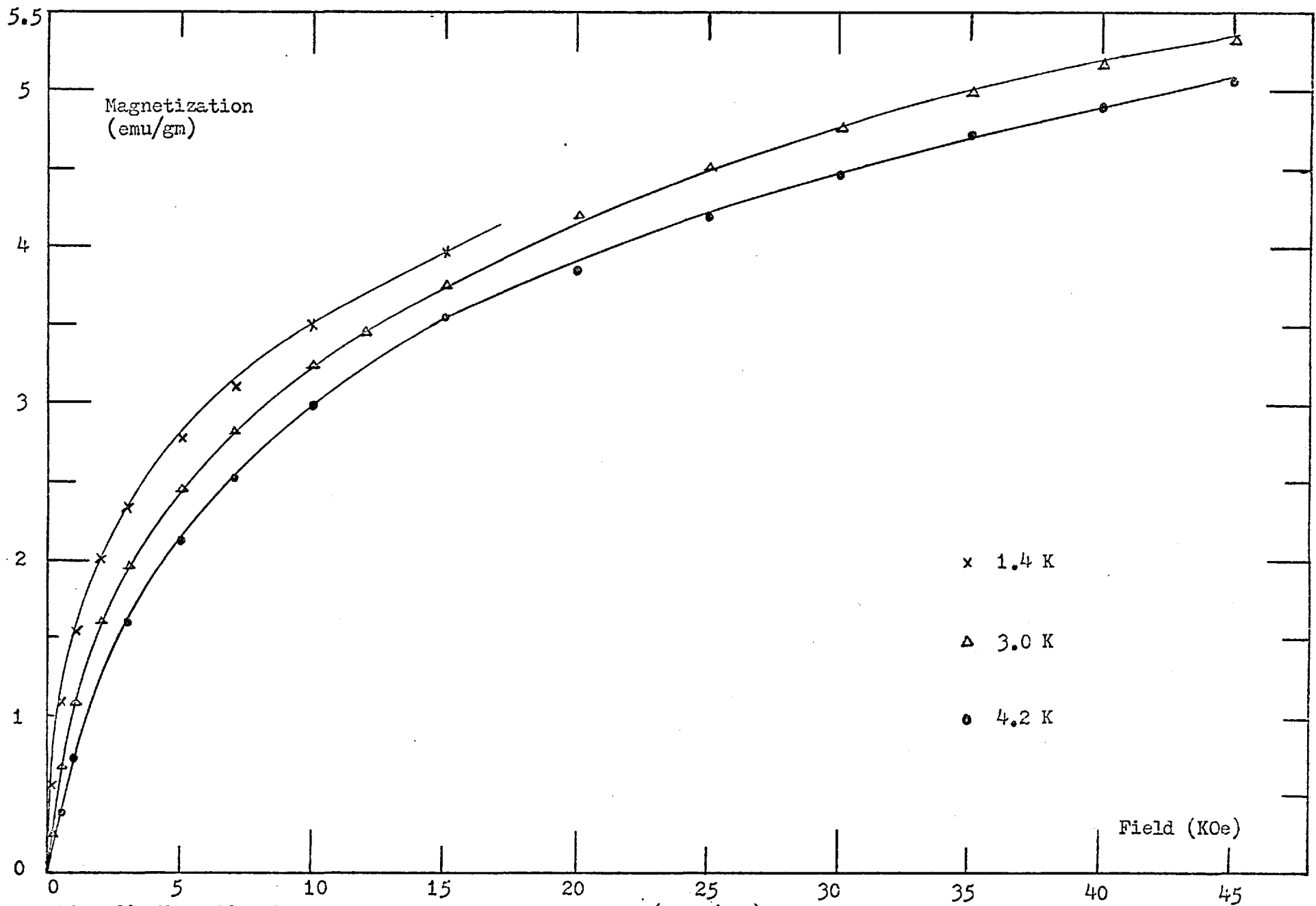
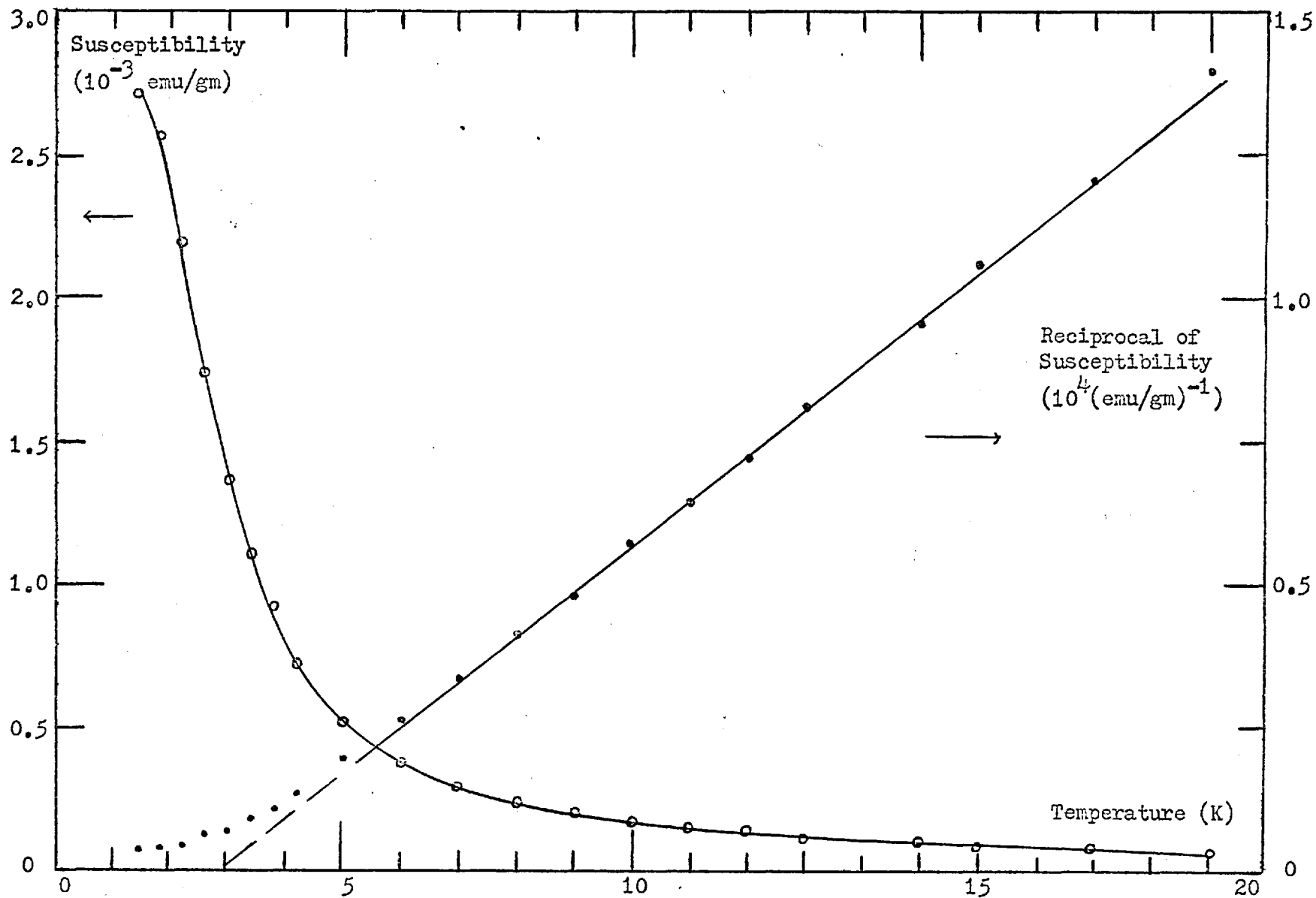Fig. 93 Magnetization versus Field for Pd$_{.95}$Pt$_{.05}$Mn (3at.% Mn) Impurity

Fig.94 Susceptibility and Reciprocal of Susceptibility for $Pd_{.95}Pt_{.05}Mn$ (3at.% Mn) Impurity

$$B = (2X_o M_o{}^2)^{-1}$$

where X_o and M_o represent the susceptibility at 0K and the saturation magnetization respectively. The plots of M^2 versus (H/M) (183-185) at various temperatures in the range considered will give a series of parallel straight lines, that at $T = T_c$ passing through the origin. By the value of T_c in combination with the intercepts and the slope, the value of X_o and M_o can also be determined.

The M^2 versus (H/M) of these two alloys have been plotted in Fig. 95 and 96. From the plots, the values of the Curie temperature $T_c = 3.5 \pm 0.1$ and 1.5 ± 0.1K have been obtained for the $Pd_{.98}Pt_{.02}Mn$ (3 at.% Mn), (x = 0.02), and the $Pd_{.95}Pt_{.05}Mn$ (3 at.% Mn) alloy respectively. The value of T_c of the (x = 0.02) alloy has also been obtained through the resistivity measurements, shown in a later part of this section, and which is in good agreement with the value obtained through the magnetic measurements. The deviations from straight line (M^2 versus (H/M)) plots at low field are presumably due to small amounts of heterogeneities in the sample (186), and the deviations at high field are presumably due to high order terms (1).

This ferromagnetic-paramagnetic states transition can also be observed from the magnetic isotherms; the magnetic isotherms measured at temperatures above the Curie temperature T_c will fall below the Brillouin function appropriate for free spins; however, the magnetic isotherms measured at temperatures below T_c will be above the Brillouin function. This effect is clearly shown in the magnetization plots of these two alloys.
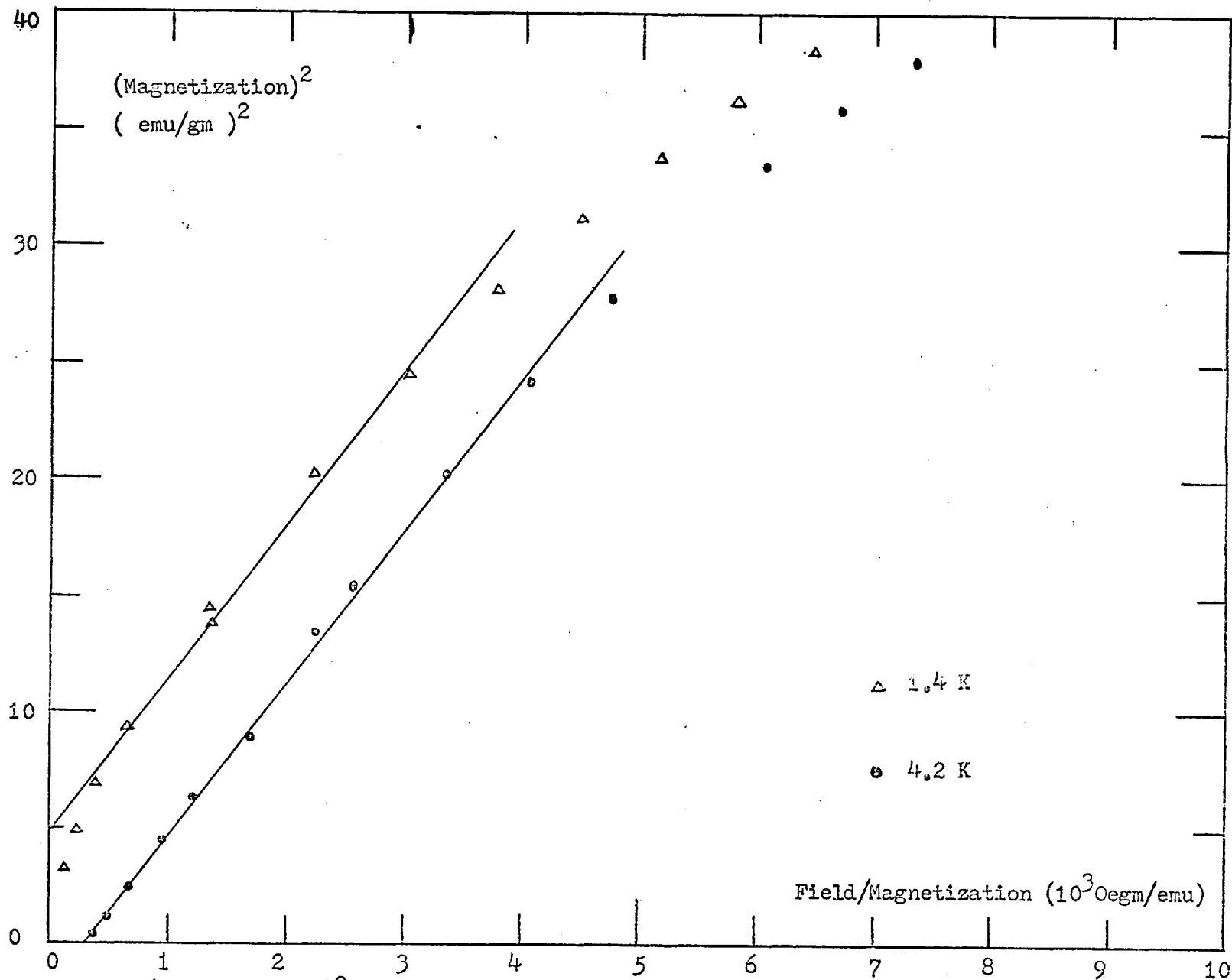
Fig.95 (Magnetization)^2 versus (Field/Magnetization) for $\underline{Pd_{.98}Pt_{.02}Mn}$ (3at.% Mn) Impurity
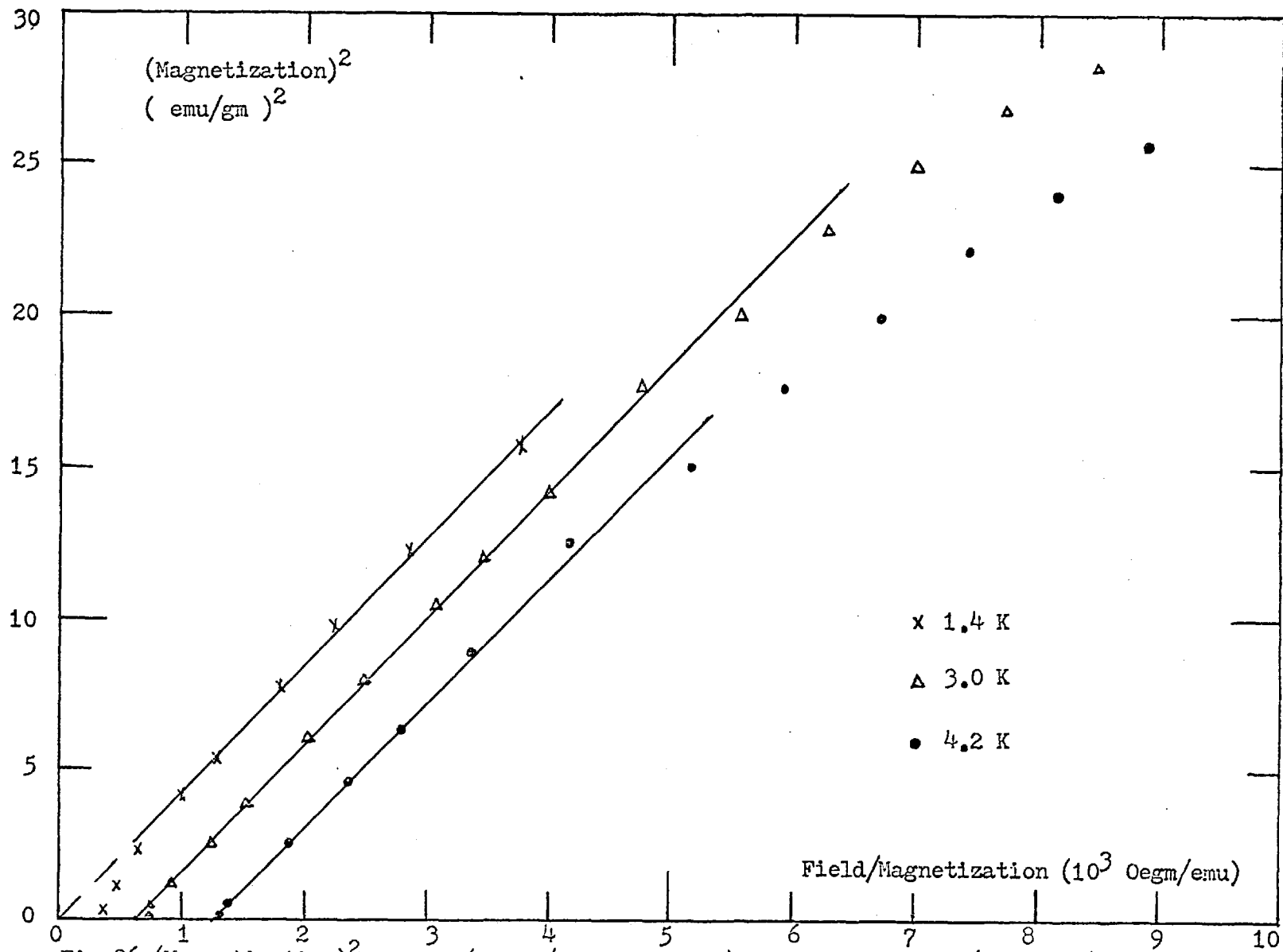
Fig.96 (Magnetization)^2 versus (Field/Magnetization) for $\underline{Pd}_{.95}Pt_{.05}Mn$ (3at.% Mn) Impurity

According to the Curie-Weiss law, the susceptibility X tends to diverge as the temperature T decreases to the paramagnetic Weiss temperature, which is very close to the Curie temperature T_c and the initial susceptibility $X \sim (T - T_c)^{-1}$ for $T > T_c$. This divergent tendency has been treated through the critical phenomena approach using the Heisenberg model, and the initial region is less explored. Early analysis proposed the relation $X \sim (T - T_c)^{-\alpha}$ when T is just above T_c and the index α has the value of about 4/3. Subsequent calculations indicate a somewhat larger index ~ 1.35 (187). The susceptibility X versus deviations from the Curie temperature $(T - T_c)$ of these two alloys have been plotted in Fig. 97 and 98. From the slopes, the α values of 1.36 ± 0.05 and 1.29 ± 0.06 have been estimated for the $Pd_{.98}Pt_{.02}Mn$ (3 at.% Mn) and the $Pd_{.95}Pt_{.05}Mn$ (3 at.% Mn) alloy respectively. These values are quite close to the theoretically proposed value.

The incremental resistivity of the $Pd_{.98}Pt_{.02}Mn$ (3 at.% Mn) and the resistivity of the $Pd_{.98}Pt_{.02}Mn$ (1.5 at% Mn) alloy from 2.6 to 4.2K are plotted in Fig. 99 and 100. The incremental resistivity P is assumed to be $P_{alloy} - P_{host}$, where P_{alloy} is the resistivity of the alloy and P_{host} is that of the host.

The spin-disordered resistivity which is caused by the scattering between the atoms which possess localized but randomly oriented spin and the conduction electrons passing through it give rise to an appreciable term in the electrical resistivity. This spin-disordered resistivity should decrease markedly upon the atomic ordering (188). This effect is clearly shown by the sudden change of the resistivity as the temperature decreases in our results.
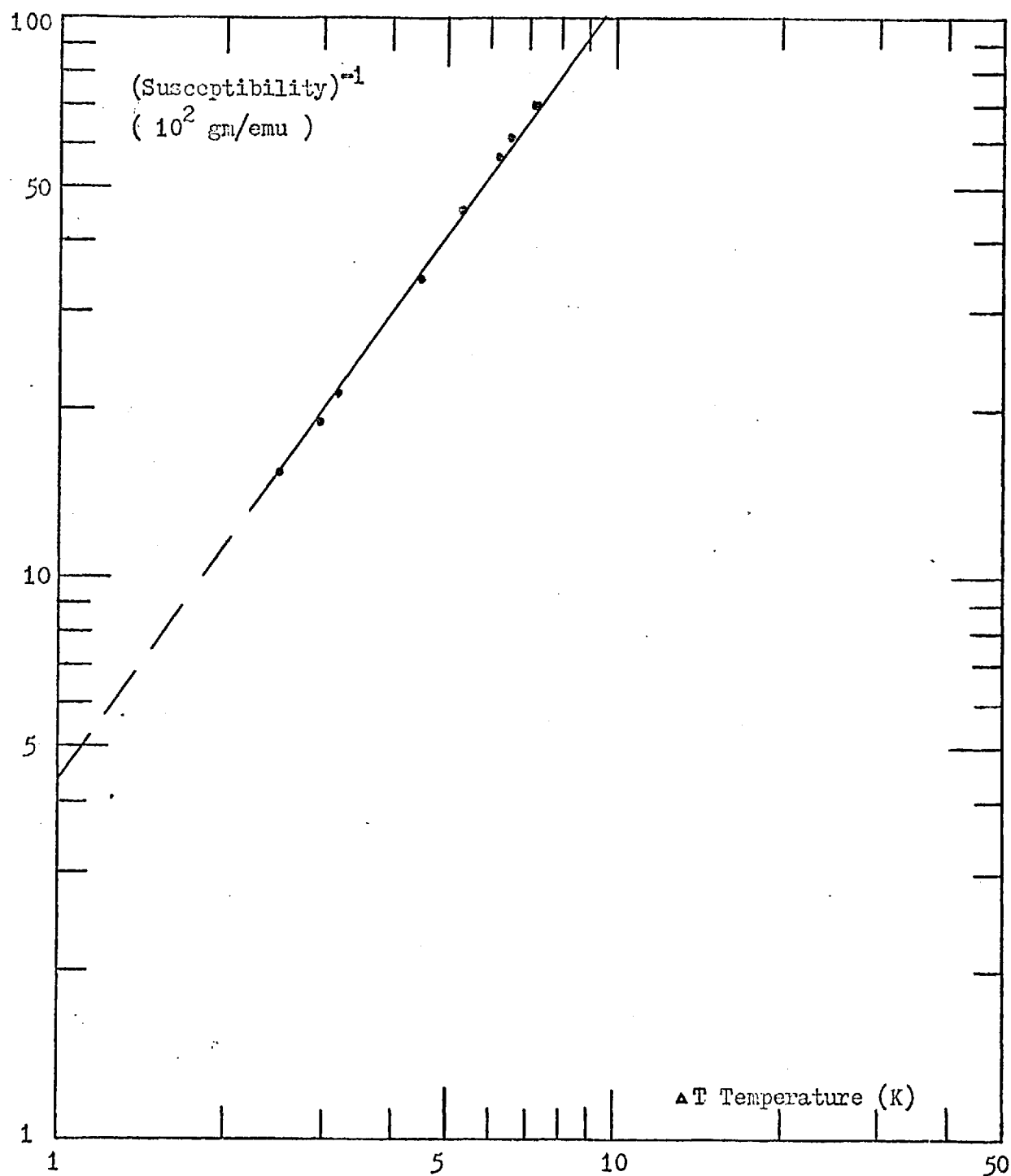
Fig. 97 Reciprocal of Susceptibility versus deviation from Curie
Temperature $\Delta T = T - T_C$ for $\underline{Pd_{.98}Pt_{.02}}Mn$ (3at.% Mn) Impurity

Fig. 98 Reciprocal of Susceptibility versus deviation from Curie
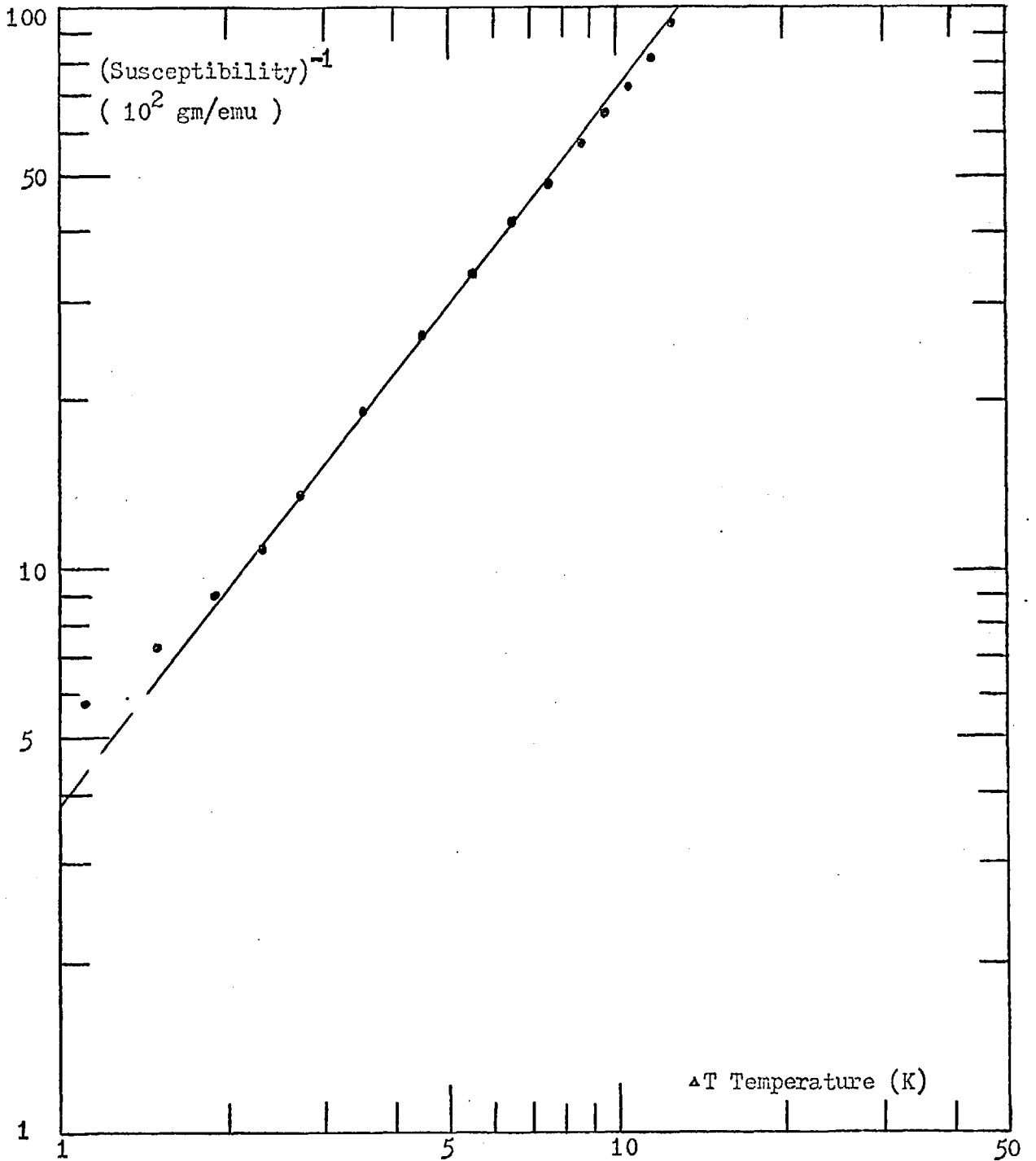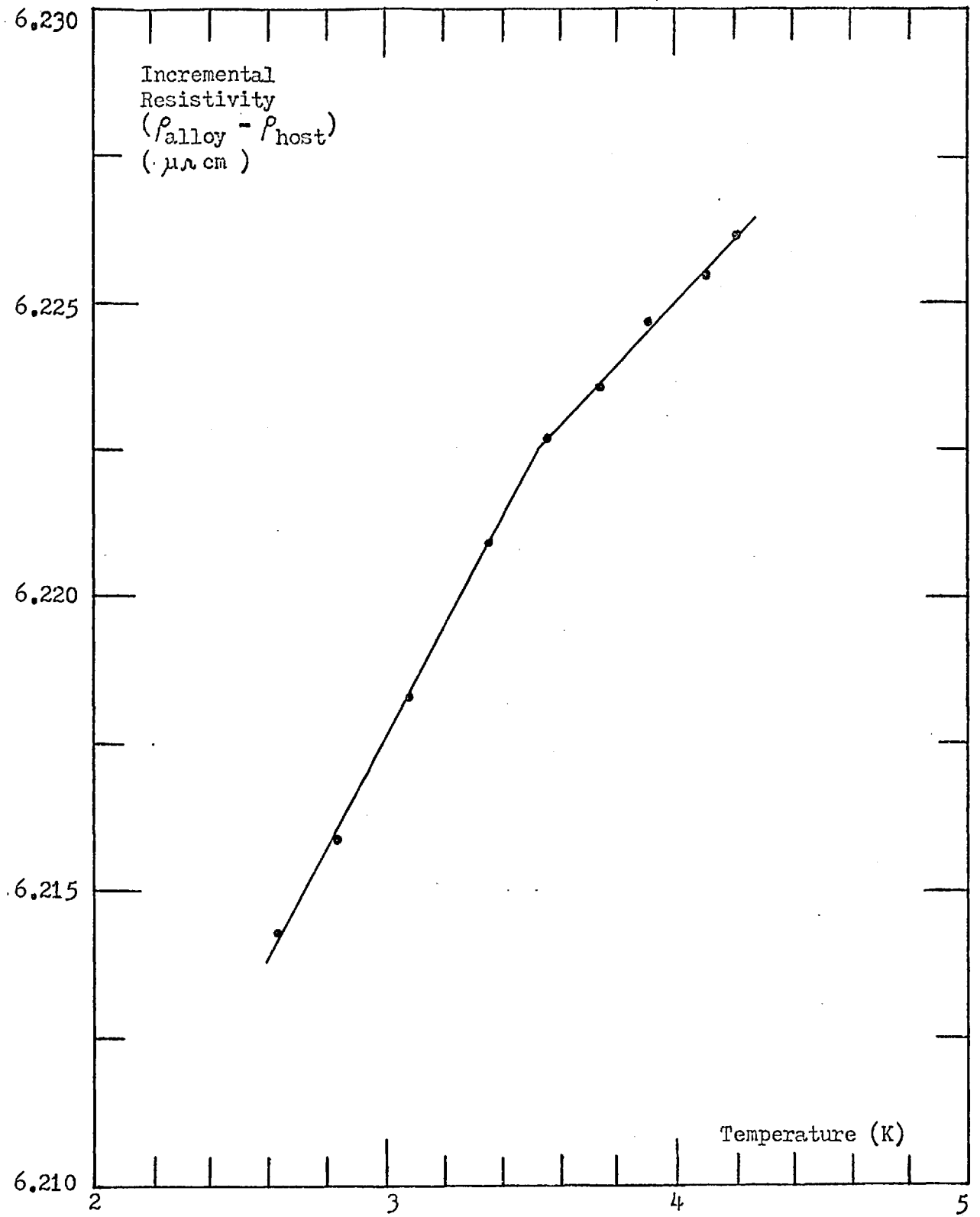Temperature $\Delta T = T - T_C$ for $Pd_{.95}Pt_{.05}Mn$ (3at.% Mn) Impurity

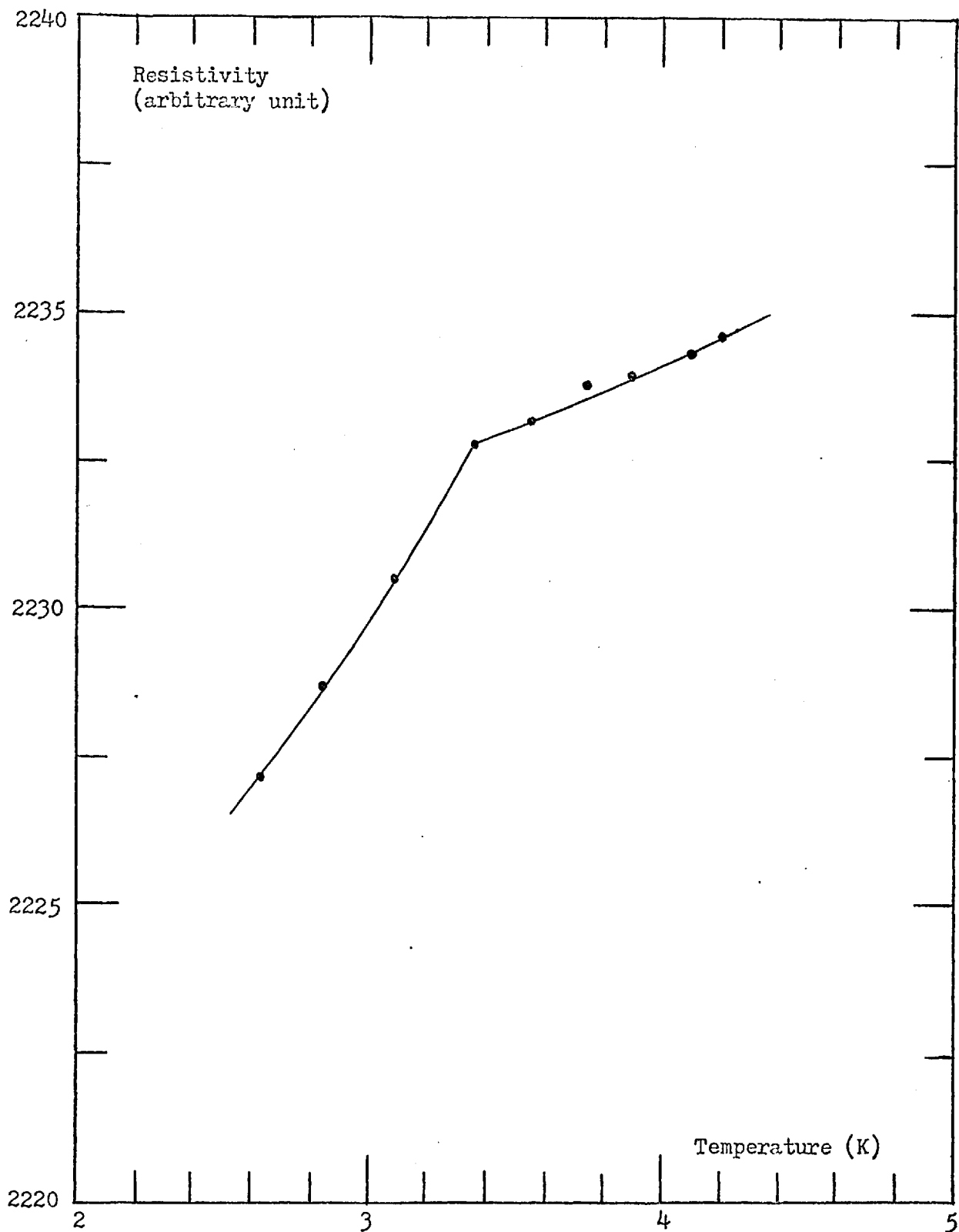Fig. 99 Resistivity versus Temperature for Pd$_{.98}$Pt$_{.02}$Mn (3at.% Mn)

Fig. 100   Resistivity versus Temperature for Pd$_{.98}$Pt$_{.02}$Mn (1.5at.% Mn)

Thus, the Curie temperature T_c of the $Pd_{.98}Pt_{.02}Mn$ (3 at.% Mn) and

the $Pd_{.98}Pt_{.02}Mn$ (1.5 at.% Mn) alloys can be determined at be 3.5 ± 0.1

and $3.3 \pm 0.1K$ respectively. This value of T_c for the $Pd_{.98}Pt_{.02}Mn$

(3 at.% Mn) alloy is in good agreement with what has been obtained through

the magnetic measurement by means of the M^2 versus (H/M) plot (1).

The $Pd_{1-x}Pt_xMn$ alloys being studied other than the above three alloys

belong to the second category, where there is a magnetic spin glass -

superparamagnetic-paramagnetic state transition occurring. For these

alloys, the low temperature magnetic isotherms M of the Mn solute versus

field H, and the low field susceptibility X and the reciprocal of the suscep-

tibility (1/X) versus temperature T from 1.4 to 20K have been plotted in

Fig. 101 to 114.

All the magnetic isotherms which have been measured fall far below

the Brillouin function. This indicates the impurity atoms behave far from

the free spin system. By comparing the magnetic isotherms of the alloys

with the same amount of impurity, 3 at.% Mn, in the $Pd_{1-x}Pt_x$ binary

matrix of different compositions, it is obvious that the approach toward

the saturation of the magnitization delays monotonically as the composition

of Pt(x) increases. By comparing the magnetic isotherms of the alloys

with different amounts of impurity, 3 at.% Mn and 4 at.% Mn in the same

$Pd_{.75}Pt_{.25}$ binary matrix, the approach toward the saturation of the

magnetization delays as the impurity concentration increases. It is, thus,

suggested that the impurity interactions increase.

A clear cross of the two magnetic isotherms, taken at 1.4 and 3K, at

field H ~ 2KOe can be seen, say, on the magnetization plot of the

$Pd_{.50}Pt_{.50}Mn$ (3 at.% Mn) alloy. This cross exhibits the competitions

Fig. 101 Magnetization versus Field for Pd$_{.85}$Pt$_{.15}$Mn (3at.% Mn) Impurity

Fig. 102   Susceptibility and Reciprocal of Susceptibility for $Pd_{.85}Pt_{.15}Mn$ (3at.% Mn) Impurity
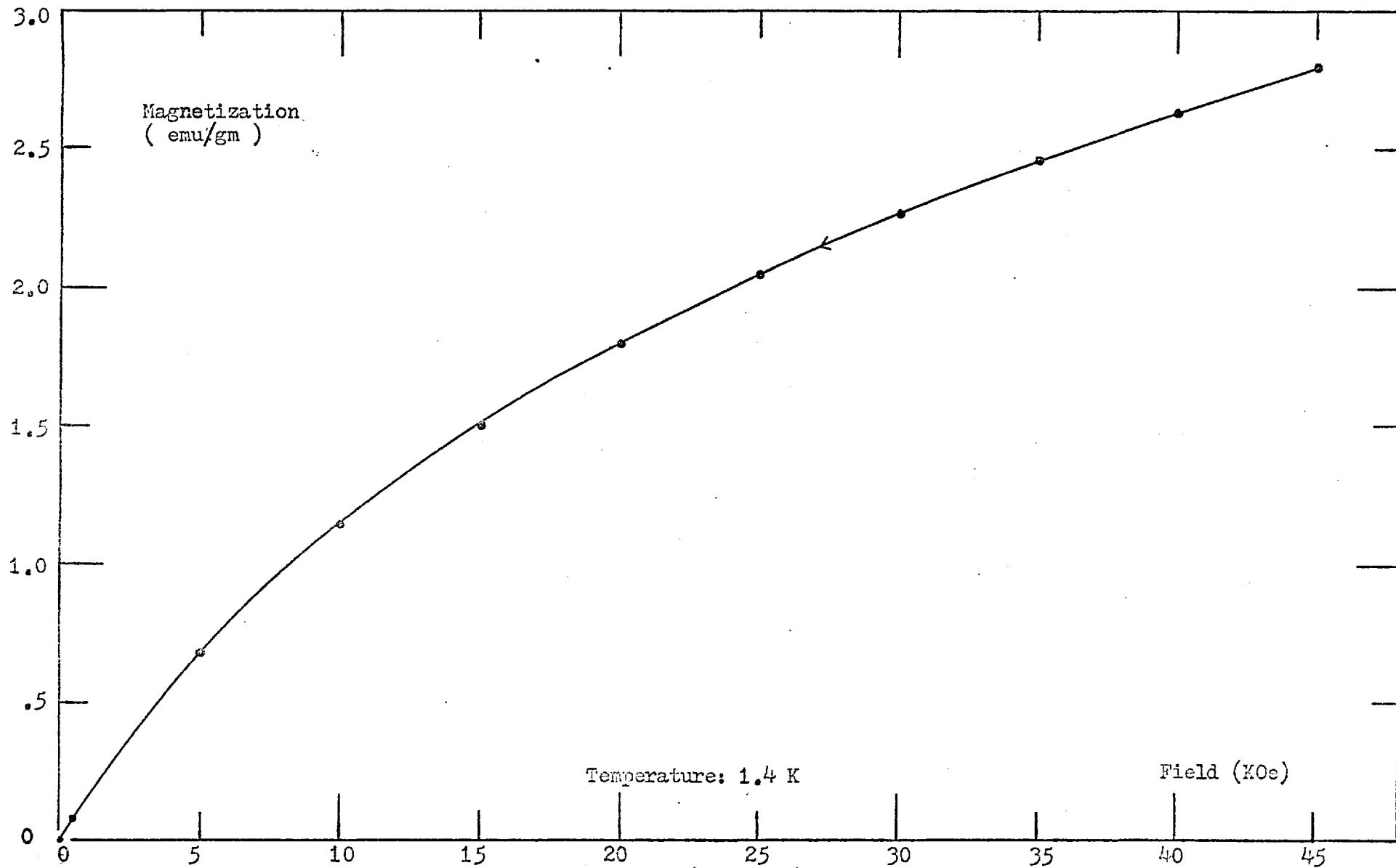
Fig.103 Magnetization versus Field for Pd$_{.75}$Pt$_{.25}$Mn (3at.% Mn) Impurity after cooling from 35K in field 45 KOe

Fig. 104 Susceptibility and Reciprocal of Susceptibility for $Pd_{.75}Pt_{.25}Mn$ (3at.% Mn) Impurity

Fig. 105 Magnetization versus Field for $Pd_{.65}Pt_3$–Mn (3at.% Mn) Impurity
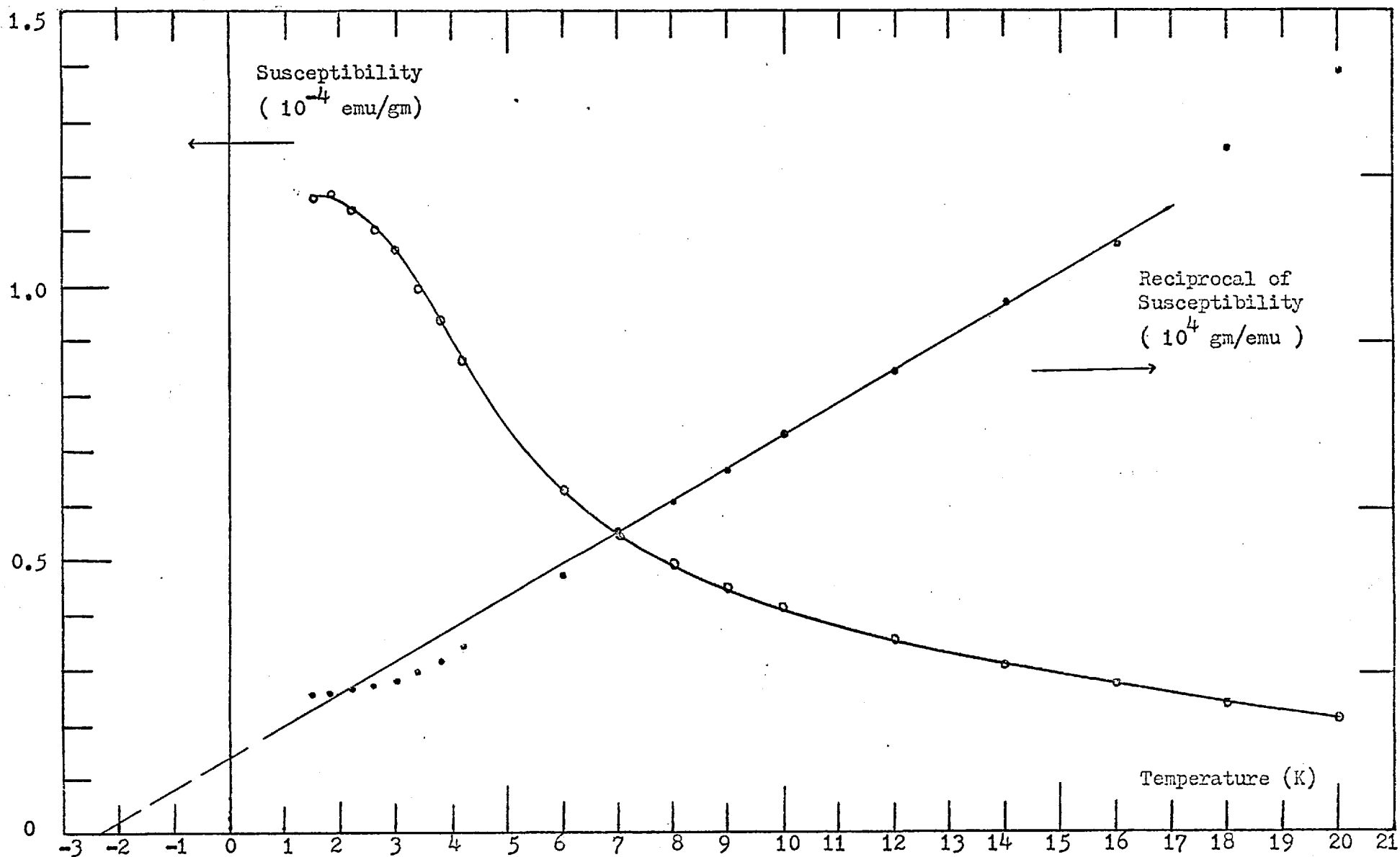
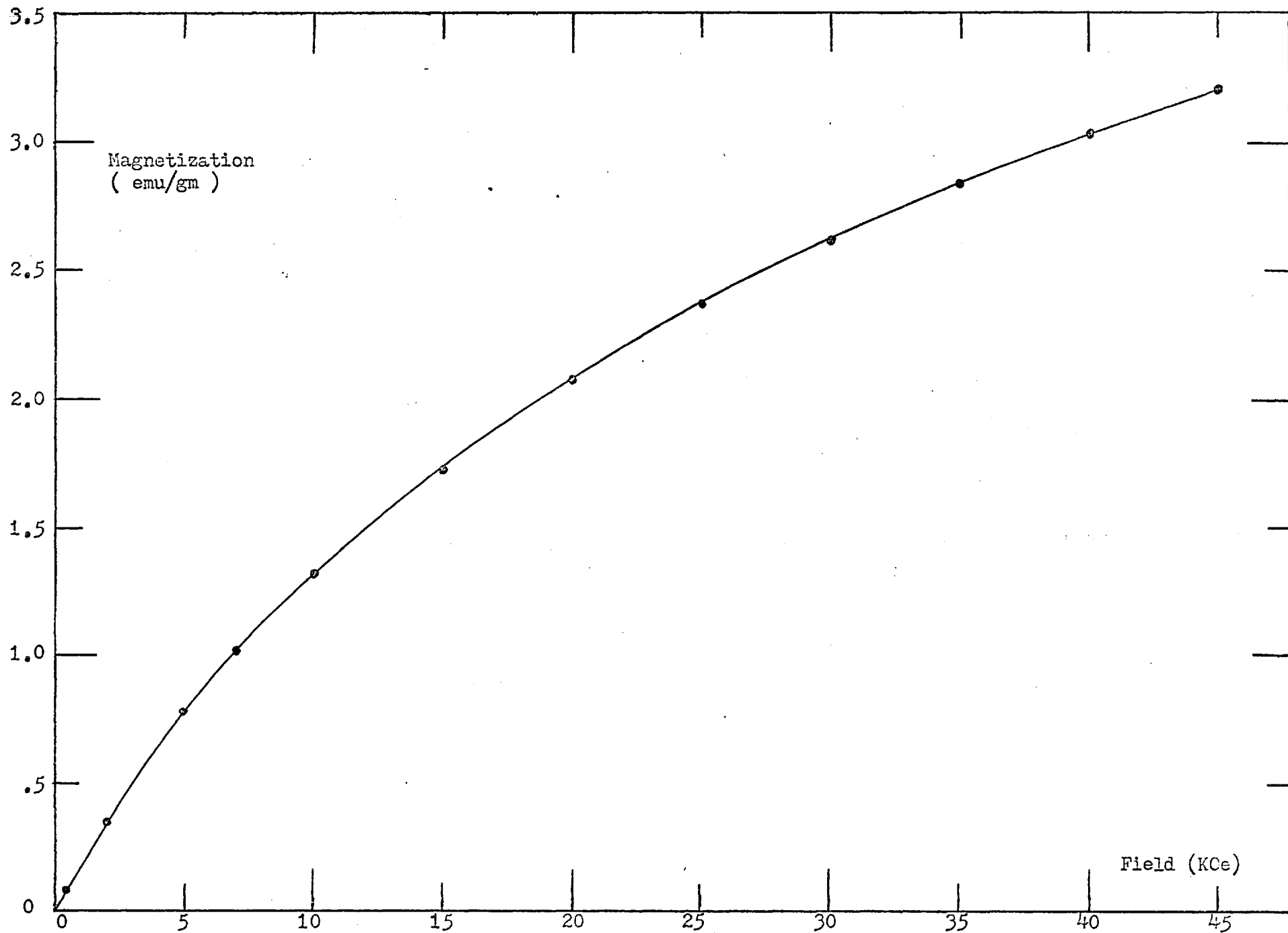Fig. 106 Susceptibility and Reciprocal of Susceptibility for $\underline{Pd_{.65}Pt_{.35}}Mn$ (3at.% Mn) Impurity

Fig. 107 Magnetization versus Field for Pd$_{.50}$Pt$_{.50}$Mn (3at.% Mn) Impurity
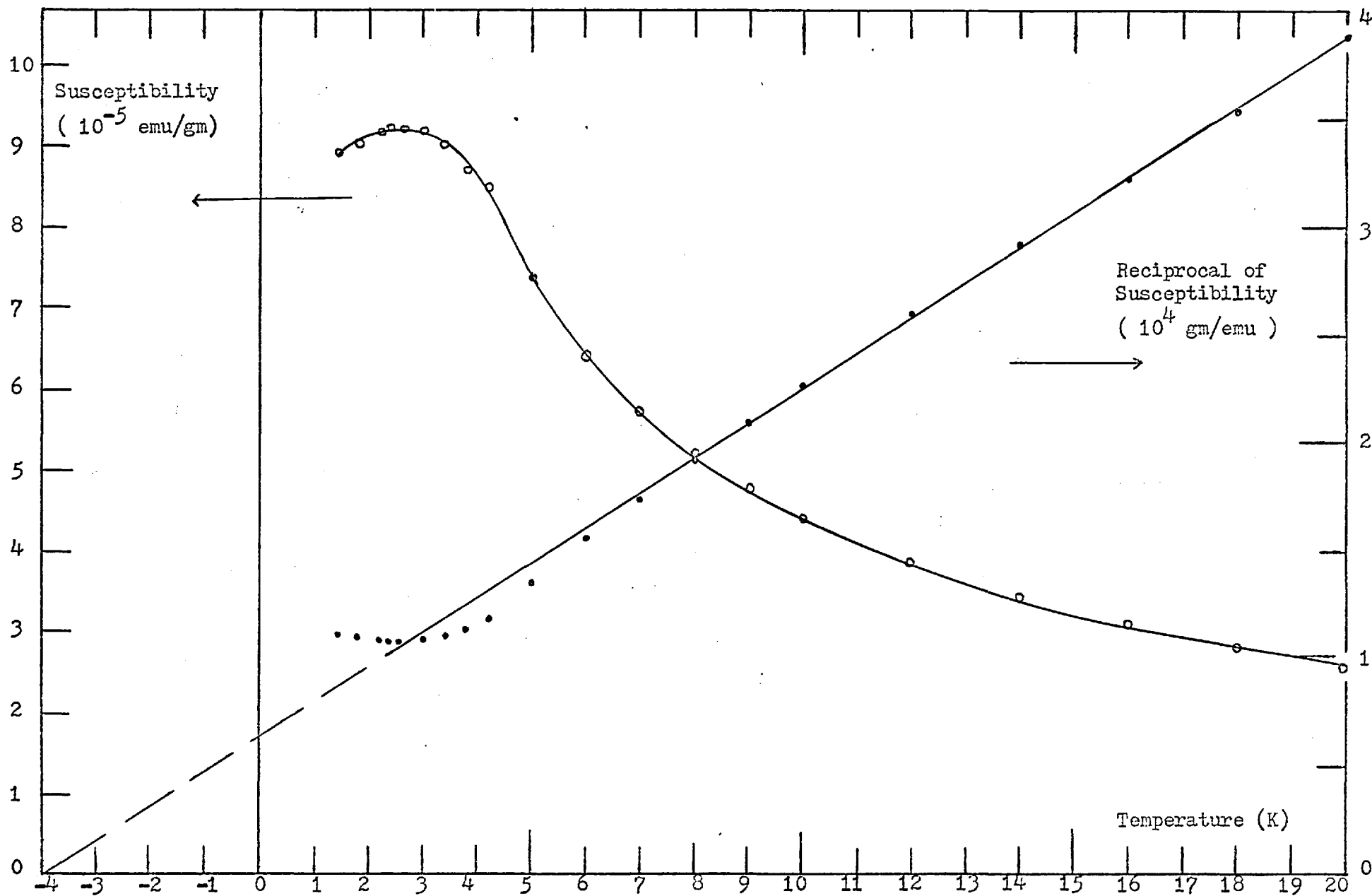
Fig. 108 Susceptibility and Reciprocal of Susceptibility for $Pd_{.50}Pt_{.50}Mn$ (3at.% Mn) Impurity

Fig. 109 Magnetization versus Field for Pd $_{.25}$Pt$_{.75}$Mn (3at.% Mn) Impurity
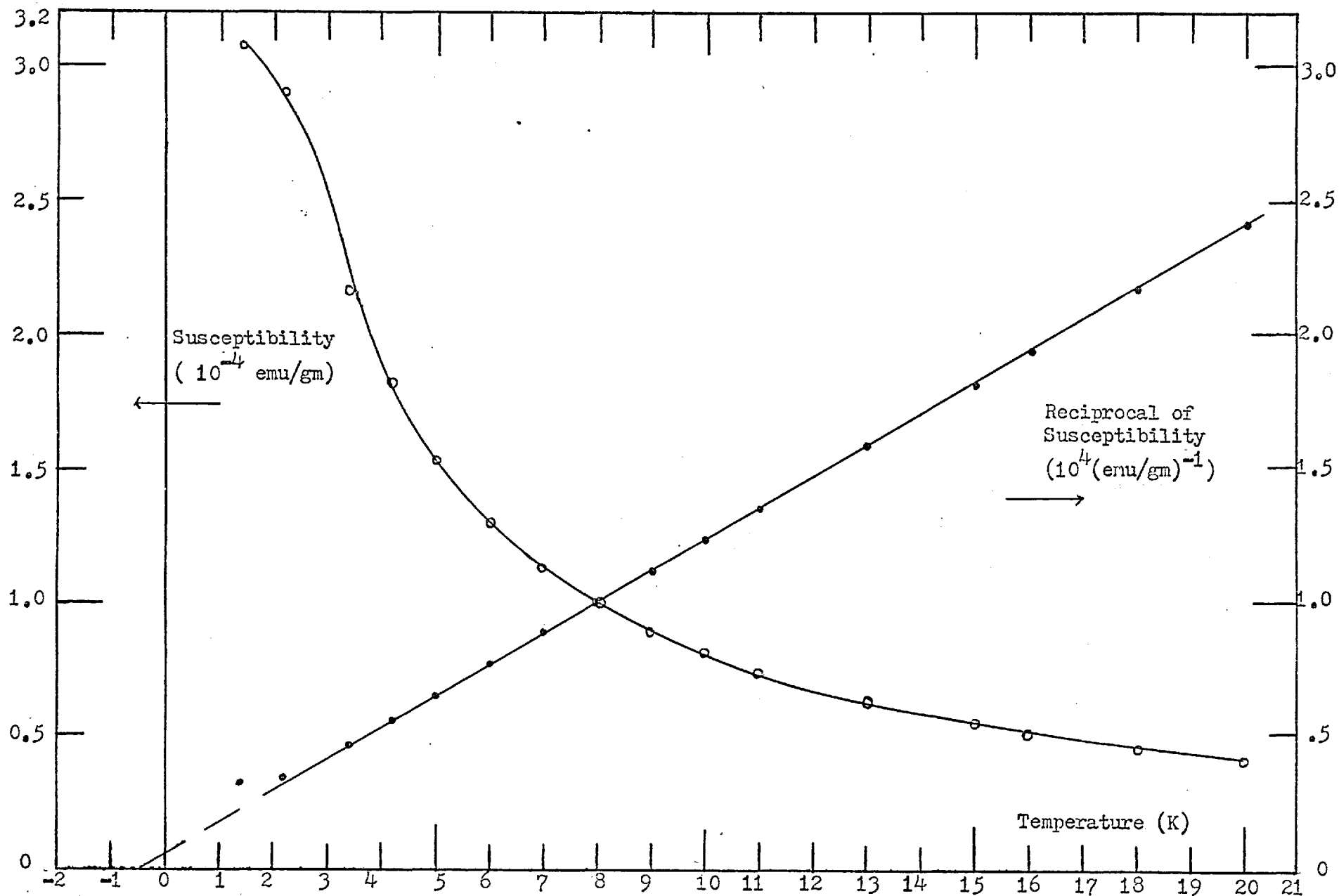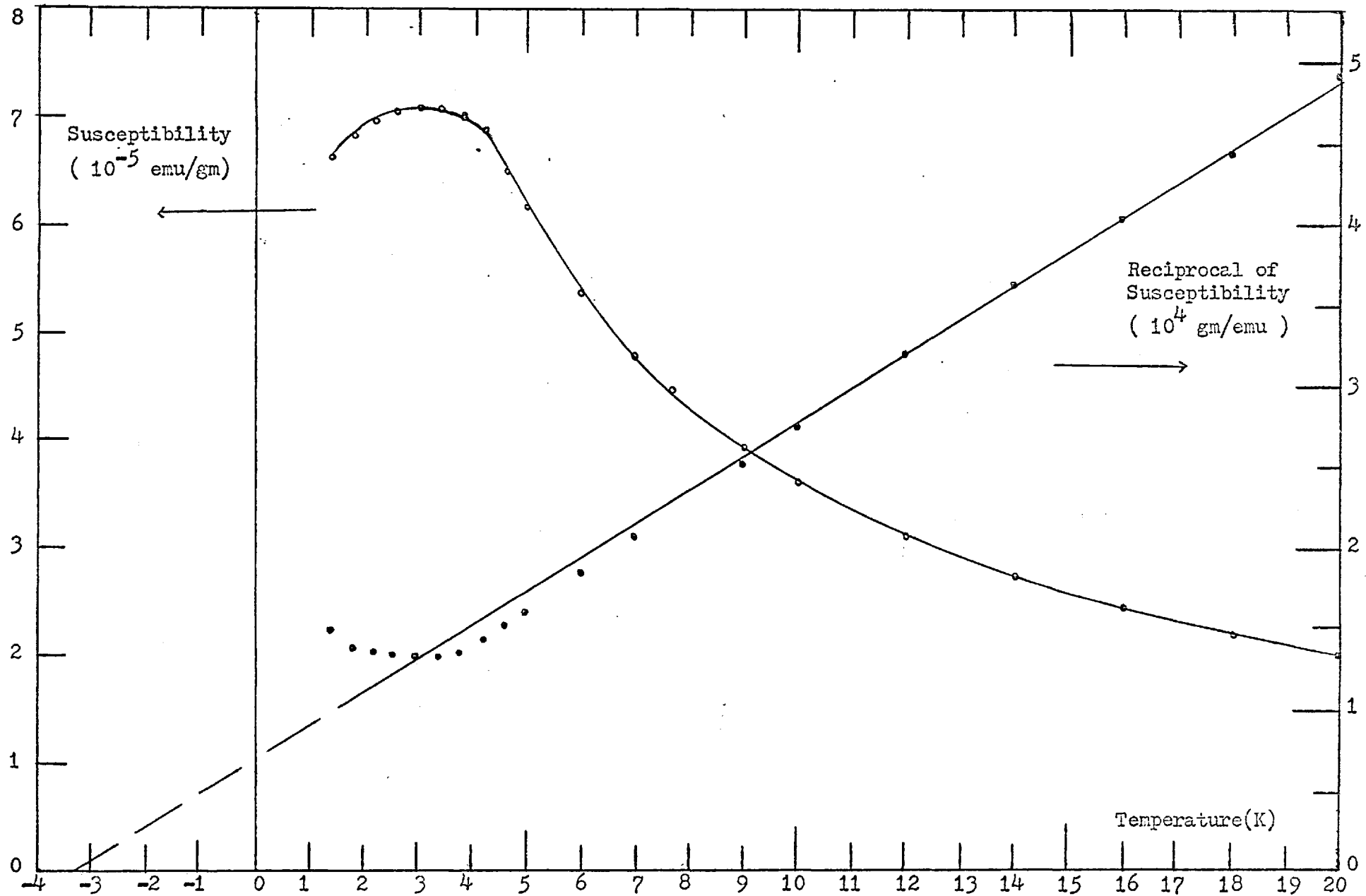
Fig. 110 Susceptibility and Reciprocal of Susceptibility for $Pd_{.25}Pt_{.75}Mn$ (3at.% Mn) Impurity
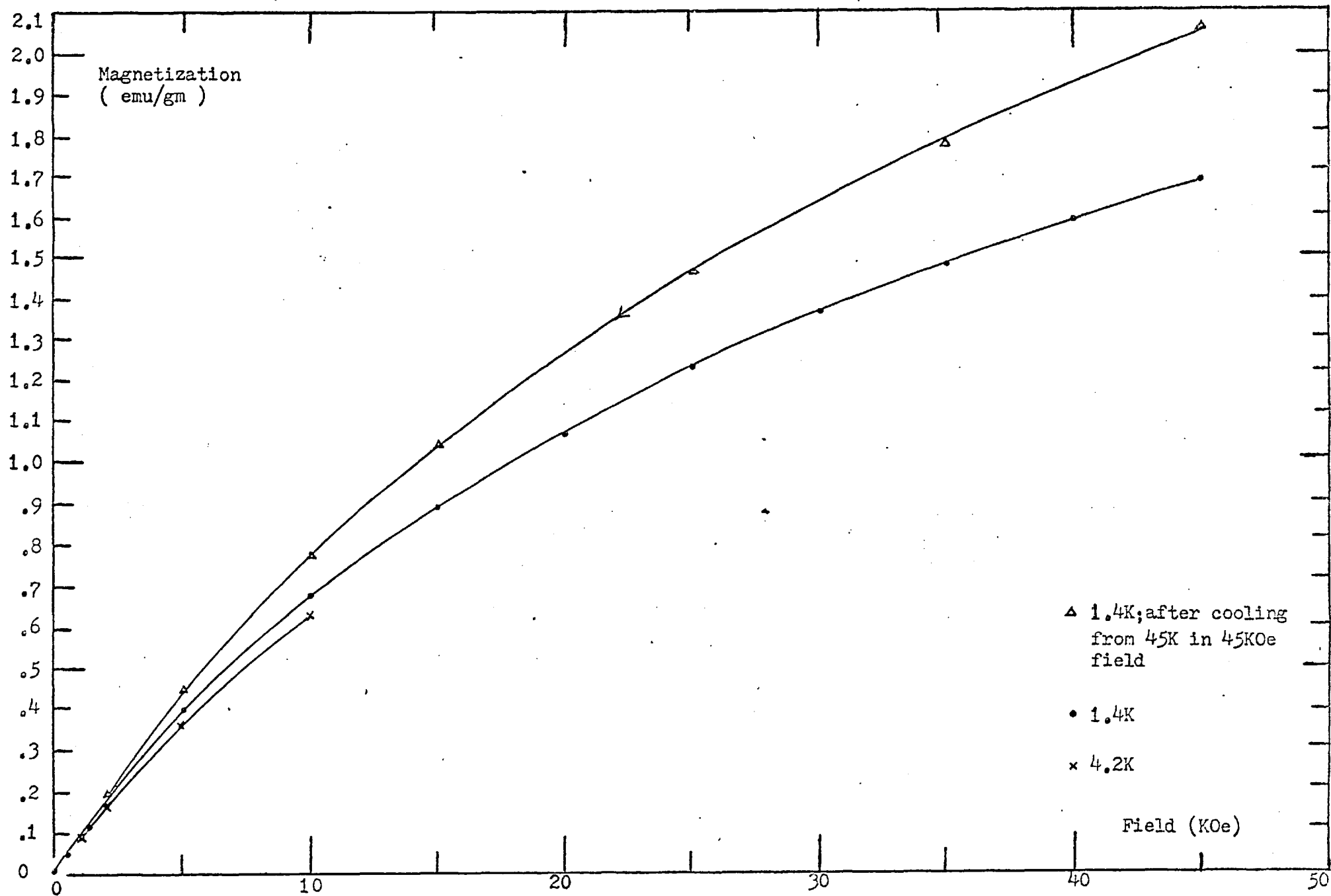
Fig. 111 Magnetization versus Field for PtMn (3 at.% Mn) Impurity
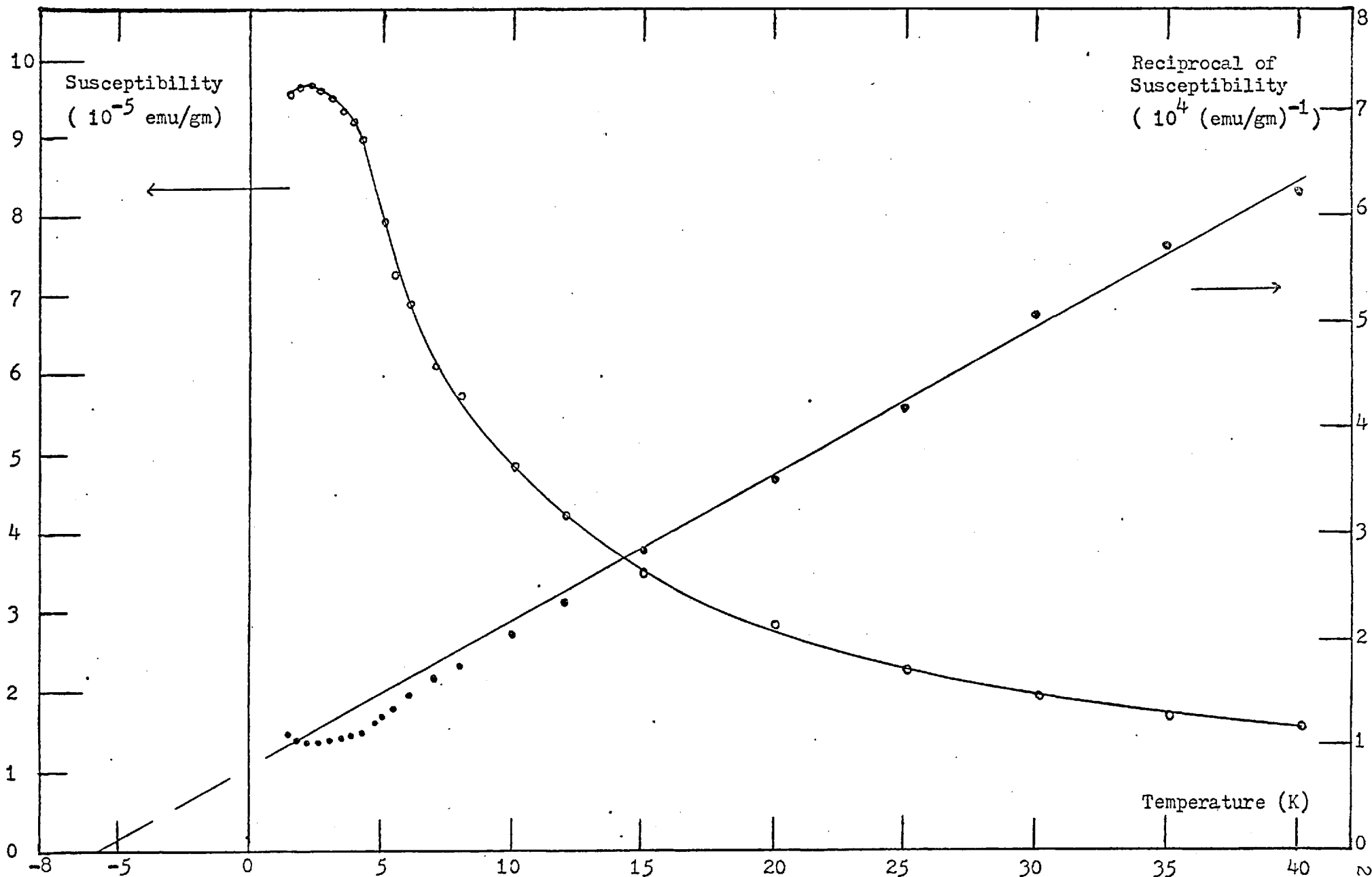
Fig.112 Susceptibility and Reciprocal of Susceptibility versus Temperature for PtMn (3 at.% Mn) Impurity
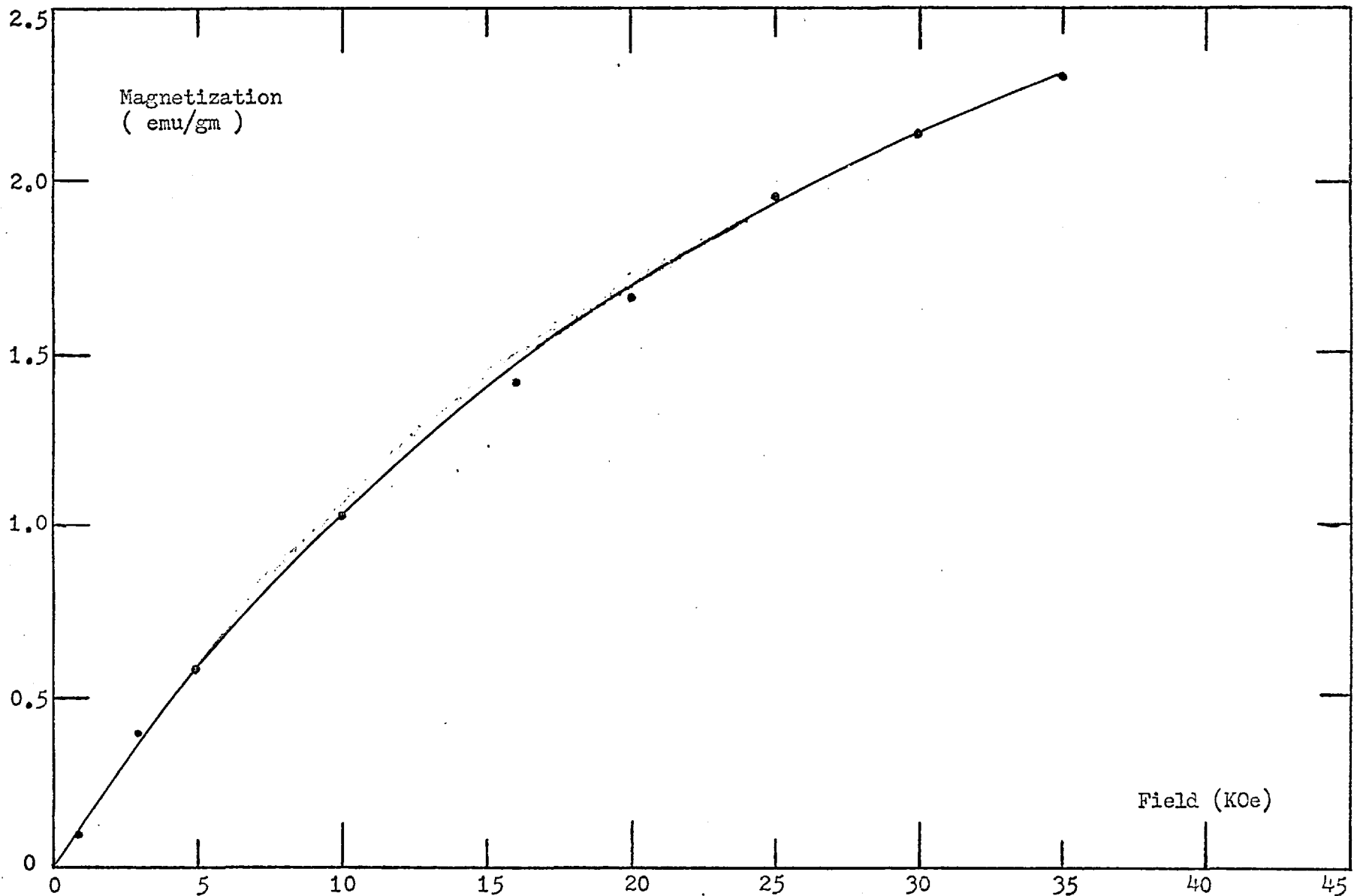
Fig. 113 Magnetization versus Field at 1.9K for Pd$_{.75}$Pt$_{.25}$Mn (4at.% Mn) Impurity

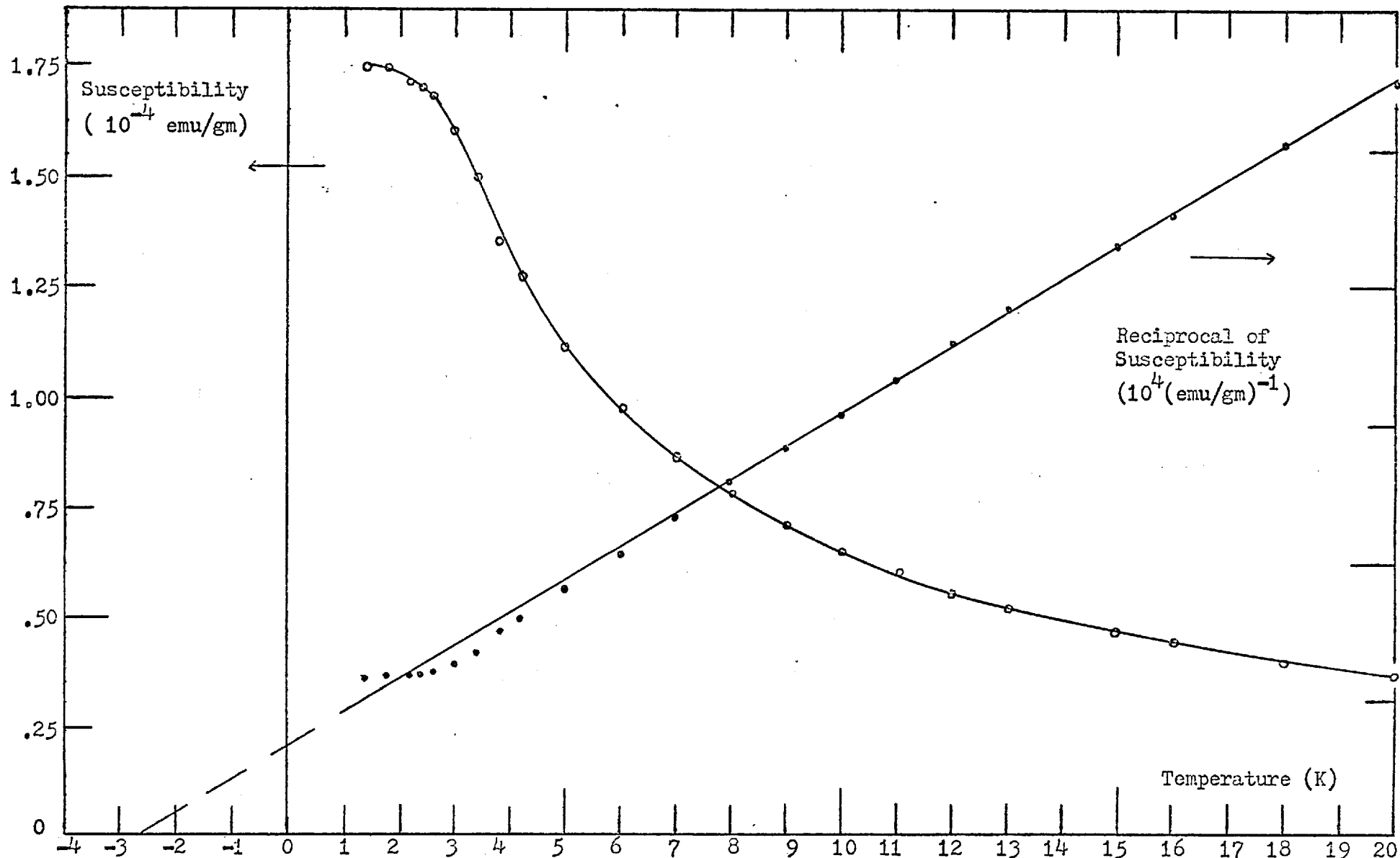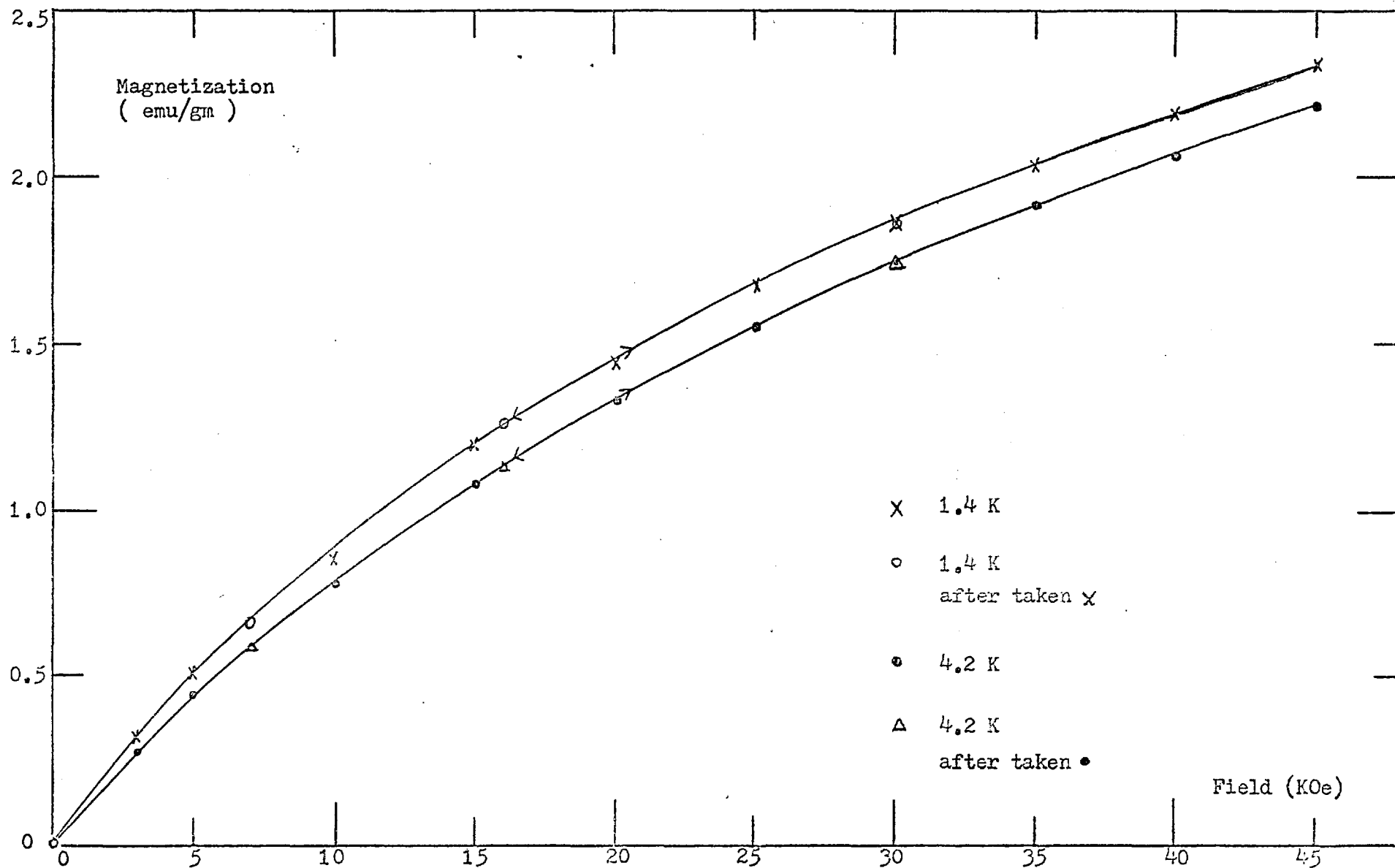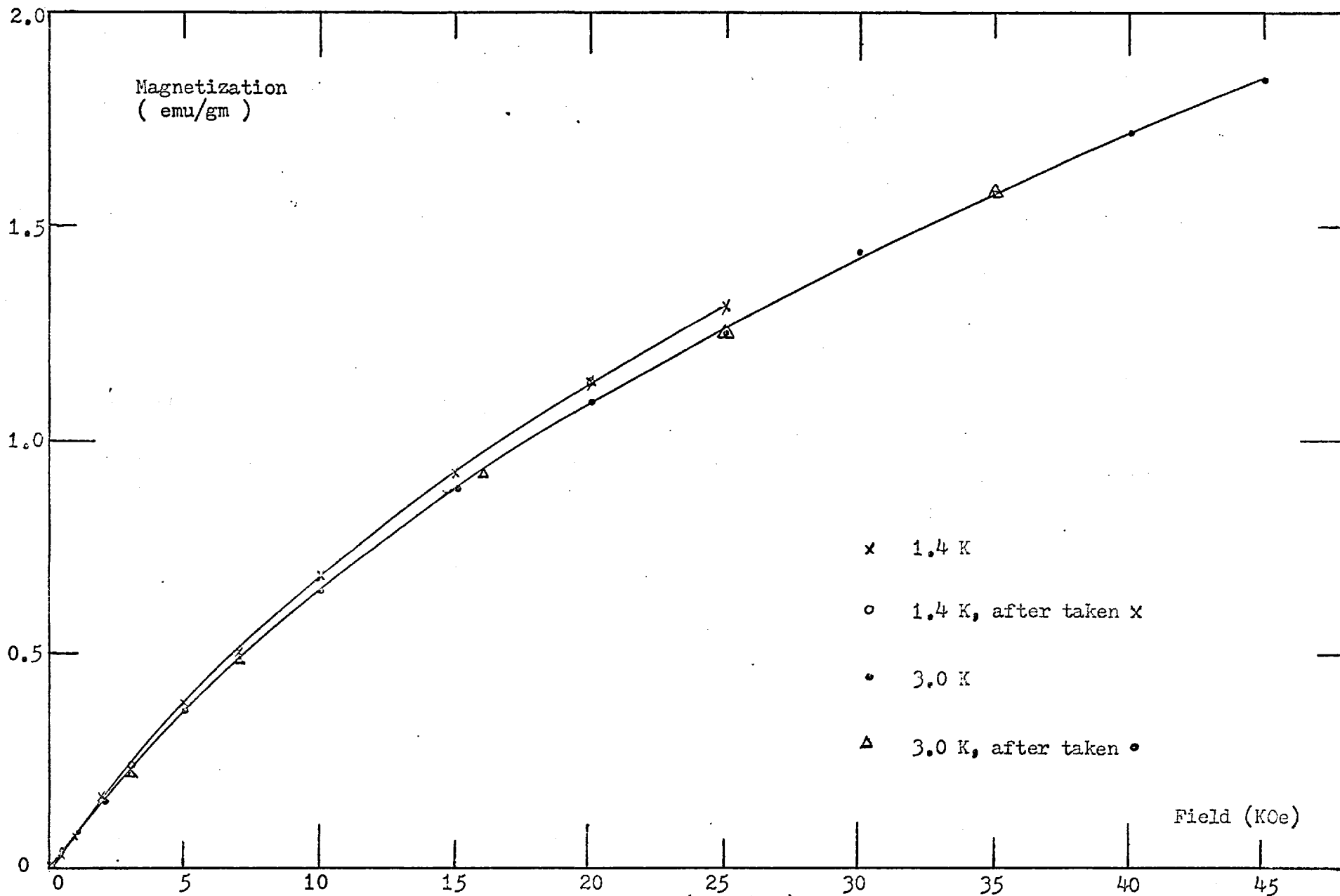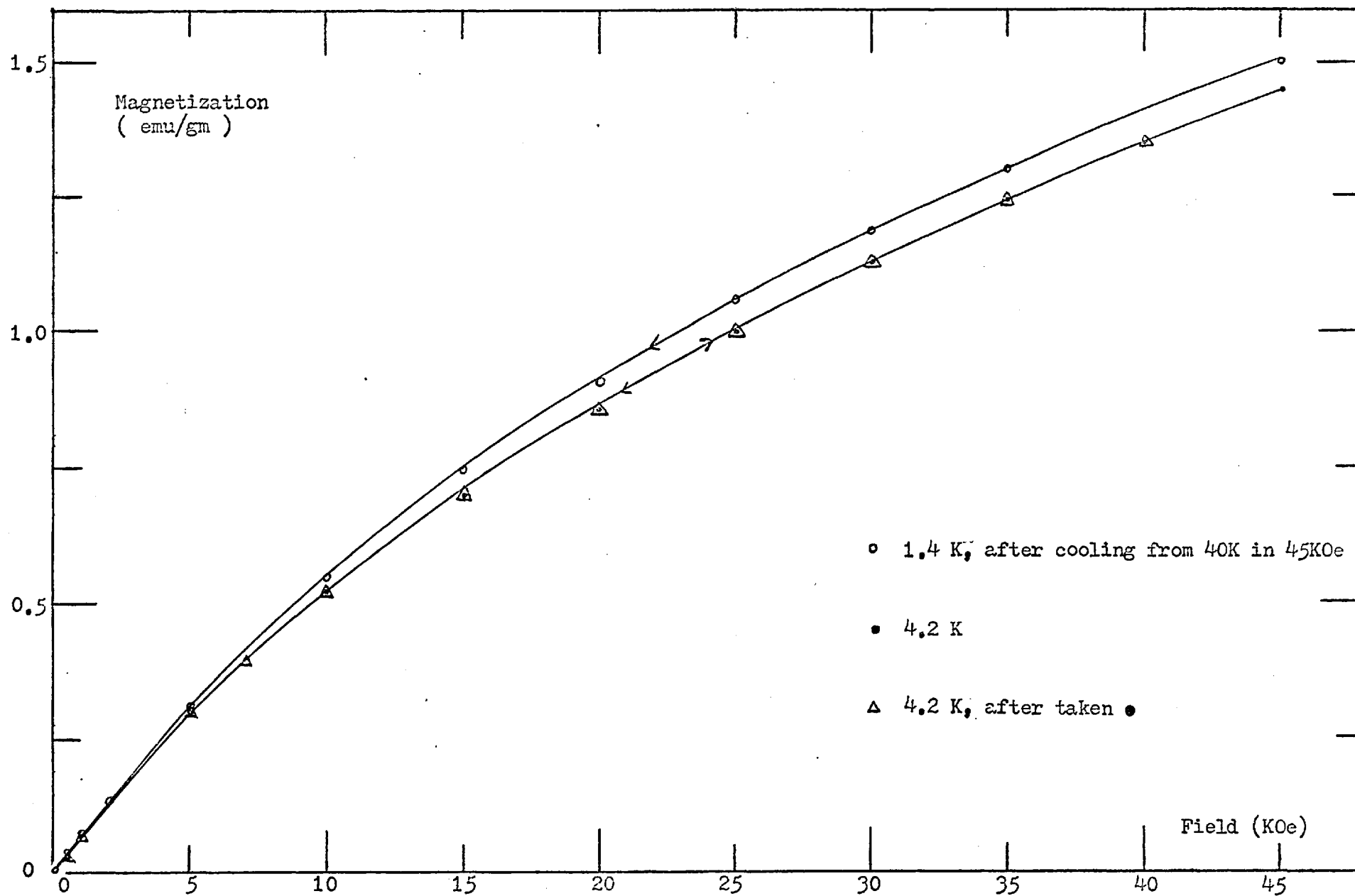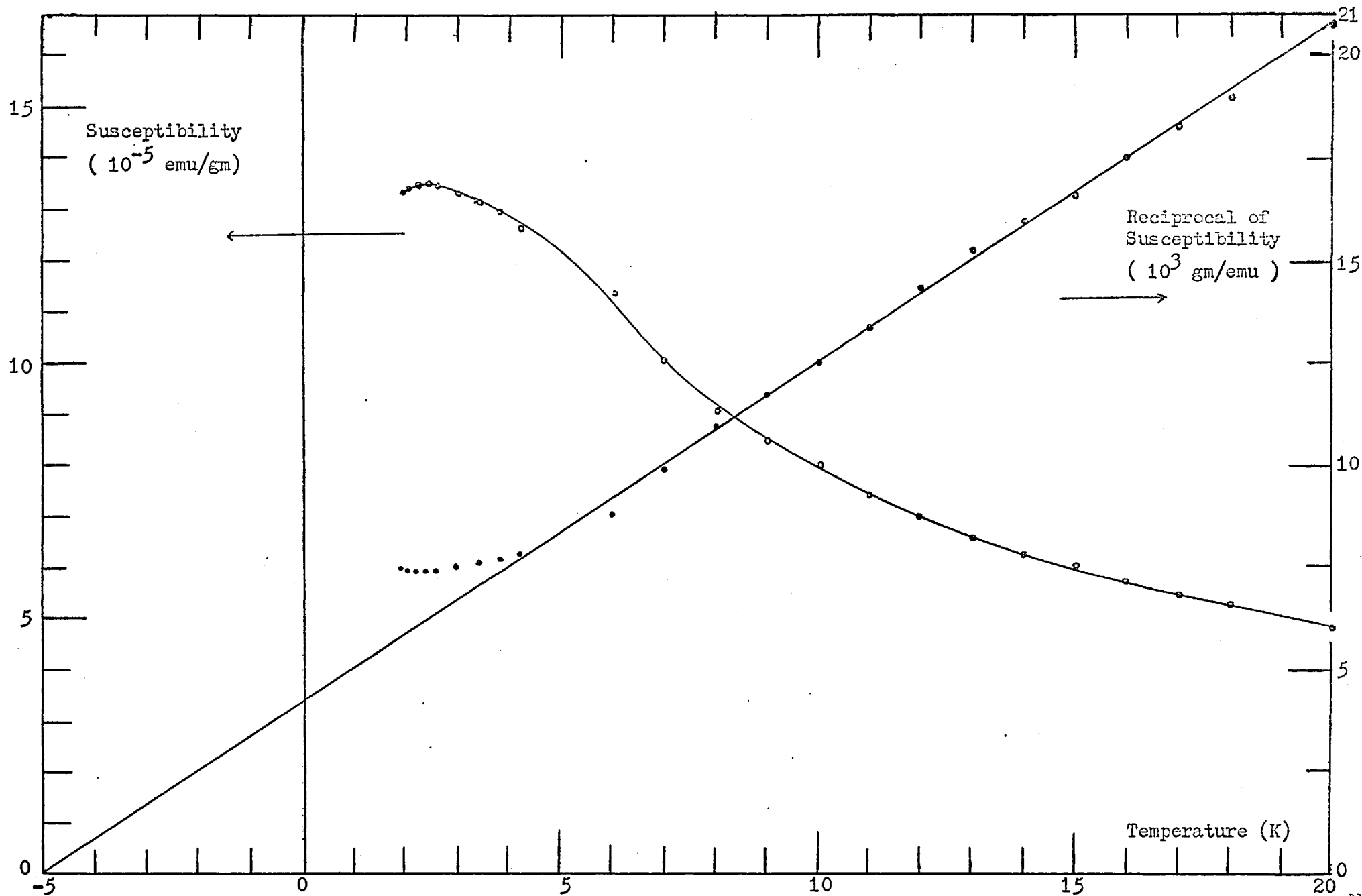Fig. 114 Susceptibility and Reciprocal of Susceptibility for $Pd_{.75}Pt_{.25}Mn$ (4at.% Mn) Impurity

among the effects of the impurity interactions, the thermal fluctuation, and the applied field. Details of this competition have been discussed in the previous chapter, Chapter 4.

The susceptibility of these alloys follow the Curie-Weiss law at temperatures above 8K. Below this temperature the susceptibility deviates to above the Curie-Weiss law which indicates the onset of the superparamagnetic state. As the temperature decreases further, a falling down of the susceptibility starts and a maximum on the suscepti-bility curve is, thus, formed at a distinct temperature T_{max}. This maximum cusp of the susceptibility with some field cooling remanence is the clear evidence of the existence of the magnetic spin glass state.

By extrapolating the reciprocal of the susceptibility between 8 and 20K, the Weiss temperatures θ have been determined. From the Curie constants, the effective magnetic moments μ_{eff} per Mn atom have been obtained. The values of the Curie temperature T_c, the Weiss temperature θ, the temperature of the susceptibility maximum T_{max}, the effective moment μ_{eff} per Mn atom and the low field susceptibility X taken at 20K of all the alloys being studied are listed in Table 7.

TABLE 7

Magnetic Properties of Some $Pd_{1-x}Pt_xMn$ Alloys

$Pd_{1-x}Pt_xMn_y$ composition		Weiss temp.	Curie temp.	Effective moment	Suscept. maximum	Mn Suscept. at 20K
x	y at.% Mn	θ (k)	T_c(k)	$\mu_{eff}(\mu_B)$	T_{max}(k)	$X(10^{-5}$emu/gm)
0.02	1.5 (a)	---	3.3 ± 0.1	---	---	---
1.00	3 (a)	-6.4 ± 0.3	---	6.1 ± 0.2	2.5 ± 0.2	2.8 ± 0.1
0.75	3 (a)	-3.5 ± 0.3	---	4.6 ± 0.2	3.0 ± 0.2	2.0 ± 0.1
0.50	3 (a)	-4 ± 0.3	---	4.9 ± 0.2	2.5 ± 0.2	2.6 ± 0.1
0.35	3 (a)	-2.5 ± 0.3	---	4.3 ± 0.2	1.6 ± 0.2	2.2 ± 0.1
0.25	3 (a)	-2.9 ± 0.3	---	5.3 ± 0.2	---	2.7 ± 0.1
0.15	3 (a)	-0.5 ± 0.3	---	5.1 ± 0.2	---	4.1 ± 0.1
0.05	3 (a)	+2.9 ± 0.3	1.5 ± 0.1	6.1 ± 0.2	---	4.1 ± 0.1
0.02	3 (a)	+5.3 ± 0.3	3.5 ± 0.1	4.6 ± 0.2	---	5.3 ± 0.1
0.00	3 (b)	+8.5	7.5	6.3	---	---
0.25	4 (a)	-5.0 ± 0.3	---	5.5 ± 0.2	2.4 ± 0.2	4.8 ± 0.1

(a) from ref. (1)

(b) from ref. (180)

The Weiss temperature θ, the Curie temperature T_c and the susceptibility maximum temperature T_{max} of the $Pd_{1-x}Pt_xMn$ alloys versus the binary matrix composition x have been plotted in Fig. 115.
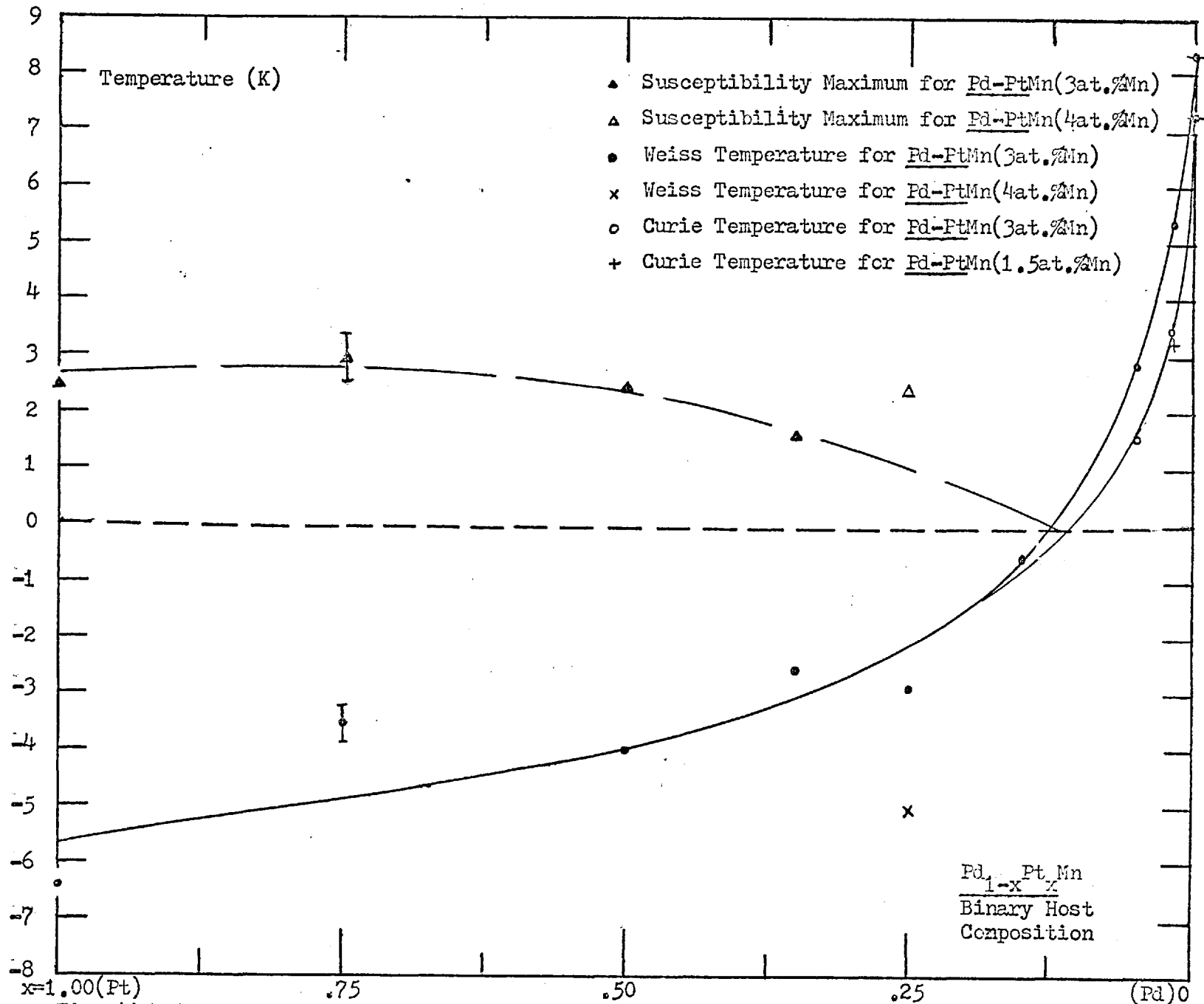
Fig. 115 Plot of Susceptibility Maximum, Weiss Temperature and Curie Temperature for Pd-PtMn

The Θ decreases monotonically from +8K approaching zero to negative, until it reaches -6K as composition Pt (x) varies from 0.00 to 1.00. The T_{max} changes naturally follow the opposite direction. These behaviours thus suggest that as the Pt composition of the binary matrix increases, the tendency towards ferromagnetism will decrease and, on the other hand, the tendency towards magnetic spin glass state will increase and vice versa.

As the concentration of Pt in the matrix increases, the interactions between solute atoms tend to stabilize the spin fluctuations, driving the atom closer to the instability which leads to magnetic ordering formation. The latter process, apparently, does not occur uniformly at every solute site through the alloy, but varies according to the local environment around the solute atoms; therefore, the magnetic state transition versus the $Pd_{1-x}Pt_x$ composition is expected to be a smooth one.

The low field susceptibility X taken at 20K and the effective moment μ_{eff} per Mn atom of the $Pd_{1-x}Pt_x$Mn versus the binary matrix composition x have been plotted in Fig. 116. The X and μ_{eff} both have a dip at the medium composition between x = 0.00 and 1.00.

The $Pd_{1-x}Pt_x$ binary matrix might be divided into roughly two regions: I and II. In Region I, for small x, the binary matrix is dominated by the Pd part of the host. The exchange enhancement factor D, and hence the size of the polarization clouds centered on the Mn atoms, will increase as the Pd composition increases in the $Pd_{1-x}Pt_x$ binary matrix. The increase of the polarization clouds will, thus, increase the alignments between the impurity atoms due to increase of the overlapping until the polarization clouds reach a certain degree where the ferromagnetic interaction between the distant Mn impurity atoms will dominate the alloy;
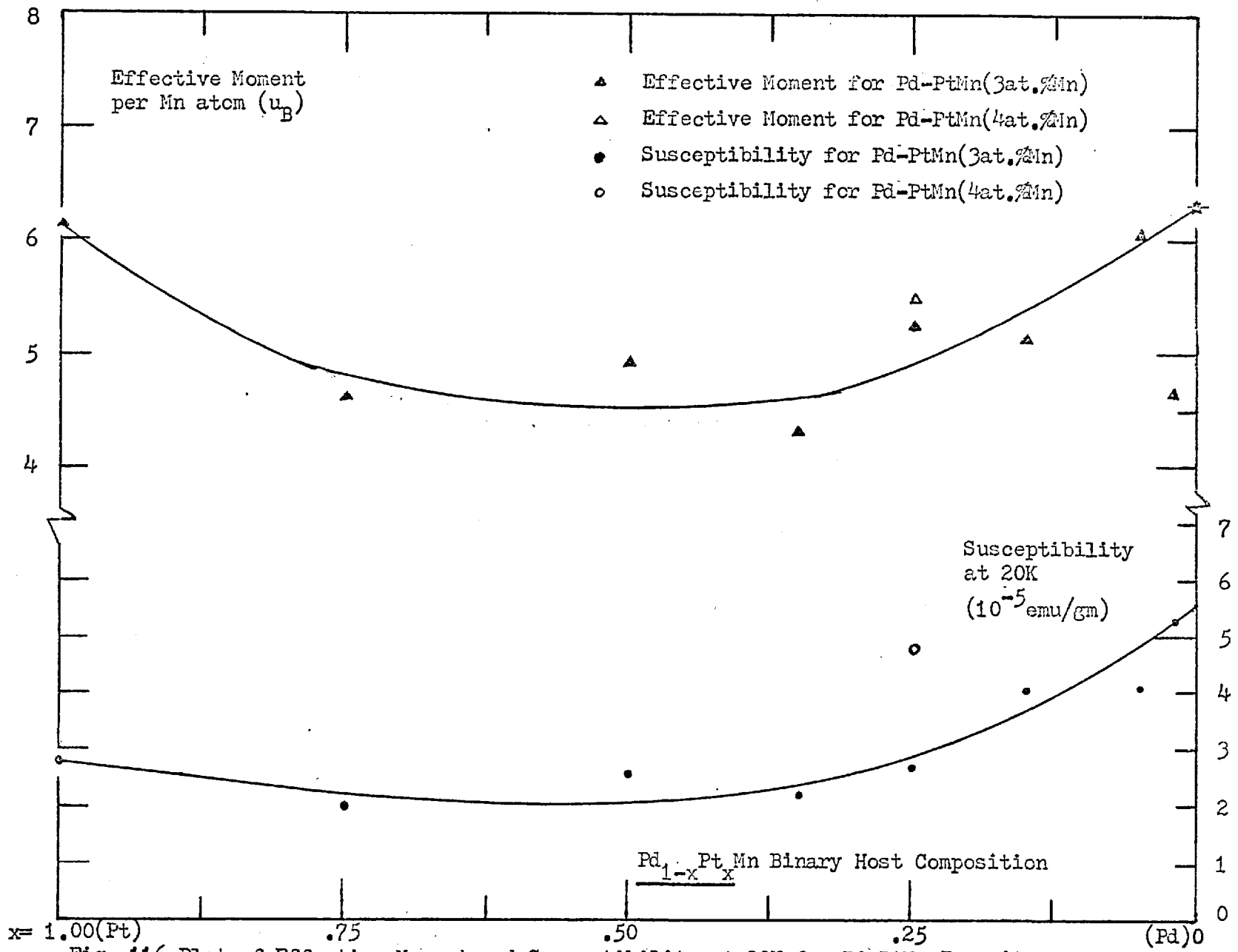
Fig. 116 Plot of Effective Moment and Susceptibility at 20K for Pd-PtMn Impurity

therefore, an onset of the ferromagnetism occurs. As the Pd composition increases further (i.e. the polarization increases further) the value of X, μ_{eff}, T_c, and θ will naturally increase to higher values. The effect of the competition between the ferromagnetic-antiferromagnetic interactions of Mn atoms can also be seen from the close values of T_c for $\underline{Pd_{.98}Pt_{.02}Mn}$ (3 at.% Mn) and $\underline{Pd_{.98}Pt_{.02}}Mn$ (1.5 at.% Mn) alloys. The increase of the ferromagnetic effect almost compensates for the increase of the anti-ferromagnetic effect due to increase of Mn concentrations.

In the Region II, for large x, the $Pd_{1-x}Pt_x$ binary matrix is dominated by the Pt part of the host. The polarization clouds centered on Mn atoms decrease as the Pt composition increases and, hence, the interactions between the distant Mn atoms become less effected. But, on the other hand, relatively, the possible nearest neighbor Mn antiferromagnetic interactions have more weight now. These mixed impurity interactions thus lead to the onset of the magnetic spin glass state. This tendency can also be seen from the high value of T_{max} of the $\underline{Pd_{.75}Pt_{.25}}Mn$ (4 at.% Mn) alloy compared with that of the $\underline{Pd_{.75}Pt_{.25}}Mn$ (3 at.% Mn) alloy. Although these two alloys have similar composition to the binary host, but the former has higher Mn impurity concentrations; thus, the nearest neighbor interaction becomes more important, and it has more tendency toward magnetic spin glass state. Since the decrease of the distant impurity interactions as the Pt composition increases, an increase of T_{max} and decrease of μ_{eff} and X should happen.

A final upturn of μ_{eff} occurs when the alloy composition is close to the $\underline{Pt}Mn$ (3 at.% Mn). This effect is analogous to the $\underline{Pt}Mn$ alloy system; when the impurity concentration decreases, the μ_{eff} increases

at low concentration range as has been shown in Chapter 4, Fig. 72.

Because when in the PtMn alloys the Mn concentration decreases, then

each Mn atom can act more freely with its surrounding local polarization

cloud in response to any external field as a giant moment; however, as

the Mn concentration increases, then the increase of impurity interactions

will influence each other more. Therefore, the overall response to

external field will decrease and result in a decreasing of μ_{eff} from the

bulk susceptibility measurements. In the rich Pt, $Pd_{1-x}Pt_xMn$ (3 at.% Mn)

alloys, even the number of Mn impurity atoms is conserved, but the

change of the composition of the binary matrix results in the change

of the exchange enhancement factor (113) and will have the same effect

on impurity interactions as changing the number of Mn atoms in the

PtMn alloy system; therefore, in an analogy to the results and analysis

of the PtMn alloys, the further increase of Pt in the rich Pt binary matrix

will result in the increase of μ_{eff} per Mn atom.

From the above experimental results, one can conclude that when a

small amount of Mn impurity, say 3 at.% Mn, is added into the $Pd_{1-x}Pt_x$

binary matrix, the behaviours of the alloys will change smoothly with the

composition of the host. At the x = 0 end, PdMn, the alloy is ferromagnetic

with a Curie temperature T_c = 8K (179,180). As the composition of Pt (x)

increases, the Curie temperature will drop and eventually a magnetic

spin glass state will be stabilized. The paramagnetic Weiss temperature θ

starts from about 8.5K for PdMn (3 at.% Mn) (180) and falls down smoothly

as x increases, to the value of -6.3K for PtMn (3 at.% Mn) (1). These

variations have been shown clearly in Fig. 115. At this stage, an obvious

question will be asked: what is the critical composition of the binary host

$Pd_{1-x}Pt_x$, at which the $\underline{Pd_{1-x}Pt_x}Mn$ (3 at.% Mn) alloy lies on the division between ferromagnetism and magnetic spin glass?

From the magnetic phase diagram of $Pd_{1-x}Pt_xMn$ alloy system, the existence of such a critical composition should not be doubted, and the alloy with such a critical composition can be easily verified by extrapolating the parallel lines on the M^2 versus (H/M) plot of magnetic isotherms to temperature T = 0K, which should pass through the origin.

Experimentally, however, to find and to make an alloy with the critical composition is rather impractical; therefore, from either side of the critical composition x_c, two usual extrapolating methods are used to approach this question. The method in dealing with the $x < x_c$ side is to plot the data points of host compositions versus Curie temperatures T_c, then extrapolate the curve connecting those data points to $T_c = 0K$ composition. But, from the only three data points we obtained for the $x < x_c$ region of the $\underline{Pd_{1-x}Pt_x}Mn$ (3 at.% Mn) alloy system, no simple relationship can be drawn.

The other method in dealing with the $x_c < x$ side is to plot the low temperature isothermal values of (X_{host}/X_{alloy}) versus host composition (178), and extrapolate this curve to the divergent point, $(X_{host}/X_{alloy}) = 0$, and the intercept is the critical composition. From the results we obtain in the $x_c < x$ region, there is no well-defined curve which can be drawn, because the data points are too far apart, and there is no simple relationship among them.

We, therefore, use the extrapolating Curie temperatures method and also take into consideration the tendency of the change of the Weiss temperatures through a wide composition range, and estimate the critical

composition of the $Pd_{1-x}Pt_xMn$ (3 at.% Mn) alloy system between ferro-

magnetism and magnetic spin glass state to be $x = 0.10 \pm 0.02$. A more

comprehensive magnetic phase diagram of the Pd-Pt Mn alloy system has

been established and is shown in Fig. 117.
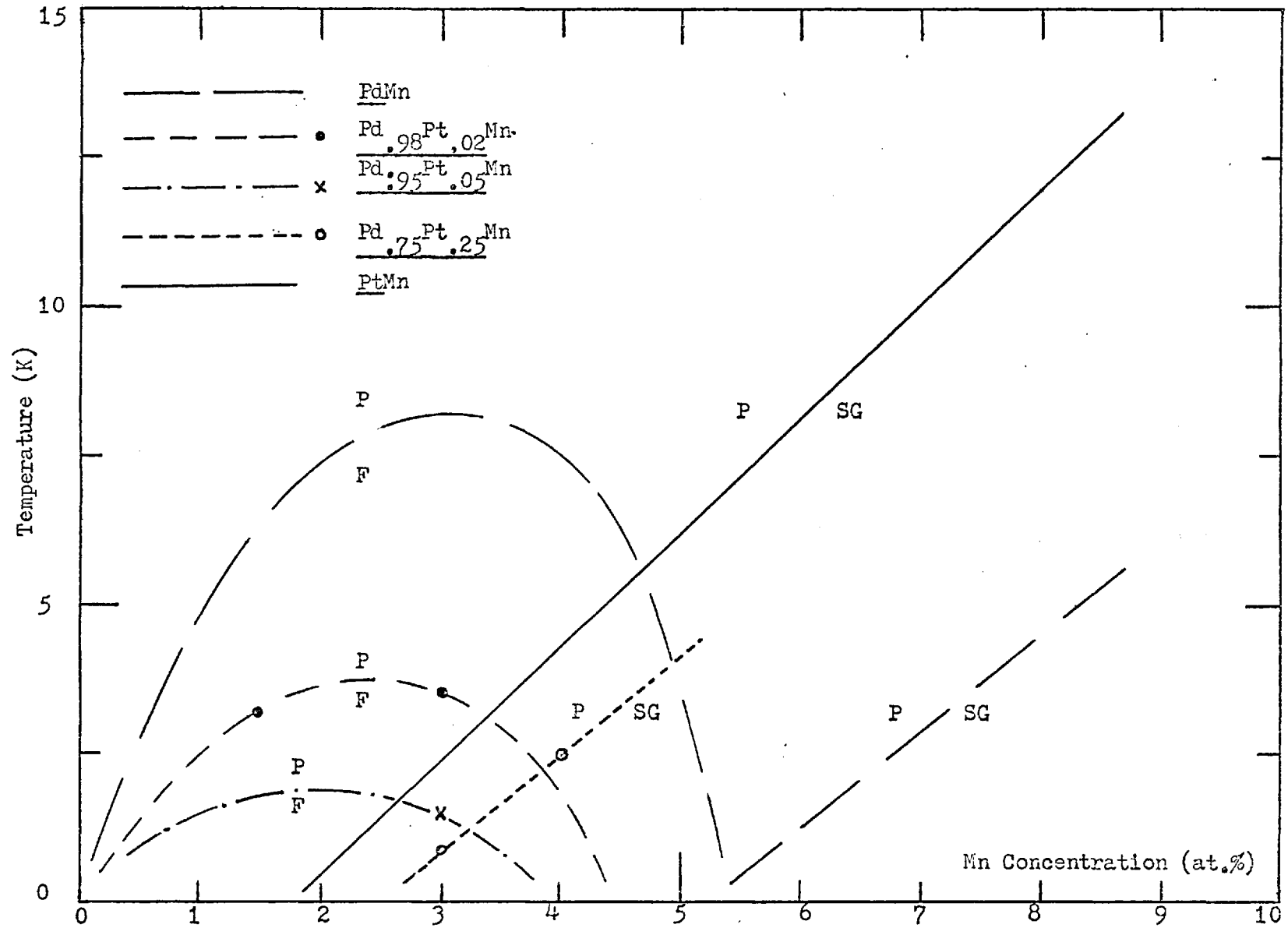
Fig. 117 Magnetic Phase Diagram for Pd-PtMn alloy system, F:Ferromagnetic, P:Paramagnetic
SG:Magnetic Spin Glass State

REFERENCES

REFERENCES

1. Pon-Wei Hou, this work

2. B.R. Coles, private communication

3. W.B. Pearson, Phil. Mag. 46, 920 (1955)

4. G. Knapp, J. Appl. Phys. 38, 1267 (1967)

5. For a careful measurement of Weiss temperature   versus impurity concentration, see F.W. Smith, Phys. Rev. B 10, 2034 (1974)

6. W. Meissper and G. Voigt, Ann. Physik 7, 761 (1970)

7. J. Kondo, Prog. Theor. Phys. 32, 37 (1964)

8. B. Knook, Thesis, Univ. of Leiden (1962)

9. M.P. Sarachik, E. Corenzeit and L.D. Longinotti, Phys. Rev. 135, A1041 (1964)

10. G.G. Low and M.F. Collings, J. Appl. Phys. 34, 1195 (1963)

11. A. Arrott, M.F. Collins, T.M. Holden, G.G. Low and R. Nathans, J. Appl. Phys. 37, 1194 (1966)

12. J. Friedel, Can. J. Phys. 34, 1190 (1956)

   Nuovo Cinento (Supp.) 7, 287 (1958)

   J. Phys. Rad. 23, 692 (1962)

13. N.F. Mott, Proc. Phys. Soc. Lond. 47, 571 (1935)

14. See, for example, E.Merzbach, Quantum Mechanics, John Wiley & Sons Inc. (1967), Chapter 16

15. See, for example, E.Merzbach, Quantum Mechanics, John Wiley & Sons Inc. (1967), Chapter 12

16. B.T. Matthias, M. Peter, H.J. Williams, A.M. Clogston, E. Corenzwit and R.C. Sherwood, Phys. Rev. Lett. 5, 542 (1960)

   Phys. Rev. 125, 541 (1962)

17. P.W. Anderson, Phys. Rev. 124, 41 (1961)

18. K. Yosida, A. Kiji and S. Chikazumi, Prog. Theor. Phys. 33, 559 (1965)

19. A.P. Klein and A.J. Heeger, Phys. Rev. 144, 458 (1966)

20. E.C. Stoner, Rept. Prog. Phys. 11, 43 (1947)

   J. Phys. Rad. 12, 372 (1951)

21. P.A. Wolff, Phys. Rev. 124, 1030 (1961)

22. A.M. Clogston, Phys. Rev. 125, 439 (1962)

23. C. Zener, Phys. Rev. 81, 440 (1951)

24. N.A. Ruderman and C. Kittel, Phys. Rev. 96, 99 (1954)

25. R. Kasuya, Prog. Theor. Phys. 16, 45 (1956)

26. K. Yosida, Phys. Rev. 106, 893 (1957)

27. P.W. Anderson and A.M. Clogston, Bull. Am. Phys. Soc. 6, 124 (1961)

28. J. Kondo, Prog. Theor. Phys. 28, 846 (1962)

29. A good review see, for example, B.N. Ganguly and C.S. Shastry, J. Phys. C 3, 1587 (1970)

30. K. Yosida, Phys. Rev. 147, 223 (1966)

31. K. Yosida, Prog. Theor. Phys. 36, 875 (1966)

32. A.A. Abrikosov, Phys. 2, 5 (1965)

33. H. Suhl and D. Wong, Phys. 3, 17 (1967)

34. Y. Nagaoka, Prog. Theor. Phys. 37, 13 (1967)

   Phys. Rev. 138, A 1112 (1956)

35. P.E. Bloomfield and D.R. Hamann, Phys. Rev. 164, 856 (1967)

36. S.D. Silverstein and C.B. Duke, Phys. Rev. 161, 456 (1967)

37. D.R. Hamann, Phys. Rev. 158, 570 (1967)

38. C. Rizzuto, Rep. Prog. Phys. 37, 147 (1974)

39. P.E. Bloomfield, R. Hecht and P.R. Sievert, Phys. Rev. B2, 3714 (1970)

40. M.D. Daybell and W.A. Steyert, Rev. Mod. Phys. 40, 380 (1968)

41. N. Rivier, M. Sunjic and M.J. Zuckermann, Phys. Lett. 28A, 492 (1969)

42. H. Suhl, Phys. Rev. Lett. 19, 442 (1967)

43. N. Rivier, Thesis, Univ. of Cambridge (1968)

44. N. Rivier and M.J. Zuckermann, Phys. Rev. Lett. 21, 904 (1968)

44a. D.R. Hamann, Phys. Rev. Lett. 23, 95 (1969)

45. J.R. Schrieffer and P.A. Wolff, Phys. Rev. 149, 491 (1966)

46. J.R. Schrieffer, J. Appl. Phys. 38, 1143 (1967)

47. K. Kume, J. Phys. Soc. Japan 23, 1226 (1967)

48. A. Narath, A.C. Go ssard and J.H. Wernick, Phys. Rev. Lett. 20, 795 (1968)

49. H. Launois, Solid St. Comm. 7, 525 (1969)

50. M.S. Green, private communication

51. L.D. Landau and E.N. Lifehitz, Statistical Physics, Pergamon (1958), Chapter 14

52. D.J. Thouless, Phys. Rev. 181, 954 (1969)

53. J.R. Schrieffer and D.C. Mattis, Phys. Rev. 140, A1412 (1965)

54. P.W. Anderson, J. Appl. Phys. 37, 1194 (1966)

55. G.W. Poo, J. Phys. F 2, 782 (1972)

56. F.T. Hedgcock and P.L. Li, Phys. Rev. B2, 1342 (1970)

57. A.J. Heeger, Solid St. Phys. 23, 283 (1969)

58. H. Frohlick and F.R.N. Naborro, Proc. Roy. Soc. London A 175, 382 (1940)

59. P.A. Wolff, Phys. Rev. 120, 814 (1960)

60. See, for example, W.A. Harrison, Solid State Theory, McGraw Hill Inc. (1970), Chapters IV and V

61. P.G. deGennes, J. Phys. Rad. 23, 630 (1962)

62. A. Blandin and J. Friedel, J. Phys. Rad. 20, 160 (1959)

63. D.G. Golibersuch and A.J. Heeger, Phys. Rev. 182, 584 (1969)

64. D.G. Golibersuch, Thesis, Univ. of Pennsylvania (1970)

65. D. Mattis, Phys. Rev. 130, 76 (1963)

66. F. Holtzberg, T.R. McGuire, S. Methfessel and J.C. Suits, Phys. Rev. Lett. 13, 18 (1964)

67. H. Suhl, Solid St. Comm. 4, 487 (1966)

68. T. Moriya, Prog. Theor. Phys. 33, 157 (1965)

69. B.R. Coles, J. Physique C4, 203 (1974)

70. P.R. Weiss, Phys. Rev. 74, 1493 (1948)

71. W. Marshall, Phys. Rev. 118, 1519 (1960)

72. M.W. Klein and R. Brout, Phys. Rev. 132, 2412 (1963)

73. M.W. Klein, Phys. Rev. Lett. 11, 408 (1963)
    Phys. Rev. 136, A1156 (1964)

74. S.H. Liu, Phys. Rev. 157, 411 (1967)

75. O.S. Lutes and J.L. Schmit, Phys. Rev. 134, A676 (1964)

76. P.J. Ford and J.A. Mydosh, J. Physique C4, 241 (1974)

77. B.W. Southern, to be published

78. I. Takahashi and M. Shimizu, Prog. Theor. Phys. 51, 1678 (1974)

Prog. Theor. Phys. 53, 41 (1975)

79. Y.C. Tsay and M.W. Klein, Phys. Rev. B7, 352 (1973)

80. P. Lederer and D.L. Mills, Phys. Rev. 165, 837 (1968)

81. H. Nagasawa, Solid St. Comm. 10, 33 (1972)

82. J.W. Loram, R.J. White and A.D.C. Grassie, Phys. Rev. B5, 3659 (1972)

83. J. Souletie, J. Low Temp. Phys. 7, 141 (1972)

84. N. Rivier and V. Zlatic, J. Phys. F2, L87 (1972)

J. Phys. F2, L99 (1972)

85. J. Souletie and R. Tournier, J. Low Temp. Phys. 1, 95 (1969)

86. A. Blandin, Thesis, Paris Univ. (1961)

87. A.I. Larkin and D.E. Khmel'nitskii, Zh. Eksp. Theor. Fiz. 58, 1789 (1970) (Sov. Phys. - JETP 31, 958 (1970))

88. E.C. Hirschkoff, O.G. Symko and J.C. Wheatley, J. Low Temp. Phys. 5, 155 (1971)

89. J.L. Tholence and R. Tournier, J. Physique C4, 229 (1974)

90. P.W. Anderson, Mat. Res. Bull. 5, 549 (1970)

91. P.A. Beck, Met. Trans. 2, 2015 (1971)

92. V. Cannella and J.A. Mydosh, AIP Conf. Proc. 18, 651 (1974)

93. A.J. Dekker, Physica 24, 697 (1958)

94. V. Cannella and J.A. Mydosh, Phys. Rev. B6, 4220 (1972)

95. V. Cannella, J.A. Mydosh and J.I. Budnick, J. Appl. Phys. 42, 1689 (1971)

96. J. Crangle and W.R. Scott, J. Appl. Phys. 36, 921 (1965)

97. A.P, Murani and B.R. Coles, J. Phys. C 3, S159 (1970)

98. B.R. Coles and R. Rusby, J. Phys. F. $\underline{4}$, 1265 (1974)

99. B.R. Coles, A Tari and H.C. Jamieson, Low Temp. Phys.

    Editors: K.D. Timmerhaus, W.J. O'Sullivan and E.F. Hammel

    (1974) $\underline{V.2}$ 414

100. L. Shen, D.S. Schreiber and A.J. Arko, Phys. Rev. $\underline{179}$, 512 (1969)

101. See, for example, G.J. Nieuwenhuys, B.M. Boerstoel, J.J. Zwart

    and G.J. van den Berg, Physica $\underline{62}$, 278 (1972)

102. S. Ehara, J. Phys. Soc. Japan $\underline{17}$, 726 (1962)

103. P.P. Craig, R.C. Perisho, R. Segnan and W.A. Steyert, Phys.

    Rev. $\underline{138}$, A1460 (1965)

104. G.G. Low and T.M. Holden, Prog. Phys. Soc. $\underline{89}$, 119 (1966)

105. B.R. Coles, Amorphous Magnetism, Editors: Hooper and de Graaf

    169 (1972)

106. V. Jaccarino and L.R. Walker, Phys. Rev. Lett. $\underline{15}$, 258 (1965)

107. C.G. Robbins, H. Claus and P.A. Beck, Phys. Rev. Lett. $\underline{24}$,

    1307 (1969)

108. Y. Ito and J. Akimitsu, J. Tech. Rept. ISSP , A560 (1972)

109. T.H. Geballe, B.T. Matthias, A.M. Clogston, H.J. Williams,

    R.C. Sherwood and J.P. Maita, J. Appl. Phys. $\underline{37}$, 1181 (1966)

110. J.W. Garland and A. Gonis, Magnetism in Alloys, Edistor: P.A.

    Peck and J.T. Waber (1972) 79

111. T.J. Hicks, B. Rainford, J.S. Kouvel, G.G. Low and J.B. Comly,

    Phys. Rev. Lett. $\underline{22}$, 531 (1969)

112. O.K. Anderson, Phys. Rev. $\underline{B2}$, 883 (1970)

113. K. Andres and M.A. Jensen, Phys. Rev. $\underline{165}$, 533 (1968)

114. A.M. Clogston, V. Jaccarino and Y. Yafet, Phys. Rev. $\underline{134}$, A650 (1964)

115. T.A. Seitchik, A.C. Gossard and V. Jaccarino, Phys. Rev. 136, A1119 (1964)

116. P. Nozieres, The Theory of Interacting Fermi Systems, W.A. Benjamin Inc. (1963)

117. S. Foner and E.J. McNiff Jr., Phys. Rev. Lett. 19, 1438 (1967)

118. G. Chouteau, R. Fourneaux and R. Tournier, Proc. Int. Conf. Low Temp. Phys. 12th Kyoto (1970)

119. G. Gruner, private communication

120. A.J. Barber, private communication

121. M. Hansen and K. Anderko, Constitution of Binary Alloys, McGraw-Hill Book Co. (1958)

122. F.A. Shunk, Constitution of Binary Alloys (Second Supplement), McGraw-Hill Book Co. (1969)

123. A.E. Bell, Thesis, Univ. of London (1973)

124. L.J. Neuringer and Y. Shapira, Rev. Sci. Instru. 40, 1314 (1969)

125. R. Berman and J. Kopp, J. Phys. F. 1, 457 (1971)

126. H.H. Sample, L.J. Neuringer and L.G. Rubin, Rev. Sci. Instru. 45, 64 (1974)

127. J.A. Poulis, C.H. Massen and J.M. Thomas, J. Sci. Instru. 43, 234 (1966)

128. A.N. Gerritsen and D.H. Damon, Rev. Sci. Instru. 33, 301 (1962)

129. H. Krupp, Vacuum 13, 297 (1963)

130. A.J. Barber, Thesis, Univ. of London (1974)

131. A. Tari, Thesis, Univ. of London (1972)

132. O. Laborde and P. Radhakrishna, Solid St. Comm. 9, 701 (1971)

133. J.L. Tholence and R. Tournier, J. Physique C1, 211 (1971)

134. K. Mizuno, J. Phys. Soc. Japan 30, 742 (1971)

135. J. Flouquet, Phys. Rev. Lett. 25, 288 (1970)

136. D.L. Martin, Phys. Rev. 141, 576 (1966)

137. D. Davidov, C. Rettori, R. Orbach, A. Dixon and E.P. Chock,

    Phys. Rev. B11, 3546 (1975)

138. A.I. Larkin, V.I. Mel'nikov and D.E. Khmel'nitskii, Zh. Eksp.

    Theor. Fiz. 60, 846 (1971) (Sov. Phys. - JETP 33, 458 (1971))

139. C.M. Hurd, J. Phys. Chem. Soc. 30, 539 (1969)

140. J.A. Cameron, J.A. Campbell, J.P. Compton, R.A.G. Lines and

    G.V.H. Wilson, Phys. Lett. 20, 569 (1966)

141. See, for example, H.P. Falke, H.P. Jablonski and E.F. Wassermann,

    Z. Physik 269, 285 (1974)

142. R.S. Newrock, B. Serin, J. Vig and G. Boats, J. Low Temp. Phys.

    5, 701 (1971)

143. G. Gruner, Adv. in Phys. 23, 941 (1974)

144. G. Gruner, Solid St. Comm. 10, 1039 (1972)

145. E. Babic, P.C. Ford, C. Rizzuto and E. Salamoni, Solid St. Comm.

    11, 519 (1972)

146. E. Babic, P.C. Ford, C. Rizzuto and E. Salamoni, J. Low Temp.

    Phys. 8, 217 (1972)

147. J.P. Kedves, M. Hordos and L. Gergely, Solid St. Comm. 19,

    1067 (1972)

148. A.D. Caplin and C. Rizzuto, Phys. Rev. Lett. 21, 746 (1968)

149. R. Aoki and T. Ohtsuka, J. Phys. Soc. Japan 26, 651 (1969)

150. C.P. Flynn, D.A. Rigney, and J.A. Gardner, Phil. Mag. 15, 1255 (1967)

151. S.F. Edwards and P.W. Anderson, J. Phys. F. 5, 965 (1975)

152. D. Sherrington and B.W. Southern, J. Phys. F. 5, L49 (1975)

153. K.H. Fischer, Phys. Rev. Lett. 34, 1438 (1975)

154. A. Gerstenberg, Physik 2, 236 (1958)

155. W.M. Star, B.M. Boerstoel, J.E. VanDam and C. Van Baarle, Proc. Int. Conf. Low Temp. 11th St. Andrews, (1967) 1280

156. A. Tari and B.R. Coles, J. Phys. F. 1, L69 (1971)

157. A.P. Murani, A. Tari and B.R. Coles, J. Phys. F. 4, 1769 (1974)

158. J.S. Kouvel, J. Phys. Chem. Solids 24, 795 (1963)

159. J.E. VanDam, Thesis, Univ. of Leiden (1972)

160. R.P. Guertin, H.C. Praddaude, S. Foner, E.J. McNiff, Jr. and B. Barsoumian, Phys. Rev. B7, 274 (1973)

161. D.M.S. Bagguley, W.A. Crossley and J. Liesegang, Proc. Phys. Soc. 90, 1047 (1967)

162. J. Crangle, Phil. Mag. 5, 335 (1960)

163. P. Lederer, Proc. NATO Adv. Study Insti. "Magnetism Current Topic," France, (1970)

164. M.P. Maley, R.D. Taylor and J.L. Thompson, J. Appl. Phys. 38, 1249 (1967)

165. G.J. Nieu wen huys, M.F. Pikart, J.J. Zwart, B.M. Boerstoel and G.J. Van Den Berg, Physica 69, 119 (1973)

166. E. Kren, G. Kadar, L. Pal, J. Solyom, P. Szabo and T. Tarnoczi, Phys. Rev. 171, 574 (1968)

167. S.J. Pickart and R. Nathans, J. Appl. Phys. 33, 1336 (1962)

168. S.S. Sidhu, K.D. Anderson and D.D. Zauberis, Bull. Am. Phys. Soc. 10, 352 (1965)

169. F. Menziger and A. Paoletti, Phys. Rev. 143, 365 (1966)

170. Y. Miyako, H. Morishita and T. Watanabe, J. Phys. Soc. Japan 27, 1071 (1969)

171. S.J. Pickart and R. Nathans, J. Appl. Phys. 34, 1203 (1963)

172. H. Nagasawa, J. Phys. Soc. Japan 27, 787 (1969)

173. W.M. Star, E. DeVroede and C. Van Baarle, Physica 59, 128 (1972)

174. R.M. Roshko and G. Williams, Phys. Rev. B9, 4945 (1974)

175. W.M. Star, S. Foner and E.J. McNiff, Jr., Phys. Lett 39A, 189 (1972)

176. N. Inoue and H. Nagasawa, J. Phys. Soc. Japan 31, 477 (1971)

177. H. Nagasawa, J. Phys. Soc. Japan 28, 1171 (1970)

178. R. Harris and M.J. Zuckermann, Phys. Rev. B5, 101 (1972)

179. G. Williams and J.W. Loram, Solid St. Comm. 7, 1261 (1969)

180. D. Shaltiel, J.H. Wernick and H.J. William, Phys. Rev. 135, A1346 (1964)

181. H. Kadomatsu, J. Sci. Hiroshima Univ. A37, 141 (1973)

182. A.M. Clogston, B.T. Matthias, M. Peter, H.J. Williams, E. Corenzwit and R.C. Sherwood, Phys. Rev. 125, 541 (1962)

182a. H. Nagasawa, J. Phys. Soc. Japan 25, 691 (1968)

183. K.P. Belov and A.N. Goryaga, Fizika Metall 2, 3 (1956)

184. A. Arrott, Phys. Rev. 108, 1394 (1957)

185. J.S. Kouvel, G.E. Res. Lab. Rept. 57-RL-1799 (1957)

186. S. Shtrikman and E.P. Wohlfarth, Physica $\underline{60}$, 427 (1972)

187. C. Domb, Ann. Acad. Sci. Fennicae A VI $\underline{210}$, 167 (1966)

188. T. Kasuya, Prog. Theor. Phys. $\underline{16}$, 58 (1956)

APPENDIX   A

Magnetic Interactions in "Dilute" AgMn Alloys

Pon-Wei Hou and B.R. Coles

Department of Physics, Imperial College, London SW7, England

Abstract

Measurements are presented of the magnetization M up to 50KG between 1.8 and 4.2K and the susceptibility X from 1.8 to 100K of three "dilute" AgMn alloys of nominal concentrations 630, 1000, and 1370 ppm Mn. Both M and X follow scaling laws well. The strength V_o of the RKKY interaction between two Mn impurities has been determined from expressions for the high field behaviour of M in the presence of such interaction, yielded by a virial expansion of the free energy. The value obtained for V_o is $(3.9 \pm 1) \times 10^{-25}$ eV cm^3. The effective $|J|$ value estimated from V_o is (0.9 ± 0.1) eV.

Recently the interest in alloy research has been shifting from the extremely dilute region ($T_I < T_K$, where T_I is the measure of average interactions between solute atoms and T_K is the Kondo temperature) in which the single-impurity Kondo effect dominates to the more concentrated region in which the interactions between impurities can be no longer neglected. The strength V_0 of the Ruderman-Kittel-Kasuya-Yosida[1] (RKKY) interaction, $V(r) = V_0 \cos(2K_F r)/r^3$ (for $K_F \gg \pi$), between two Mn impurities and the effective $|J|$ value in $\underline{Ag}Mn$ alloys have been determined by magnetization measurements at high fields and are presented here. The $\underline{Ag}Mn$ alloy system was chosen because T_K is very small so that in the dilute limit the solute has a good magnetic moment down to very low temperature ; and because the electronic structure of Ag is simple it can be safely approximated to by a free electron model. It is thus unlike $\underline{Au}Fe$, for example, where the effect of T_K on the interaction behaviour is clear in the results of Laborde and Radhakrishna[2].

Three $\underline{Ag}Mn$ alloys with respective nominal concentrations of 630, 1000, and 1370 ppm Mn were examined. The starting materials were 99.9999% "Specpure" Ag (Johnson Matthey) and 99.99% pure Mn from Koch-Light Labs Ltd. The samples were made by diluting a 5.43 at.% $\underline{Ag}Mn$ master alloy in an arc furnace filled with two-thirds atmosphere argon, and forming into short cylinders of about 3 mm diameter. All samples were cleaned by a solution containing equal amounts of 25% NH_4OH and 20 vols H_2O_2. Measurements were carried out by a force (Faraday) method using a superconducting solenoid (0-50KG) with separate superconducting gradient field coils; the forces were measured with a Beckman microbalance LM-600. Temperatures T were derived from the He vapour pressure from 1.8 to 4.2K, from the resistance of an Allen Bradley carbon resistor from 4.2 to 25K and at higher temperatures from the readings of a copper-constantan thermocouple with a reference junction in liquid nitrogen.

The magnetic susceptibility χ of the Mn solute was assumed to be $\chi_{alloy} - \chi_{Ag}$, where χ_{alloy} is the susceptibility of the alloy and χ_{Ag} is that of Ag. χ_{Ag} has been measured from 1.8 to $100°K$, and since it changes only very slightly with temperature compared with the change of χ, the value -1.86×10^{-7} emu/gm for χ_{Ag} was used as the correction for the whole of this temperature range. The initial susceptibility follows a Curie-Weiss behaviour and from the Curie constant the spin $S = 2.23 \pm 0.01$ per Mn atom was determined, which is in good agreement with the values of Mizuno[3] and Flouquet[4], where in this and later calculations the assumption $g = 2$ was made.

The RKKY impurity-impurity interaction and the single impurity Kondo effect will both reduce the magnetization M below the Brillouin function appropriate for free spins, and also inhibit the approach to saturation of M. From the RKKY interaction, scaling laws[5]

$$(M/n) = F_1 (T/n, H/n)$$

and $\chi = F_2 (T/n)$ were derived, where H was the magnetic field and the concentration n acted as the scaling parameter. The (M/n) vs (H/n) behaviour has been plotted in Fig. 1 for the three alloys by fixing the "reduced temperature" $T/n = 3.0 \times 10^{-3} °K/ppm$ Mn and χ vs (T/n) in Fig. 2 for the 630 and 1370 ppm alloys. The experimental results follow the scaling laws well. Another characteristic feature of magnetic interaction which arises from the RKKY interaction is that the magnetization per impurity atom, at a given H and T, decreases as n increases. This characteristic feature can be seen implicitly in Fig. 3. The above evidence thus suggests that the RKKY interaction, rather than single impurity Kondo effect or crystal field splitting dominates the magnetic behaviour of the alloys measured.

By using a virial expansion of the free energy in a power series of the

concentration of magnetic impurities to investigate the effect of the RKKY

interaction on the thermodynamic function of dilute magnetic alloys, Larkin

and Khmel'nitskii[6] derived the following temperature independent expression

for magnetization M at the $kT < g\mu_B H$ limit,

$$M = g\mu_B \bar{S}n \left[1-2(2\bar{S}+1)n \, V_0 / 3g\mu_B H \right] \qquad \text{where } \bar{S} = (S(S+1))^{\frac{1}{2}}$$

and effective moment $\mu_{eff} = g\mu_B \bar{S}$. However, under practical laboratory

conditions (say H = 45 KG) the $kT << g\mu_B H$ limit might be difficult to achieve

and the effect of temperature should be considered as well. This can be done,

as Larkin and Khmel'intskii[6] suggested, by introducing the free energy in second order

$$F^{(2)} = (\tfrac{2}{3})n^2 V_0 \, Re \, \psi' \left[\tfrac{1}{2} - (\tfrac{i}{2\pi}) \ln (1+2ch \, (g\mu_B H/kT)) \right]$$

where ψ' is the logarithmic derivative of the Γ function. We obtained the

following temperature-dependent expression for the small $kT/\mu_B H$ case

$$M = g\mu_B \, \bar{S}n \left\{ 1-2(2\bar{S}+1) (nV_0/3g\mu_B H) \left[1+(\tfrac{1}{3}) (\pi k/g\mu_B H)^2 T^2 \right] \right\}$$

The fractional deviation of magnetization M (taken at field H = 45 KG) from

the saturation magnetization, assuming this to be $n\mu_{eff} = ng\mu_B \bar{S}$, has been

plotted as $(1-M/g\mu_B \bar{S}n)$ vs T^2 in Fig. 3. A T^2 dependence is observed

clearly, and a linear relation between $(1-M/g\mu_B \bar{S}n)$ vs n at a fixed T can also

be seen implicitly. From the intercepts at T^2 = 0 of the straight lines, the

strength of the RKKY interaction between two Mn atoms in AgMn $V_0 = (3.9 \pm 1) \times 10^{-25} eVcm^3$

has been determined, where 1-ppm Mn = 5.91×10^{16} Mn atoms/cm^3.

The effective |J| value of the s-d exchange interaction $V_{sd} = -J \, \underset{\sim}{S} \cdot \underset{\sim}{s}$

between the spin operators $\underset{\sim}{S}$ and $\underset{\sim}{s}$ for the spin momenta of Mn and conduction electron

of Ag can be estimated by putting the above obtained values of V_0 and S into the

following equation[7]

$$V_o/2 = 9\pi^2 J^2 S(S+1)/64\sqrt{2}\ E_F K_F^3$$

where the $\frac{1}{2}$ factor at left appears because V_o is the strength defined between two impurities, with $E_F = 5.48$ eV and $K_F = 1.2 \times 10^8$ cm^{-1}.[8] The effective $|J|$ value of (0.9 ± 0.1) eV has been determined, which is between that of 1.1 eV obtained by Mizuno[3] from NMR studies and the value of 0.22 eV derived by Flouquet[4] from γ-ray anisotropic measurements.

An alternative approach can be used to estimate roughly the order of magnitude of the effective $|J|$ value from V_o as follows. The results for AgMn alloys show that in this system when n lies between 630 and 1370 ppm Mn the RKKY interaction dominates. From the recent ESR results for dilute AgMn alloys by Davidov et al[9], we estimate by the behaviour of the g value that the $nV_o \sim kT_K$ condition holds when n $\sim$ 200 ppm. Using the above V_o value, the AgMn Kondo temperature $T_K = 55 \pm 10$ mK has been estimated which is close to the value 40 mK obtained by Flouquet[4]. This value of T_K gives the effective $|J| \approx (0.27 \pm 0.02)$ eV from $T_K \approx T_F \exp(-1/2\ |J|\ \rho)$[10], with $T_F = 6.39 \times 10^4$ K and $\rho = 0.137$ eV^{-1},[8] which is of the same order as the above calculated $|J|$ value.

References

1. N.A. Ruderman and C. Kittel, Phys. Rev. 96, 99 (1954)

   R. Kasuya, Prog. Theor. Phys. 16, 45 (1956)

   K. Yosida, Phys. Rev. 106, 893 (1957)

2. O. Laborde and P. Radhakrishna, Solid State Comm. 9, 701 (1971)

3. K. Mizuno, J. Phys. Soc. Japan 30, 742 (1971)

4. J. Flouquet, Phys. Rev. Lett. 25, 288 (1970)

5. J. Souletie and R. Tournier, J. Low Temp. Phys. 1, 95 (1969)

6. A.I. Larkin and D.E. Khmel'nitskii, Zh. Eksp. Theor. Fiz. 58, 1789 (1970)

   (Sov. Phys. - JETP 31, 958 (1970))

7. See, for example, W.A. Harrison, Solid State Theory, Chap.IV and V,

   McGraw Hill Inc. 1970.

8. D.L. Martin, Phys. Rev. 141, 576 (1966).

9. D. Davidov, C. Rettori, R. Orbach, A. Dixon and E.P. Chock, to

   be published.

10. A.A. Abrikosov, Phys. 2, 5 (1965).

    Y. Nagoaka, Phys. Rev. 138, A1112 (1965).

    H. Suhl and D. Wong, Phys. 3, 17 (1967).

Figure Captions

Fig. 1   Impurity magnetization M divided by concentration n as a function of magnetic field H divided by n at the fixed "reduced temperature" $(T/n) = 3.0 \times 10^{-3}$ °K/ppm Mn for 630, 1000 and 1370 ppm Mn AgMn alloys.

Fig. 2   Magnetic susceptibility χ as a function of "reduced temperature" (T/n) for 630 and 1370 ppm Mn AgMn alloys.

Fig. 3   Fractional deviation of magnetization M, taken at field
H = 45 KG, from the saturation magnetization $n\mu_{eff} = g\mu_B \bar{S} n$,
$(1 - M/g\mu_B \bar{S} n)$ as a function of T^2 for 630, 1000 and 1370 ppm Mn AgMn alloys.
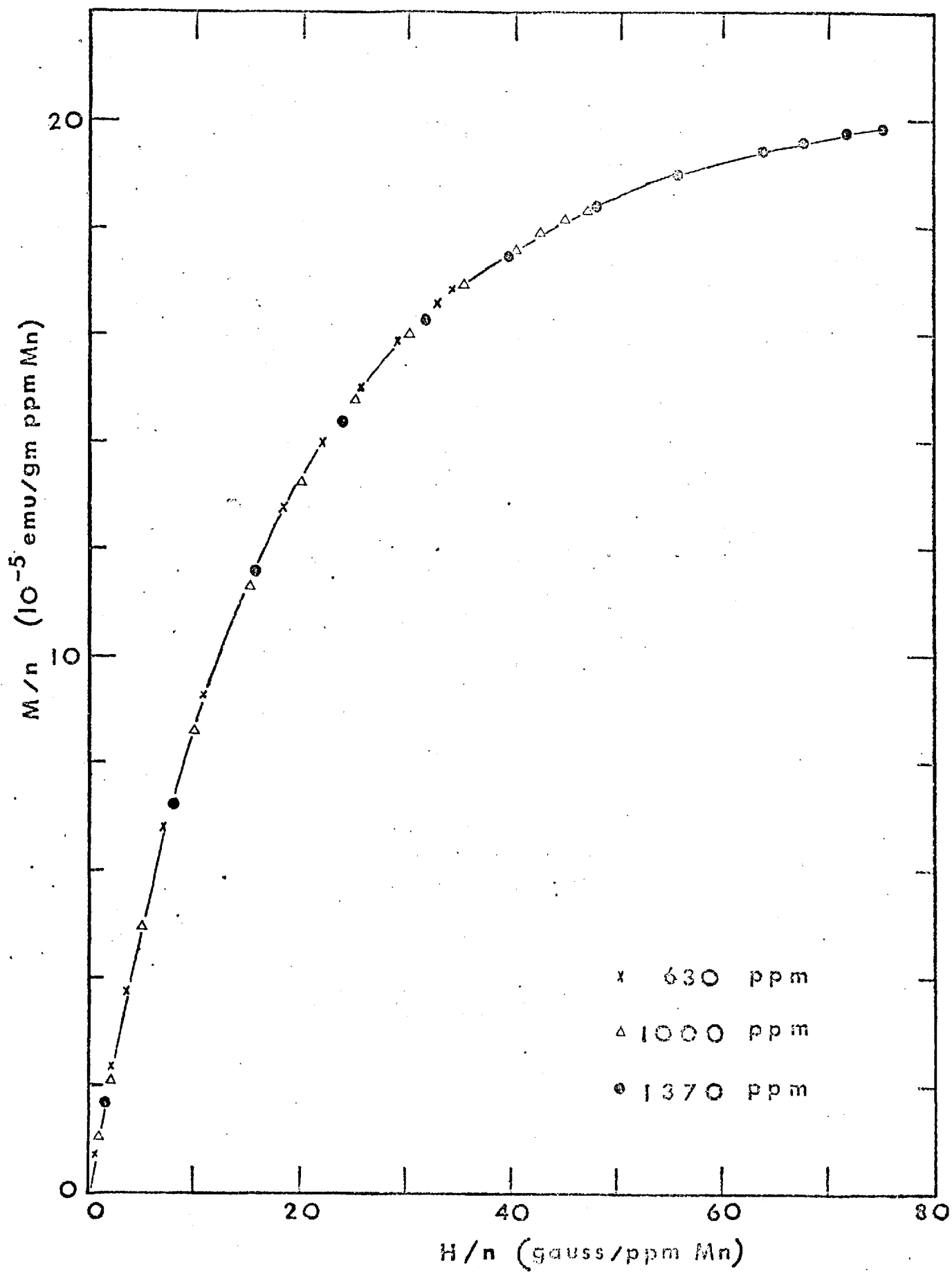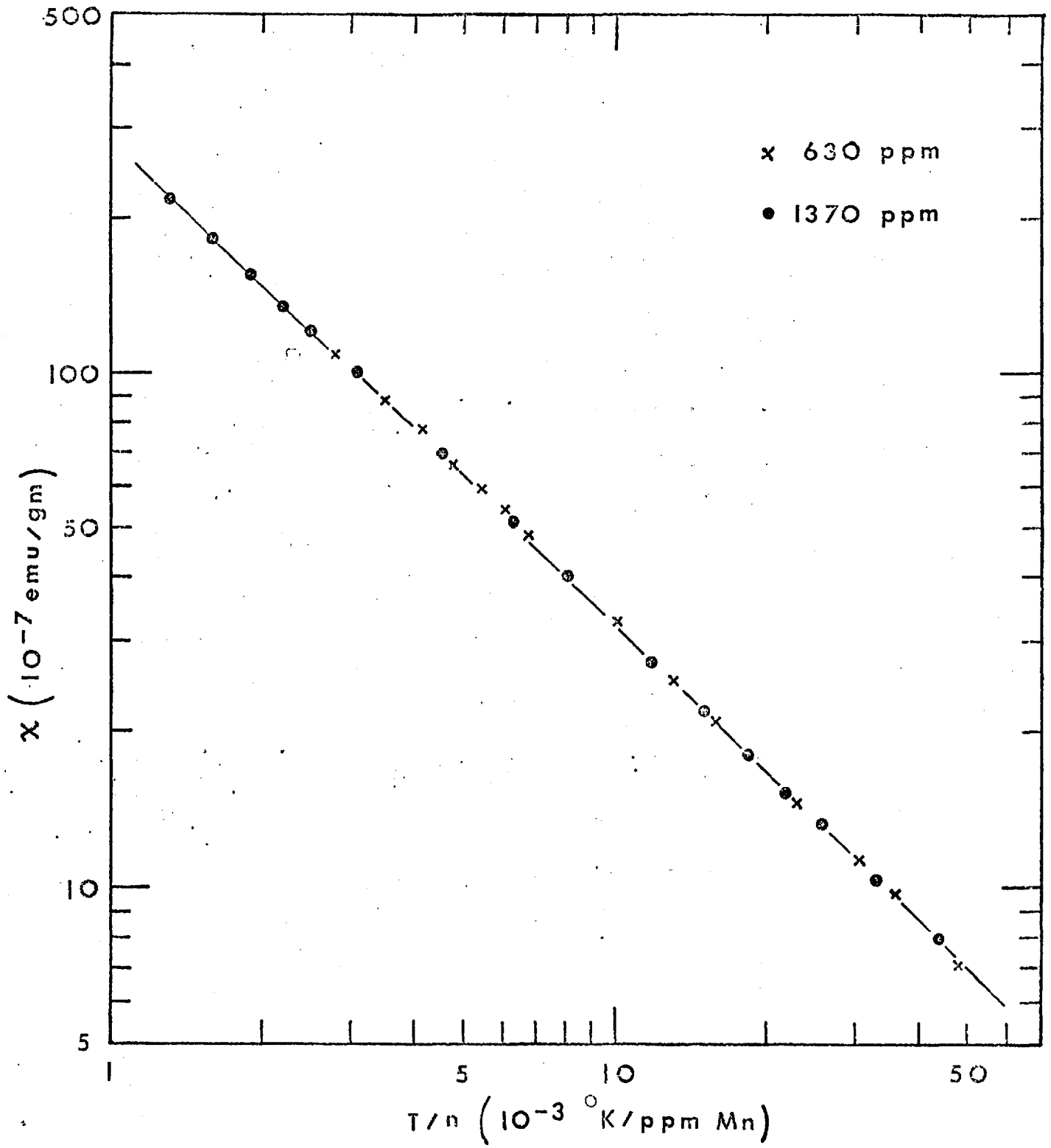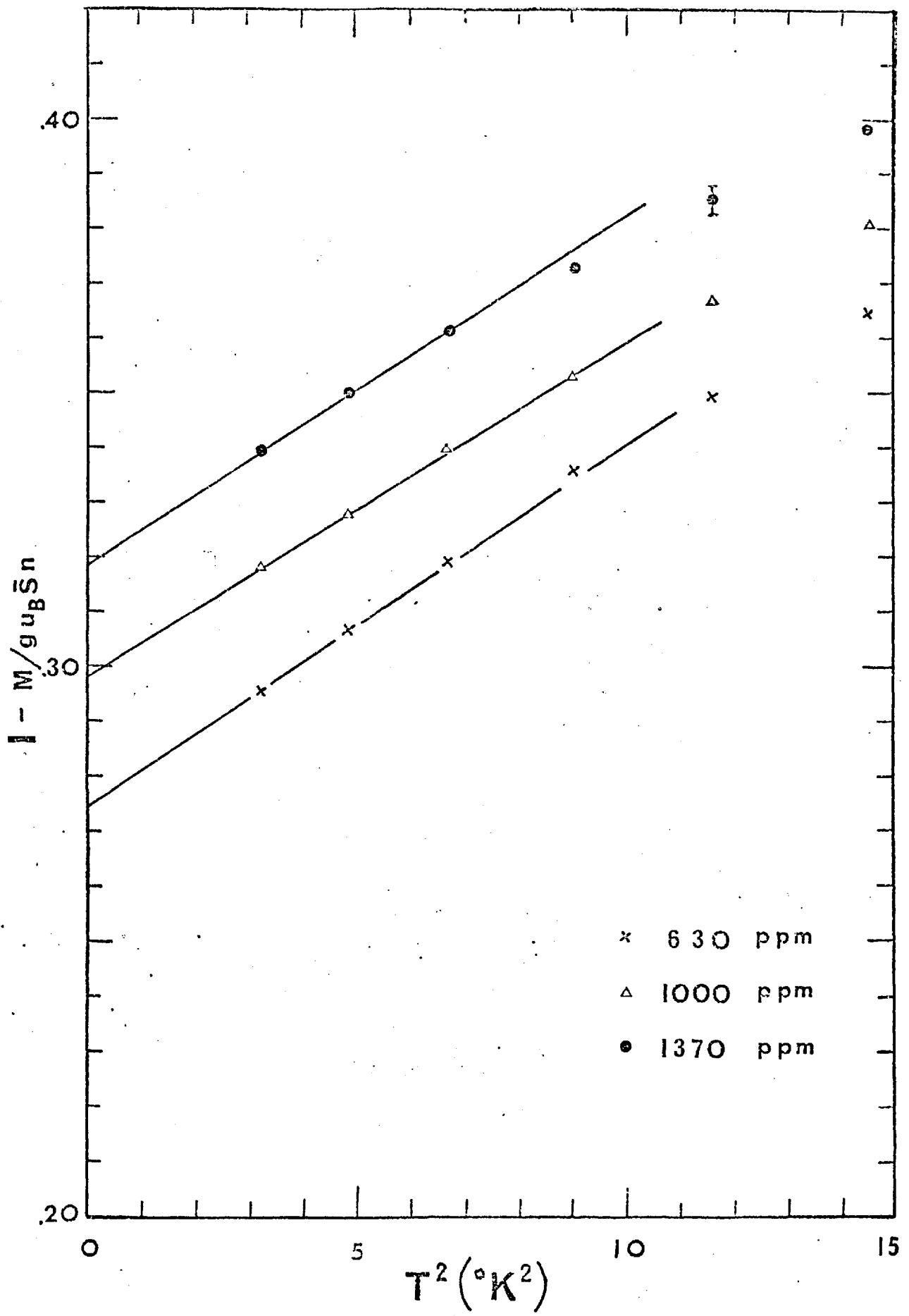
APPENDIX   B

Extended Far Vacuum Ultraviolet Transmission Spectrum of Uracil Thin Film

Pon-Wei Hou   Department of Physics, Imperial College, LONDON SW7

R.P. Rampling   Department of Physics,   Queen Elizabeth College, LONDON W8

Abstract

The direct sublimation of a thin film of specimen onto a scintillator method has been used to extend the vacuum ultraviolet (UV) transmission spectrum. With a He light, the far vacuum UV transmission spectrum of a thin film of uracil from 4 eV to 21 eV (300 to 60 nm) has been obtained and is presented here. The results are in good agreement with UV spectra previously obtained up to 10 eV and with electron energy loss measurements up to 21 eV.

1. Introduction

In order to obtain transmission spectra in the far vacuum ultraviolet (UV) region of the electromagnetic spectrum very thin films of the specimen material are needed (~50 nm). The structural integrity of such films will only be maintained if they are supported on specimen beds which must themselves be transparent in this region. Typically thin lithium fluoride (LiF) or quartz plates are used and UV light transmitted by the specimen supported in this way is subsequently detected by a scintillator-photomultiplier combination. Since LiF and quartz become strongly absorbing at wavelengths shorter than ~155 nm and 105 nm respectively the useful range of this method is restricted to wavelengths longer than this bottleneck.

An alternative method is used in electron microscope and X-ray diffraction by mounting the thin film of specimen onto another thin film but with stronger structure, say a thin carbon film on Cu grids, to extend the range of spectra; then subtract the spectra of this supporting film out of the collected data to obtain the spectra of the specimen. However this method is not fruitful in UV spectra, because of the relative weak energy, low intensity and instability of the UV light.

In order to overcome the problem of the high energy cut-off of the specimen bed and thus extend the vacuum UV transmission spectrum beyond 12 eV a new method was used (Vickers[1]). This involved subliming the specimen directly onto the scintillator (P - terphenyl) which need be supported only by a material which is transparent to scintillated light, say a glass plate. Using specimens prepared in this way the vacuum UV transmission spectrum for uracil ($C_4 N_2 O_2 H_4$) was measured from 300 nm to 60 nm (4 to 21 eV). The results are presented together with corresponding results obtained by other workers using more traditional methods up to the limit of ~ 10 eV and with electron energy loss measurements, with relatively poor resolution, which cover the remainder of the region.

II. Experiments

The spectral measurements were made on an automated Hilger and Watts E 766 near-normal incidence monochromator constructed by Rampling and Vickers[2]. Data were collected on punched paper tape for subsequent anal/sis on a CDC 6600 computer. The dispersion element was a Bausch and Lomb reflection grating with 600 lines mm $^{-1}$ blazed for a wavelength of 150 nm. The specimen was at room temperature in an ambient pressure of ~5 x 10^{-5} torr.

The light source was a McPherson 630 lamp used in an AC discharge mode with hydrogen gas down to 90 nm and in a condensed spark mode with molecular sieve purified helium gas for shorter wavelengths. Experiments were made with a resolution of about 5 nm and the light was assumed to be unpolarised and each reading was checked for the effects of stray light. The photomultiplier was a EMI 6094 with 1200 volts potential supply.

The specimen was prepared as follows. The p – Terphenyl scintillator was sublimed in a vacuum of 5 x 10^{-5} torr and at a temperature of 130 ° C onto a clean, 1 mm thick glass slide. This formed a uniform smooth layer ~3,600 nm thick. Half of this slide was covered and a film of uracil ~50 nm thick was slowly sublimed at a temperature of 150° C onto the other half under similar vacuum conditions. The construction of the slide is shown in figure 1. The chemicals used were from BDH without further purification.

p – Terphenyl was chosen as the scintillator rather than the more usual sodium salicylate because it could be prepared with a much smoother surface whilst having a comparable quantum efficiency.

III Results

At each wavelength the amplified photomultiplier voltage was recorded for the three positions of the specimen in the beam shown as A, B and C in figure 1. The voltage recorded from position B corresponds to the dark current I_B and the incident light intensity I_o can be taken to correspond to $(I_A - I_B)$. Similarly the transmitted light I_t corresponds to $(I_C - I_B)$ and the optical density O.D. can be written

$$O.D. = \frac{1}{d} \log\left(\frac{I_o}{I_t}\right)$$

where d is the specimen thickness.

Figure 2 shows the optical density for a 50 nm uracil film calculated as a function of wavelength and energy. This result remained substantially the same as the film thickness was varied up to 100 nm.

Table 1 shows a comparison of the positions of the peaks in the transmission spectrum for uracil specimens prepared in a number of ways. The sublimed thin film results obtained using traditional methods are those of Yamada and Fukotome [3], the aqueous solution results are from Voet et al [4], the vapour results from Clark et al [5] all of which go only to 10 eV. The electron energy loss results of Isaacson [6] up to 20 eV are also shown. The good agreement between this work and previous results is encouraging evidence of the usefulness of the direct sublimation method for extending the range of vacuum UV spectra of thin films.

IV Acknowledgements

We thank A.F. Vickers for general discussion and for a copy of his thesis which forms a background for this work. We also thank S. Onari and H. Fukutome for information on scattering from thin films and J.E.G. Wheaton and R.E. Huffman for helpful discussion on light source. We appreciate the warm hospitality of Department of Physics, Queen Elizabeth College, where this experiment h as been carried out.

1. A. F. Vickers, Private Communication

2, R. P. Rampling and A. F. Vickers, J. Phys. E, $\underline{6}$, 871 (1973)

3. T. Yamada and H. Fukutome, Biopolymers, $\underline{6}$, 43 (1968)

4. D. Voet, W. B. Gratzer, R. A. Cox and P. Doty, Biopolymers, $\underline{1}$, 193 (1963)

5. L. B. Clark, G. Peschel and I. Tinoco Jr., J. Phys. Chem., $\underline{69}$, 3615 (1965)

6. M. Isaacson, J. App. Phys., $\underline{56}$ 1803 (1972)

Figure Captions

Fig1. Schematic diagram of the ultraviolet transmission spectra system. The block (dashed line) is moved horizontally for each of the incident monochromatic light frequency taken. The data of I_A, I_B and I_C corresponding to the readings when position A, B or C is located at the straight position between incident light and photodetector.

Fig2. The optical density vs the energy loss for a 50nm uracil film.

Table 1, <u>Positions of the Peaks in the Optical Spectra</u>

Ultraviolet Spectra				
Direct Sublimed Film (This work)	Indirect Sublimed Film [3]	Aqueous Solution [4] (PH 7.0)	Vapor[5]	Electron Energy Loss[6]
4.7 ± 0.1 (eV)	4.66 (eV)	4.79 (eV)	5.09 (eV)	4.70 (eV)
6.21 ± 0.15	6.07	6.14	6.05	5.93
6.80 ± 0.15	6.96	----	----	6.93
7.50 ± 0.20	7.90	----	----	----
8.68 ± 0.15	8.60	----	----	8.45
13.1 ± 0.4	----	----	----	13.9
16.9 ± 0.4	----	----	----	16.9